A High Pressure Shock Tube and Rapid Compression Machine Study of *n*-Butylcyclohexane and its Mixtures with *n*-Heptane

Christine Conroy, B. Sc.

Supervisor: Prof. Henry Curran

Head of School: Dr. William Carroll

Abstract

This study presents a high pressure experimental and modelling investigation on the ignition of *n*-butylcyclohexane and its mixtures with *n*-heptane. Mixtures were chosen to represent a surrogate for *n*-decylcyclohexane, a constituent of transportation fuels which has an extremely low vapour pressure and hence it is currently impossible to carry out gas phase experiments using this fuel. Thus, mixtures of 53% *n*-butylcyclohexane and 47% *n*-heptane were prepared and studied to mimic the same hydrogen/carbon ratio as *n*-decylcyclohexane.

Ignition delay times were measured in two heated shock tubes in the temperature range 800 – 1550 K, at reflected shock 1, 10, 30 and 50 atm and at equivalence ratios of 0.3, 0.5, 1.0 and 2.0 in air for both *n*-butylcyclohexane and mixtures of *n*-butylcyclohexane / *n*-heptane.

The shock tubes used in this study consists of a 3 m driver section and 5.73 m driven section separated by a double diaphragm section. Upon rupture of the diaphragm a shock wave is generated. This shock wave moves into the driven section compressing and heating the test gas. The ignition delay time is defined as the time from the arrival of the shock wave at the end wall to the ignition of the fuel. Ignition delay times were measured from 50 μs to 3 ms.

Ignition delay times were also measured in a heated rapid compression machine in the temperature range 580 – 800 K, at compressed gas pressures of 10 and 30 atm for both *n*-butylcyclohexane and mixtures of *n*-butylcyclohexane / *n*-heptane at the equivalence ratios outlined for the shock tube.

The rapid compression machine used in this study is a twin opposed system capable of compression of test gas mixtures up to 60 atm with a compression time of approximately 16 ms. Ignition delay times were measured from 3 ms to 100 ms.

Due to the low vapour pressures of the fuels used in this study homogeneous heating of the equipment was essential to ensure that the fuel remained in the gas phase. Heating systems were installed onto the shock tubes and rapid compression machine, mixing tanks and manifolds.

Experimental results obtained for both *n*-butylcyclohexane and mixtures of *n*-butylcyclohexane / *n*-heptane were compared to simulations of two models which are available in the literature, JetSurF 2.0 and Natelson *et al.*. The models failed to capture the experimental data.

In addition ignition delay times are also measured in the low pressure shock tube. This is a stainless steel shock tube with a 6.22 m driven section and a barrel shaped driver section. This is a single diaphragm shock tube. During an experiment the diaphragm is ruptured by a cross shaped cutter housed inside the driven section of the shock tube. Increased drive gas pressure caused the diaphragm to bulge and come in contact with the cutter resulting in the bursting of the diaphragm. Ignition delay time is defined as the time from the arrival of shock wave at the end wall to the maximum rise in $CH^{\star}$ emission. Ignition delay times were measured from 50 μs to 1000 μs.

Ignition delay times of the isomers of pentene were measured in the low-pressure shock tube. Experiments were carried out using 1- and 2-pentene in the temperature range 1250 – 1900 K, at a reflected shock pressure of 1 atm and at equivalence ratios of 0.5, 1.0 and 2.0 at 1% fuel concentration. Experimental results were used to validate the model of Mehl *et al.* *This work* was presented at the 33rd Internal Symposium on Combustion.

Ignition delay times were also measured for 2,5-dimethylfuran in the low pressure shock tube.

Experiments were carried out in the temperature range 1300 – 2000 K, at a reflected shock pressure of 1 and 2 atm and at equivalence ratios of 0.5, 1.0 and 2.0 at 0.75% fuel concentration. This works builds upon a study previously carried out by G. Black at NUI Galway where low pressure shock tube ignition delay times were measured at 1 atm, $\phi = 1.0$ and 2.5. Experimental results from this study were used for model validation. Ignition delay times were also measured for 2,5-dimethylfuran in the low pressure shock tube. Experiments were carried out in the temperature range 1300 – 2000 K, at a reflected shock pressure of 1 and 2 atm and at equivalence ratios of 0.5, 1.0 and 2.0 at 0.75% fuel concentration. This works builds upon a study previously carried out by G. Black at NUI Galway where low pressure shock tube ignition delay times were measured at 1 atm, $\phi = 1.0$ and 2.5. Experimental results from this study were used for model validation.

Contents

List of Figures

List of Tables

Chapter 1

Introduction

1.1 Energy Usage

Combustion occurs as a result of a reaction between a fuel and an oxidiser. The energy is released in the form of heat, light and mechanical energy. This energy can be harnessed by humans. At a very basic level fire provides us with a source of warmth, light and a means to cook food. It can be used to produce electricity and power engines. Fire is one of the oldest known technologies and was vital in human evolution.

At present approximately 90% of the world's energy demand is met by combustion. Hence, a fundamental understanding of combustion processes is of vital importance to utilise our remaining fossil fuel resources to their full potential, while still considering environmental factors such as toxic emissions and particulate matter.

In Ireland we rely heavily on fossil fuels. For example in 2010, 95% of the total energy produced was from the combustion of such fuels. To meet this energy demand 86% of our energy needs are imported in the form of oil, coal and natural gas. Some natural gas deposits exist with two gas fields, Kinsale and Corrib, yet 92% of total natural gas consumed in Ireland is imported. Figure 1.1 illustrates the energy sources and the area in which it is consumed in Ireland in 2010, usage is given in tonne of oil equivalent (toe). Sources are shown on the left hand side while uses are shown on the right. It is clear that imported oil is the major contributer to energy production, accounting for 50% of total energy production. It is also evident that most energy is consumed by the transportation sector with 31% of total energy production being used in this sector [1].

With some estimates showing that peak oil has been reached it is of vital importance that the resources that are available be utilised in an efficient manner. This can be achieved via a better understanding of the chemical reactions that lead to the combustion of fuels and hence improvements in the efficiency of combustion processes.

1.2 Transportation Fuels

Transport fuel consists of a number of components which can be grouped into well defined categories of hydrocarbons, including 4 – 8% alkanes, 2 – 5% alkenes, 25 – 40% iso-alkenes, 3 – 7% cycloalkanes, 1 – 4% cycloalkenes and from 20 – 50% aromatics by volume [2]. The composition of transport fuels varies depending on the origin of the crude oil and refining processes. For example in the U.S. petrol typically consists of 45% branched alkanes, 11% ethers, 5% alkenes and 30% aromatics, while diesel is composed of 31% alkanes, 24% alkyl-cyclohexanes, 15% alkyl decalins, 9% alkyl benzenes and 19% polycyclic naphthenoaromatics [3].

It is clear that straight-chained and cyclic alkanes form a substantial component of both

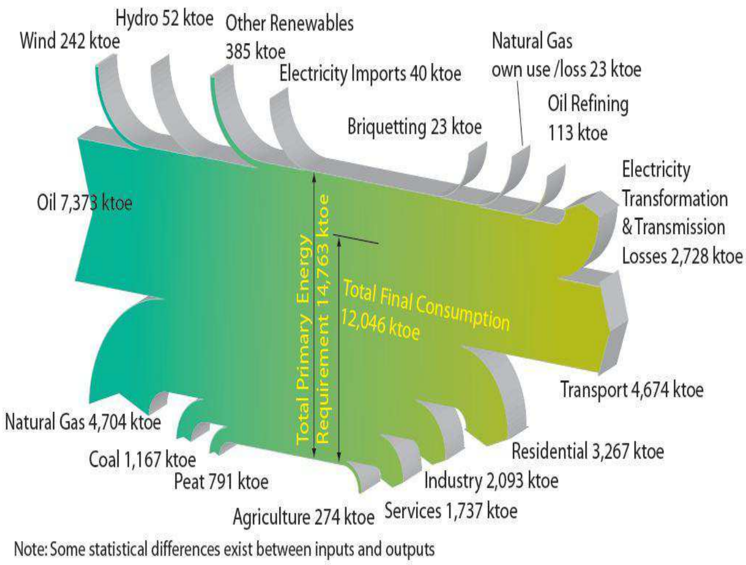

Figure 1.1: Overall energy flow, Ireland, 2010 [1].

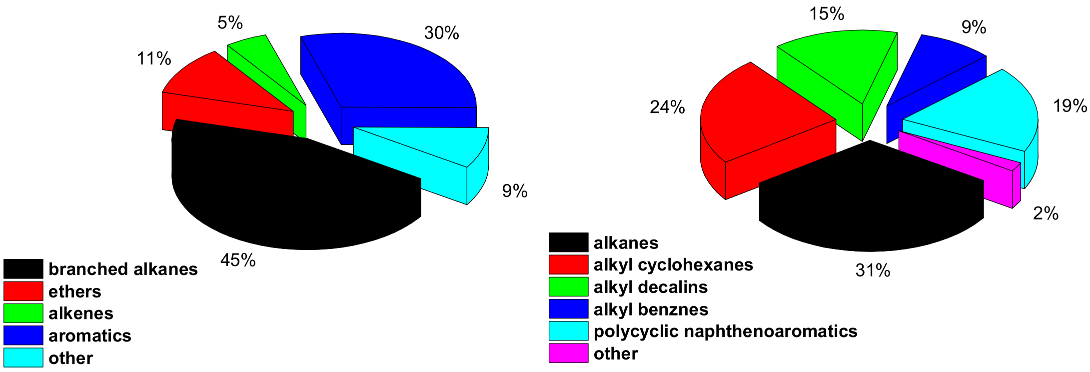

(a) Petrol (b) Diesel

Figure 1.2: Composition of petrol and diesel [3].

petrol and diesel fuels. It is for this reason that the ignition characteristics of such molecules are of great interest. This thesis is concerned with studying the ignition characteristics of n-butylcyclohexane and an n-decylcyclohexane surrogate, composed of n-butylcyclohexane and n-heptane, as it is currently impossible to study this fuel experimentally due to its low vapour pressure.

While extensive research has been carried out on n-heptane [5–10], little has been published on n-butylcyclohexane. Of the work which has been published most has been concerned with the use of n-butylcyclohexane as a component of a surrogate to mimic aviation fuel [11–13]. In recent years, since 2010, work has been reported in the literature on the combustion of n-butylcyclohexane. This work includes a laminar flame speed study [14], a shock tube study [15], a flow reactor study [17] a single cylinder engine study [16] and non-premixed flames [18].

1.3 Surrogate Fuels

Conventional fuels, diesel, petrol and aviation fuels, are composed of many different classes of hydrocarbons. Within these classes there are a large number of molecules hence it would be impossible to conduct meaningful experiments with such a vast number of chemicals contained in one mixture. In order to overcome this problem surrogate fuels are used. These are well defined mixtures of a small number of hydrocarbon compounds whose relative concentrations can be adjusted so that the physical and chemical properties of their combustion approximate those of a fuel that is difficult to study experimentally [19]. Surrogates can be divided into two groups; physical surrogates and chemical surrogates. Physical surrogates are selected to reproduce the physical properties, for example boiling point, density, viscosity and vapour pressure of a fuel. Chemical surrogates on the other hand, are chosen to have the same chemical-class composition as the surrogate fuel; they are selectively constructed in order to reproduce a fuel's combustion characteristics [13].

Surrogates may also be used to emulate a fuel component which may be difficult to study experimentally due to its low vapour pressure. For example in this study a mixture of *n*-butylcyclohexane and *n*-heptane is used as a surrogate for *n*-decylcyclohexane. *n*-Decylcyclohexane is a large molecular weight component which is found in diesel and aviation fuels. Cycloalkanes account for approximatley 24% of diesel [3] and approximatley 17% of aviation fuels [20] Gas phase experiments of this fuel are difficult to carry out due to its extremely low vapour pressure, Camin *et al.* report it to be 52.08 Torr at 196.8°C [21].

Surrogate fuels are typically used in order to provide a baseline for performance and emission as well as providing a tool which can facilitate the development of a kinetic model.

1.4 Vapour Pressure

The vapour pressure is the pressure exerted by a vapour of a solid or liquid when in equilibrium with its condensed phases in a closed system at a given temperature. The vapour pressure of any substance increases with temperature. This relationship is non-linear. Table 1.4 gives the vapour pressures of cyclohexane and a number of alkylcyclohexanes at room temperature. Figure 1.3 shows the vapour pressures for methyl-, ethyl-, *n*-propyl- and *n*-butylcyclohexane over a range of temperatures. It can be clearly seen that with increasing alkyl chain length the vapour pressure of the fuel decreases. *n*-Butylcyclohexane has a vapour pressure of approximately 100 Pa at room temperature (20°C), compared to methylcyclohexane which has a vapour pressure 6270 Pa at 20°C [22] . This makes gas phase experiments of *n*-butylcyclohexane and higher alkyl cyclohexanes difficult if not carried out a low fuel concentrations. In order to carry out high fuel concentration gas phase experiments with such low vapour pressure fuels, uniform heating of the experimental equipment is essential to ensure that all of the fuel remains in the gas phase and that condensation does not occur. In this study heating the shock tubes and of the rapid compression machine was vital. Installation of these heating systems will be outlined in detail in Section 4.2.

1.5 Combustion Chemistry

The oxidation of hydrocarbon fuels, RH, can be divided into two distinctive sets of reactions, high-temperature and low-temperature. High-temperature chemistry dominates at temperatures in excess of approximately 1100 K, while low-temperature chemistry is important in the region 600 – 1100 K [6]. Figure 1.4 illustrates a lumped kinetic scheme of primary oxidation reaction for a hydrocarbon fuel, RH.

Fuel	Vapour pressure at 20°C (Pa)
Cyclohexane	13773
Methylcyclohexane	6270
Ethylcyclohexane	1299
n-Propylcyclohexane	356
n-Butylcyclohexane	101
n-Pentylcyclohexane	30
n-Hexylcyclohexane	10
n-Heptylcyclohexane	3
n-Octylcyclohexane	1.5

Table 1.1: Vapour pressures of cyclohexane and a number of alkylcyclohexanes at room temperature [22].

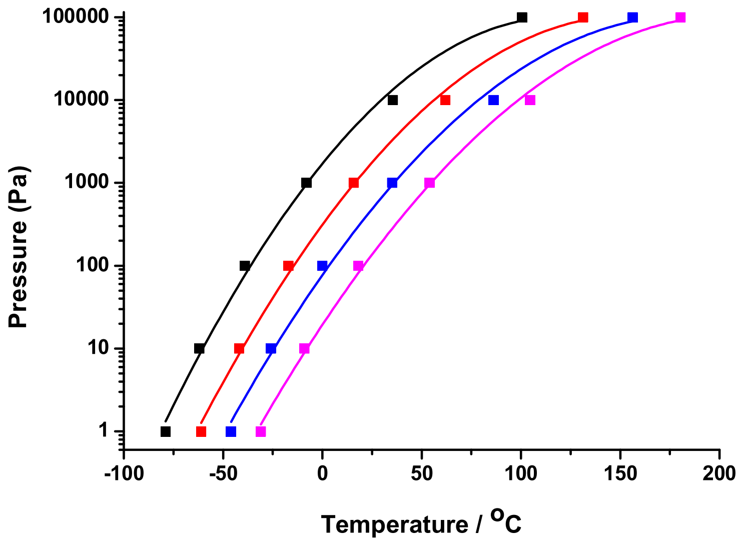

Figure 1.3: Vapour pressures of alkylcyclohexanes over a range of temperatures. ■ – methylcyclohexane, ■ – ethylcyclohexane, ■ – *n*-propylcyclohexane, ■ – *n*-butylcyclohexane [22].

1.5.1 High-Temperature

High-temperature oxidation takes place at temperatures in excess of approximately 1100 K [6]. In this temperature regime unimolecular fuel decomposition and hydrogen atom abstraction reactions from the fuel are important. At high-temperature, the chemistry is dominated by the chain branching reaction of hydrogen atom reacting with molecular oxygen to give a hydroxyl radical and an oxygen atom:

$$\dot{H} + O_2 \longrightarrow \dot{O}H + \ddot{O}$$

- Unimolecular fuel decomposition results in the formation of two alkyl radicals or an alkyl radical and a hydrogen atom.

$$RH \longrightarrow \dot{R} + \dot{R}'$$
$$RH \longrightarrow \dot{R} + \dot{H}$$

- Hydrogen atoms can be abstracted from the fuel by a number of species such as $\dot{H}$, $\ddot{O}$, $\dot{O}H$, O_2, $H\dot{O}_2$ and alkyl radicals, such as methyl radical, step 1, Fig. 1.4.

$$RH + \dot{H} \longrightarrow \dot{R} + H_2$$

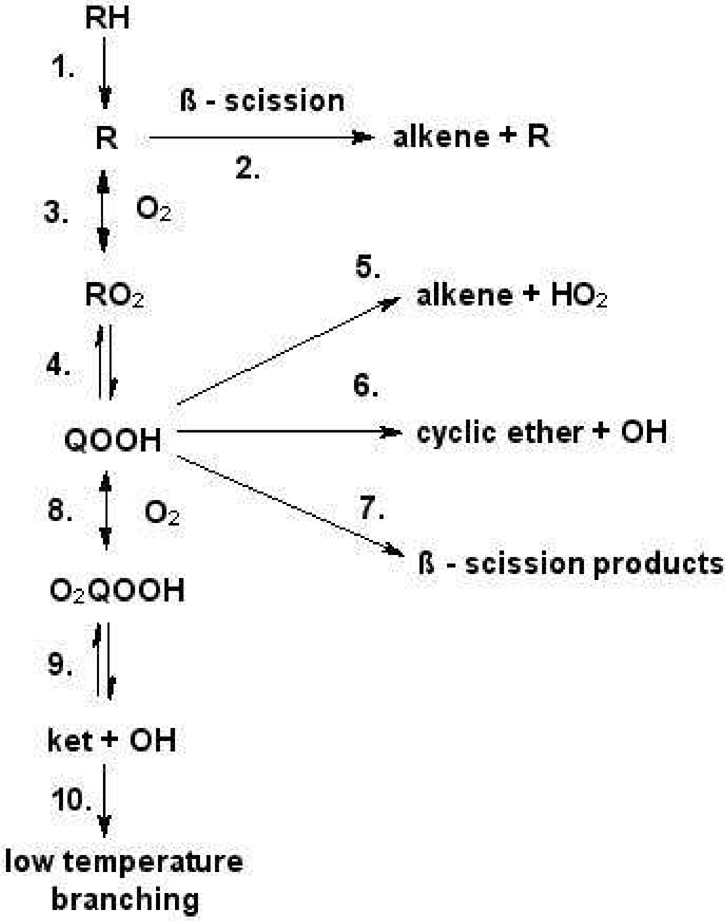

Figure 1.4: Lumped kinetic scheme of the primary oxidation reaction [6]. RH refers to the fuel, R the fuel radical, QOOH the product of internal isomerisation of the RO_2 species and ket a ketone species.

$$\begin{aligned} \mathrm{RH} + \ddot{\mathrm{O}} &\longrightarrow \dot{\mathrm{R}} + \dot{\mathrm{O}}\mathrm{H} \\ \mathrm{RH} + \dot{\mathrm{O}}\mathrm{H} &\longrightarrow \dot{\mathrm{R}} + \mathrm{H_2O} \\ \mathrm{RH} + \mathrm{O_2} &\longrightarrow \dot{\mathrm{R}} + \mathrm{H}\dot{\mathrm{O}}_2 \\ \mathrm{RH} + \mathrm{H}\dot{\mathrm{O}}_2 &\longrightarrow \dot{\mathrm{R}} + \mathrm{H_2O_2} \\ \mathrm{RH} + \dot{\mathrm{C}}\mathrm{H_3} &\longrightarrow \dot{\mathrm{R}} + \mathrm{CH_4} \end{aligned}$$

- Hydrogen peroxide can decompose via the following chain branching pathway;
  $$\mathrm{H_2O_2}\ (+\mathrm{M}) \longrightarrow \dot{\mathrm{O}}\mathrm{H} + \dot{\mathrm{O}}\mathrm{H}\ (+\mathrm{M})$$

- The alkyl radicals formed may undergo β-scission, step 2, Fig. 1.4 or may react with O_2 to form an alkene and $\mathrm{H}\dot{\mathrm{O}}_2$.

- The alkenes formed have a number of fates. These species can undergo hydrogen abstraction by $\dot{\mathrm{H}}$, $\ddot{\mathrm{O}}$, $\dot{\mathrm{O}}\mathrm{H}$ etc. to form an alkenyl radical [6].

1.5.2 Low-Temperature

Low-temperature oxidation of hydrocarbon fuels is dominated by a series of chain branching reactions [6], these reactions are shown in Fig. 1.4.

- Low-temperature oxidation involves the addition of a hydrocarbon fuel radical, $\dot{R}$, to molecular oxygen. This reaction results in the formation of an alkyl peroxy radical, $R\dot{O}_2$, step 3, Fig. 1.4.
- This alkyl peroxy radical has a number of fates. Firstly it can decompose to give an alkene and $H\dot{O}_2$. Secondly alkyl peroxy radical can undergo reactions with $H\dot{O}_2$ or other radicals and H_2O_2. Thirdly the peroxy radical can also undergo internal hydrogen-atom isomerisation. This proceeds through a transition state. This is mostly likely to proceed via a 5, 6, 7 or 8-membered intramolecular H-atom isomerisation reaction. This results in the formation of a hydroperoxy alkyl radical species, $\dot{Q}OOH$, step 4, Fig. 1.4.
- The $\dot{Q}OOH$ species can undergo a number of reactions; it can decompose to give an alkene + $H\dot{O}_2$, epoxide + $\dot{O}H$ or β-scission products. The $\dot{Q}OOH$ species can also add to molecular oxygen to form a $\dot{O}_2QOOH$ species, step 8, Fig. 1.4.
- The $\dot{O}_2QOOH$ species undergoes a further internal hydrogen-atom isomerisation reaction and goes on to low-temperature chain branching, steps 9 and 10, Fig. 1.4.

1.5.3 Negative Temperature Coefficient Behaviour

In *this study* the fuels used, *n*-butylcyclohexane and *n*-butylcyclohexane / *n*-heptane mixtures, exhibited strong negative temperature coefficient (NTC) behaviour. In combustion systems NTC behaviour marks the temperature range where the reactivity of the fuel decreases despite increasing temperature, i.e. longer ignition delay times are observed with increasing temperature. This is due to the underlying chemistry. In the NTC region the $\dot{Q}OOH$ species undergoes propagation reations to form alkenes, cyclic ethers and β-scission products, septs 5, 6 and 7, Fig. 1.4. These reactions compete with the chain branching step of addition of molecular oxygen to the $\dot{Q}OOH$ species. This reduces the number of radicals producd and has the effect of decreasing the reactivity of the system, hence longer igntion delay times are observed.

1.6 Alkyl-Cyclohexanes

Alkyl-cycloalkanes are common components in hydrocarbon fuels, with alkyl fragments ranging from methylcyclohexane and ethylcyclohexane to very large alkyl segments with as many as 15 or 20 carbon atoms. The literature to date is mainly concerned with the oxidation of the lower alkyl-cyclohexanes, cyclohexane itself, methylcyclohexane, ethylcyclohexane and to a lesser extent *n*-propylcyclohexane. The work that has been carried out on mono substituted alkyl-cyclohexanes to date will be described here briefly.

1.6.1 Methylcyclohexane

Methylcyclohexane is the smallest of the alkyl cyclohexanes. Its relatively high vapour pressure (6250 Pa at 20°C) makes it favourable for use in gas phase experiments and hence a number of experimental studies have been completed and kinetic models are available for its oxidation [23–26, 28].

Zeppieri *et al.* [23] carried out a study on the oxidation and pyrolysis of methylcyclohexane. It was conducted in a flow reactor at high temperatures in the range of 1050 – 1200 K. On pyrolysis, the major intermediates formed were ethene, 1,3-butadiene, methane and propene. It was found that these intermediates were also formed during the oxidation of the fuel with other oxygenates including CO and CO_2.

Orme *et al.* [24] studied the oxidation of methylcyclohexane at equivalence ratios of 0.5, 1.0 and 2.0. This work was carried out in a shock tube at reflected shock temperatures in the range 1200 – 2100 K and reflected shock pressures of 1.0, 2.0 and 4.0 atm. In addition as part of this study a kinetic reaction mechanism was developed to describe the oxidation of methylcyclohexane and was used, not only to simulate shock tube experiments, but also the flow reactor experiments of Zeppieri *et al.* [23]. The model consisted of 190 species and 904 reversible reactions and was found to be in good agreement with experimental data.

Pitz *et al.* [25] carried out experiments using methylcyclohexane in a rapid compression machine at a compression ratio of 10.5:1 and at compressed gas temperatures in the range 680 – 980 K. Using this experimental data the model developed by Orme *et al.* for the oxidation of methylcyclohexane was altered to include low-temperature kinetics. Some changes were also made to the high-temperature reaction mechanism. It was found that the ignition delay times predicted for *n*- and *iso*-alkenes based on estimates of $R\dot{O}_2$ isomerisation rate constants were too long when compared to data obtained experimentally. They also concluded that the relative rates of 5-, 6-, 7- and 8-membered ring methylcyclohexylperoxy isomerisations are critical to the prediction of ignition delay times in the NTC region.

Vanderover and Oehlschlager [26] carried out experiments on methylcyclohexane diluted in air using a shock tube. Experiments were carried out in the temperature range 881 – 1319 K, at pressures from 10.8 to 69.5 atm and at equivalence ratios of 0.25, 0.5 and 1.0.

Yang and Boehman [28] studied cyclohexane and methylcyclohexane in a motored engine at low- to intermediate-temperatures. They varied the compression ratio from 4 to 15 at an equivalence ratio of 0.25. The initial intake temperatures were 120°C and 200°C. Results showed that overall the reaction activity, which was monitored by the fuel conversion to carbon monoxide, was influenced by the presence of the methyl group. Cyclohexane showed stronger NTC behaviour than methylcyclohexane. For methylcyclohexane oxidation four conjugated olefin were detected: 1-, 3- and 4-methylcyclohexenes and methylenecyclohexene. Reaction pathways to these products were proposed.

1.6.2 Ethylcyclohexane

Ethylcyclohexane has not been studied as extensively as methylcyclohexane. A small number of experimental comparative studies have been carried out where ethylcyclohexane ignition delay times and flame speeds are compared with those of other mono-alkylated cyclohexanes [26, 29].

Vanderover and Oehschlager [26] carried out a shock tube study using ethylcyclohexane diluted in air. Experiments were carried out in the temperature range 881 – 1319 K, at equivalence ratios of 0.25, 0.5, and 1.0 and pressures from 10.8 to 69.5 atm. The ignition delay times observed for ethylcyclohexane were shorter than those for methylcyclohexane under all conditions studied. This indicated that an increasing alkyl side chain length in alkyl cyclohexanes increases reactivity. This is also true for alkyl benzenes [27].

Wu *et al.* [29] have studied laminar flame speeds of cyclohexane and mono-alkylated cyclohexanes. Experiments were carried out using cyclohexane, methylcyclohexane and ethylcyclohexane at pressure of 1, 2 and 5 atm and an unburned gas temperature of 353 K. It was found that increasing alkyl chain length reduces the laminar flame speed. This effect becomes more prominent as pressure increases. Flame speed measurements from this study were compared to those of Ji *et al.* [14] and were found to be in good agreement. Model predictions from JetSurF 2.0 [30] were found to be in good agreement with the experimental values.

Husson *et al.* [31] carried out a product analysis of the oxidation of ethylcyclohexane in the low- to intermediate-temperature regimes. This work was carried out in a jet-stirred reactor with online gas chromatography for the analysis of reaction products. Experiments were carried out at near atmospheric pressure (800 Torr), in the temperature range 500 – 1100 K, with a residence time of 2 seconds for equivalence ratios of 0.25, 1.0 and 2.0. Experimental results were simulated using a kinetic model from the literature. The model captured fuel, oxygen and products profiles such as carbon monoxide, carbon dioxide, methane, ethane, 1,3-cyclopentadiene and 1,3-cyclohexadiene, however it failed to accurately predict concentration profiles for other species such as acetylene, ethylene, propene, and 1- and 2-butene.

1.6.3 *n*-Propylcyclohexane

n-Propylcyclohexane has been studied in some detail with ignition delay time and speciation data available in the literature. Experimental studies include a jet stirred reactor [32], rapid compression machine [33], shock tube ignition delay times [34], spherical bomb [35] and laminar flame speed studies [36].

Ristori *et al.* [32] studied the oxidation of *n*-propylcyclohexane at atmospheric pressure in a jet-stirred reactor in the temperature range 950 – 1250 K at equivalence ratios (ϕ) of 0.5 and 1.5. Concentration profiles of reactants, intermediates and final products formed are reported at a reaction time of 70 ms. A model including 176 species and 1369 reactions attempted to trace some of the main pathways which proceed via H-atom abstraction to form seven different propylcyclohexyl radicals that react via β-scission to yield products such as ethylene, propene, methylenecyclohexane, cyclohexene, and 1-pentene. The model captured the species concentrations well.

Crochet *et al.* [33] have studied the oxidation of *n*-propylcyclohexane in an RCM over a range of equivalence ratios, $\phi = 0.3$, 0.4 and 0.5, at compressed pressures of 9.0 – 13.4 bar, 6.3 – 9.2 bar and 4.5 – 6.4 bar and at compressed temperatures of 620 – 930 K. For all experiments pressure and light emission signals were recorded. Chemical analysis was also performed to identify the stable oxidation products formed. Samples collected were analysed using GC/MS. The major products detected were propenal, propanal, cyclohexene, methylenecyclohexane, cyclohexanone, propyl-4-cyclohexene, propyl-3-cyclohexene and cyclohexanespiro-(ethyl-2-ox-2-irane).

Dubois *et al.* [35] studied the oxidation of *n*-propylcyclohexane using a shock tube and a spherical bomb. Ignition delay times were measured at temperatures in the range 1250 – 1800 K, at pressures of 10 and 20 bar and at equivalence ratios in the range 0.2 – 1.5. In addition laminar flame speeds were determined using a stainless steel spherical bomb at an initial temperature of 403 K and at a pressure of 1 bar. Using the experimental data obtained a detailed kinetic mechanism of 100 species and 690 reactions was developed based on models in the literature [32, 37, 38]. Good agreement between the model and the experimental data was observed.

Dubois *et al.* [34] have also recorded ignition delay times for *n*-propylcyclohexane and oxygen diluted in argon in a heated shock tube. Experiments were carried out in the temperature range of 1250 – 1750 K, at pressures of 9 – 12 bar and for equivalence ratios from 0.3 to 1.0. This experimental data was simulated using *n*-proplycyclohexane mechanisms from the literature [38, 39]. The results of the simulations showed an overall reasonable agreement with the experimental data for the activation energies but failed to reproduce ignition delay times. For all cases predicted times were longer than those observed experimentally.

Pousse *et al.* [36] have studied lean laminar premixed methane flames doped with *n*-propylcyclohexane. In the study inlet gases containing 0.81% *n*-propylcyclohexane, 7.1% methane and 36.8% oxygen were used. This corresponds to an equivalence ratio of 0.68. The flame was stabilised on a burner surface at a pressure of 6.7 kPa (50 Torr) using argon as the diluent with a gas velocity at the burner of 49.2 cm s^{-1} at 333 K. Samples were collected via a quartz microprobe and analysed using gas chromatography. Species concentrations were measured as a function of distance above the burner. An oxidation mechanism was also presented as part of this work. This mechanism predicted accurately the consumption of both fuel components and oxygen and also major products with the exception of propyne, allene, propene, propane and 1-butene which were vastly under-predicted. Both flame speciation data and jet-stirred reactor data were used to validate this mechanism. This work on *n*-propylcyclohexane is part of a larger study investigating the effect of doping methane flames with components of diesel fuel. *n*-

Propylcyclohexane is one such component. Also investigated was *n*-butylbenzene and indane [40, 41]. Indane and *n*-butylbenzene were added to lean methane flames in similar concentrations to that of *n*-propylcyclohexane. A comparison of the findings from the three investigations was given in Part III of this paper series [41]. It was concluded that, in the presence of non-aromatic cyclic reactants, the formation of alkenes and non-aromatic aldehydes is favoured, while in the presence of aromatic cyclic reactants, a greater number of aromatic products are formed.

1.6.4 *n*-Butylcyclohexane

n-Butylcyclohexane has been used as a component in surrogate jet fuels for some time and a number of studies have been reported in the literature. Recently flame speed [14, 18], ignition delay [15], flow reactor and single cylinder engine [17] studies have been reported in the literature for pure *n*-butylcyclohexane.

Lai and Song [42] have carried out a pyrolysis study of cyclohexane and seven other *n*-alkyl-cyclohexanes (alkyl side chain C_nH_{2n+1} where n = 1, 2, 3, 4, 6, 8 and 10). This work was carried out to investigate the thermal stability of the fuels. Experiments were carried out in or near supercritical phase conditions using a batch reactor at 450°C, at pressures 2 MPa. With side chain lengths n $\geq$ 3 the main products of the decomposition reactions favour cleavage of the side chain as opposed to ring opening cracking reactions. One example includes *n*-butylcyclohexane, where reactions take place to give alkylcyclohexanes and cyclohexenes. Reaction pathways for the pyrolysis of these longer side chained alkylcyclohexanes were also proposed in this paper. It was concluded that the thermal stability of alkyl cyclohexanes decreases with increasing side chain length.

Yu and Eser [43] performed a study of the thermal decomposition of *n*-butylbenzene and *n*-butylcyclohexane under supercritical conditions. Experiments were carried out in a Pyrex glass tube reactor and in a 316 stainless steel tubing bomb reactor to obtain gas samples. The reactors were heated to 450°C prior to performing the experiments. Reaction products were identified via GC-MS analysis. Product distributions for the thermal decomposition of *n*-butylcyclohexane were provided. Both liquid and gaseous decomposition product distributions were outlined and thermal decomposition pathways were proposed. Liquid products observed include cyclohexane, methylene cyclohexane, cyclohexene, methylcyclohexene, vinylcyclohexane, allycyclohexane as well as C_{10} alkenes. Also high molecular weight compounds were observed, C_{13} to C_{18} hydrocarbons. From this study it was also concluded that the formation of gaseous products are not favoured, gaseous products which were observed include hydrogen, methane, ethane, propane, propylene, butane and butene. A reaction mechanism for the decomposition of *n*-butylcyclohexane was proposed.

In a similar report Yu and Eser [12] have carried out work under super critical conditions on the thermal decomposition of *n*-decane, *n*-dodecane, *n*-tetradecane, *n*-butylbenzene, *n*-butylcyclohexane, decalin and tetralin. These molecules were analysed using a Pyrex glass tube reactor or a 316 stainless steel bomb reactor at temperatures in the range 400 – 475°C. Decomposition products for the fuels studied were reported. Both gaseous and liquid products for the decomposition of the fuel components were given as were species concentration profiles as a function of pressure.

Humer *et al.* [11] carried out experimental studies on the characterisation of the non-premixed combustion of jet fuel and a number of its surrogates in laminar non-uniform flows. Critical conditions of extinction and autoignition were measured for jet fuels JP-8, Jet-A and Fischer Tropsch JP-8. A detailed chemical kinetic model for the combustion of many of the components in JP-8 was not available, hence chemical kinetic models were developed by working on surrogates of the fuels. Previous studies suggested the use of four or five components for a suitable surrogate jet fuel, however, two or three components are used by Humer *et al.* In total 13 possible surrogates were developed consisting of *n*-decane, methylcyclohexane, toluene, o-xylene, *n*-dodecane,

n-butylcyclohexane, n-butylbenzene, trimethylbenzene, n-propylbenzene, iso-octane, decalin, 1-methylnaphthalene and tetralin. The surrogates were ranked by how well they reproduced the critical conditions of autoignition, hydrogen/carbon ratio, simplicity and how well they reproduced critical conditions of extinction. While surrogates containing n-butylcyclohexane were used it was found that the most suitable surrogate was a mixture of 60% n-dodecane, 20% methylcyclohexane and 20% o-xylene.

Colket *et al.* [44] also carried out work on surrogate jet fuels where numerous surrogates were suggested. One such surrogate which was discussed in detail contained 50% n-decane, 25% n-butylbenzene and 25% n-butylcyclohexane by volume. Firstly, laboratory experiments were carried out using a non-premixed opposed jet flame to test ignition and extinction limits. Experiments were carried out at atmospheric pressure and at 110°C. Secondly, a pressurised flow reactor study was performed at 0.8 MPa, at temperatures from 600 – 800 K and at ϕ = 0.3. Gas mixtures were prepared at 80% dilution. The conditions studied spanned the NTC regime which was followed by measuring the production of CO. Finally a single cylinder engine study was carried out at 500 K, at a compression ratio of 15 at ϕ = 0.23. It was concluded that the surrogates used in this study were of greater reactivity than that of the jet fuel.

Natelson *et al.* [45] have also carried out work on the low- and intermediate-temperature oxidation of n-decane, methylcyclohexane, n-butylcyclohexane, toluene and n-butylbenzene. Experiments was carried out on the pure fuels and on select mixtures in a pressurised flow reactor at temperatures in the range 600 – 800 K at 0.8 MPa, under fuel lean conditions (ϕ = 0.3). In addition, a single cylinder co-operative fuels research engine was used. This is a spark-ignition test engine which allows for compression ratio to be adjusted. Experiments were carried out at compression ratios from 14:1 to 16:1, at temperatures in excess of 500 K and at an equivalence ratio of 0.23. During the oxidation of the fuel CO production was analysed. It was found that n-butylcyclohexane was reactive under these conditions, while by comparison, methylcyclohexane did not exhibit any reactivity.

Natelson *et al.* [13] also carried out an investigation into the use of n-butylcyclohexane as a component in a possible surrogate for jet and diesel fuels. The surrogates chosen were a 2:1:1 and a 1:1:1 n-decane:n-butylcyclohexane:n-butylbenzene mixture. These surrogates and the real fuels were oxidised in a pressurised flow reactor at a pressure 0.8 MPa, at temperatures between 600 – 800 K at $\phi = 0.3$. The volumetric mixture of 1:1:1 n-decane:n-butylcyclohexane:n-butylbenzene was selected as a possible surrogate to match the properties and composition of diesel fuel, while the 2:1:1 n-decane:n-butylcyclohexane:n-butylbenzene mixture was chosen as a possible surrogate for jet fuel. While both surrogates matched the average composition and key properties of the respective fuels, the surrogates were of significantly greater reactivities. In order to develop better surrogates that mimic the real fuels in greater detail, Natelson *et al.* recommended the addition of iso-paraffins to reduce the low-temperature reactivity and to approximate the carbon number of real fuels.

Glaude *et al.* [46] have studied the oxidation of n-butylcyclohexane as a component of a surrogate for diesel fuel. One such surrogate used in their study was a mixture composed of n-butylcyclohexane (39%), n-decane (31%), n-butylbenzene (16%) and α-methylnaphthalene (14%). This work was performed to evaluate $NO_{\times}$ emissions from diesel and biodiesel fuels. It was concluded that the concentrations of $NO_{\times}$ emissions were influenced by both the operating conditions of the engine and the composition of the fuel. For example, when biodiesel was used in place of conventional diesel the concentration of $NO_{\times}$ increased slightly.

More recently Natelson *et al.* [16] carried out a study using a single-cylinder engine and a flow reactor. As in their previous study [45], JP-8 surrogates composed of 2:1:1 and 1:1:1 mixtures of n-decane:n-butylcyclohexane:n-butylbenzene. The pressurised flow reactor conditions were identical to those used in a previous study [45], namely at a pressure of 0.8 MPa, at temperatures in the range 600 – 800 K at an equivalence ratio of 0.3. Conditions for the single cylinder engine were as follows; compression ratios of 14:1, 15:1 and 16:1, inlet temperatures of 500 K, at atmospheric pressure, at an equivalence ratio of 0.23 and at an engine speed of 800 RPM. It was found that both surrogates were more reactive than the jet fuel, which had the longest autoignition times. They also found that the 2:1:1 surrogate was more reactive than the 1:1:1 surrogate.

More recently Ji *et al.* [14] have measured laminar flame speeds of cyclohexane and a number of mono-alkylated cyclohexanes. Cyclohexane, methylcyclohexane, ethylcyclohexane, *n*-propyl-cyclohexane and *n*-butylcyclohexane diluted in air were investigated at atmospheric pressure and at an unburned mixture temperature of 353 K. Experiments were simulated using JetSurF 1.1 [47]. Its was found that cyclohexane/air flames propagate faster than those of the alkylated cyclohexanes. It was also shown that the laminar flame speeds for the alkylated cyclohexanes (methylcyclohexane to *n*-butylcyclohexane) were quite similar. The model was in good agreement with the experimental results.

Natelson *et al.* [17] have also carried out an investigation into the low-temperature oxidation of *n*-butylcyclohexane in a pressurised flow reactor. Temperatures in the range 600 – 820 K were studied while other inlet conditions were kept constant at 0.8 MPa, at 0.120 s residence time and at an equivalence ratio of 0.38. The concentrations of CO, CO_2 and O_2 were measured as a function of temperature. Stable intermediates (formaldehyde, cyclohexanone, ethene, 1-butylcyclohexene and 4-butylcyclohexene) were measured at five temperatures. Samples were analysed using a GC/MS system. As part of this study methylcyclohexane and *n*-butylbenzene were also analysed under somewhat similar inlet conditions, at temperatures in the range 600 – 800 K, at a residence time of 0.120 s and at an equivalence ratio of 0.30. Under these conditions both fuels were found to be unreactive. This demonstrates the importance of the alkyl side chain in the low-temperature oxidation of alkylcyclohexanes. Natelson *et al.* [17] have developed a reaction set of 80 reactions and 42 species which was incorporated into JetSurF 1.1 to capture the low-temperature chemistry of the fuel. At these experimental conditions the combined model predicts the overall low-temperature reactivity of the fuel.

Hong *et al.* [15] have carried out a shock tube study of cyclohexane, methylcyclohexane and *n*-butylcyclohexane. Ignition delay times were measured behind reflected shock wave pressures of 1.5 and 3 atm at equivalence ratios of almost 0.5 and 1.0, in the temperature range 1280 – 1480 K. In addition to ignition delay times, H_2O and $\dot{O}H$ time histories were also recorded for cyclohexane, methylcyclohexane, *n*-butylcyclohexane, iso-octane and *n*-heptane under similar test conditions. It was found that *n*-butylcyclohexane is the most reactive of the three fuels studied. Model predictions were calculated using JetSurF 2.0 [30]. The simulations were found to be in good agreement with the experimental results.

Liu *et al.* [18] have measured ignition temperatures for cyclohexane and mono-alkylated cyclohexanes in non-premixed flames. Flames were measured in a counterflow configuration at atmospheric pressure, a free stream of fuel/N_2, a local strain rate of 120 s^{-1} and fuel mole fractions ranging from 1 – 10 %. From the experimental results obtained in this study it was found that cyclohexane flames exhibited the highest ignition propensity of the fuels studied. By comparing the data of the alkyl-cyclohexanes it was found that the length of the alkyl side chain had no measurable effect on ignition temperatures. The experimental data obtained was compared with simulation results from JetSurF 2.0 [30]. This model reproduced data for cyclohexane, methyl-, ethyl- and propyl-cyclohexane. However, it over-predicted the ignition temperature of butylcyclohexane by 20 K.

It can be concluded that the work that has been carried out to date on *n*-butylcyclohexane is mainly concerned with its use as a surrogate for aviation fuels. More recently flame speed, shock tube and flow reactor data has been reported. The aim of *this work* is to produce shock tube and rapid compression machine ignition delay times, at elevated pressures for *n*-butylcyclohexane and also use *n*-butylcyclohexane in mixtures with *n*-heptane as a surrogate for *n*-decylcyclohexane which then can be used for model validation.

1.7 *n*-Heptane

n-Heptane is a primary reference fuel for both the research octane number and motor octane number. On both scales *n*-heptane has a value of 0. *n*-Heptane has been extensively studied at a range of experimental conditions and hence its combustion characteristics are well known. For this reason the literature review given here is not comprehensive, it is a brief overview of the ignition delay time studies which have been carried out previously.

Ciezki and Adomeit [4] have studied *n*-heptane in a single-pulse high-pressure shock tube. Experiments were carried out at reflected shock pressures in the range 3.2 – 42 bar, reflected shock temperatures in the range 660 – 1350 K and equivalence ratios between 0.5 and 3.0. Pressure and $CH^{\star}$ (431.5 nm) emission time histories were recorded and used to measure ignition delay times. Under the conditions of the study NTC behaviour and two stage ignition was observed.

Minetti *et al.* [5] investigated the oxidation and autoignition of *n*-heptane in a rapid compression machine. The combustion products were identified using GC/MS analysis. Sampling was carried out between cool flame and normal flame activity and particular attention was paid to two stage ignition. It was concluded that no important chemical reactions occurred during the compression period nor during the induction period preceding the cool flame. A chemical model was produced to accurately simulate the experimental data.

Curran *et al.* [7] studied the oxidation of automotive primary reference fuels *n*-heptane and iso-octane. Experiments were carried out using a flow reactor at temperatures of 550 – 880 K at 12.5 atm. Shock tube experiments were carried out at reflected shock wave temperatures in the range of 690 – 1220 K and at a pressure of 40 atm. Both pure *n*-heptane and pure iso-octane were used as well as mixtures of the two fuels. Experiments were carried out under stoichiometric conditions. Experimental data was used in the validation of a chemical kinetic model predicting the oxidation of the primary reference fuels under engine-like conditions.

In addition Curran *et al.* [6] have developed a detailed chemical kinetic mechanism for a wide range of experimental data including flow reactor, shock tube and rapid compression machine. *n*-Heptane experiments were carried out in initial pressure ranges from 1 – 42 atm, temperature in the range 550 – 1700 K, with equivalence ratios from 0.3 to 1.5. Good agreement was achieved between computed and experimental data.

Herzler *et al.* [8] have carried out a study using lean, $\phi = 0.1 - 0.4$, *n*-heptane/air mixtures. This work was carried out in a shock tube at temperatures in the range 720 – 1100 K and high pressures, 50 atm. Under these conditions NTC behaviour and two stage ignition was observed.

Silke *et al.* [9] have studied the nine isomers of heptane including *n*-heptane in a rapid compression machine. This study was carried out to investigate the effect of fuel structure on ignition delay times. Experiments were carried out using stoichiometric fuel mixtures in air, at compressed pressures of 10, 15 and 20 atm for *n*-heptane and at 15 atm only for all other isomers, over a compressed temperature range of 640 – 960 K. For each of the fuels studied a characteristic NTC behaviour was observed. It was found that for the more branched isomers of heptane reduced reactivity was observed. This is in line with the research octane number of each of the fuels.

Davidson *et al.* [10] have studied *n*-heptane in a shock tube. In this study the concentration time histories were measured behind the reflected shock wave during *n*-heptane oxidation. Experiments were carried out at reflected shock wave temperatures in the range of 1300 – 1600 K and a pressure of 2 atm. Stoichiometric *n*-heptane mixtures diluted in argon were used. Concentrations of *n*-heptane, C_2H_4, $\dot{O}H$, CO_2 and H_2 were recorded using laser absorption.

Heufer *et al.* [84] have studied *n*-heptane as well as methane and ethanol in a shock tube. This investigation was carried out using a new high-pressure shock tube and results were compared to those available in the literature. Experiments were carried out using stoichiometric *n*-heptane mixtures in air at reflected shock pressures of 13.5 and 38 bar, at reflected shock temperatures in the range 690 – 1250 K. In this temperature range NTC behaviour was observed. The ignition delay times obtained for *n*-heptane were compared to those of Fieweger *et al.* and were found to be in good agreement.

In this thesis *n*-heptane has been blended with *n*-butylcyclohexane. This binary mixture is intended to act as a surrogate for *n*-decylcyclohexane. *n*-Decylcylohexane is a large cycloalkane fuel component. It is currently impossible to carry out gas phase experiments using this fuel because of its low vapour pressure. In the literature there are numerous examples of *n*-heptane being used in a blend with other fuel components. Recent examples of such studies include the work of Sante [48] and Zhang *et al.* [49].

Sante [48] studied *n*-heptane/toluene mixtures in a rapid compression machine. Experiments were carried out with pure *n*-heptane and mixtures with increasing toluene concentrations from 25% to 100%. Experiments were carried out at compressed temperatures in the range 710 – 814 K and at compressed pressures in the range 7.96 – 10.38 bar.

Zhang *et al.* [49] carried out a shock tube study of *n*-heptane/*n*-butanol mixtures. In this work the ignition delay times *n*-heptane, *n*-butanol and three mixtures of the two fuels were investigated. Experiments were carried out in the temperature range 1200 – 1500 K, at pressures of 2 and 10 atm and at equivalence ratios of 0.5 and 1.0.

This aim of *this thesis* is provide shock tube and rapid compression machine ignition delay times for *n*-butylcyclohexane and an *n*-decylcyclohexane surrogate over a range of pressures, temperatures and equivalence ratios which can be used for model validaition.

Chapter 2

Shock Tube

Shock tubes are used to generate shock waves which are in turn used to compress almost instantly a test gas mixture to a higher pressure and temperature. This action mimics a single stroke of a piston within an engine while providing a more controlled environment in which measurements can be taken; for example shock wave velocity, light emission and ignition delay time. Where the correct facilities exist, shock tubes can allow for experimental data to be obtained in the temperature range 500 – 5000 K, in the pressure range from 1 – 1000 atm and ignition delay times of the order of tens of microseconds to a number of milliseconds.

2.1 A Brief History

Shock tubes can be used to investigate a number of phenomena. Such topics include detonation characteristics, chemical kinetics and fluid properties. Shock tubes have been in use for over 100 years with the first known investigations having been carried out in 1899 [50]. The shock tube has stood the test of time due to its simplicity and its reliability. This simple piece of apparatus in conjunction with various detection methods can be used for a range of applications.

One of the first known studies carried out using a shock tube was that by the French engineer Vieille. This work consisted of a series of experiments where spherical glass bulbs, which had been placed at the end of a 6 m long cylindrical tube, were burst under pressure. Later Vieille divided this tube into two sections separated by a thin diaphragm. An investigation was also carried out into the use of various diaphragm materials such as metal foil, glass, paper and collodion [50].

Dixon [51] investigated the movement of flames in a horizontal tube in 1902. In this investigation the photographic analysis of detonation waves and the reflections of these waves was carried out.

Paymen and coworkers [52–57] carried out a number of investigations concerning detonation processes in a tube associated with the problem of explosion danger in UK mines. Their work led to the design of the shock tube as we know it today, where a shock wave is created by the bursting of a diaphragm separating areas of high and low-pressure. In a six part publication series a number of topics were investigated. In the first publication a new photographic method was discussed and this method was used to capture the disturbance produced as the result of a bullet in flight [52]. In the second publication the shock waves and products produced by blasting detonators were discussed [53]. In a further publication combustible mixtures of ethylene and oxygen as well as carbon monoxide and oxygen were investigated [54]. Mixtures were ignited using a spark ignition source. A similar publication looked at the detonation of mixtures of methane and air [55]. In this case ignition was achieved using a detonator. Paymen and Shepherd also investigated the disturbance produced when diaphragms are burst using compressed air [56]. Copper diaphragms were used to carry out this investigation. The movement of the disturbance produced by the rupturing of the diaphragm was captured by Schlieren photography. This technique photographs the flows of fluids of varying density. In the final installment of this series the detonation velocities of cylinders of TNT (trinitrotoluene) was investigated [57]. Purity, crystal size, diameter and the degree of confinement were all varied to study the effect on the detonation velocity.

During, and immediately after, World War II, shock tubes were rapidly developed as a tool for aeronautical research and by the 1950's shock tubes had been installed in many universities and government laboratories. Studies were being carried out to investigate supersonic flows over a body [58, 59]. From the mid 1950's onwards there had been a rapid increase in the number of institutions using shock tubes. This simple piece of laboratory equipment used in conjunction with various detection methods can be used for a number of applications including those relating to aeronautics, chemistry and physics.

2.2 Shock Tube Design

All shock tubes consist of the same simple design, composed of two sections, the driver or high-pressure section and the driven or test section, Fig. 2.1. In most shock tubes these two sections are separated by a diaphragm composed of metal or plastic. To carry out an experiment a gaseous test mixture (fuel/oxygen/inert gas) is allowed to flow into the evacuated test section. An inert driver gas is allowed to flow into the driver section. The diaphragm ruptures due to the increase in pressure or due to a cutting mechanism placed inside the shock tube. The sudden release of pressure creates a shock wave that travels the length of the tube.

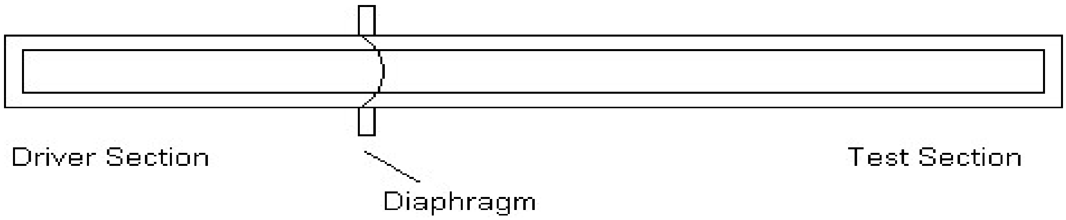

Figure 2.1: Schematic of a basic shock tube consisting of a driver and test section separated by a diaphragm.

2.3 Shock Waves and Shock Wave Phenomena

A shock wave is a propagating disturbance created as a result of a sudden release of energy. This energy can be electrical, mechanical or nuclear, released in a confined space. These are very narrow regions, which are generally considered to be infinitely thin, across which pressure, temperature and fluid density can change. With the correct engineering shock waves can be easily generated and their properties controlled.

The most important event for the formation of the shock wave is the rupturing of the diaphragm, which leads to the formation of the incident and reflected shock wave, contact surface and the rarefaction fan, Fig. 2.2.

- Incident and Reflected Shock Wave

  When the diaphragm ruptures the incident shock wave moves into the test section continuing until it reaches the endwall. The incident wave heats and compresses the test gas. Upon reaching the endwall the wave is reflected and becomes the reflected shock wave.

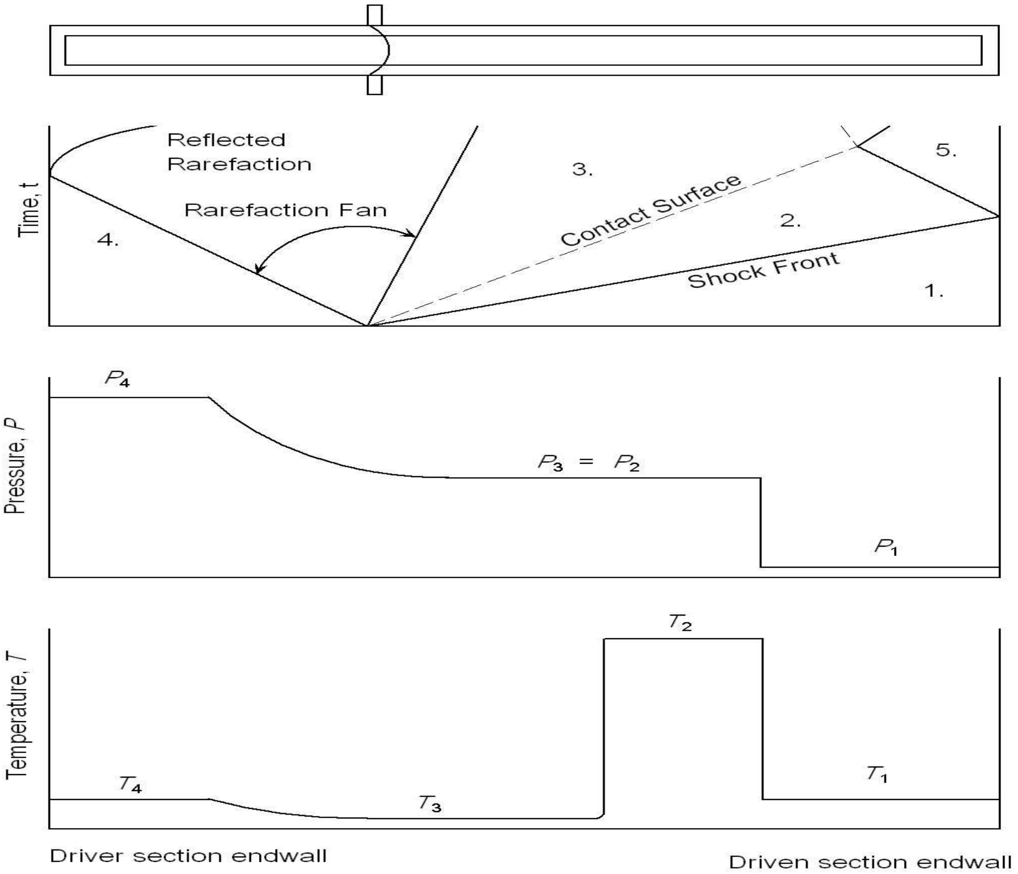

Figure 2.2: Shock wave phenomena, temperature and pressure changes due to shock wave phenomena [50].

This wave travels in the opposite direction to the incident shock and heats and compresses the gas for a second time, further increasing the temperature, pressure and density of the gas. The reflected shock wave allows for the realisation of temperatures and pressures that would only be achievable with incident shock waves using extremely high pressures of driver gas.

- Contact Surface

  The contact surface is the boundary between the driver gas and test gas. In reality this boundary is not well defined as there is some mixing and inter-diffusion of the gases.

- Rarefaction Fan

  When the diaphragm ruptures a group of waves making up the rarefaction fan move into the driver section. This set of waves spread out and cause a decrease in the density, temperature and pressure of the gas below the initial conditions. The rarefaction head moves into the driver section where it is reflected off the driver section endwall into the driven section of the tube. The gas is still moving but accelerates as it travels through the gas that is already moving down the length of the shock tube. The speed of the rarefaction wave will be greater than that of the incident wave for this reason. The interaction of the rarefaction fan with the test gas will result in quenching of all chemical reactions.

Figure 2.2 also illustrates the change in temperature and pressure due to the various wave phenomena where the area denoted 1.) is the undisturbed test gas, 2.) is the region between the contact surface and the shock front, 3.) is the region between the contact surface and the rarefaction fan, 4.) is the driver gas at its initial conditions; and finally 5.) denotes the reflection of the shock wave off the endwall. The corresponding temperatures and pressures for these regions are denoted by a subscript of the individual numbers, for example the corresponding temperature and pressure for the undisturbed test gas are T_1 and p_1. Similar notation may be applied to Fig. 2.3 and Fig. 2.4. It can be seen that as the shock front moves into the low-pressure or test section of the shock tube both pressure (p_2) and temperature (T_2) rise dramatically.

2.4 Shock Tube Test Time

In a shock tube the maximum time available for measurements in uniform conditions behind the reflected shock wave is defined as the time between the arrival of the shock wave at the endwall and the arrival of the first disturbance from the contact surface which reaches the endwall.

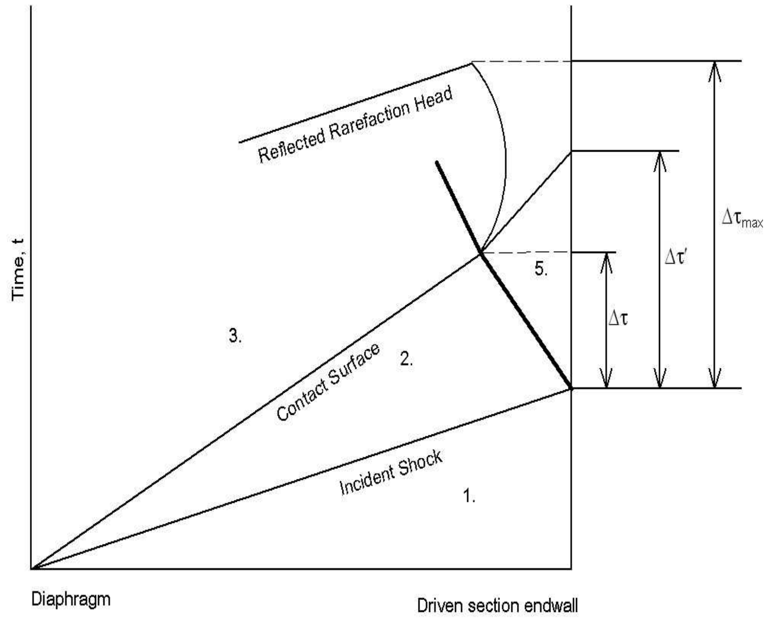

Figure 2.3: Schematic of the available test time in a shock tube [50].

Figure 2.3 is a schematic representation of the available test time in a given shock tube experiment. These wave phenomena are critical in the understanding of the available test time in such a system.

In Fig. 2.3 $\Delta\tau$ is defined as the time between the arrival of the incident shock wave at the endwall, its reflection and its collision with the contact surface.

$\Delta\tau'$ is defined as the time between the reflection of the incident shock wave at the endwall, its collision with the contact surface and its arrival back at the endwall.

$\Delta\tau_{max}$ is defined as the time between the arrival of the incident shock wave at the endwall and the arrival of the reflection rarefaction head.

For data acquisition system close to the endwall of the shock tube, where the observation time is greatest,$\Delta\tau'$ is the longest possible time where uniform conditions persist and measurements can be taken.

In carefully engineered conditions the incident shock wave is not reflected back to the endwall from the contact surface, which now remains stationary in the shock tube. Under such conditions the observation time can then be increased to $\Delta\tau_{max}$, Fig. 2.4(c). $\Delta\tau_{max}$ is now theoretically the longest time where uniform conditions exist. This is defined as the time between the arrival of the incident shock wave at the endwall and the arrival of the rarefaction head in the test section.

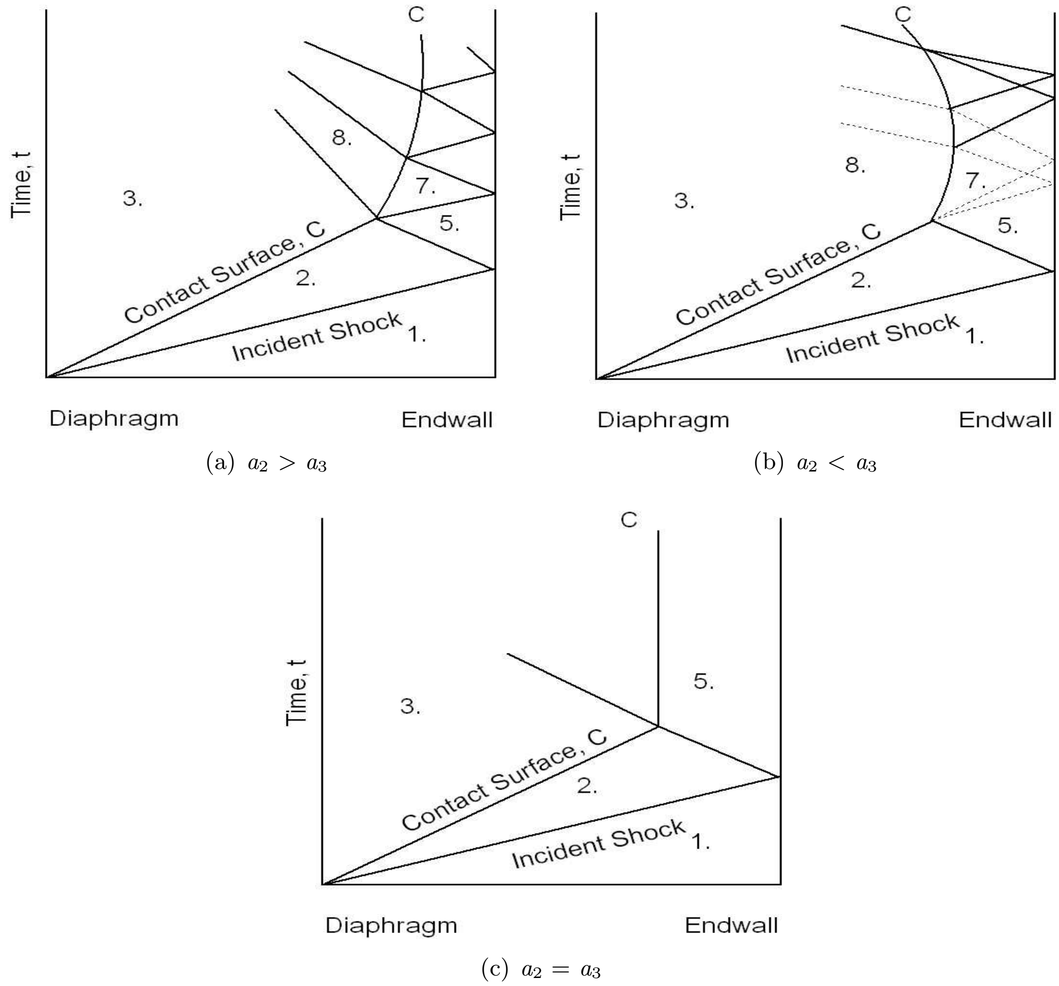

Figure 2.4: Three possible interactions of the contact surface with the reflected shock wave [50].

Figure 2.4 illustrates the three possible conditions produced as a result of the interactions of the contact surface with the reflected shock wave, where a is the local speed of sound.

In Figure 2.4(a) where $a_2 > a_3$, the shock wave is reflected off the endwall and gives rise to multiple, progressively weakening shock reflections between the endwall and the contact surface.

In Figure 2.4(b) where $a_2 < a_3$, the reflection from the contact surface is in the form of a rarefaction wave. The disturbances between the endwall and the contact surface alternate between a rarefaction wave and a shock wave.

Figure 2.4(c) illustrates a special case where $a_2 = a_3$. In this case the reflected shock wave passes thought the contact surface without a change in speed. The contact surface is brought abruptly to a halt in this interaction. In this case uniform conditions persist for longer than those observed in Fig. 2.4(a) and 2.4(b). This interface is said to be tailored, this allows for longer test times. A tailored interface can be achieved with careful consideration for the temperature and composition of the driver gas used in an experiment.

In the shock tube facility at NUI Galway a precise quantity of nitrogen gas is added to the helium driver gas in order to attain a tailored interface. In the literature there are a number of reported ways of obtaining a tailored interface [60–62]. These include the use of helium/air, helium/carbon dioxide, helium/propane and helium/argon driver gases.

The driver gas composition for a tailored interface can be found using using the following method.

A driver gas composition curve is firstly plotted. The molecular weight and specific heat ratio of an ideal gas mixture can be determined using species mole fractions, x_i

$$MW_n = \sum x_i MW_i \tag{2.1}$$

$$\gamma_n = \frac{\sum \frac{x_i \gamma_1}{\gamma_1 - 1}}{\sum \frac{x_i \gamma_1}{\gamma_1 - 1} - 1} \tag{2.2}$$

Using the above equations gas mixture curves for various combinations of driver gases can be plotted, Fig 2.5.

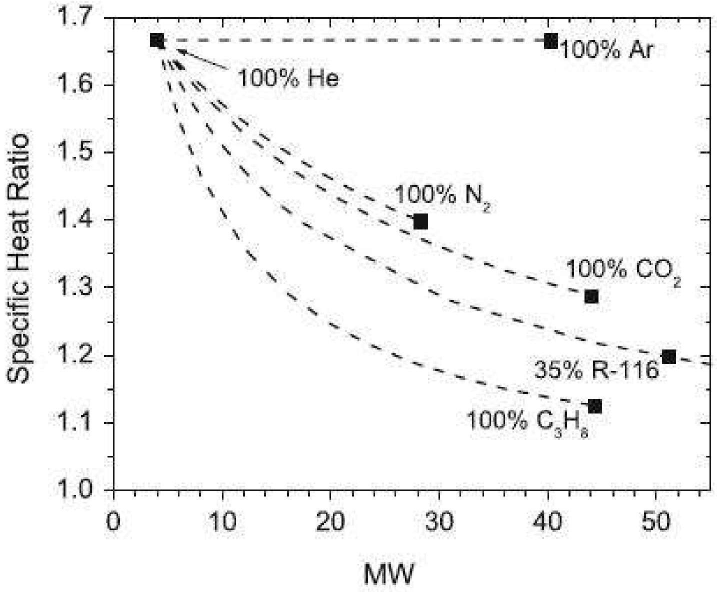

Figure 2.5: Driver gas composition curves for a number of gas mixtures [61].

For a bath gas (MW_1, γ_1) initial shock tube temperature, T_4 and T_1, and a test temperature, T_5, solving for the equation below a tailoring curve can be obtained.

$$\frac{\gamma_4 MW_1 T_3}{\gamma_1 MW_4 T_2} = \frac{\left(1 + \frac{\gamma_4+1}{\gamma_4-1}\frac{p_5}{p_2}\right)\left(\frac{2\gamma_4}{\gamma_4-1}\right)}{\left(1 + \frac{\gamma_1+1}{\gamma_1-1}\frac{p_5}{p_2}\right)\left(\frac{2\gamma_1}{\gamma_1-1}\right)}\left[\frac{\frac{2}{\gamma_1-1}}{\frac{2}{\gamma_4-1}}\right]^2 \tag{2.3}$$

The point of intersection of the of the tailoring curve and the composition curve is the driver gas composition that provides a tailored interface for the corresponding test temperature.

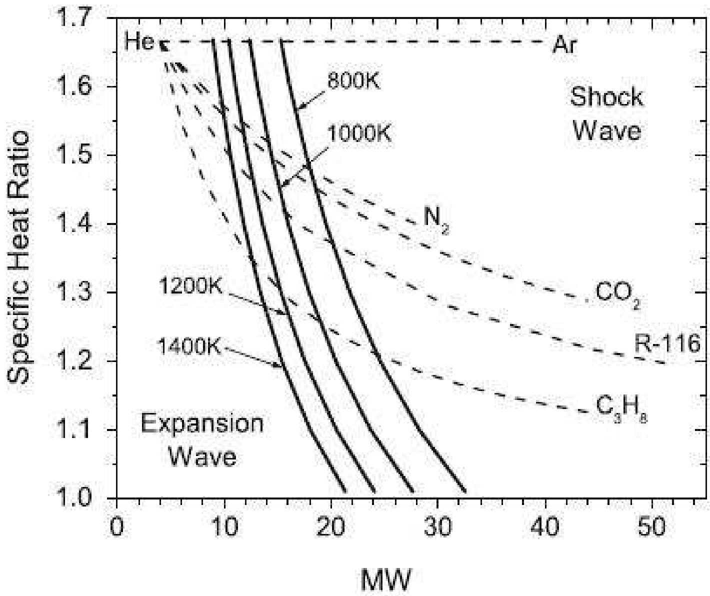

Figure 2.6: Gas composition curves (dashed lines) and tailoring curves (solid lines) for test temperatures (T_5) of 1,400, 1,200, 1,000, and 800 in argon bath gas (T_1 = T_4 = 298 K) [61].

Chapter 3

Rapid Compression Machine

Rapid compression machines are typically used to simulate a single cycle of an internal combustion engine allowing the study of phenomena such as spontaneous ignition under more favourable conditions than those found in engines without the risk of contamination due to oil mist or metal particles. This is achieved by rapidly compressing a fuel/oxygen/diluent mixture using one or two pistons driven by compressed air. Unlike a shock tube, where its basic design can be said to be characteristic of all shock tubes, the same cannot be said for rapid compression machines. Modern rapid compression machines have the common feature that they have pistons driven by compressed gas. The development of such machines evolved over time. An overview of these machine designs that led to the development of the modern rapid compression machine will be outlined briefly.

3.1 A Brief History

Rapid compression machine designs can be categorised as first, second and third generation.

The first rapid compression machines consisted of a free falling weight system, where an impact set a piston in motion until the opposing pressure caused by either increasing pressure in the chamber in non-reactive gases, or the increasing pressure due to ignition in reactive mixtures, stopped and returned the piston to its original position. These are referred to as first generation machines. In these machines a delay was observed between the compression of the test gas and its ignition. It was referred to as the pre-flame period. However, due to the nature of the experimental setup with was not possible to make mesurments of this time as detection methods were not included.

Second generation machines were built with a more heightened importance of ignition delay time. These machines were designed to allow for the piston to be stopped and held in position. Such machines were limited by their compression ratios and the speed of their operation.

Third generation machines are designed to overcome the problems associated with second generation machines. They are characterised by having pistons driven by compressed gas and achieving compression times of under 20 ms. Due to the high driving pressure used in these machines a major emphasis has been placed on mechanisms to stop the movement of the piston so that there is no rebound. There are a number of ways in which this is achieved and these will be discussed briefly.

3.1.1 First generation

First generation rapid compression machines include those built by Falk [63], Dixon *et al.* [64] and Dixon and Crofts [65].

Falk (1906)

The machine built by Falk is among one of the first reported [63]. This machine consisted of a steel cylinder which screwed into a wrought iron plate. Into this cylinder the piston and piston rod topped with an iron plate was inserted. To ensure no loss of gas during compression, three grooves in the side of the piston were wound with hemp and lubricated with lanolin. A brass ring fitted to the piston rod, which could only be moved with considerable force, indicated the smallest volume of gas in the cylinder during a compression. In order to bring about compression for the gas in the cylinder a free falling weight was allowed to fall onto the iron plate. Falk used this apparatus to measure the ignition temperature of gas mixtures.

Dixon (1914)

Dixon *et al.* [64] built a machine that consisted of a glass tube held in an horizontal position by using wooden clamps with its closed end against a wooden support. A free falling pendulum suspended from the ceiling by three meters of trellis work was then used to rapidly force the steel piston into the tube. The design of this machine allowed for the easy variation of compression ratio as wooden blocks and steel plates could be used to bring the pendulum to a stop. The image of the flame was focused onto a photographic film which could be revolved a known number of revolutions per second. This apparatus had the advantage of allowing for the control of the final volume and photographic records of ignition. Dixon and co-workers noted that some time had elapsed between the motion of the piston and the moment when the flame started. They referred to this as the pre-flame period, more commonly known today as ignition delay time. For the set of experiments performed the pre-flame period was reported to be of the order of 10 milliseconds.

Dixon and Crofts (1914)

Dixon and Crofts [65] built a modified version of the machine first built by Falk. Modifications were made so that the cylinder was sufficiently wide to prevent appreciable cooling from the walls, the apparatus had to be sufficiently long to give a final volume that could be measured accurately, the piston had to be driven rapidly, had to be gas tight without lubricant coming into contact with the gas mixture and had to be stopped the moment it had compressed the gas to ignition. Despite these modifications two serious problems remained; firstly, there was no mechanism installed to stop the piston at the end of the stroke and, secondly, there was no way to measure the pressure in the cylinder.

3.1.2 Second generation

Second generation rapid compression machines were designed, building on the knowledge and experience obtained from the work of Falk and Dixon *et al.* and also with a greater desire to investigate ignition delay times.

Second generation machines include those built by Cassel [66], Ricardo [67–69], Pignot [70] and Fenning [71].

Cassel (1917)

The rapid compression machine developed by Cassel was designed to compress gas mixtures without rebound of the piston [66]. Cassel noted that rebound of the piston at the end of compression would result in cooling of the gas and would hence quench ignition. The machine which was developed consisted of a heavy steel cylinder with a threaded opening near the bottom to allow for addition of the test gas. The piston was housed within this cylinder. The piston was set in motion on impact with a falling weight. This motion was guided by a set of steel rods which were screwed into the base of the machine. Attached to the head of the piston was a rod with a stylus. This stylus pressed against a drum which was rotated with a known constant speed around the combustion chamber. The stylus was used to scratch a record of the motion of the piston onto the rotating drum. To prevent rebound of the piston at the end of compression a set of break shoes were installed to hold the weight which was falling onto the piston, also a set of lead washers were used to dissipate the energy.

Ricardo (1920 – 22)

The machine developed by Ricardo was used by Tizard and Pye for an investigation carried out on engine detonations [67,68]. This machine consisted of a flywheel which rotated on a central shaft, kept at 360 RPM, a crank, an internally expanding clutch, piston and combustion cylinder. The combustion cylinder on this machine could be raised or lowered to alter the compression ratio. An optical pressure indicator, Hopkinson type, measure it possible to measure the variation in pressure before and after compression. Later modifications were made to this machine by Tizard and Pye. These modifications included the use of two cylinders in tandem, an upper cylinder which included an oil bath that could be heated to 150 – 180°C, and another lower cylinder which was maintained at room temperature [69]. This meant that the initial temperature of the gas could be raised without exposing the leather seals to high-temperature which would cause them to degrade.

Pignot (1929)

The machine built by Pignot [70] was based on the design of Dixon. This machine had a method of adjusting the length of the stroke by moving a plug up or down the threaded piston rod. It had a heating coil surrounding the combustion cylinder to regulate the initial temperature of the gas mixture. A thermocouple was inserted directly into the cylinder to monitor the initial temperature. In order to hold the piston in place a number of spring-loaded clamps snapped into a groove on the piston rod upon compression. This was found to be insufficient to stop the piston from rebounding after compression of the gas mixture.

Fenning and Cotton (1930)

Fenning and Cotton carried out a number of experiments to determine ignition temperatures using Tizard and Pye's machine [71]. They found that the results which they obtained were not reproducible due to the behaviour of the machine, which was found to be due to surface effects, fine particles suspended in the combustion cylinder and friction in the moving parts of the machine. To overcome these problems the machine was modified by replacing the upper cylinder with a mild steel plate to which a rubber bulb was clamped. This rubber bulb was used to hold the test mixture while the remainder of the cylinder, which now could be lubricated, was filled with air. It transpired that this method also led to non-reproducible results. It was found that this was due to adsorption of the test gas by the rubber bulb.

3.1.3 Third generation

With the development of third generation rapid compression machines higher compression ratios and shorter compression times could be achieved. These machines are characterised by compressed gas driven piston assemblies. There are a number of such machines are in operation in various research groups worldwide, a number of which are described briefly here.

Affleck and Thomas (1968 – 69)

Currently there are two twin opposed piston rapid compression machines in operation at NUI Galway. The first was originally built by Shell engineers in the 1960's [72] and was brought to NUI Galway in the 1990's where various modifications were carried out. The second is an automated replica/clone of the original machine, installed in 2010. The two units comprise of a piston sleeve and piston, hydraulic control section and driving section with a central combustion chamber fitted with a pressure transducer.

University of Science and Technology, Lille (1991)

The rapid compression machine in use at the University of Science and Technology, Lille [73] is a right-angle machine with two pistons connected to each other by a cam in order to compress a test mixture in a short time in the reaction chamber. By separating the driving and the compression pistons, the driving piston can be stopped at the end of the stroke by using a shock absorber. The system is set in motion by building the gas pressure in the driving gas receiver and by releasing the hydraulic lock. The reaction chamber is equipped with an inlet / exhaust valve, pressure transducer and optical windows.

Leeds University (1990)

The rapid compression machine at Leeds University [74] is based on the design of Affleck and Thomas. This rapid compression machine differs in so far as is it incorporates only one piston.

Massachusetts Institute of Technology (1990)

The rapid compression machine at the Massachusetts Institute of Technology [75] is the first known to incorporate a creviced piston design in an effort to curtail the formation of corner vortices. This is an air driver and oil dampened single piston machine.

University of Michigan (2004)

The rapid compression machine at the University of Michigan is a free-piston facility [76]. This consists of a driver section 5.54 m in length. This section is separated from the driven section via a globe valve. The driver section, 2.74 m in length, is connected to the test manifold. This test manifold consists of four components, the convergent section, extension section, thermocouple manifold and instrumented section. The extension section provides the contact surface used to halt the motion of the sabot. The sabot is constructed in two parts, an acetal resin body and an ultra-high molecular weight polyethylene replaceable nose cone. Spring loaded U-rings seal the sabot to the test section. In order to compress test gas mixtures the driver section is filled to a high-pressure with a driver gas. The glove valve to the driver section, which is filled with a test gas mixture, is then opened. This release of high-pressure gas pushes the sabot forward down the driven section, compressing the test gas ahead of it.

Several other rapid compression machine facilities exist such as those found at Argonne National Laboratory, University of Stuttgart, Technical University Munich, RWTH Aachen University, Gifu University, Hosei University, Nagoya Institute of Technology and Tokyo University.

3.2 Achieving Desired Compressed Temperature in a Rapid Compression Machine

The compressed temperature, T_c, is the temperature reached as a result of compression of the test gas from low-pressure to high-pressure. In doing this the initial temperature of the gas is raised considerably. A desired compressed temperature can be reached in three ways; firstly by carefully selecting the diluent gas or mixture of gases, secondly by varying the compression ratio of the machine and thirdly by varying the initial temperature of the gas charge. All three methods are currently being employed in the rapid compression machine facilities at NUI Galway.

A number of diluent gases were used including argon, nitrogen and carbon dioxide. By using the various gases or mixtures of gases desired compressed temperatures can be achieved using the same initial temperature and pressure of fuel/diluent charge. For example if argon is used as a diluent gas a higher compressed temperature will be achieved compared to nitrogen under the same conditions, due to the heat capacity of the gases, which is the amount of energy required to increase one mole of a substance temperature by 1 K. The heat capacity of argon is 20.786 J K^{-1} mol^{-1}, that of nitrogen is 29.124 J K^{-1} mol^{-1} and that of carbon dioxide is 37 J K^{-1} mol^{-1} [22]. Hence on compression, higher temperatures are reached with argon than with nitrogen or carbon dioxide. However, the use of high concentrations of argon is undesirable due to its high thermal diffusivity (α) resulting in significant heat losses which lowers the core temperature resulting in longer observed ignition delay times. Thermal diffusivity is the ratio of a substance thermal conductivity (κ), its ability to conduct heat, to its density (ρ) and heat capacity (C_p).

The compression ratio is defined as the ratio of the initial volume to the final volume. Variation of the compression ratio can be easily achieved in a rapid compression machine by using various interchangeable piston heads. A number of piston heads are available, each with a different cylindrical height which reaches differing lengths into the reaction chamber resulting in a change of the compressed volume. At higher compression ratios higher compressed temperatures are reached. This also precludes the need to use argon as a diluent.

To vary the initial temperature of the test gas charge a heating system was installed on the chamber and sleeves of the RCM. This heating system, which is described in Section 4.4, allows for homogeneous heating of the RCM up to a temperature of 130°C.

3.3 Temperature Inhomogeneity and Roll-Up Vortices

Temperature inhomogeneities occur in the reaction chamber during an experiment due to the formation of roll-up vortices. These vortices are formed as a result of the motion of the pistons. As the pistons are set in motion they compress the test gas in the reaction chamber. During this motion the flat head of the pistons scrape the colder boundary layer off the reaction chamber wall. This colder boundary layer gas is then mixed with the hot, adiabatic reacting core gas resulting in a temperature inhomogeneity in the chamber. The formation of this roll-up vortex can be dampened, if not eliminated, by the use of carefully engineered crevices incorporated into the cylindrical face of the pistons. Such pistons are designed to incorporate a crevice of specific dimensions and a clearance channel such that the boundary layer gas is consumed by the crevice. Such work has previously been carried out by Würmel [77] where computational fluid dynamic simulations were used to predict the movement of the gases during an experiment and a number of designs for creviced pistons were proposed. Figure 3.1 illustrates the effect of the design of creviced pistons on temperature inhomogeneity during an experiment. It can be seen that, for non-creviced pistons, a vortex is formed leading to an inhomogeneous temperature distribution in the reaction chamber. Figure 3.1 also emphasises the importance of the crevice design. The crevice must be sufficient size so that it can consume the boundary gas. With careful engineering of the crevice a homogeneous temperature field can be attained in the chamber.

Brett *et al.* [78] studied the autoignition of hydrogen and methane in the RCM at NUI Galway. In this work experimental data using both creviced and non-creviced pistons were compared. Better agreement was observed between experimental and simulated pressure histories when creviced piston heads were used. When flat piston heads were used the simulation significantly over-predicted the compressed pressure for hydrogen experiments. Methane experiments carried out using creviced piston heads were more accurately predicted by the model. It was concluded that creviced piston heads allow for greater agreement between the simulation and experimentally obtained pressure histories. However, the model failed to predict the measured ignition delay times accurately.

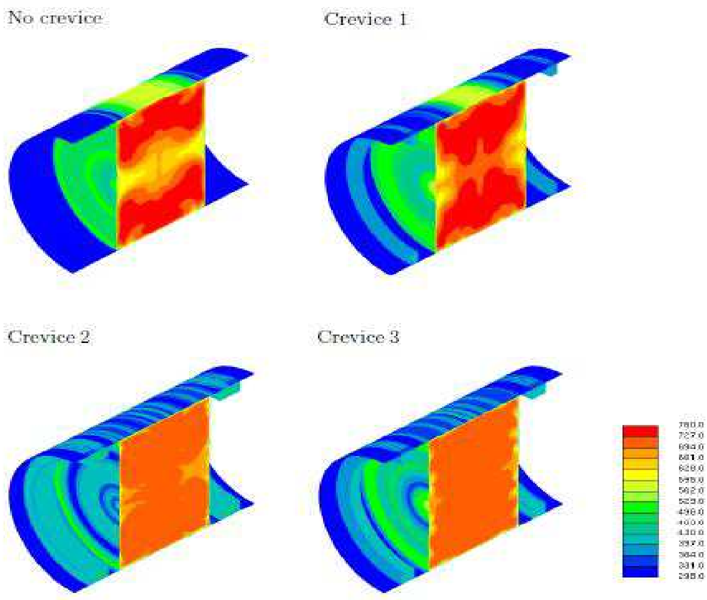

Figure 3.1: Temperature distribution during compression as seen with flat head pistons and three designs of creviced pistons [77].

Chapter 4

Experimental

4.1 Low-Pressure Shock Tube

The low-pressure shock tube at NUI Galway has been extensively characterised by Smith [79], who carried out the redesign and replacement of various elements of the shock tube as well as its characterisation.

Driver and Driven Sections

At its simplest a shock tube consists of a driver and driven section separated by a diaphragm. The details of the low-pressure shock tube are briefly described below:

Driver Section

- The driver section consists of a 63 cm long, 52 cm diameter barrel which is connected to a 10 cm long steel tube with an internal diameter of 10.24 cm. This steel tube is fitted with a flange with eight equispaced bolt holes, an identical flange on the driven section allows for the conjunction of the two sections. A diaphragm is held between the two sections and viton o-rings mounted in both flanges ensure that a seal is created.
- Attached to the driver section is a pressure gauge (Swagelok). This allows for the monitoring of the diaphragm burst pressure and ensures that a sufficient vacuum is achieved in this section prior to experiments.
- On the underside of the driver section is a flange port connected to a flexible stainless steel braided hose which in turn is connected to a rotary pump (Edwards E2M5). This is used to evacuate the driver section prior to experiments.
- At the top of the driver section is an inlet which allows for the high-pressure driver gas (helium) to enter this section. Depending on the reflected shock wave pressure required, the pressure of the driver gas varies. For example using 125 μm diaphragm to create a 1 atm shock, approximately 800 mbar of driver gas is required. This inlet can also be used to add nitrogen to the system in order to bring it to a greater than atmospheric post-shock pressure.
- Located at the top of the driver section is a tap that allows for the shock tube to be vented. This is used to bring the tube to atmospheric pressure before opening the flanges to remove the ruptured diaphragm.

Driven Section

- The driven section consists of a 622 cm long steel tube with an internal diameter of 10.24 cm.

- Housed in the driver section in close proximity to the diaphragm is a cross shaped cutter. The purpose of this cutter is to cause the diaphragm to petal under pressure. Petaling the diaphragm reduces the likelihood of diaphragm pieces breaking off and being carried down the tube. This cutter is on a threaded housing unit. It is capable of being moved forward for weaker shock waves or back for stronger shock waves in which a lesser and greater pressure of driver gas is used respectively.

- Attached to the driven section is a manifold. This manifold allows for the addition of the test gas mixture into the shock tube, the evacuation of the shock tube and the preparation of test gas mixtures. Attached to the manifold are two pressure gauges (MKS Baratron 390HA, Chell) and vacuum pumps (Edwards E2M5, Speedivac E02). A glass manifold allows for cold fingers containing high vapour liquid fuels to be attached.

- Close to the endwall are four pressure transducers (PCB 113A21). These are mounted flush to the interior wall of the tube at 494.9, 365.9, 236.9 and 29.9 mm from the endwall. The signals produced by the pressure transducers are amplified (PCB 483A02) and sent to three counters (Philips/Fluke PM6666) which captures the time taken for the shock wave to pass each transducer. These times can be used to calculate the shock velocity.

- At the end of the shock tube is a capping plate, i.e. the endwall. The endwall is fitted with a pressure transducer (Kistler 601B). The pressure transducer produces a signal which is then amplified (Kistler 5001) and sent to an oscilloscope (Tektronix TSD 2024). This signal indicates the arrival of the shock wave at the endwall.

- At the endwall a quartz window allows for optical access. A photodetector (PDA55) with a $CH^{\star}$ filter, centred at 426.8 nm, captures the emission of light and sends a signal to an oscilloscope (Tektronix TSD 2024).

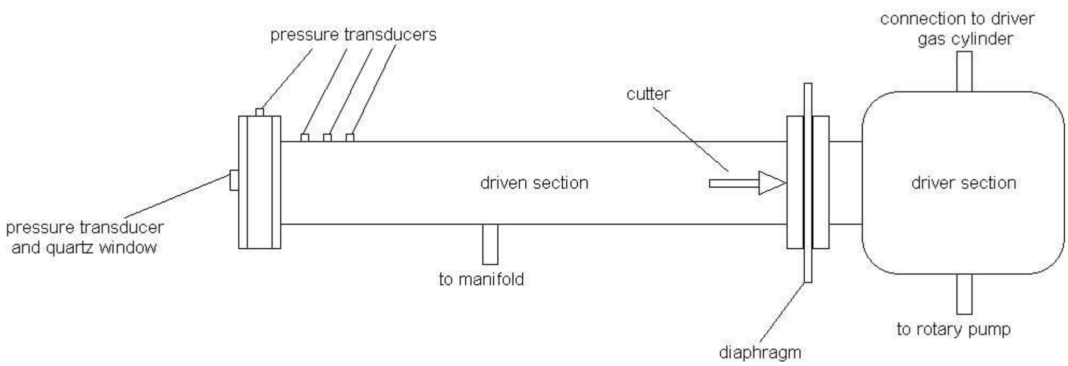

Figure 4.1: Schematic of the low-pressure shock tube.

Diaphragms and Diaphragm Rupturing Mechanism

Prior to performing an experiment in the low-pressure shock tube a polycarbonate diaphragm is placed between the flanges and viton o-rings of the driven and driver sections. These flanges are then bolted together with 4 × 8 mm nuts and bolts. During an experiment the diaphragm is allowed to rupture under pressure with assistance from a cross shaped cutter housed inside the tube. The increase in driver gas pressure in the driver section causes the diaphragm to bulge. The cutter causes the diaphragm to petal and with this there is a sudden release of the driver gas into the driven section.

It is often necessary to test if the combination of the cutter position and the diaphragm thickness is sufficient to achieve a desired reflected shock wave pressure. Such tests may be carried out using an un-reactive initial charge of argon in the driven section of the shock tube. Knowing the initial conditions of temperature, pressure, test charge composition and shock velocity the reflected shock wave pressure may be calculated. Slight adjustment of the cutter is often needed and this process is repeated until such time as the desired reflected shock pressure is achieved.

Gas Mixture Preparation

Prior to the preparation of a mixture the stainless steel mixing tank is firstly isolated from the shock tube, tap 1, Fig. 4.2, and evacuated roughly to 10^{-2} Torr (Edwards E2M5) and then evacuated to a low-pressure, 10^{-4} Torr, using a water cooled oil diffusion pump (Speedivac E02) backed by a two-stage rotary oil pump (Edwards E2M5).

The liquid fuel is placed in a glass finger with a small quantity of molecular sieve, here the molecular sieve is used a desiccant. The glass finger is then attached to a glass manifold. This liquid fuel was subjected to repeated freeze-pump-thaw de-gassing stages. This is carried out by freezing the fuel, removing the evolved gas, allowing the fuel to thaw and repeating a number of times. The aim of this procedure is to eliminate the presence of dissolved gases in the fuel.

All gas mixtures were prepared manometrically. Firstly the mixing tank was isolated from the vacuum pump, tap 3, Fig. 4.2. The desired quantity of fuel vapour was then allowed to flow from the glass finger to the evacuated mixing tank, tap 4, Fig. 4.2. The pressure of fuel was read to a high degree of accuracy using an MKS Baratron (390HA), which is capable of measuring up to 100 Torr with an accuracy of 0.01 Torr. When the desired quantity of fuel vapour had been added, the tap to the tank, tap 5, Fig. 4.2, and the isolation tap to the glass portion of the manifold, tap 4, Fig. 4.2 were closed. The manifold was then evacuated, tap 3, Fig. 4.2. Next the required amount of oxygen was added, tap 2, Fig. 4.2, and the manifold was pressurised with oxygen to a greater pressure than that of the fuel in the tank. This was carried out in order to prevent fuel from escaping from the tank. The tap to the mixing tank was then opened and the oxygen gas was added. The pressure of the gas was monitored by a pressure gauge (Chell), capable of measuring up to 800 Torr. When the desired quantity of oxygen was added the tap to the tank was closed and again the line was evacuated. The diluent gas, usually Ar, was added following the same procedure as for oxygen.

Mixtures were allowed to equilibrate, preferably overnight. When this was not possible a minimum of 4 hours standing time was observed.

Pre-Experimental Procedure

Prior to carrying out experiments the following should be performed:

- Check that the extraction fan is running.

- Ensure that a new diaphragm is placed between the flanges of the driver and driven section, also ensure that the flanges are bolted together.

- Check that the flow of water to the oil diffusion pump is on and sufficient.

Figure 4.2: Low-pressure shock tube driven section manifold.

Experimental Procedure

When carrying out experiments using the low-pressure shock tube the following procedure should be followed.

Pre-shock:

- Prior to turning on the driver and driven section rotary pumps close the air admittance valves. The rotary pumps can be now turned on.
- At the driven section open the manifold and shock tube to the rotary pump. Also open the driver section to the rotary pump.
- Fill the liquid nitrogen trap of the diffusion pump. Allow the diffusion pump to heat for 30 minutes prior to use.
- When the diffusion pump has been heating for the required period of time the shock tube can be now evacuated using this pump provided the vacuum produced by the rotary pump is sufficient.
- Turn on and ready all electronics, this includes gauge read outs, computers, times, oscilloscope, amplifiers, light detector etc.

Filling the shock tube:

- The shock tube and manifold are firstly isolated from the rotary and diffusion pumps.

- Ensuring the tap to the shock tube is open, open the tap to the mixing tank containing the test gas mixture. Allow the required pressure of gas mixture to flow from the tank to the evacuated shock tube. The tap to the tank is then closed.
- The required test gas charge is now in the shock tube. At this stage the shock tube should be isolated from the manifold.
- Ready all diagnostic equipment.
- At the driver section the rotary pump is then isolated from the shock tube.
- Helium driver gas is then allowed to flow into the driver section, this high-pressure gas causes the diaphragm to push against the cutter and rupture, thus creating a shock wave.

Post-shock:

- If the final pressure within the shock tube is greater than atmospheric pressure the shock tube can be vented through the exhaust. If the final pressure in the shock tube is below atmospheric pressure the pressure in the shock tube must be first raised by adding nitrogen to the system and then venting. This minimises potential contaminants entering the shock tube.
- The bolts of the flange are now opened and the ruptured diaphragm removed. Ensure that all petals remain attached to the ruptured diaphragm. Remove any diaphragm pieces which may have broken off. A new diaphragm is inserted and flanges of the driver and driven sections are then bolted closed again.
- Note times captured on timers and also the ignition delay time.

Shutting down:

- Turn off all electrical equipment with the exception of the driven section rotary pump.
- The diffusion pump is turned off and allowed to cool for 45 minutes.
- After such time that the diffusion pump has cooled the water supply and rotary pump can be turned off and the air admittance valve opened.

Determination of Ignition Delay Time

An ignition delay time is defined as the time between the arrival of the shock wave at the endwall and the ignition of the fuel. This time can be measured by using the maximum rise in pressure or the onset of unflitered light emission due to the ignition event. In the low-pressure shock tube a pressure transducer (Kistler 601B) located in the endwall captures the arrival of the shock wave at the endwall. Light in the form of $CH^\star$ emission (431.5 nm) was captured by a detector (PDA55). A narrow bandpass filter with a spectral bandwidth of 10 nm and the detector are aligned with the quartz window fitted in the endplate. These signals were amplified and sent to an oscilloscope (Tektronix TDS 2024) where the signal was displayed and the ignition delay time measured. Figure 4.3 is a typical trace obtained in a low-pressure shock tube experiment. The initial pressure rise observed is due to the arrival of the shock wave at the end wall. The pressure remains constant for some time followed by a rise in pressure which coincides with a peak in light intensity. This is due to fuel ignition.

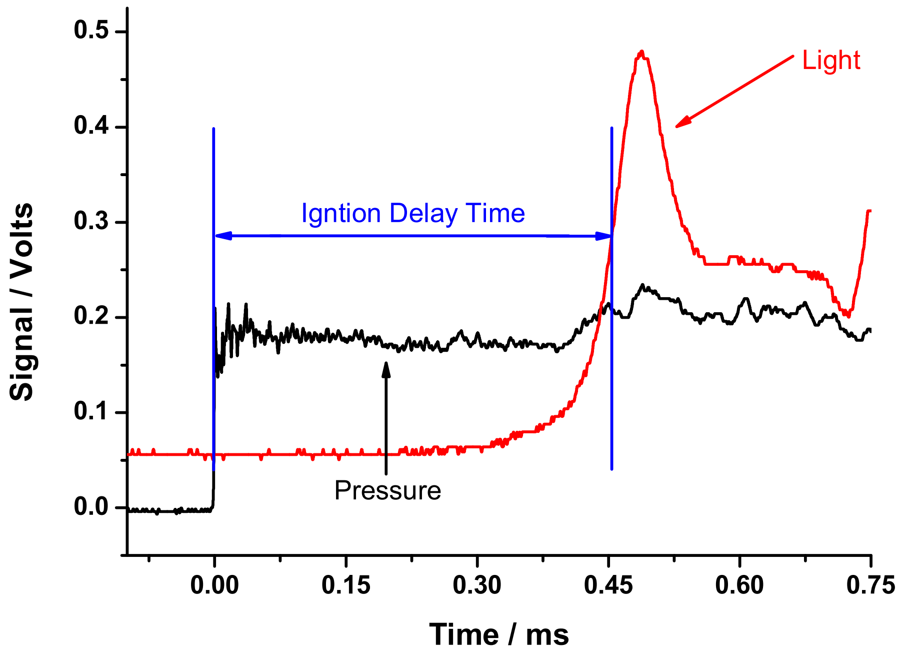

Figure 4.3: Typical pressure and light intensity trace obtained for a 2,5-dimethylfuran low-pressure shock tube experiment, reflected shock wave pressure of 2.0 atm, $\phi = 2.0$.

Incident Shock Velocities

After diaphragm rupture a shock wave is generated. This shock wave then moved into the driven section of the tube. Four pressure transducers (PCB piezotronics, 113A21) mounted flush to the internal wall of the shock tube at distances of 494.9, 365.9, 236.9 and 29.9 mm from the endwall capture the movement of the shock wave in the tube. As the shock wave passes each of the pressure transducers an electrical signal is produced which is then amplified (PCB 483A02) and relayed to a timer (Philips/Fluke PM6666). Three such timers are used. These timers display the time taken for the shock wave to pass these fixed points in the shock tube. In order to find the velocity of the shock wave at the endwall the incident velocities are extrapolated. This is easily done knowing the distances between the transducers and the times taken for the shock wave to travel these distances.

Reflected Shock Temperatures and Pressures

Knowing the test gas composition, the velocity of the shock wave, the initial temperature and pressure of the test gas used in an experiment the temperature and pressure behind the reflected shock wave can be calculated using GasEq [80]. GasEq uses thermochemical data of the species present in the test gas in conjunction with frozen chemistry to predict these values. This program solves equations for the conservation of mass, momentum and energy.

Cleaning of the Shock Tube

On a periodic basic and before changing fuels the shock tube was cleaned thoroughly. It was brought to atmospheric pressure and the flanges that hold the diaphragm opened and the end-plate removed. Firstly the shock tube was cleaned from the endplate using a solution of citric acid and lint free cloth. Acetone and lint free cloth was then used to remove any remaining traces of citric acid.

4.2 Intermediate-Pressure Shock Tube

The pre-existing intermediate-pressure shock tube at NUI Galway underwent extensive modification in order to be used as part of this project. A heating system was installed onto the shock tube, manifold and mixing tanks to allow for work to be carried out with low vapour pressure fuels. To allow for experiments to be carried out at high-pressure both the driver and driven section manifolds were replaced to ensure that they could withstand high-pressures.

This stainless steel shock tube is capable of withstanding pressures of up to 40 atm. Experiments were carried out at reflected shock pressures of 10 and 30 atm.

Through this work a number of modifications were made to the pre-existing intermediate-pressure shock tube. These modifications and the validation of the apparatus were made through a combined effort of a group of people. I was directly involved in the installation of the new driven section manifold, the installation of various heating systems and the installation of the new driven section manifold as described in this section. All validation work was carried out others in the group.

Driver and Driven Sections

Driver Section

- The driver section consists of a 3 m long stainless steel tube with an internal diameter of 6.3 cm. This section terminates in a flange with six equispaced bolt holes. 6 × 8 mm bolts are used to hold the driver section flange, driven section flange and buffer section together. Four viton o-rings, one located in the flange of the driver section, another located in the flange of the driven section and one on both sides of the buffer section create a seal.

- Attached to the driver section is a manifold with connections to three pressure gauges (Swagelock), driver gas cylinders, taps to regulate the flow of the driver gases to the driver section and buffer section and a vacuum pump. The three Swagelock pressure gauges, connected to the driver section manifold, are collectively capable of reading from 1 to 200 bar. These gauges are used when pressurising the driver and buffer sections and also to ensure a suitable vacuum has been reached.

- A vacuum pump (Edwards RV5) is connected to the manifold. This pump allows the driver section to be evacuated to a sufficiently low-pressure before the addition of the driver gas.

Buffer section

- This stainless steel section is a 6.3 cm in diameter and 7 cm in length which sits between the flanges of the driver and driven sections.

- The purpose of this section is to allow for stronger, higher reflected-pressure shock waves to be created. The driver and buffer sections are firstly raised to an equal intermediate-pressure, the buffer section is then closed and the larger driver section is pressurised to a higher pressure. The diaphragms are ruptured by rapidly evacuating the buffer section. This was achieved by using a solenoid valve and dump tank. When the required final pressure had been reached the solenoid valve was opened to the dump tank, evacuating the buffer section and rupturing the diaphragms.

Driven Section

- The stainless steel driven section is 5.73 m long with an inner diameter of 6.3 cm.
- The driver section can be attached to the buffer section and driver section by six equispaced holes that allow 6 × 8 mm bolts to be passed through and bolted together. Two diaphragms are places between the two flanges prior to tightening the bolts. Four viton o-rings, one on each flange and one on each side of the buffer section, ensure a seal is created.
- Attached to the driver section is a manifold that allows for the addition of the test gas, the preparation of test gas mixtures and the evacuation of the shock tube. Attached to the manifold is a vacuum pump (BOC Edwards XDS 5). This vacuum pump is capable of evacuating the shock tube and the mixing tanks to a pressure of 0.2 Torr. Three MKS pressure gauges that collectively are capable of measuring up to 5000 Torr are also attached to the manifold. These gauges are used in the preparation of test gas mixtures and in measuring the initial charge pressure at the beginning of an experiment.
- Along the shock tube four pressure transducers (PCB 113A24) are mounted flush to the interior wall at 50, 20 and 9.9 cm from the endwall and one mounted flush to the endwall. These pressure transducers produce an electrical signal which is amplified (PCB Piezotronics 482A22) and sent to three timers (Fluke PM 6681, Philips/Fluke PM 6666). These capture the time taken for the shock wave to pass the transducers. Pressure traces are recorded using an oscilloscope (Tektronix TDS 2024/ Sigma LDS Nicolet).
- The shock tube is capped by an endplate which is fitted with a pressure transducer (PCB 113A24). This records the arrival of the shock wave at the endwall and monitors the pressure rise within the tube during ignition. The signal is amplified and sent to an oscilloscope (Sigma LDS Nicolet). The design of this endwall also allows for optical access. A sapphire window mounted in the endwall allows for light emission to be captured and recorded. Unfiltered light is detected using a photomultiplier (Thor Labs PDA 55) and a signal is sent to the oscilloscope (Sigma LDS Nicolet) where it can be used to measure the ignition delay time.

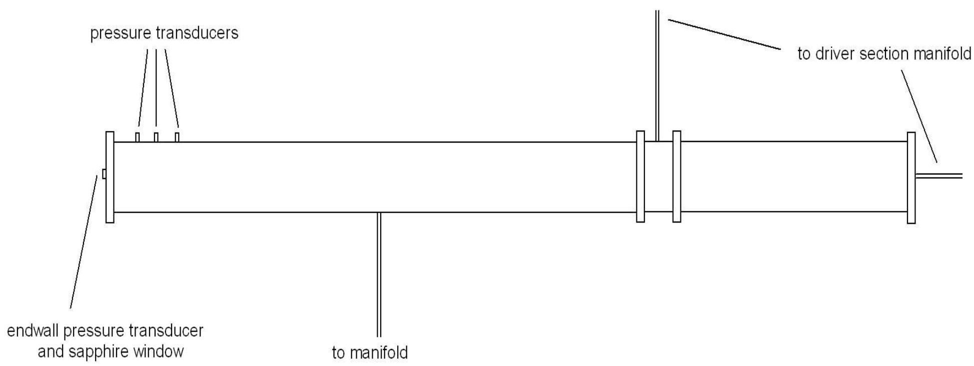

Figure 4.4: Schematic of the intermediate-pressure shock tube.

Gas Mixture Preparation

There are two possible ways of preparing a test gas mixture using liquid fuels; the cold finger method and the direct injection method. The method used is dependent on the vapour pressure of the fuel.

Cold Finger Method

This method involves the used of a glass cold finger containing the liquid fuel which is then attached to the manifold. Prior to the preparation of the fuel mixture the 50 L mixing tank is left to evacuate to a sufficiently low-pressure (0.2 Torr).

The fuel is then subjected to several freeze-pump-thaw de-gassing cycles. The liquid fuel and a small amount of molecular sieve are placed in a cold finger and clamped in place on the glass section of the manifold. De-gassing was carried out by freezing the liquid fuel with liquid nitrogen, removing any gases, allowing the fuel to thaw and repeating.

The mixture is then prepared manometrically. The required pressure of the fuel is allowed to flow into an evacuated mixing tank. The tap to the mixing tank and the isolation tap the glass section of the manifold are now closed. The manifold is then evacuated. The oxygen cylinder is now opened and a line charged to a higher pressure with oxygen than that of the pressure of the fuel in the tank. The tap of the tank is then opened and the required pressure of oxygen added. The bath gas is then added in a similar fashion. Pressures were measured using three MKS pressure gauges one capable of measuring to 100 Torr, a second capable of measuring to 1000 Torr and a third capable of measuring to 5000 Torr.

When the mixture preparation procedure was completed mixtures were allowed to sit to equilibrate of a period of two hours in a heated mixing tank or up to four hours in an unheated mixing tank before use.

Injection Method

This method is used for liquid fuels with low vapour pressures where the cold finger method would result in low fuel concentration mixtures. The injection method follows the same procedure as described for the cold finger method the only difference being that the fuel is injected directly into a heated mixing tank fitted with a suitable injection port. A gas tight glass syringe is used for this method. This syringe is weighted before and after the addition of the fuel to the tank. An increase in pressure inside the mixing tank was observed with the injection of the fuel. Again the mixture is prepared manometrically with the required quantities of oxygen and bath gas being added in the same manner as in the cold finger method.

Again when the mixture preparation procedure was completed mixtures were allowed to sit in the heated mixing tank for two hours to equilibrate before use in experiments. It is also of great importance that the mixing tank remain at a constant temperature to ensure that the fuel remains in the gaseous phase and no condensation of the fuel occurs. Condensation would result in inaccuracies in the mixture composition.

Gaseous Fuels

Gaseous fuel mixtures may also be prepared. Gas cylinders containing the gas to be studied may be attached directly to the manifold and test gas mixtures prepared using a similar procedure to that outlined previously.

Preparation of Multiple Fuel Component Gas Mixture

As part of this study mixtures of *n*-butylcyclohexane and *n*-heptane were investigated. These fuel mixtures were prepared by firstly weighing a clean dry glass vial. The balance was then zeroed and an appropriate weight of *n*-heptane was added dropwise using a syringe to an accuracy of significant figures. *n*-Butylcyclohexane was then added using a similar procedure. The vial was then capped and shaken to insure that the two liquids mixed thoroughly. Test gas mixtures using this fuel were prepared via the direct injection method outlined previously.

Diaphragms and Diaphragm Rupturing Mechanism

The intermediate-pressure shock tube employs a double diaphragm system. This system used two diaphragms of similar or differing thicknesses. In order to use this system two diaphragms are placed between the flanges of the tube sections and the buffer section and 6 × 8 mm bolts are used to hold these pieces together. If it is the case that two diaphragms of the differing thickness are used the thicker of the two is placed to face the driver section. With a known pressure of test gas in the driven section of the tube and the diaphragms in place, high-pressure driver gas is allowed to flow into the driver section and also the smaller buffer section. When the two sections are at the desired intermediate-pressure, the buffer section is then closed and the driver section isolated. The driver section is then brought to a greater final pressure. When a sufficiently high-pressure has been reached the driver section is then closed. To rupture the diaphragm the smaller section between the two diaphragms is rapidly evacuated. This causes a differential in pressure which in turn causes the diaphragms to rupture and results in the formation of a shock wave.

Throughout this study polyester diaphragms were used.

Pre-Experimental Procedure

Prior to performing experiments the following should be carried out:

- Turn on the extraction fan and ensure that it is running.
- Ensure that new diaphragms of the correct thickness are placed between the flanges of the driver, driven and buffer sections, also ensure that these sections are bolted together.
- Turn on the heating system of the shock tube, mixing tanks and manifold. Ensure that the temperature controllers are set to the required temperature for the experiment.
- Replace the septum of the injection port of the mixing tank if necessary.

Experimental Procedure

When carrying out experiments using the intermediate-pressure shock tube the following procedure is followed:

Pre-shock:

- Before turning on the rotary pump the air admittance valve must be closed. The rotatory pump can now be turned on.
- Open the driver section to the pump and allow it to evacuate.
- At the driven section turn on the scroll pump, open it to the shock tube and manifold and allow it to evacuate.
- Turn on and ready all electronics, i.e. gauge read outs, times, oscilloscope, amplifiers etc.
- The shock tube and manifold are firstly isolated from the vacuum pump.

- Record the temperatures from the thermometer readings. Ensuring that the temperature required for the experiment has been reached and that the temperature is homogeneous throughout the length of the shock tube.
- Ensuring the tap to the shock tube is open, open the tap to the mixing tank containing the test gas mixture. Allow the required pressure of gas mixture to flow from the tank into the tube. The tap to the tank is then closed.
- With the required pressure of gas in the tube, it is then isolated from the manifold.
- At this stage all of the thermostat controllers should be turned off as it was found that these controls interfere electronically with the timers used to measure shock velocity.
- All diagnostic equipment are to be readied at this point.
- At the driver section the rotary pump is then isolated form the shock tube.
- Driver gas is allowed to flow into the driver and buffer sections to a required intermediate-pressure. The smaller buffer section is then closed and the larger driver section is filled to a greater pressure.
- The diaphragms are ruptured by rapidly evacuating the buffer section.

Post-shock:

- Note and record the times captured on the counter timers and the ignition delay time.
- The heating system is turned on again.
- The high-pressure gas remaining in the shock tube is vented and brought to atmospheric pressure by opening the tap connected to the buffer section.
- When the shock tube has reached atmospheric pressure the venting tap can now be closed and the shock tube is evacuated thought the driver section manifold. The tap to the pump is then closed and the shock tube brought back to atmospheric pressure by adding nitrogen to the system.
- The diaphragms are replaced.
- Any small pieces that became detached from the main piece of diaphragm should be removed so as not to interfere with the next experiment.
- The diaphragms are replaced and the flanges of the driver and driven sections are then re-sealed.

Shutting down:

- Turn off the heating system.
- Turn off all diagnostic equipment.
- Turn off the vacuum pumps. Open the air admittance valve of the rotary pump.
- Turn off the extraction fan.

Determination of Ignition Delay Time

The ignition delay time is defined as the time between the arrival of the shock wave at the endplate to the maximum rate of rise of the pressure signal or the onset of light emission. Light emission was only used as a diagnostic when carrying out measurements at a reflected shock wave pressure of 1 atm due to the small pressure rise on ignition of the fuel. Figure 4.5 is a typical pressure trace from an intermediate-pressure shock tube experiment. This pressure rise was measured using a pressure transducer (Kistler 603B) located in the endplate, Fig **??**. This pressure transducer produces an electrical signal which was sent to an amplifier (Kistler 5018). This signal was in turn recorded on an oscilloscope (Tektronix TDS 2024 / Sigma LDS Nicolet) where the pressure trace was displayed. Also it was possible to use light as a diagnostic for this purpose. Located in the centre of the endwall is a sapphire window. Located just in front of the window was a photomultiplier (Thor Labs PCB 55). This detector captures and amplifies unfiltered light emission due to ignition of the fuel. This signal was also recorded on the oscilloscope (Tektronix TDS 2024 / Sigma LDS Nicolet) where it can be used to measure the ignition delay time. This method was of particular use when fuel-lean mixtures were being examined and also at low reflected shock wave pressures where the pressure rise due to ignition was not sufficient to accurately measure the ignition delay time.

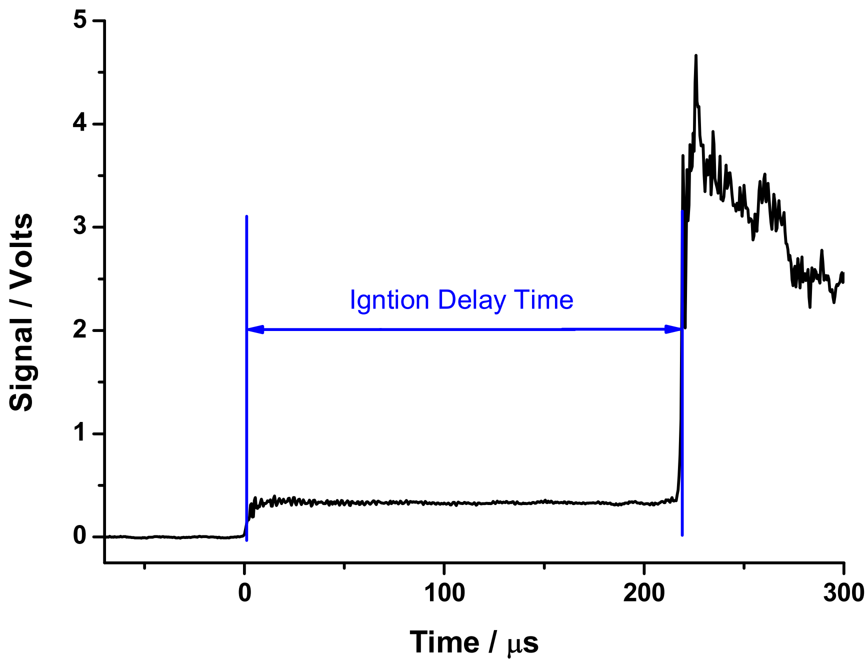

Figure 4.5: Typical pressure trace obtained for a n-butylcyclohexane intermediate-pressure shock tube experiment, reflected shock wave pressure of 30 atm, $\phi = 2.0$.

Incident Shock Velocities

After the diaphragm ruptures a shock wave is created. This shock wave travels the length of the driven section towards the endwall. Three pressure transducers (PCB 113A24) mounted flush to the interior wall of the shock tube at 50, 20 and 9.9 cm from the endwall and one mounted in the endwall produce an electrical signal as the shock wave passes. Each signal is then sent to a amplifier (PCB Piezotronics 482A22) which amplifies the signal which is then sent to a timer

(Fluke PM 6681, Philips/Fluke PM 6666). There are three such timers. These timers display the time taken for the shock wave to pass these fixed points. The velocity of the shock wave when it reaches the endwall can be easily obtained by extrapolation of the known times and distances.

Reflected Shock Temperatures and Pressures

As with the low-pressure shock tube, GasEq [80] was used to calculate reflected shock temperatures and pressure knowing the test gas composition, shock wave velocity, initial pressure of gas used and initial temperature of the gas.

Cleaning of the Shock Tube and Mixing Tanks

A problem encountered in the used of large hydrocarbon was sooting. Sooting is a result of incomplete combustion of the hydrocarbon fuel and was a particular problem when using high pressures and fuel rich mixtures.

Shen *et al.* [82] have reported on the effects of sooting in an RCM. It was reported that contamination of the combustion chamber resulting from sooting showed a pre-ignition energy release and shorter ignition times in the experimental data obtained. A similar situation was observed in the intermediate-pressure shock tube where *n*-butylbenzene data that had been taken previously in the intermediate-pressure shock tube was repeated. The ignition delay times for the new data set were much faster than what was expected. This was found to be due to soot contamination in the tube.

Loose soot particles and small fragments of diaphragm were easily removed by cleaning the shock tube with a lint free cloth and acetone. This was sufficient to remove soot and loose diaphragm material but because of the diaphragm material used small fragments of the diaphragm can make their way to the endwall where they melt and adhere to the walls. Efforts were taken to remove the majority of the larger fragments but despite our best efforts smaller pieces remained. In an effort to remove the residue remaining on the shock tube walls and endwall a fine grade emery paper was used. The walls and endwall were then cleaned with acetone after this process. Occasionally the driven section was also cleaned to remove soot and loose pieces of diaphragm.

In addition to sooting it was also discovered that, because of the low vapour pressure fuels used, there was a problem of cross contamination of the fuels. In order to overcome this a procedure was put in place where the tanks were roughly evacuated. Approximately 5 ml of ethanol (low grade) was then injected into each of the tanks and allowed to stand. After some time the tanks are again evacuated. Following this 1 atm of nitrogen was allowed to flow into the evacuated tanks and again allowed to stand. The tanks are then allowed to evacuate overnight. This procedure was carried out on a regular basis and when changing fuels.

Modifications Made to Intermediate-Pressure Shock Tube

Installation of New Manifold

A new stainless steel manifold was designed, built and installed to allow for a uniform system that could withstand high-pressures, Fig. 4.6. The manifold is the part of the shock tube that controls the volumes of fuel, oxygen and diluent gases that are prepared in the mixing tank. The manifold further controls the quantity of fuel mixture allowed into the driven section prior to an experiment.

The stainless steel manifold is connected via a flexible, heated stainless steel braided hose and a valve, tap 5, Fig. 4.6. The valve is used to open and close the flow of the gaseous fuel mixtures to the shock tube. The manifold has one horizontal, three upper and four lower taps. Two of the upper taps and the horizontal tap, taps 1, 2 and 4, Fig. 4.6, are equipped with pressure transducers capable of measuring up to 5000 torr. These pressure transducers are used to measure the pressure inside the manifold during experiments and the pressure of the diluent gases and fuel upon preparation of the fuel mixture. The middle upper tap, tap 3, Fig. 4.6, is attached to two gas cylinders (oxygen and nitrogen) via two high-pressure Swagelok tubes (SS-8R4-TP4-TP4) using a three way stainless steel junction.

The leftmost lower tap, tap 6, Fig. 4.6, is connected to a mixing tank that holds the gaseous fuel, oxygen and diluent gas. The second lower tap, tap 7, Fig. 4.6, is connected to a vacuum gauge (BOC Edwards Pirani 501) used to measure the pressure inside the manifold. The pressure gauge and the manifold are connected at two Swagelok VCR junctions held together using a steel clamp. The crevice of each junction is fitted with viton o-rings to withstand high-temperatures and pressures of up to 200°C and 5 atm. The fourth lower tap is connected to the vacuum pump, tap 8, Fig. 4.6.

Connected to the horizontal and first and third upper taps are three pressure gauges (MKS Instruments), taps 1, 2 and 4, Fig. 4.6. The first of these pressure gauges is capable of measuring up to 100 Torr and is mainly used to measure the pressure of the fuel during mixture preparation.

The second pressure gauge is capable of measuring up to 1000 Torr. This is normally used to measure the pressure of oxygen gas during mixture preparation. Both of these pressure gauges are connected to the manifold via VCR junctions fitted with viton o-rings and held together using steel clamps.

The third pressure transducer is capable of measuring up to 5000 Torr and is used to measure the pressure of the diluent gas on mixture preparation. This gauge is attached to the manifold via a Swagelok NW junction which requires a gasket and a steel clamp to keep the junction in place. The VW crevices have been fitted with 16 mm viton o-ring.

The three pressure transducers connected to the upper portion of the manifold are attached to three signal conditioners (MKS Instruments type 121 - 100, 1000, 5000 Torr). These are in turn connected to two digital pressure readouts (MKS PR 4000B) from which the pressure is recorded.

The centre upper tap of the manifold is attached to the oxygen and nitrogen cylinders via a three way steel junction that is screwed into place. The fourth lower tap is connected to a vacuum pump (Edwards XDS 5) and held in place at two Swagelok VCR junctions using a steel clamp. These junctions do not require viton o-rings because they are not exposed to excessive temperatures or pressures.

Installation of Heating System to Shock Tube

Recent modifications to the intermediate-pressure shock tube have seen the installation of a heating system to the shock tube itself and also to the connected mixing tanks and manifold. This modification to the system is of great importance when dealing with liquid fuels of low vapour pressure as the heating of the system allows the fuel to remain in a gaseous state without condensation allowing for gaseous phase experiments to be carried out at pre-heated temperatures of up to 130°C.

The various methods used when installing the intermediate-pressure shock tube heating system are outlined. Over time it was found that certain aspects of the system were insufficient for maintaining a homogeneous temperature and modifications were made. These modification are outlined below.

First Heating System

The first heating system was installed on the driven section of the shock tube only. Ten sil-

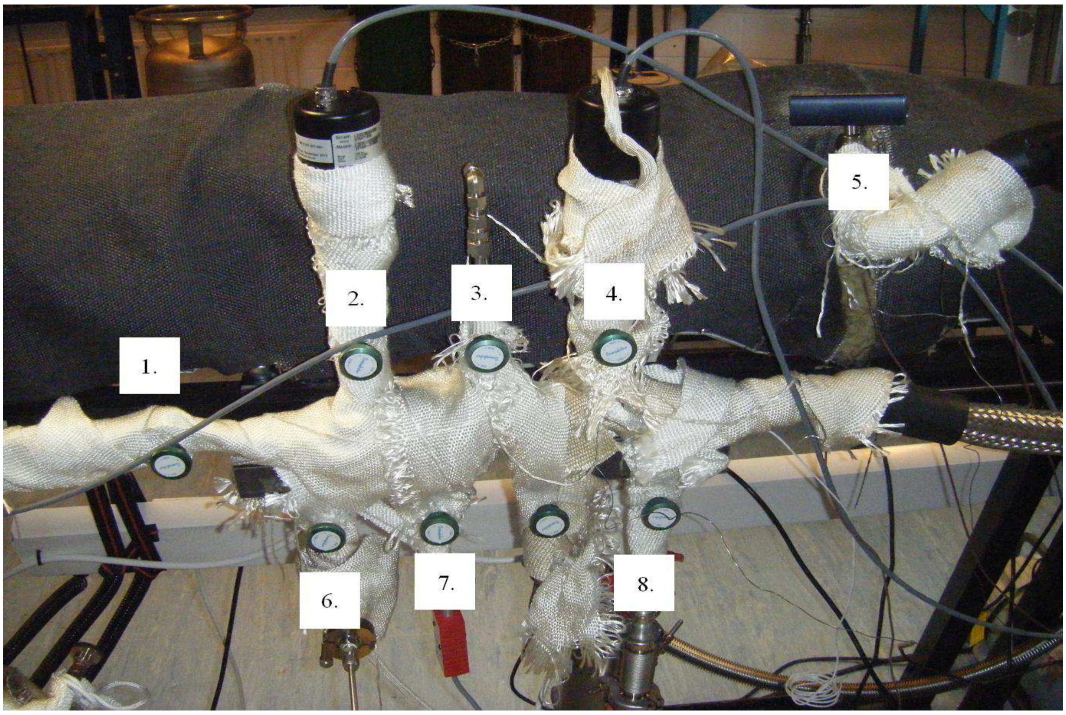

Figure 4.6: New intermediate-pressure shock tube driven section manifold.

icon patch thermometers (Omega SA2C-RTD-3-100-B-40) were placed on the surface of the tube, one on the endplate and nine others at a distance of 30, 60, 140, 220, 300, 380, 460, 540 and 570 cm from the endplate. Two patch thermometers were then connected to one dual input digital output (Omega HH804). Six thermocouples were placed on the shock tube and each was connected to a 16 amp thermostat (Flexelec FX/ST - 220). Heating tapes (Flexelec RVI 1250W) were then wrapped around the shock tube over the patch thermometers and the thermocouple. The heating tapes were wound around the shock tube tightly without over lap. The heating tapes were then connected in duplicate to the thermostat controllers (Flexelec FX/ST - 220). Then a layer of fibre glass was placed over the heating tapes. This was then covered with insulation tape (Zetex 1000) ensuring that no fibre glass was left exposed. To test this system the temperature at each point along the tube was measured and recorded over a period of 60 minutes.

This method of heating resulted in a large non-uniformity and deviation in temperatures of up to 17°C (%RSD 4.54%) along the tube, Fig. 4.7. This was caused by the direct contact of the thermometer sensor with the heating tape. This temperature was found to be not representative of the actual temperature of the shock tube itself, hence this method of heating the shock tube was found to be unsuitable.

Second Heating System

A new system was designed to address the problem of large temperature deviations along the tube and to ensure that recorded temperatures were representative of the temperatures inside the tube itself. Ten silicon patch thermometers (Omega SA2C-RTD-3-100-B-40) were placed on the surface of the shock tube, one at the endplate and at 30, 60, 140, 220, 300, 380, 460, 540 and 570 cm from the endplate. Two patch thermometers were connected to one dual input digital output (Omega HH804). Three layers of insulation tape (Zetex 1000) were wrapped around the length of the tube. Heating tape (Flexelec RVI 1250W) was wrapped over the insulation tape and connected to 16 amp thermostats (Flexelec FX/ST - 220). Each thermocouple was

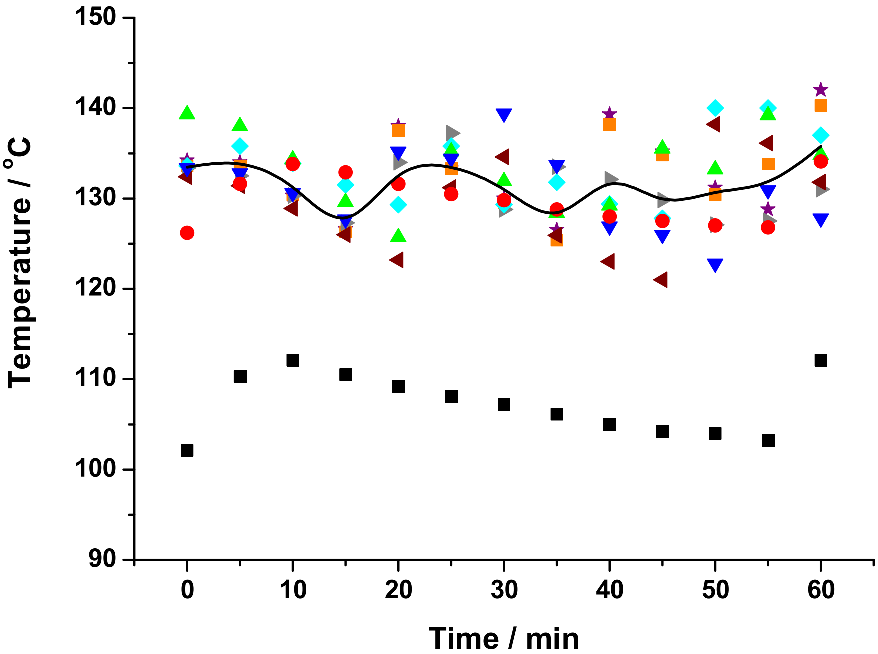

Figure 4.7: Temperature deviations along the shock tube as a result of the first heating system. Distance from the endplate; ★ – 30 cm, ■ – 60 cm, ▶ – 140 cm, ◀ – 220 cm, ♦ – 300 cm, ▲ – 380 cm, ▼ – 460 cm, ● – 540 cm, ■ – 570 cm

placed underneath the heating tape. Heating tapes were connected in duplicate to each of the thermostat controllers. Rope heaters (Omega FGR) were wrapped around the buffer section and endplate of the test pressure section and controlled by two thermostat controllers (Vulcanic 30633). A final layer of insulation tape (Zetex 1000) was placed over the heating tape (Flexelec RVI 1250W) to ensure a minimal heat loss to the atmosphere. Again to test this system the temperature at each point along the tube was measured and recorded over a period of 60 minutes.

This second heating method resulted in temperature deviations that were significantly reduced (3.5°C, %RSD 1.87%), Fig. 4.8. A number of thermocouples were placed on the internal wall of the tube at known distances from the endwall. The temperatures recorded on the external wall were found to be representative of the temperatures inside the tube.

A small section of the driver section was insulated in the same way as the driven section to avoid excessive heat loss to this section. This ensured the temperature at the diaphragm end of the low-pressure section was maintained.

Over time it was found that the temperature of the shock tube was very difficult to control. This was due to the large number of heating tapes and poor insulation. This method of heating tended to result in the formation of hot spots, in particular near the endwall, and as a result heating was no longer uniform along the length of the tube. It was for this reason that it was decided to remove this heating system and install a new, more heavily insulated one.

Third Heating System

Firstly the two sections of the shock tube were raised by approximately 6 cm to allow for the large amount of insulation needed for this new heating system. Ten silicon patch thermometers (Omega SA2C-RTD-3-100-B-40) were placed on the surface of the shock tube, one at the

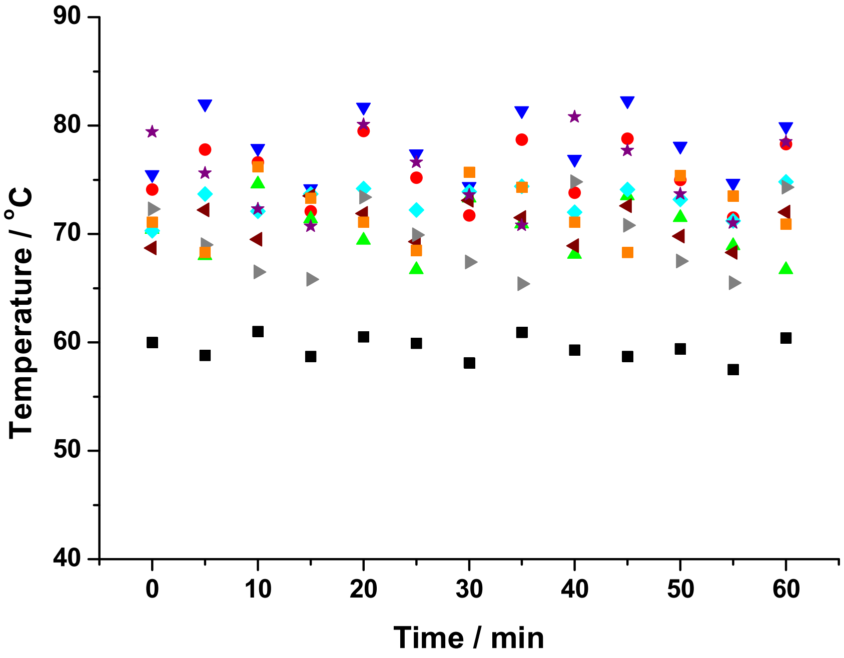

Figure 4.8: Temperature deviations along the shock tube as a result of the second heating system. Distance from the endplate; ★ – 30 cm, ■ – 60 cm, ▶ – 140 cm, ◀ – 220 cm, ♦ – 300 cm, ▲ – 380 cm, ▼ – 460 cm, ● – 540 cm, ■ – 570 cm

endplate and at 30, 60, 140, 220, 300, 380, 460, 540 and 570 cm from the endplate. A total of four heating tapes (Flexelec RVI 1250W) were used. The previous heating system incorporated 12 heating tapes. Three of these tapes were wrapped around the driven section of the shock tube, one was placed on the driver section. The tapes were spaced evenly over the length of the tube. Four thermocouples (Flexelec FX/ST - 220) were attached to the tube, the heating tapes would be later connected to the thermostat controllers. Following this one layer of insulation tape (Zetex 1000) was added in order keep the heating tapes in place. Next a thick covering of fibreglass insulation (approximately 15 cm) was added leaving the area close to the buffer section and the endwall uncovered. This was then covered with a layer of aluminium tape ensuring that no fibreglass insulation was left exposed. The areas left uncovered were later covered with an easily removable insulation.

Testing of this heating system showed that it allowed for a more homogeneous temperature distribution.

Installation of Heating System to Manifold

A heating system was installed on the manifold. The upper and lower taps of the manifold were wrapped with rope heaters (Omega FGR). Each of the ropes were attached to separate temperature controllers (Vulcanic 30633). A thermometer and thermocouple were placed under the heating ropes on the surface of the manifold. The remaining surface was wrapped with two heating tapes connected separately to thermostats (Vulcanic 30633). The heating ropes were finally wrapped with insulation tape (Zetex 1000).

As with the heating system on the shock tube that on the manifold was also modified. After removing the existing system the existing heating tapes (single strand Flexelec RVI 1250W) were re-positioned over the entire manifold. Following this the manifold was insulated with a large amount of fibreglass insulation which was then covered with aluminium tape.

Installation of Heating System to Mixing Tank

A heating system was place on each of the mixing tanks to ensure that the low vapour pressure liquid fuels remained in the gaseous phase while mixtures were being prepared and used. Each of the three 50 L mixing tanks were heated in a similar manner to the shock tube. Thermometer sensors (Omega SA2C-RTD-3-100-B-40) were place at three points on the tanks, the bottom, mid-way and near the top of the tank. The tank was then wrapped with three individual layers of insulation tape (Zetex 1000) with minimal overlap. Heating tape (Flexelec RVI 1250W) was them wrapped around the tank over the 3 layers of insulation tape (Zetex 1000). A final layer of insulation tape was them placed over the heating tape.

In order to heat the bottom of the tank a similar approach was taken. A thermometer was placed on the bottom of the tank. The insulation tape (Zetex 1000) was arranged into four sheets. One sheet was placed on a table, heating tape (Flexelec RVI, 1250W) was arranged in a zig-zag fashion on this sheet with a thermocouple. This heating tape was connect a thermostat controller (Flexelec FX/ST - 220). The remaining three sheets were placed on top of this and finally the mixing tank was placed on top of the insulating sheets and heating tape. The heating tapes were attached to temperature controllers and power supplies. The tank was then connected to the manifold.

While modifications were made to the heating systems on the shock tube and the manifold no modification was made to the heating of the tanks.

Installation of a New Manifold to Driver Section

The manifold of the driver section allows for the addition of driver gases to the buffer and driver sections, the mixing of such gases and the evacuation of driver section prior to an experiment. The manifold used previously was composed of stainless steel tubing and brass Swagelok fittings. This manifold was found to leak at pressures greater than 30 bar and was therefore unsuitable for use at high-pressure. A new manifold of similar design was built using stainless steel tubing and stainless steel Swagelok fittings. This manifold was tested and was found to hold pressures in excess of 60 bar.

This stainless steel manifold is connected to the shock tube via two high-pressure Swagelok tubes (SS-8R4-TP4-TP4). The manifold has five upper and three lower taps. Three of the upper taps are equipped with pressure gauges. The remaining two upper taps are connected to the shock tube, one at the driver section and one at the buffer section. Two of the three lower taps are connected to driver gas cylinders. The third lower tap is connected to a vacuum pump.

Three of the five upper taps are connected to Swagelok pressure gauges. The first, left-most upper portion of the manifold is connected to a Swagelok gauge capable of measuring from 1 – 200 bar.

The second upper tap, Fig. 4.9, tap 1, is also connected to a Swagelok pressure gauge. This pressure gauge is capable of measuring from 1 – 40 bar.

The third upper tap, Fig. 4.9, tap 2, is connected to the final Swagelok pressure gauge. This pressure gauge is capable of measuring pressure from 1 – 2.5 bar.

These pressure gauges are used to measure pressure in the driver section of the shock tube, ensure that the correct pressure of driver gas is used and finally to ensure that the shock tube is correctly vented after each experiment.

The two remaining taps, Fig. 4.9, taps 3 and 4, are connected to the driver and buffer sections of the shock tube via flexible high-pressure Swagelok tubing (SS-8R4-TP4-TP4). These are used when filling the driver section during an experiment. Firstly the driver and buffer sections are filled to an intermediate-pressure. When this has been achieved the right-most tap to the buffer section is closed allowing for the driver section only to be filled to the higher final pressure.

The two left-most lower taps, Fig. 4.9, taps 5 and 6, are connected to driver gas cylinders, nitrogen and helium. The third, right-most lower tap, Fig. 4.9, tap 7, is connected to a vacuum pump (Edwards RV5) which is used to evacuate the driver section prior to carrying out an experiment and also to evacuate the shock tube after carrying out an experiment before opening the buffer section to remove and replace the ruptured diaphragms.

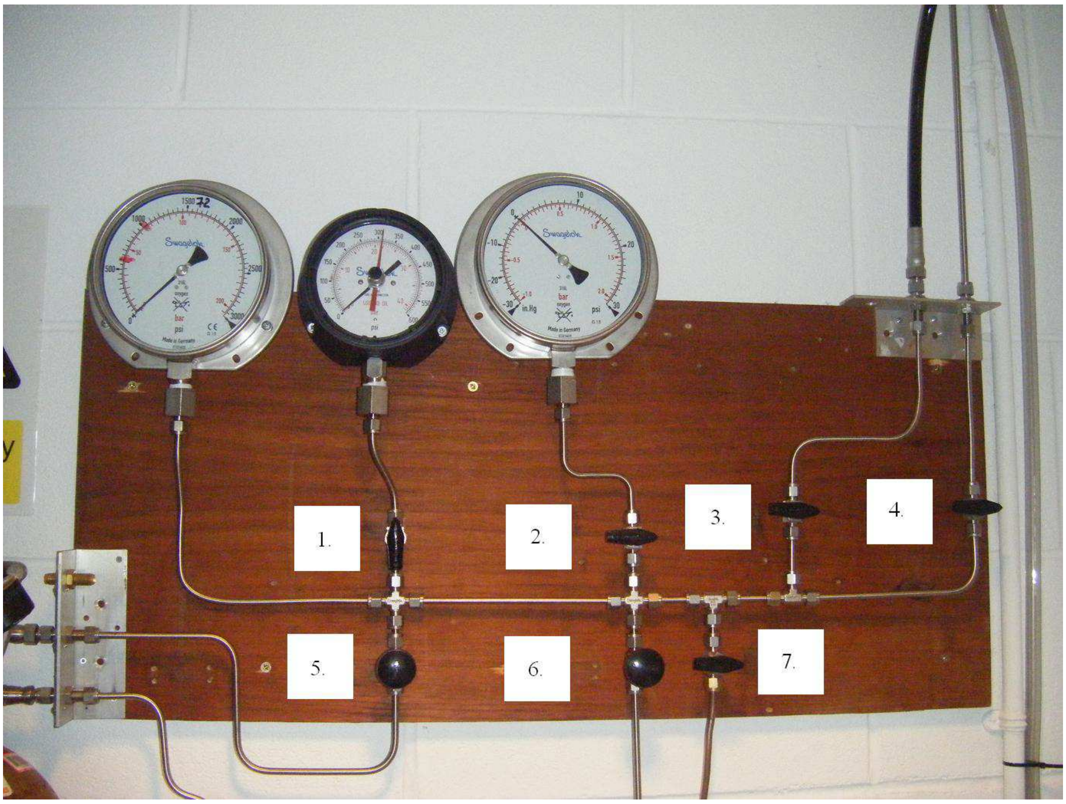

Figure 4.9: New intermediate-pressure shock tube driver section manifold.

Validation of the Intermediate-Pressure Shock Tube

Validation of the intermediate-pressure shock tube was carried out at both room temperature and at elevated temperatures using the newly installed heating system. Experiments were carried out using n-heptane at $\phi = 1.0$ at a reflected shock pressure of 10 atm. n-Heptane, provided by Sigma-Aldrich (97%), was chosen for this validation because a large quantity of ignition delay time data exists for this fuel in the literature. Comparisons to literature data can be used to show that the shock tube is operating efficiently.

Validation carried out at room temperature tested two methods of fuel addition to the mixing tank; the traditional method of using a cold finger and a new method whereby the fuel is injected via an injection port on top of the mixing tank. A 1.8% fuel, $\phi = 1.0$, in air mixture was prepared using both the cold finger and direct injection methods.

Validation of the shock tube at elevated initial temperatures was carried out at 75°C and 120°C. The shock tube and manifold were heated to the specified temperatures. All temperatures at the surface of the shock tube and manifold were recorded at regular intervals. Before the heated experiments were started a temperature profile of the manifold and low-pressure section of the shock tube was obtained at five minute intervals over one hour. This allowed the deviation in temperature along the length of the shock tube to be determined to establish the degree of error. It was found that the standard deviations on the manifold were 1.74°C at 75°C and 1.0°C at 125°C.

For this validation study polyester diaphragm were used. For experiments carried out at 75°C two 125 μm thick diaphragms were used. Experiments at 125°C were carried out using 250 μm and 125 μm (high-pressure and low-pressure side respectively) thick diaphragms. The reason for using the differing thicknesses of diaphragm material for the various initial temperatures is due to the reduced strength of the diaphragm material with increasing temperature. Hence at higher temperatures thicker diaphragm material should be used to ensure that the desired driver gas pressure and hence reflected shock pressure is realised. Before each experiment at elevated temperatures all the temperatures at regular points along the manifold and shock tube were noted to ensure unusually large deviations in temperature.

The results of these validation experiments were in very good agreement with that of the data produced at Stanford University [83], Fig.. 4.10.

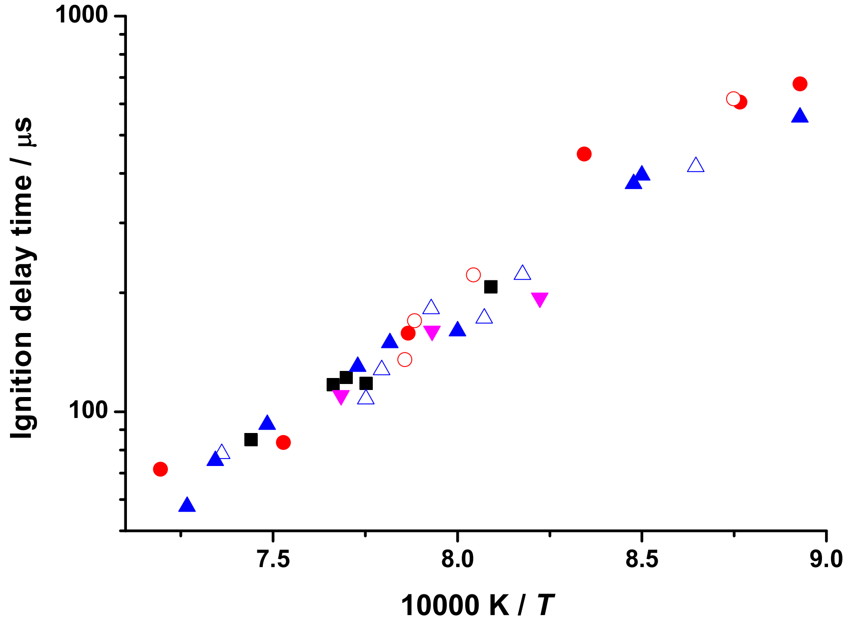

Figure 4.10: Validation data of intermediate-pressure shock tube carried out using, 1.8 %, ϕ = 1.0 n-heptane at refelected shock wave pressure of 10 atm, ■ – Stanford University [83], ● – cold finger method, room temperature, ○ – direct injection, room temperature △ – direct injection, 75°C, ▲ – direct injection, 125°C, ▼ – direct injection with new endwall, 100°C.

4.3 High-Pressure Shock Tube

In order to safely carry out experiments at elevated pressures a new stainless steel high-pressure shock tube was designed, fabricated, installed and validated in early 2012. This stainless steel shock tube is capable of withstanding pressures up to 450 bar and can be heated to 200°C.

The installation, heating and validation of the high-pressure shock tube was achieved though the combined effort of the group. I was directly involved in the installation of the shock tube itself and the installation of the heating system as described in this section. Validation work was carried out by others in the group.

Driver and Driven Sections

Driver Section

- The driver section consists of a 3 m long stainless steel tube with an internal diameter of 65.3 mm and a wall thickness of 15.3 mm. This section consists of two tube sections connected via a 78 mm long tube connection piece. The tube sections terminate in a short threaded section. To this threaded section a flange is attached via this buttress thread. These flanges contain six equispaced holes through which 6 × 20 mm bolts are passed and the flanges bolted together.

- To both ends of this section a flange, with six equispaced bolt holes, is mounted via a buttress threading. An identical is located on the driven section of the tube. 6 × 20 mm bolts allow of the tube sections, the buffer section and two diaphragms to be held together. Four o-rings, one located in the flange of the driver section, another located in the flange of the driven section and one on both sides of the buffer section creates a sufficient seal. To cap the driver section a stainless steel cap and viton o-ring are placed on the tube and are bolted in place using a steel end plate.

- Connected at two points along the tube are two Maximator (21V9M071) taps capable of withstanding extremely high-pressures. These taps are located at the buffer section and tube connection piece of the driver section. These taps are used in the evacuation of the driver section, in the addition of driver gases before an experiment and in the venting of the shock tube after an experiment.

- Attached to the driver section is a manifold. This manifold is identical to that used in the intermediate-pressure shock tube experiments.

Buffer section

- The buffer section is located between the driver and driven sections. Two diaphragms are placed in this section, one between the driver section and the buffer section and the other between the driven section and buffer section. Four viton o-rings crate a sufficient seal. Aluminium diaphragms only are used. These diaphragms were composed of a high grade aluminium and were cut in-house.

- A Maximator (21V9M071) tap attached to the buffer section allows for the addition of driver gases, for the venting of the tube after an experiment and also for the evacuation of the driver section before an experiment.

- The purpose of this section is to allow for stronger shock waves to be created. The driver and buffer sections are firstly raised to an equal intermediate-pressure, the buffer section is then closed and the driver section is pressurised to a greater pressure. The diaphragm is ruptured by rapidly evacuating the buffer section.

Driven Section

- The driven section of the shock tube had an internal diameter of 65.3 mm and a wall thickness of 15.3 mm and is 5.7 m in length.

- The driven section is composed of four individual sections, three 1.5 m sections and one 1 m diagnostic section. Each end of the tube sections is threaded with a buttress threading to which a flange can be easily attached. The tube sections are connected via a 78 mm long tube connection piece and bolted together using 6 × 20 mm bolts.

- The driven section is attached to the buffer section and driver section using 6 × 20 mm bolts which are passed through six equispaced holes in the driver and driven section flanges. Two diaphragms are places between the two flanges prior to the tightening of the bolts.

- Attached to the driver section is a manifold. This manifold is identical to that of the intermediate-pressure shock tube.

- The 1 m diagnostic section of the shock tube is equipped with a number of access ports. These may be used for optical access or may be fitted with a pressure transducer. Six pressure transducers (PCB 1128A) are mounted flush to the internal wall and are located at 1, 15, 43, 61, 102.5 and 258.5 cm from the endwall. The electrical signal produced is amplified (PCB Piezotronics 482 signal conditioner) and is sent then relayed to the oscilloscope (TiePie Handyscope HS4 oscilloscope) where the pressure trace is recorded and can be viewed.

- The driven section is capped with a plug-style endwall which sits into the tube. When the plug has been mounted a capping plate is bolted in place via a flange using 6 × 20 mm bolts. Housed in the endwall is a pressure transducer (Kistler 603B). The electrical signal produced by this pressure transducer is relayed to a signal conditioner (Kistler 5018). The output from the signal conditioner is then sent to the oscilloscope (TiePie Handyscope HS4 oscilloscope) where the pressure trace is recorded and can be viewed. This pressure transducer is used to measure the arrival of the shock wave at the endwall and also to measure the ignition delay time during an experiment.

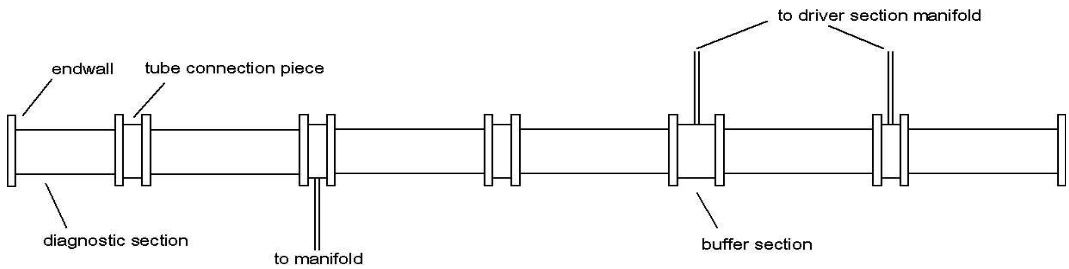

Figure 4.11: Schematic of the high-pressure shock tube.

Installation of the Shock Tube

The initial step in the assembly of the high-pressure shock tube facility was the mounting of the tube supports, Fig. 4.12(a). These supports were bolted to the pre-existing shock tube stand. There is a total of twelve such supports, eight of which are fixed to the stand at the driven section. The remaining four are mounted on movable runners at the driver section. This allows for the shorter driver section to be moved easily allowing for convenient access to the buffer section.

A buttress thread at the end of each tube section allows for the easy mounting of the flanges. The flanges of the various sections were installed as the tube sections were placed on the stand.

Alignment of the tube was initiated at the diagnostic section, Fig. 4.12(b). This section was inserted into the shock tube supports and was ensured to be horizontally level by using a sprint level.

A laser pointer was used to align the remaining sections. This laser was attached to a stand and aligned so that the laser beam pointed down the middle of the diagnostic section, Fig. 4.12(c). To ensure that the beam was in the middle of the section a number of discs of a transparent plastic material with a cross hair in the middle of each disc were printed. These were then attached to the open ends of the tube sections. The remaining sections were adjusted so that the laser beam was in line with the cross hairs at each section end.

To connect the tube sections stainless steel connectors were used, each 78 mm in length. These connecting pieces contain o-ring grooves on both sides into which viton o-rings were placed. Each of these connecting pieces also has an access point for a pressure transducer, for connection to a manifold, or for optical access. Each of these shock tube connecting pieces were held in place while a shock tube section was slid into place to maintain the overall alignment. Each of the three sections were then bolted together using 6 $\times$ 20 mm bolts, Fig. 4.12(d).

Installation of the Shock Tube Heating System

The shock tube was heated in a somewhat similar manner to the previous shock tube although many improvements were made. For this heating system one 5 m heating tape (Flexelec RVI, 1250 W) was used to heat one tube section. The heating tapes were spread over the length of the individual tube sections. Crossover of the heating tape was avoided as was non-uniform distribution of the tape which could lead to the formation of hot or cold spots. Each of the flanges were wrapped with a 1.5m heating tape (Flexelec RVI, 1250 W). This procedure was carried out along the entire driven section.

Heating tapes were also attached to the buffer section. One 1.5 m heating tape was used for each of the flanges of this section with the excess from each tape used to heat the middle of this section. Also the first section of the driver section was heated to ensure that excess heat was not being lost to the colder driver section.

After all heating tapes had been mounted on the tube, type T thermocouples were attached to the surface of the tube using aluminium tape. These thermocouples are used to measure the outer wall temperature of the shock tube. Each heating tape was controlled by an individual temperature controller (Tycothermal 4848-P-A). Before proceeding to the insulating step the heating system was turned on to ensure that all individual components of the system were fully functional.

To insulate the heating system a layer of rockwool was placed over the heating tapes ensuring that the tapes or thermocouples did not slip out of place. Thereafter an insulating blanket was then place over the rockwool and secured ensuring that no rockwool was left exposed. Specially manufactured insulating jackets were used to insulate the endwall and buffer section as easy access to these areas is needed for changing the diaphragms and cleaning the tube.

The heating system of the manifold and mixing tanks has been outlined previously and

(a) Shock tube mount

(b) Initial alignment of the shock tube

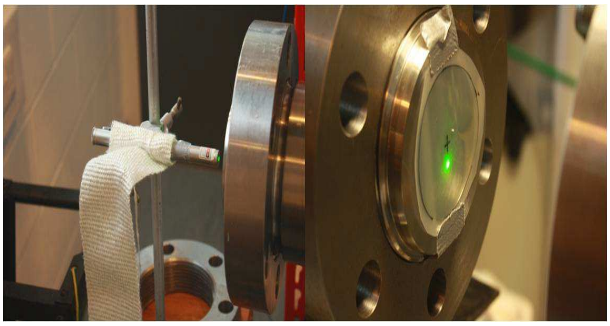

(c) Alignment of the shock tube

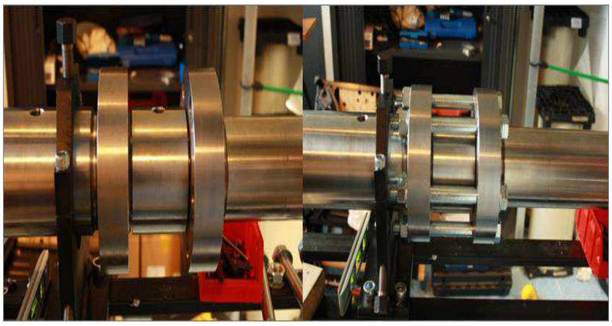

(d) Tube connection piece

Figure 4.12: Installation of the new high pressure shock tube.

remains unmodified.

Data Acquisition System

Six pressure transducers (PCB 1128A) are mounted along the diagnostic section of the tube flush to the internal wall at distances of 1, 15, 43, 61, 102.5 and 258.5 cm from the endwall. The signals from these pressure transducers were amplified by a signal conditioner (PCB 428) and then relayed to an oscilloscope (TiePie Handyscope HS4 oscilloscope). These transducers record the movement of the shock front in the tube and hence can be used to calculate shock velocities.

The ignition delay time is defined as the time between the arrival of the shock wave at the endwall and the rise in pressure due to the ignition of the fuel. The pressure transducer (Kistler 603B) mounted in the endwall was used exclusively to capture the arrival of the shock wave at the endwall and to measure ignition delay times. The signal from this pressure transducer was amplified by a signal conditioner (Kistler 5018) and was then sent to an oscilloscope (TiePie Handyscope HS4 oscilloscope) where the ignition delay time can be measured.

There was also the possibility of using optical detection methods as a window can be easily inserted into the tube via one of the numerous ports in the diagnostic section. However for this study this was not necessary as experiments were carried out at high-pressure. The pressure rise due to ignition was sufficient to determine the ignition delay time.

All pressure traces are displayed on a PC using oscilloscope software (TiePie Multichannel Software). All raw data can then be then exported to a program, which was built in-house. Using the shock velocity, the reflected shock pressure and temperature are calculated. This program also allows the user to measure ignition delay time and shock attenuation. A print out gives all

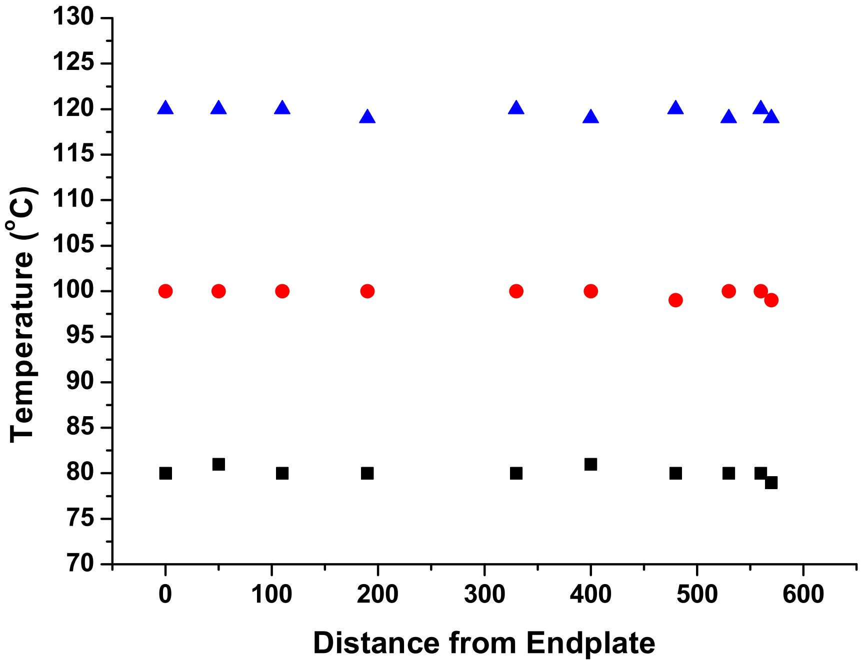

Figure 4.13: Heating profile of high pressure shock tube at ■ – 80°C, ● – 100°C, ▲ – 120°C.

relevant information.

Validation of High-Pressure Shock Tube

The newly installed high-pressure shock tube was validated against data obtained previously in the intermediate-pressure shock tube and data from literature [83,84]. Ignition delay times were obtained for mixtures of 1.8% *n*-heptane diluted in air at a reflected shock pressures between 10 and 13 atm at an equivalence ratio of $\phi = 1.0$. Experiments were carried out over a large reflected shock wave temperature range, 670 – 1430 K. In this temperature range NTC behaviour was observed. The data obtained in the validation of this shock tube was in good agreement with the data obtained in the validation of the intermediate-pressure shock tube and data in the literature, Fig. 4.14.

Gas Mixture Preparation

For all experiments carried out using this shock tube gas mixtures were prepared via direct injection of the liquid fuel into the evacuated mixing tank. This procedure has been outlined previously.

For high-pressure experiments it was, on occasion, necessary to prepare test gas mixtures in the shock tube. This was due a limit in the operating pressure of the mixing tanks, approximately 2000 Torr. Gas mixtures were prepared in the tube in a similar way to that used when preparing mixtures via direct injection of the fuel into the mixing tank. Such procedures are limited by the vapour pressure of the fuel and the maximum working pressure of the pressure gauges.

Firstly the shock tube and the mixing tank were evacuated until sufficiently low vacuum was reached, approximately 0.02 Torr. The tap to the vacuum pump was closed at this stage and the fuel was injected into the mixing tank and allowed to flow into the shock tube. The manifold was then evacuated roughly, approximately 1 Torr. The tap to the vacuum pump was then closed

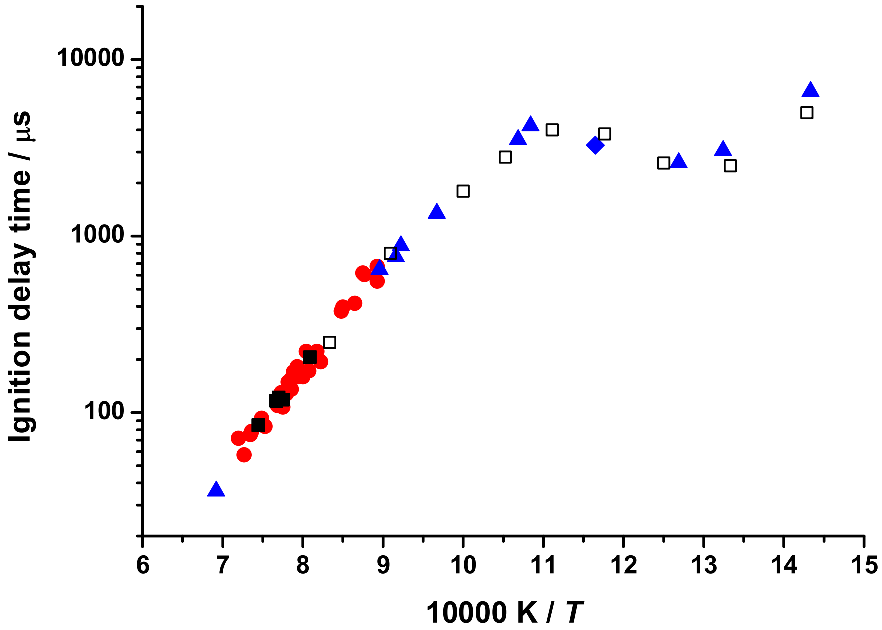

Figure 4.14: Validation of the new high-pressure shock tube using *n*-heptane diluted in air reflected shock pressure between 10 and 13 atm at an equivalence ratio of ϕ=1.0. ■ – Davidson et al. [83], □ – Heufer et al. [84] ● – previous validation, ▲ – current validation.

and oxygen was then allowed to flow into the manifold. The manifold was charged to a greater pressure of than the pressure of the fuel in the shock tube. The desired pressure of oxygen was then added. The same procedure was followed for the addition of nitrogen.

Gas mixtures made in the shock tube were allowed to mix for a longer time that those prepared in the mixing tanks. Typically for mixtures prepared in the mixing tanks a preferred mixing time of two hours was observed. It was found that mixtures which were prepared in the shock tube were subject to slow diffusion due to the long length and small diameter of the shock tube, hence it was preferable to leave such mixtures overnight in order to ensure a homogeneous gas mixture.

Diaphragms and Diaphragm Rupturing Mechanism

The high-pressure shock tube used in this study incorporates a double diaphragm system. Two diaphragms of similar or differing thicknesses may be used. For all experiments carried out in this shock tube aluminium diaphragms only were used. Aluminium of high purity and a number of thicknesses was obtained. Diaphragms were cut in-house by means of a hydraulic press. This press cuts the outline of the diaphragm and also places a cross shaped score in its centre. The depth of the score can be varied by use of a number of different spacers, each of varying thickness, which are easily interchangeable. The combination of material thickness and score depth allows for easy variation of the shock wave strength as the driver pressure can be controlled.

The aluminium used for this purpose is of high purity. It was found that new orders of the same thickness of aluminium with the same depth score did not always burst at an expected pressure due to small variation in the composition of the metal. For this reason new orders of aluminium were tested to ensure the correct spacer was being used to achieve a desired burst pressure.

The double diaphragm system used in this shock tube is similar to that used previously in the intermediate-pressure shock tube. Firstly the driver section and the section between the two diaphragms was brought to an intermediate-pressure. This area between the diaphragms was then closed and the driver section brought to the final pressure. The diaphragms were ruptured by a sudden change in pressure.

Experimental Procedure

The pre-experimental and experimental procedure for this shock tube is similar to that of the intermediate-pressure shock tube, differing only in the pre-experimental procedure. Prior to the experiment the conditions required to obtain a desired reflected shock pressure and temperature can be calculated using a predictive code written in-house by Dr. A. Heufer. Given the desired final conditions this code uses shock tube theory to calculate the required initial conditions. This also allows for the calculation of tailored interface conditions which allows for the realisation of longer ignition delay times.

Cleaning of the Shock Tube and Mixing Tanks

It was seen that in the intermediate-pressure shock tube, regular cleaning of the tube and mixing tanks was of vital importance. The same is also true of the high-pressure shock tube. Only aluminium diaphragms were used in this shock tube the hence plastic diaphragm particle adhering to the inner wall of the tube were no longer a concern. However due to the nature of the experiments carried out, i.e. high reflected shock wave pressure, low reflected shock wave temperature and large hydrocarbon fuels, a high degree of sooting still look place. Care was taken to clean the tube and mixing tanks on a regular basis as per the procedures outlined for the intermediate-pressure shock tube.

4.4 Rapid Compression Machine

The rapid compression machine (RCM) used in this study is a replica of the machine previously installed at NUI, Galway. This machine was originally built by Shell engineers and operated at the Thornton Research Centre until it was moved to NUI Galway in 1996 where it was re-commissioned and returned to full working order. This machine has been described in detail elsewhere [72]. The replica machine only differs for the original machine in its control mechanism. The original machine has to be operated manually, while its newer counterpart is automated.

The installation, heating and validation of the rapid compression machine was achieved though the combined effort of the group. I was directly involved in the heating of the mixing tanks, manifold and early heating of the chamber as described in this section. Validation work and modifications to the heating of the chamber were carried out by others in the group.

Description of Machine Used

The rapid compression machine used in this study is a twin opposed piston system. The two identical units comprise of a piston sleeve and piston, hydraulic control section and driving section with a central combustion chamber, Fig. 4.15.

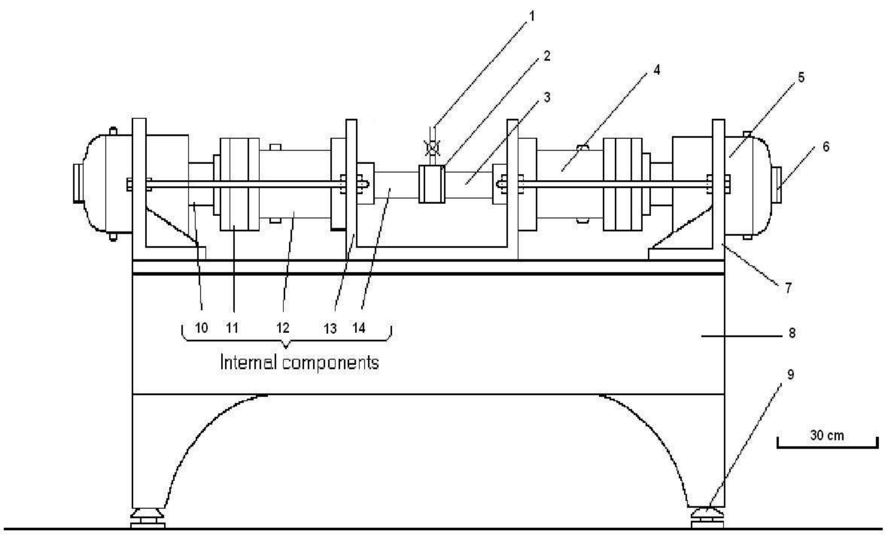

Figure 4.15: Schematic of rapid compression machine.
1.) chamber inlet 2.) reaction chamber 3.) sleeve 4.) hydraulic chamber 5.) drive chamber 6.) piston position sensor 7.) drive chamber bracket 8.) machine bed 9.) cushioned feet 10.) driving piston 11.) rear gland assembly 12.) speed control 13.) front gland assembly and stopping block 14.) compression piston.

The hydraulic section, Fig. 4.16, has three functions. Firstly, to hold the pistons in place before the start of compression. By applying the hydraulic lock to the retracted piston, sufficient pressure is applied to the piston assembly in this position to allow for the driving section to be pressurised. When the hydraulic lock is broken, by venting a small portion of the fluid from the hydraulic chamber, the driving pressure is no longer in balance with that of the pressure exerted by the hydraulic fluid and the piston assembly accelerates forward.

The second function of the hydraulic section is to control the speed of the piston. Motion of the piston results in displacement of fluid through the annular clearance between the control piston and speed control profile. Here excess fluid pressure acts on the front surface of the control piston to provide a thrust sufficient to maintain constant piston velocity.

The final function of the hydraulic section is to bring the piston to rest. This is achieved by a stopping ring in the stopping groove. Precisely machined clearances between the ring and the groove allow for the progressive venting of the compressed fluid at a rate such that roughly uniform deceleration is achieved. In the final stage the decelerating force and piston velocity are reduced to zero so that the piston stops without rebound.

The driving sections are located to the extreme left and right of the machine. These sections have two functions; firstly to allow the pistons to retract at the beginning of an experiment. Secondly to allow for the addition of compressed air which is used to drive the pistons forward during experiments.

Connecting the two units are piston sleeves with a central reaction chamber where the pre-mixed test charge is loaded. This chamber is equipped with a pressure transducer (Kistler 603B) to measure the pressure history in the chamber.

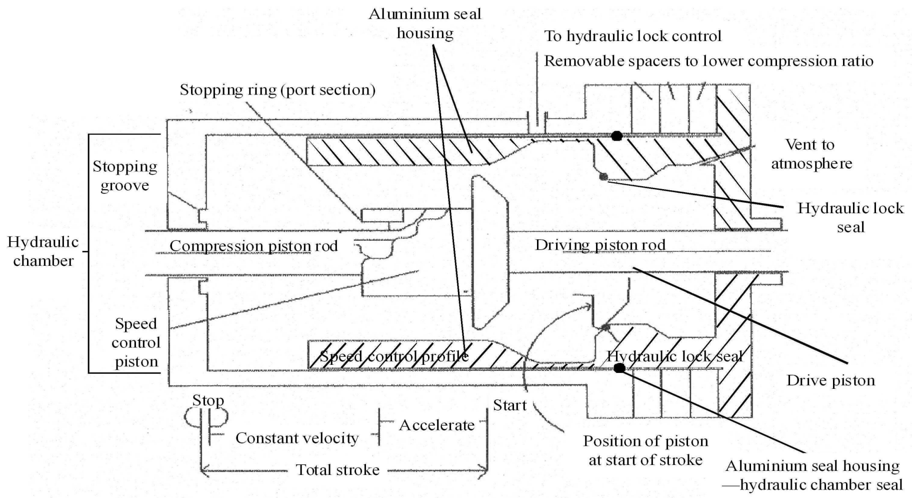

Figure 4.16: Schematic of rear gland assembly.

Installation of the Manifold

The manifold consists of eight needle valve taps; four upper taps, two lower taps and two horizontal taps. The first upper tap, tap 1, Fig. 4.17, is connected via a four way junction to the oxygen and diluent gas cylinders. The second upper tap, tap 2, Fig. 4.17, is connected to a vacuum gauge (BOC Penning 8). This is used to ensure that an appropriate vacuum is achieved prior to mixture preparation or carrying out experiments. The third upper tap, tap 3, Fig. 4.17, is idle at present but can be fitted with a pressure gauge in the future if required or can also be used for the addition of extra diluents such a carbon dioxide. The fourth and final upper tap, tap 4, Fig. 4.17, is connected to a pressure gauge (MKS Instruments) capable of measuring pressures up to 5000 Torr, which is in turn connected to a digital pressure readout (MKS PR4000B). This pressure gauge has a number of functions. It is used to measure the pressure inside the manifold during experiments and also to measure the pressure of fuel, oxygen and diluent gases during gas mixture preparation.

The right hand lower tap, tap 6, Fig. 4.17, is connected to a vacuum pump (Edwards RV5) which is used to evacuate the manifold and reaction chamber when necessary. The other lower tap, tap 7, Fig. 4.17, is connected via a long horizontal stainless steel tube containing four Swagelok VCR junctions. The stainless steel connector is held in place using a stainless steel clamp. The stainless steel four junction tube is connected to the mixing tanks at each junction. The junctions are held in place using stainless steel clamps and viton o-rings ensures a sufficient seal is created. Currently attached to the four junction stainless steel tube are two 35 L stainless steel mixing tanks with injection ports, with the possibility of adding two more tanks if necessary. The horizontal tap on the left, tap 5, Fig. 4.17, is connected between the manifold and a horizontal glass finger to control the volume of fuel that enters the mixing tank from the finger upon preparation of the fuel mixture. Fuel samples that are provided in the gaseous state (*n*-butane, *iso*-butane, etc.) can be attached via a Swagelok VCR junction. The second horizontal tap on the left, tap 8, Fig. 4.17, allows for the manifold to be isolated from the combustion chamber.

This setup allows for the addition of fuel via three methods: cold finger method, direct injection through the injection port on top of the mixing chamber and direct addition of already gaseous fuel samples.

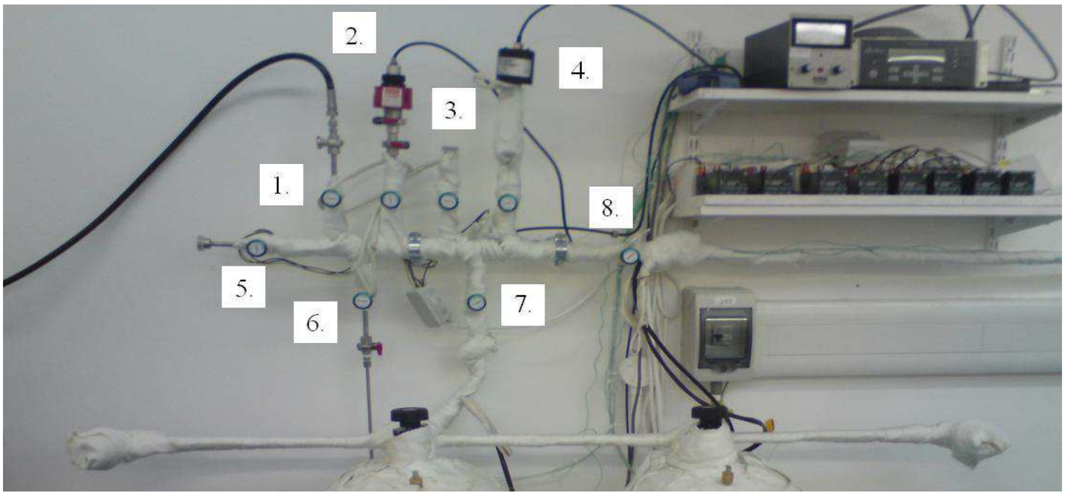

Figure 4.17: RCM manifold

Heating of the Manifold and Mixing Tanks

Due to the low vapour pressure of the fuels studied in this project it was necessary to design and install a heating system that maintains the temperature of the system above the saturation vapour pressure of the fuel. A heating system was designed and installed on the manifold and mixing tanks of the RCM.

Sixteen type K thermocouples were attached to the manifold using aluminium foil tape at various locations. Following this heating tapes (Flexelec RVI, 1250 W) were wrapped around the manifold. Care was taken to ensure that all surfaces were covered fully. The thermocouples were connected to both heating tapes via a temperature controller (Cal 9900 thermostat) and a thermocouple data logger (Pico TC-08 USB) which in turn was connected to a PC. The heating tapes were connected in duplicate to one thermocouple via the thermostat while another thermocouple (located under one of these tapes) was connected to the data logger, meaning that in essence two thermocouples were required to control and measure the temperature of two heating tapes.

The mixing tanks were heated in the same manner as the manifold with the exception that each tank was placed on top of a stirring mantle to ensure homogeneous mixing of the test gases. The top and side walls of the tank were heated as described above, the bottom of the tank was heated using a single heating tape (Flexelec RVI, 1250 W). This heating tape was placed under the tank and covered with insulation tape (Zetex 1000). These heating tapes were also connected in duplicate as described for the manifold.

Heating of Chamber and Piston Sleeves

When carrying out experiments in the rapid compression machine the initial temperature of the test gas mixture is varied to investigate the ignition behaviour of the fuel over a range of compressed temperatures. For this reason the reaction chamber and its connecting sleeves must be heated, not only to ensure that the fuel remains in the gaseous phase, but also to vary the initial temperature of the experiment. The design of the heating system for the chamber and piston sleeves has been improved a number of times during the course of this study. Each improvement was carried out in order to improve the temperature homogeneity of the system.

First Heating System

The initial heating system installed on the chamber and piston sleeves consisted of one type J thermocouple which was attached to the outside of the reaction chamber with aluminium foil tape. The chamber and sleeves were then covered with one 5 m heating tape (Flexelec RVI, 1250 W) and this in turn was covered with insulation tape (Zetex 1000). A thermometer was placed again in a specific location which could read the external temperature of the chamber. The thermocouple and heating tape were connected to a temperature controller (Cal 9900 thermostat) which was capable of heating the system to approximately 200°C. In order to avoid damage to the transducer and the chamber tap temperatures did not exceed 130°C. This system resulted in an uneven temperature distribution as only one heating tape was used throughout the entire system.

Second Heating System

To attain a more homogeneous temperature profile the heating system was updated greatly. Previously, the sleeves and chamber of the RCM were heated with one 5 m Flexelec (Flexelec RVI, 1250 W) heating tape. This was found to create an inhomogeneous temperature profile. Due to heat loss the temperature was much lower at the face of the piston heads, Fig. 4.18. The new heating system consisted of each individual sleeve and the chamber being wrapped in an individual heating tape. In total three 1 m heating tapes (Flexelec RVI, 1250 W) were used. Each heating tape was controlled by an individual temperature controller and thermocouple. The heating tapes were then covered with insulation tape (Zetex 1000). This heating system allowed for more controlled heating of the chamber and piston sleeves. While the temperature distribution was much improved the problem of a much lower temperature at the face of the pistons still remained.

Third Heating System

In order to overcome the problem of heat loss to the pistons new sleeves were designed and manufactured each to house six cartridge heaters (Hotset HHP 6.5 mm). This new design was incorporated into the pre-existing heating system. Each of the two sets of six cartridge heaters were controlled by an individual temperature controller and thermocouple. Figure 4.18 is a plot of two temperature profiles at various distances from the face of the piston, one without cartridge heaters and one with cartridge heaters. It can be seen that, by incorporating the cartridge heaters into the heating system design, there is greater heat conductivity to the piston heads and a more homogeneous heating of the sleeves and chamber.

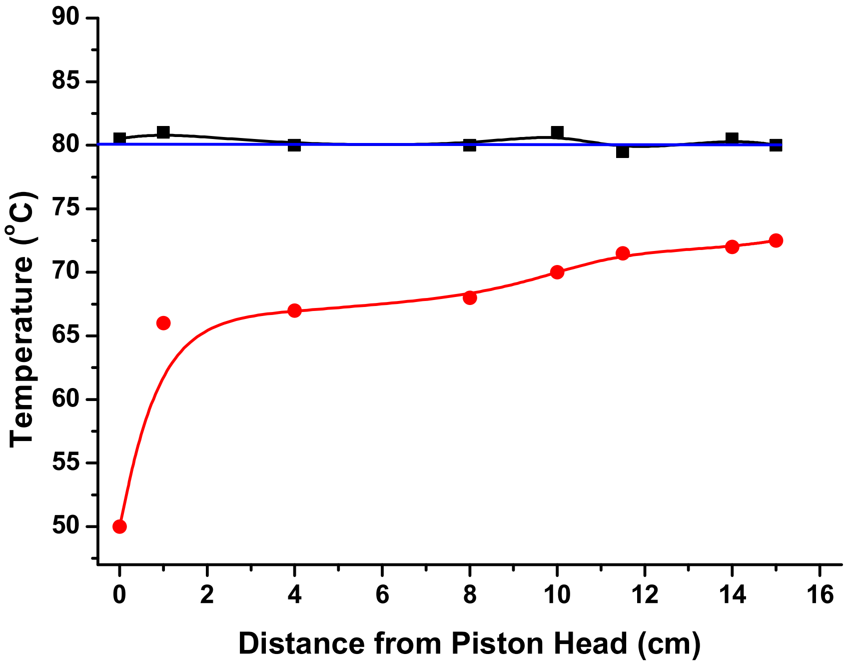

Figure 4.18: Temperature profiles obtained by new and old heating systems in the setting temperature of 80°C. ● – previous heating system with heating tapes only ■ – new heating system with cartridge heaters, —— – temperature controller setting.

Validation of Rapid Compression Machine

Extensive validation of the RCM was carried out using n-butane at a compressed pressure of 20 atm and at $\phi = 0.5$ in air over the temperature range 670 – 1000 K. Argon and nitrogen gases were used as diluents in a number of compositions, argon being used for higher compressed temperatures and nitrogen being used for lower temperatures. The results obtained were compared to results which had been previously obtained on the original rapid compression machine and were found to be in good agreement, see Fig. 4.19.

Calculation of Compression Ratio

To calculate the compression ratio a stainless steel bulb with a known volume of 300 cm^3, V_b, was attached to the manifold via one of the vertical inlets. The bulb was filled to a known pressure with nitrogen, p_i, and the valve on the bulb was closed and the manifold was evacuated. The tap leading to the reaction chamber was closed and the vacuum pump was isolated. The contents of the bulb were then expanded into the manifold. The final pressure, p_f, was recorded after approximately 30 seconds and the pressure was recorded. The procedure was repeated by simply expanding the nitrogen gas from the bulb and manifold into the line leading to the reaction chamber while keeping the reaction chamber tap closed. The volume of the manifold and line could then be calculated separately using the equation:

$$p_i V_b = p_f V_b \tag{4.1}$$

The above steps were repeated a number of times for both the manifold and line to ensure all the calculated volumes were reproducible at varying initial pressures. The procedure was used with the tap leading to the reaction chamber open and with the pistons in the pre-fired position

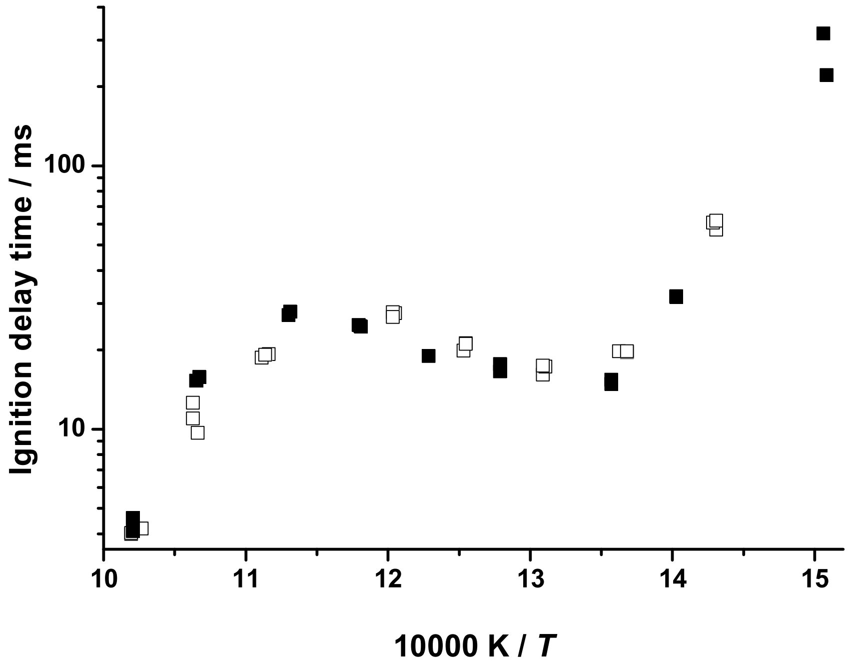

Figure 4.19: Rapid compression machine validation, n-butane, ϕ = 0.5, 20 atm. ■ – old RCM, □ – new RCM.

and in the compressed position. Knowing the volume of both the manifold and line connecting the manifold to the reaction chamber from the initial volume and pressure in the bulb, the volume of the reaction chamber with the pistons in the pre-fired and compressed positions was calculated using Formula 4.1. The compression ratio, CR, the ratio of the pre-fired volume to the fired volume, was calculated. Through out this study two differing sets of piston heads were used. These piston heads have a compression ratio of approximately 10 and 12.

Perfluoropropane

Tests were carried out on the new and original rapid compression machines to compare their compression ratios and their ability to maintain a constant pressure at full compression to ensure that there are no leaks in the system even when there is a high compressed pressure charge present in the chamber. The chamber was charged with 500 mbar of perfluoropropane (γ = C_p / C_v = 1.06) and a compression experiment was performed. When a gas with a $\gamma \approx 1$ is compressed there is negligible adiabatic heating and any pressure changes are solely caused by the mechanical compression. Both RCMs maintain a constant pressure after full compression with a less than 10% pressure drop recorded on both machines after 100 ms. Figure 4.20 shows a typical trace from a perfluoropropane and nitrogen compression, the perfluoropropane pressure trace has been scaled to reach the same compressed pressure as the nitrogen experiment. Note the nearly constant pressure of perfluoropropane after compression. In this experiment the drop in pressure after 100 ms is 8.2% indicating that the machine is holding pressure well. Nitrogen ($\gamma \approx 1.4$) results in a much greater pressure drop after compression, 27.9% after 100 ms.

It was found that the new RCM has a slightly lower compression ratio to that of the old one. This difference in compression ratio leads to a difference in the final pressure achieved in both machines, and can be attributed to a variation in the distance between the piston heads at full compression.

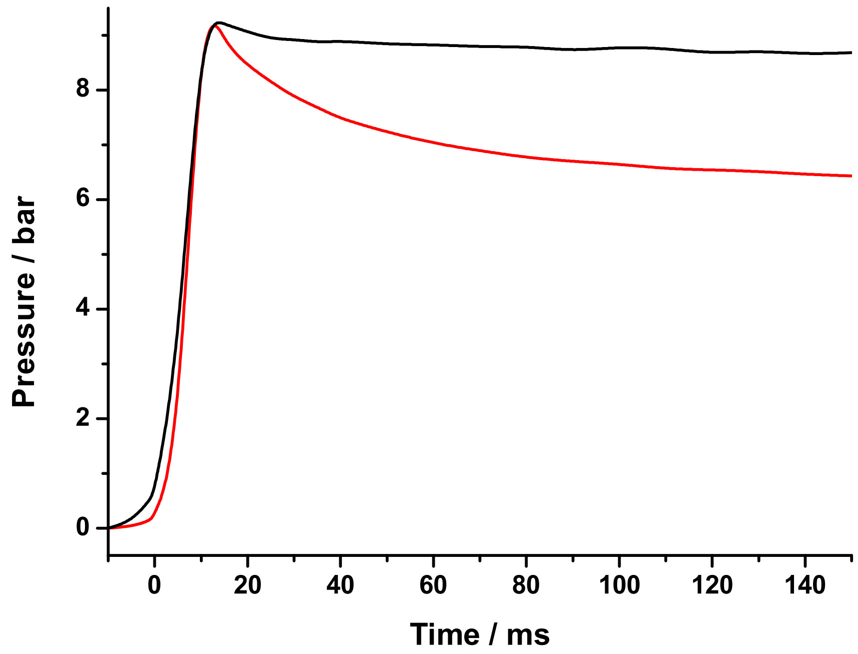

Figure 4.20: Typical nitrogen and perfluoropropane compressions carried out in the rapid compression machine. —— Perfluoropropane, —— Nitrogen.

Cleaning of the Rapid Compression Machine

Due to the high sooting nature of the fuels used it in this study it was of vital importance that the chamber, piston sleeves and piston heads be removed and cleaned on a regular basis.

To clean the RCM firstly the insulation and heating tapes of the heating system were removed, the cartridge heaters need not be removed from the sleeves. Next the pistons were retracted and the hydraulic lock applied. Thereafter the chamber and sleeves were removed and set aside. The pistons were then brought forward so that the piston heads and o-rings could be removed. All parts were cleaned thoroughly using ethanol and lint free cloth. At this stage the various components of the machine were also inspected for any damage. Piston head seals were also replaced.

Once cleaned the various components of the rapid compression machine were replaced. Firstly the piston head and new seals were replaced. When the grub nuts have been tightened the pistons were retracted. When the hydraulic lock had been applied the sleeves were replaced followed by the reaction chamber and all parts bolted into place and the heating system replaced.

Gas Mixture Preparation

The method used for the preparation of test gas mixtures was similar to that used in the intermediate- and high-pressure shock tubes. The low vapour pressure fuel used in this study was injected directly into a heated, evacuated mixing tank, via an injection port, using a gas tight syringe. The required pressures of oxygen and diluent or diluents were then added as per the procedure outline previously.

RCM experiments by their nature involve heat losses. During compression the test gas is heated to a temperature much greater than the initial temperature of the gas. The temperature distribution after compression is not entirely homogeneous as a cooler boundary layer exist between the hot core gas and the walls of the chamber. After some time this heat will dissipate from the hot core thought the boundary layer to the even cooler walls. These heat losses influence the ignition delay time of the test mixture and as a result should be accounted for if the data is to be successfully simulated. Therefore a series of non-reactive experiments were carried out. Non-reactive gas mixtures were prepared by substituting oxygen in the mixture for the diluent gas being used. Experiments were carried out in same manner as to those with the reactive fuel mixtures. Only pressure rise due to compression of the gas was observed for experiments carried out with non-reactive fuel mixtures.

Experimental Procedure

Pre-experimental procedure:

- Check that the extraction fan is on and running.
- Ensure that the chamber and piston heads have been cleaned and that the piston seals have been replaced.
- Turn on the power at the wall.
- Ensure that the pressure line valve is open. If not open slowly until the gauge reads 140 psi.
- Check oil level in hydraulic reservoir, top-up if required.
- Turn on the vacuum pumps.
- Turn on the heating system on the manifold and tanks ensuring that the temperature is sufficiently high to ensure no condensation of the fuel occurs.
- Turn on the heating system on the chamber and sleeves. Ensure that the heating system is set to the required temperature.
- Replace the septum on the mixing tank if necessary.

To carry out an experiment:

- Open the reaction chamber to the vacuum pump and evacuate.
- Set the drive pressure to the required value by turning the "Drive Pressure" knob.
- Retract the pistons by pressing Retraction/Vacuum button. When the pistons are fully retracted the "Locking Pressure" button will light up indicating that you should now proceed to the next step.
- After retracting the pistons the hydraulic lock should now be applied by pressing the illuminated "Locking Pressure" button. When the system is pressurised the "Drive Pressure" button will light up.
- Pressurise the drive chamber by pressing the illuminated "Drive Pressure" button.
- Charge the evacuated chamber with the test gas and close the tap to the chamber
- Confirm that the test mixture is in the combustion chamber by turning the "Confirm Test Gas" key.

- Ready the oscilloscope and note the initial temperature of the experiment.
- When the driving pressure has been reached the machine can be fired. This is achieved by pressing the flashing "Initiate" button.
- Open the tap to the chamber and evacuate the exhaust gas through the manifold. The machine will automatically reset and will proceed to the first step in preparation for the next experiment.
- Note the ignition delay time and piston timing.

Shutting down:

- Turn off thr heating system on the manifold, mixing tanks and reaction chamber.
- Close the tap to the vacuum pump on the manifold. Turn off both vacuum pumps.
- Turn off the main power at the wall.
- Close the pressure line valve.

Determination of Ignition Delay Time

The ignition delay time is defined as the time between the end of compression and the ignition of the fuel as seen by a sharp rise in pressure. Mounted flush to the internal wall of the combustion chamber is a pressure transducer (Kistler 603B). The electrical signal produced by the transducer due to the rise in pressure in the chamber is sent to a signal conditioner (Kistler 5018) and is then in turn relayed to an oscilloscope (Picoscope PC oscilloscope) where a pressure trace is recorded. The ignition delay time is measured directly from the oscilloscope. Figure 4.23 is a typical trace obtained in an RCM experiment. The initial pressure rise due to compression can be clearly seen as can the pressure rise due to ignition of the fuel.

For the rapid compression machine used in this study the shortest measurable ignition delay times are in the region of $4 - 5$ ms.

Piston Timing

It was also possible to measure the piston timing using the oscilloscope. Mounted in each section of the rapid compression machine are displacement sensors. The displacement sensors capture the movement of the pistons and relay the signal to an oscilloscope. The difference in the timing of the motion of the pistons relative to each other can be read directly from the oscilloscope. While carrying out a set of experiments it was important that the difference in the timing of the pistons be as small as possible. It was desirable that the difference in the timing of the two pistons be no more than 1 ms. However some drift of this timing was observed over the course of a set of experiments. The timing can be easily adjusted by controlling the amount of oil allowed into the hydraulic section of the machine. Two needle valves located on the top left and top right of the machine can be adjusted when required and the motion of the pistons relative to one another can be easily controlled.

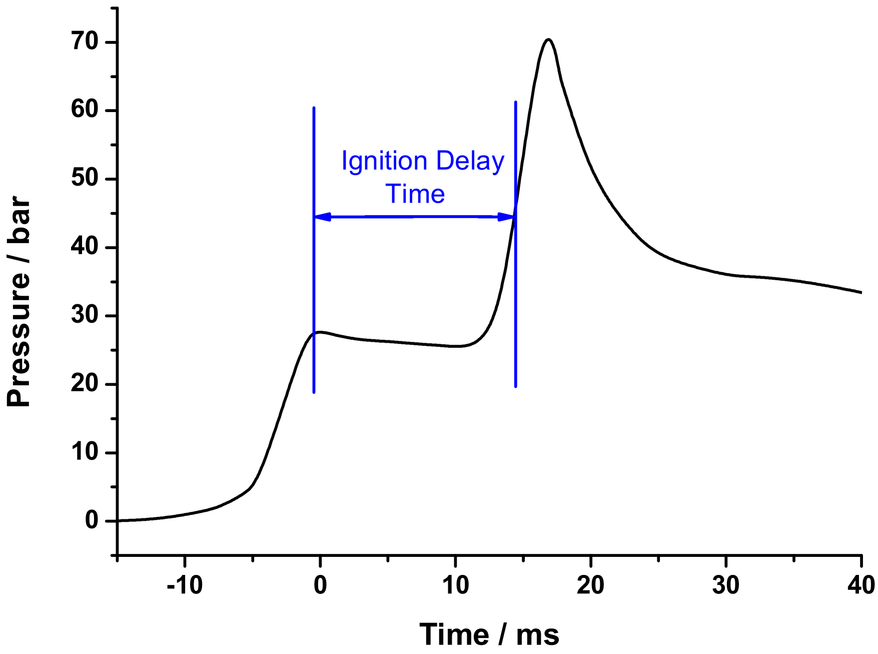

Figure 4.21: Typical pressure trace obtained for an n-butylcyclohexane, $\phi = 2.0$, RCM experiment in air, 50% nitrogen, 50% carbon dioxide diluent, $p_i = 1.626$ bar, $T_i = 115°$C resulting in a compressed pressure of 30 atm.

Determination of Compressed Pressure and Temperature

From the recorded pressure trace in an experiment the pressure rise in the chamber due to compression can be measured. The compressed pressure, p_c, of the gas can be easily calculated by adding the initial pressure, p_i, to the measured change in pressure.

Knowing the composition of the test gas, the initial temperature of the chamber, T_i, the initial pressure of the gas charge, p_i, and the compressed pressure of the gas, p_c, the compressed temperature, T_c, of the gas can be calculated using adiabatic compression/expansion and frozen chemistry in GasEq [80]. GasEq uses the temperature dependence of the ratios of specific heats, γ, according to the following equation;

$$ln\left(\frac{p_c}{p_i}\right) = \int_{T_i}^{T_c} \frac{\gamma}{\gamma - 1} \frac{dT}{T} \tag{4.2}$$

Use of Various Diluents

Throughout this study a number of diluent gases and diluent gas mixtures were used. The majority of the work was carried out in nitrogen and mixtures of nitrogen and carbon dioxide. Due to the high reactivity of the fuels used in this study it was not possible to perform experiments in mixtures containing high percentages of argon as it was found that ignition occurred on compression although some high-temperature experiments were carried out with low concentrations of argon in nitrogen. Various diluents were used in order to reach desired compressed temperatures.

Modifications Made to Rapid Compression Machine

High-Pressure Combustion Chamber

In order to carry out experiments at higher compressed pressures a new combustion chamber was designed and manufactured. It was found that in the previous chamber design the tap which was used was not capable of withstanding peak combustion pressures of approximately 60 bar. At such pressures the o-ring sealing of the tap would fail and result in a loss of pressure from the chamber. This was sufficient for 30 atm experiments carried out under fuel lean conditions, but under rich conditions ignition pressures were found to be in the range of 80 – 90 atm.

In order to overcome this problem a chamber with an improved tap was design was manufactured. This stainless steel tap can withstand greater ignition pressures thus allowing for high-pressure experiments to be carried out safely.

New Piston Head Design

In order to obtain higher compressed temperatures without the use of high concentrations of argon new piston heads were designed and manufactured. Figure 4.22 is a schematic of both set of pistons heads used in this study. The piston heads which were previously used in the RCM have a total length of 9 cm and achieve a compression ratio of approximately 10 when tested with pure nitrogen. The new piston heads have a total length of 16 cm and achieve a compression ratio of approximately 12 when tested with pure nitrogen.

These new piston heads were used mainly for higher temperature experiments where nitrogen diluent was used where traditionally the lower compression ratio piston heads would have been used with a large percentage of argon as a diluent. The new higher compression ratio piston heads also allow for a lower initial pressures of fuel / diluent charge hence reducing the likelihood of fuel condensation in the combustion chamber.

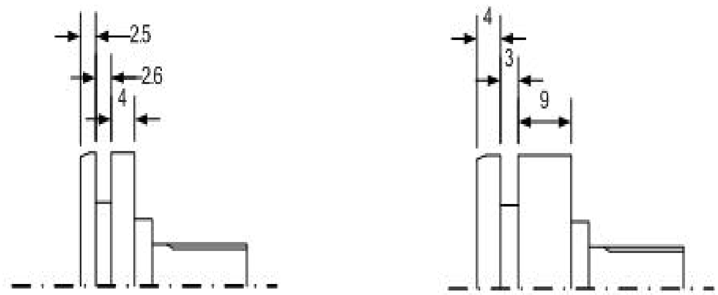

(a) Old piston heads

(b) New piston heads

Figure 4.22: Rapid compression machine piston heads, all dimensions in mm.

4.5 Infrared Laser Absorption System

Background

In order to determine if fuel condensation occurred while experiments were being carried out in the RCM an infrared test cell was installed and validated. The laser absorption system at NUIG was based upon the work of Mével *et al.* [81], who measured the gas phase absorption cross section of twenty-one hydrocarbons using infrared light at 3.39 μm in the temperature range 303 –

413 K. The results of their study demonstrated that the absorption cross sections are temperature independent in the range studied and that the aromatic and substituted hydrocarbons exhibit much smaller cross sections than n-alkanes with an identical number of C—H bonds.

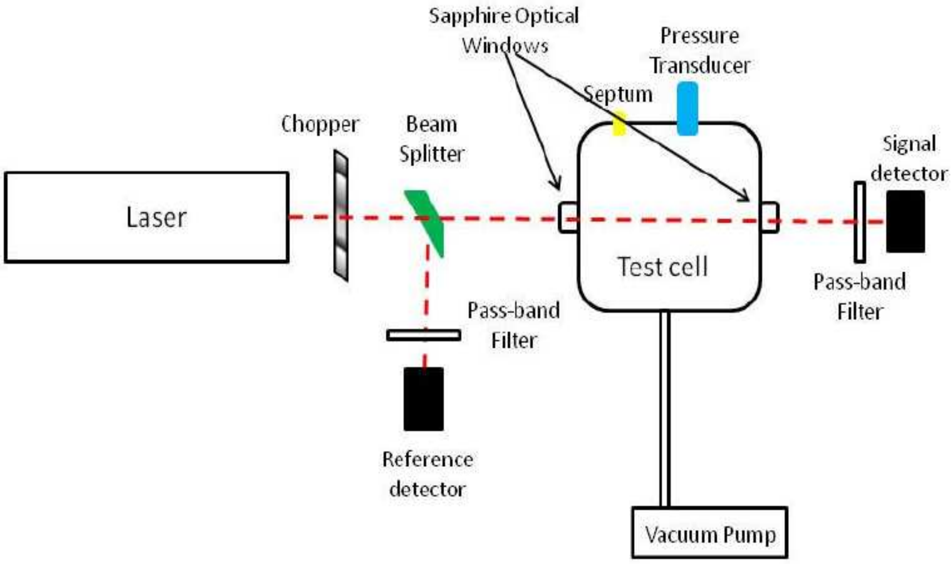

Figure 4.23: Schematic of infrared test cell.

Experimental Set Up

The experimental apparatus consists of a 3.39 μm infrared radiation source (2mW He-Ne laser ThorLabs H339P2). The detectors used in this set up can not detect a steady signal hence a signal chopper (ThorLabs optical chopper system with MC1F10 blade) operating at 300 Hz was used to create an on-off signal. A beam splitter (ThorLabs CM1-BP145B4) was used to send one half of the beam to a reference detector (ThorLabs PDA20H-EC) while the other half was passed through the 10.16 cm long test cell. A second detector (ThorLabs PDA20H-EC) measures the intensity of the beam which has been passed thought the test cell. Pass band filters (LASER2000, CW = 3400 nm, FWHM = 68nm) fitted just before the detectors select the wavelength at which the infrared radiation interacts with the C—H bond absorption line.

The test cell is equipped with two sapphire windows, septum and pressure transducer. Both the test cell and line were heated and insulated in the same way as the RCM and shock tube. Two temperature controllers ensure a homogeneous temperature within the cell. Prior to carrying out measurements the test cell was evacuated and the initial signal intensities recorded. The liquid fuel was then injected into the cell via the septum and the pressure and signal intensities recorded. The fuel concentration can be calculated assuming ideal gas behaviour.

The ratio of the incident intensity, I^0, to the transmitted intensity, I, at a given frequency, ν, can be related to the concentration of the fuel, C_{fuel}, using the Beer-Lambert Law;

$$I = I^0 \exp(-L.C_{fuel}.\sigma_\nu) \tag{4.3}$$

where L is the path length and σ is the absorption cross section at frequency ν. A reference detector was used and hence the absorption can be expressed as;

$$\sigma_\nu = \frac{1}{L.C_{fuel}} \ln\left(\frac{I_{sig} I^0_{ref}}{I_{det} I^0_{sig}}\right) \tag{4.4}$$

where *sig* and *ref* refer to the signal and reference, respectively. The absorption cross section corresponds to the slope of;

$$-\frac{A}{L} = f(C_{fuel}) \tag{4.5}$$

where A is;

$$A = \ln\left(\frac{I_{sig} I^0_{ref}}{I_{det} I^0_{sig}}\right) \tag{4.6}$$

Operation of the Infrared Absorption System

- Turn on the heating system and set to the required temperature.
- Open the lens of the laser. A small-flat head screwdriver is required for this.
- Turn on the He-Ne laser on approximately 15 minutes prior to carrying out tests. This is give the laser adequate time to heat up.
- Ensure that the vacuum pump, chopper and detectors are turned on.
- Open the test cell to the vacuum, or chamber for in-situ tests, and allow to vacuum. Ensure that there are no leaks present.
- Load the standard settings onto the oscilloscope and set to run.
- Ensure that a steady signal is being realised on the oscilloscope and the difference between the reference and signal outputs are consistent. Record the signal intensities for this condition.
- Fill the test cell. Record the pressure and the signal intensities from the oscilloscope.
- Vacuum the test cell and repeat with varying pressures of fuel, recording pressures and signal intensities.
- To shut down turn off all equipment ensure that the lens cover of the laser is closed.

Validation

Validation of the infrared test cell was carried using *n*-pentane and *n*-propylbenzene. Signal intensities were measured at a variety of temperatures and using a number of initial pressures of fuel. These *n*-pentane results were compared to those of Mével *et al.* [81], Fig 4.24. It can be seen that good agreement was observed between the results in the literature and the results recorded in our test cell.

In addition to *n*-pentane, test cell measurements were also carried out using *n*-propylbenzene, using a number of fuel concentrations at 338 K. As before results were compared to those of Mével *et al.* [81], Fig 4.25. Good agreement was observed between the two sets of data.

Test cell and in-situ RCM tests were carried out for *n*-butylcyclohexane. These results will be discussed in Section 5.4.

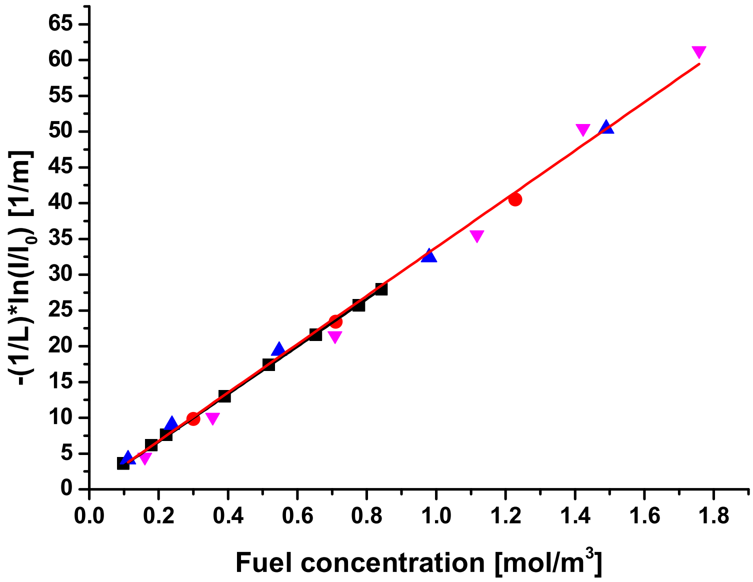

Figure 4.24: Results obtained from n-pentane validation of infrared absorption system. ■ – Mével *et al.*, ● – 273 K, ▲ – 323 K, ▼ – 338 K. Mével *et al.* y = 33.26x, R^2 = 0.999, NUI Galway y = 33.82x, R^2 = 0.998.

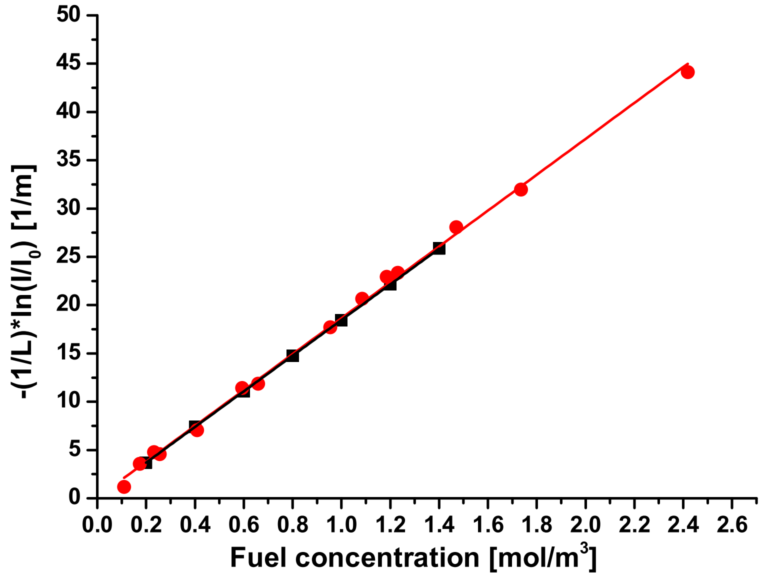

Figure 4.25: Results obtained from n-propylbenzene validation of infrared absorption system. ■ – Mével *et al.*, ● – 338 K. Mével *et al.* y = 18.46x, R^2 = 1, NUI Galway y = 18.57x, R^2 = 0.998.

.

Chapter 5

n-Butylcyclohexane Ignition Delay Time Study

This work was carried out using heated high-pressure shock tubes and a heated rapid compression machine. *n*-Butylcyclohexane (99%) was supplied by TCI. Oxygen (99.99%), nitrogen (99.95%) and helium (99.99%) gases were supplied by BOC. All reagents were used without further purification. Gas mixtures were prepared as per the procedure for direct fuel injection outlined previously for the high-pressure shock tube, Section 4.2, and the rapid compression machine, Section 4.4. Mixture compositions are provided in Table 5.1.

ϕ	*n*-Butylcyclohexane	Oxygen	Nitrogen
0.3	1.0	50.0	188.09
0.5	1.0	30.0	112.86
1.0	1.0	15.0	56.43
2.0	1.0	7.5	28.21

Table 5.1: Composition of *n*-butylcyclohexane / air gas mixtures.

5.1 Shock Tube Study

n-Butylcyclohexane was studied in the intermediate-pressure (1, 10 and 30 atm) and high-pressure (low temperature 30 atm and 50 atm) shock tubes over a range of equivalence ratios and pressures. Experiments were carried out at equivalence ratios of 0.3, 0.5, 1.0 and 2.0 in air. Experiments were carried out as per the procedure outlined previously, Section 4.2. All gas mixtures were prepared via direct injection of the fuel into the mixing tank.

5.2 Rapid Compression Machine Study

To extend the temperature range of the data obtained experimentally in the shock tube, experiments were also carried out in the RCM at compressed pressures of 10 and 30 atm. Due to the limitations of the rapid compression machine experiments were not carried out at 1 atm. Reactive and non-reactive gas mixtures were prepared via direct injection of the fuel into the mixing tank.

5.3 Results and Discussion

5.3.1 Effect of Equivalence Ratio

1 atm

Ignition delay times were measured at a reflected shock pressure of 1 atm at equivalence ratios of 0.5, 1.0 and 2.0 in air in the temperature range 900 – 1820 K. Experiments were not carried out at an equivalence ratio of 0.3. Due to the low reflected shock pressure which these experiments were carried out at the pressure rise due to ignition was weak and ill-defined. Hence it was difficult to accurately determine the ignition delay time.

Given the experimental set up, recording reliable and reproducible data was extremely difficult at this pressure. This was due to a large signal to noise ratio which resulted in the timer counters not capturing the passing shock wave. Times, which were then used to calculate the shock velocity, were measured using the traces recorded on the oscilloscope. In addition, the pressure rise due to ignition was often very weak and not well defined, resulting in an inaccurate determination of the ignition delay time. At the higher reflected shock wave pressures of this study clearly defined pressure rises were observed. Unfiltered light emission was also used as a diagnostic. This was also unsuccessful as there was not sufficient light emitted to accurately measure ignition delay times. Experimental data which was obtained was sporadic with no clearly defined trend, Fig. 5.1.

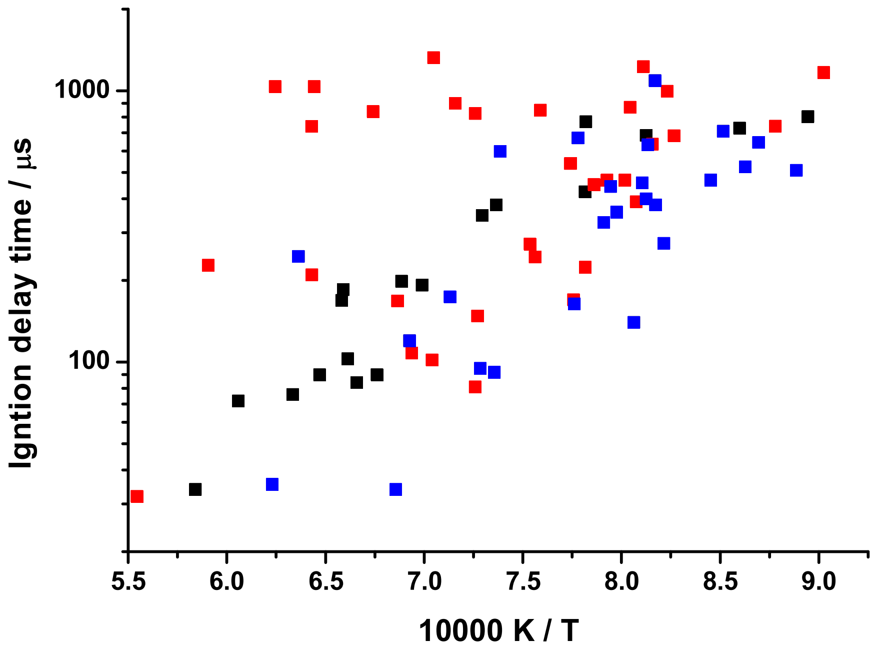

Figure 5.1: Effect of equivalence ratio on ignition delay time of *n*-butylcyclohexane in air at 1 atm, ▲ – ϕ = 0.5, ● – ϕ = 1.0, ■ – ϕ = 2.0.

10 atm

Ignition delay times were measured at a reflected shock pressure and compressed gas pressure of 10 atm at equivalence ratios of 0.3, 0.5, 1.0 and 2.0 in air in the temperature range 610 – 1530 K,

Fig. 5.2(a). Good agreement was observed between ignition delay times measured in the shock tube and those measured at lower temperatures in the RCM.

At higher temperatures (> 1250 K) fuel-lean mixtures were fastest to ignite and fuel-rich mixtures were slowest, while at lower temperatures fuel-rich mixtures were fastest and fuel-lean mixtures slowest to ignite. The reactivities of the equivalence ratios crossover at approximately 1200 K. In the temperature range studied in the RCM, 700 – 1000 K, *n*-butylcyclohexane exhibits a strong NTC behaviour.

It was found that there was little effect of equivalence ratio in the temperature range 1000 – 1450 K. At 1100 K the ignition delay times for the various equivalence ratios are: $\phi = 0.3$ – 648 μs, $\phi = 0.5$ – 606 μs, $\phi = 1.0$ – 516 μs, $\phi = 2.0$ – 446 μs, and so the ignition time decreases by 6.5% from $\phi = 0.3$ to 0.5, by 14.9% from $\phi = 0.5$ to 1.0 and 13.6% from $\phi = 1.0$ to 2.0, with a decrease in ignition delay time of 31.2% from $\phi = 0.3$ to 2.0.

In the NTC region the greatest effect of equivalence ratio was observed, which was centred at approximately 810 K. At this temperature the ignition delay times for the various equivalence ratios are: $\phi = 0.3$ – 30 ms, $\phi = 0.5$ – 11 ms, $\phi = 1.0$ – 3.6 ms, $\phi = 2.0$ – 1.9 ms. The ignition time decreased by 63.3% from $\phi = 0.3$ to 0.5, by 67.3% from $\phi = 0.5$ to 1.0 and 47.2% from $\phi = 1.0$ to 2.0, with a decrease in ignition delay time of 93.7% from $\phi = 0.3$ to 2.0.

At lower temperatures (625 – 700 K) there was a lesser effect of equivalence ratio observed and the ignition delay times again converge. At this temperature the ignition delay times for the various equivalence ratios are: $\phi = 0.5$ – 27.7 ms, $\phi = 1.0$ – 17.6 ms, $\phi = 2.0$ – 10 ms, and so the ignition time decreases by 36.5% from $\phi = 0.5$ to 1.0 and 43.2% from $\phi = 1.0$ to 2.0, with a decrease in ignition delay time of 63.9% from $\phi = 0.5$ to 2.0.

In order to carry out experiments in the rapid compression machine at compressed temperatures lower then 730 K at $\phi = 0.3$ and a compressed pressure of 10 atm a considerable portion of the diluent gas (N_2) was replaced by CO_2. It was found that the pressure rise due to ignition at these lower compressed temperatures was ill-defined, hence it was impossible to determine the ignition delay time, Fig 5.3. It was not possible to use light as a diagnostic as the chamber used in this study was not equipped with optical access.

30 atm

Ignition delay times were also measured at a reflected shock pressure and compressed gas pressure of 30 atm at equivalence ratios of 0.3, 0.5, 1.0 and 2.0 in air in the temperature range 625 – 1380 K, Fig. 5.2(b). Good agreement was observed between ignition delay times measured in the shock tube and those measured at lower temperatures in the RCM.

At the highest temperatures of the study, 1000 – 1380 K, there was a noticeable effect of equivalence ratio. At 1150 K the ignition delay times for the various equivalence ratios are: $\phi = 0.3$ – 240 μs, $\phi = 0.5$ – 190 μs, $\phi = 1.0$ – 130 μs, $\phi = 2.0$ – 100 μs. The ignition time decreases by 20.8% from $\phi = 0.3$ to 0.5, by 31.6% from $\phi = 0.5$ to 1.0 and 13.1% from $\phi = 1.0$ to 2.0, with a decrease in ignition delay time of 71.4% from $\phi = 0.3$ to 2.0.

The greatest effect of equivalence ratio was observed in the NTC region. At 875 K the greatest effect of equivalence ratio was observed between the $\phi = 0.5$ and 1.0 data. At this temperature the ignition delay times for the various equivalence ratios are: $\phi = 0.3$ – 2.6 ms, $\phi = 0.5$ – 1.8 ms, $\phi = 1.0$ – 0.99 ms, $\phi = 2.0$ – 0.63 ms. The ignition time decreases by 30.8% from $\phi = 0.3$ to 0.5, by 45% from $\phi = 0.5$ to 1.0 and 36.4% from $\phi = 1.0$ to 2.0, with a decrease in ignition delay time of 75.8% from $\phi = 0.3$ to 2.0.

At the lowest temperatures of the study, 625 – 715 K, the ignition delay time again converge. At 675 K the ignition delay times for the various equivalence ratios are: $\phi = 0.3$ – 22.3 ms, $\phi = 0.5$ – 14.5 ms, $\phi = 1.0$ – 8.7 ms, $\phi = 2.0$ – 5.5 ms. The ignition time decreases by 34.9% from $\phi = 0.3$ to 0.5, by 40% from $\phi = 0.5$ to 1.0 and 36.8% from $\phi = 1.0$ to 2.0, with a decrease in ignition delay time of 75.3% from $\phi = 0.3$ to 2.0.

Throughout the temperature range of this study fuel-rich mixture are fastest and fuel-lean mixtures are slowest to ignite. At the highest temperatures of the study, approximately 1200 K, the equivalence ratios converge, with a possible crossover of reactivities outside the range available experimentally. NTC behaviour was observed under these conditions.

50 atm

Experiments were also carried out at a reflected shock pressure of 50 atm at equivalence ratios of 0.3, 0.5, 1.0 and 2.0 in air in the temperature range 680 – 1220 K, Fig. 5.2(c). These experiments were carried out exclusively in the high-pressure shock tube.

At the highest temperatures of this study, 900 – 1220 K, the effect of equivalence ratio was less than that observed at lower temperatures. At 1050 K the ignition delay times for the various equivalence ratios are: $\phi = 0.3$ – 420 μs, $\phi = 0.5$ – 300 μs, $\phi = 1.0$ – 200 μs, $\phi = 2.0$ – 130 μs. The ignition time decreases by 28.5% from $\phi = 0.3$ to 0.5, by 33.3% from $\phi = 0.5$ to 1.0 and 35% from $\phi = 1.0$ to 2.0, with a decrease in ignition delay time of 69% from $\phi = 0.3$ to 2.0.

At lower temperatures there was a greater difference in the ignition delay times of the various equivalence ratios studied. At 870 K the ignition delay times for the various equivalence ratios are: $\phi = 0.3$ – 1320 μs, $\phi = 0.5$ – 750 μs, $\phi = 1.0$ – 420 μs, $\phi = 2.0$ – 260 μs. The ignition time decreases by 43.2% from $\phi = 0.3$ to 0.5, by 44% from $\phi = 0.5$ to 1.0 and 38.1% from $\phi = 1.0$ to 2.0, with a decrease in ignition delay time of 80.3% from $\phi = 0.3$ to 2.0.

Throughout the temperature range fuel-rich mixture were fastest and fuel-lean mixtures were slowest to ignite. There was a clear separation of the equivalence ratios though out the temperature range of the study. Again strong NTC behaviour was observed.

Due to the high reactivity of *n*-butylcyclohexane it was not possible to obtain ignition delay time data for this fuel in the rapid compression machine at a compressed pressure of 50 atm. The ignition delay times of such experiments is less than 5 ms, which was outside the range available experimentally in the RCM.

In order to carry out experiments at a reflected shock pressure of 50 atm an initial pressure of approximately 5 atm was required. However, due to the low vapour pressure of the fuel condensation occurred during the preparation of large test gas mixture which were prepared in the shock tube. To overcome this problem the initial temperature of the shock tube was increased. This was sufficient to overcome the issue of condensation for the fuel-lean cases. It was found that for stoichiometric and fuel-rich conditions it was impossible to overcome the issue of condensation and hence it was not possible to perform experiments for these conditions.

Moreover, it was not possible to measure ignition delay times for temperatures higher than 1050 K for the fuel-rich, $\phi = 2.0$ mixtures. It was found that for these experiments the observed ignition delay times were less than 50 μs. A number of such experiments were carried out but none proved to be successful.

5.3.2 Effect of Pressure

For all mixtures studied, at constant temperature increasing the pressure results in greater reactivity leading to shorter ignition delay times. Figure 5.4 shows the effect of reflected shock pressure and compressed pressure on the ignition delay times of *n*-butylcyclohexane at equivalence ratios of $\phi = 0.3$, 0.5, 1.0 and 2.0 studied. Shock tube ignition delay times are plotted with closed symbols, RCM igniting delay times are plotted with open symbols. For all equivalence ratios the fuel was more reactive at higher pressures. Figure 5.4(d) is a plot of the ignition delay times of *n*-butylcyclohexane, $\phi = 0.3$ at 10, 30 and 50 atm. It is clear that the 10 atm ignition delay times are longer than those measured at 30 atm, which are in turn longer than those measured at 50 atm.

5.4 Infrared Absorption

Infrared absorption of n-butylcyclohexane was carried out using the newly installed laser absorption system at NUI Galway, Section 4.5.

Signal intensities were recorded for vacuum conditions and varying pressures of n-butylcyclohexane at a number of temperatures in the test cell, Fig. 5.5. In-situ laser absorption tests were performed in the RCM using a reaction chamber fitted with sapphire windows for various initial pressures of n-butylcyclohexane. A quantity of n-butylcyclohexane liquid was injected into a heated mixing tank and allowed to flow into the manifold and reaction chamber. The pressure was allowed to equilibrate and absorption signals measured.

For 30 atm, $\phi = 2.0$ experiments carried out in the RCM an initial test gas charge of approximately 1.5 bar were used. This corresponds to an initial pressure of 40 mbar of n-butylcyclohexane. This was the largest amount of test charge used throughout this study and would be the most likely condition for condensation to occur. In situ tests were carried using initial pressures of n-butylcyclohexane up to 47 mbar. The results of the in-situ tests were found to be in good agreement with the test cell results hence confirming that no condensation of the fuel occurred under the initial conditions used in all n-butylcyclohexane RCM experiments.

It was not necessary to carry out IR absorption test for mixtures of n-butylcyclohexane and n-heptane and this fuel has a significantly higher vapour pressure than n-butylcyclohexane due to the n-heptane component of the fuel.

To investigate the addition of a long alkyl chain on the reactivity of n-butylcyclohexane ignition delay times were also measured for a mixture of n-butylcyclohexane and n-heptane. This mixture act as a surrogate for n-decylcyclohexane which is impossible to study in the gaseous phase due to its extremely low vapour pressure. Ignition delay times were measured at similar conditions to the n-butylcyclohexane study.

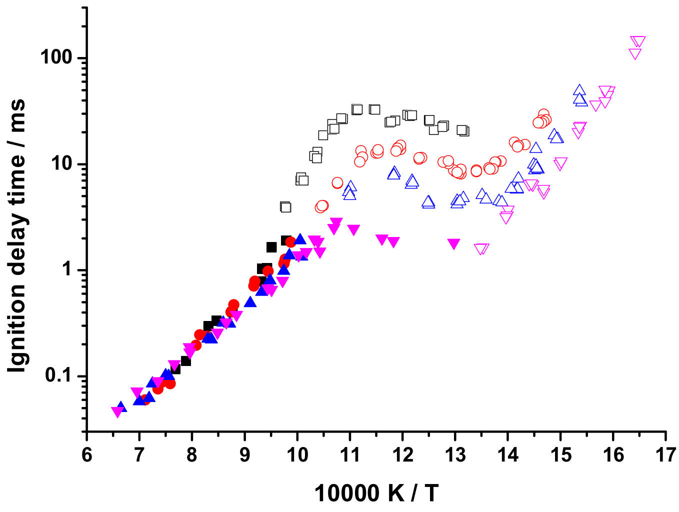

(a) 10 atm

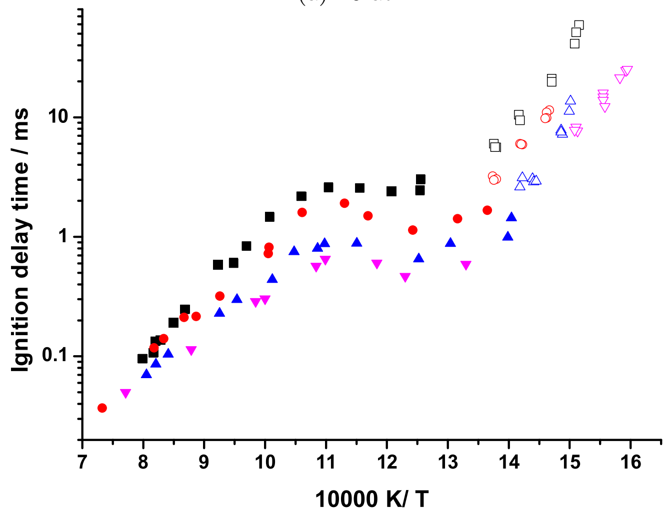

(b) 30 atm

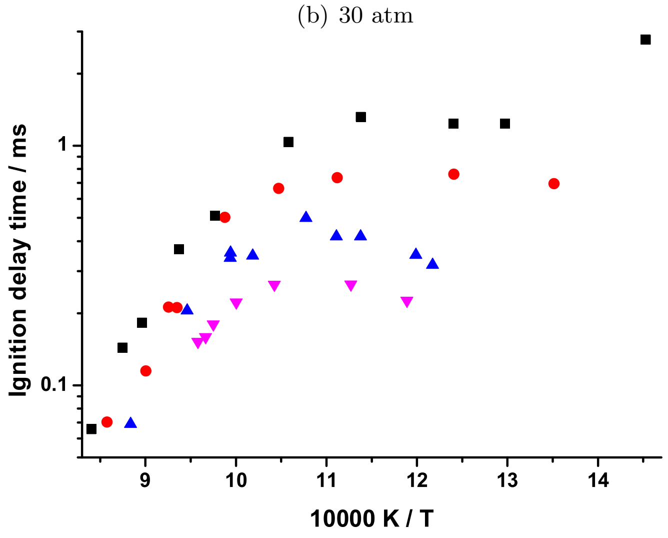

(c) 50 atm

Figure 5.2: Effect of equivalence ratio on ignition delay time of n-butylcyclohexane in air at 10, 30 atm and 50 atm, ■ – $\phi = 0.3$, ● – $\phi = 0.5$, ▲ – $\phi = 1.0$, ▼ – $\phi = 2.0$, filled symbols – shock tube data, open symbols – RCM data.

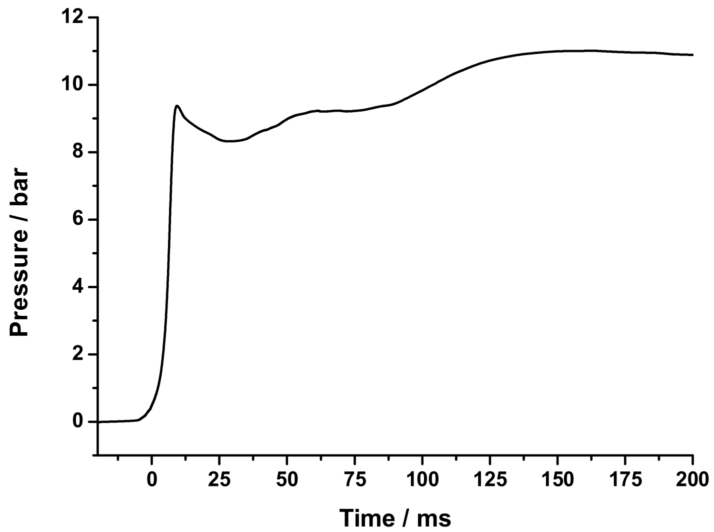

Figure 5.3: RCM trace for an n-butylcyclohexane experiment carried out $\phi = 0.3$, at a compressed pressure of 10 atm using 50% N_2 / 50% CO_2 diluent. Note the broad pressure peak making the ignition delay time difficult to measure.

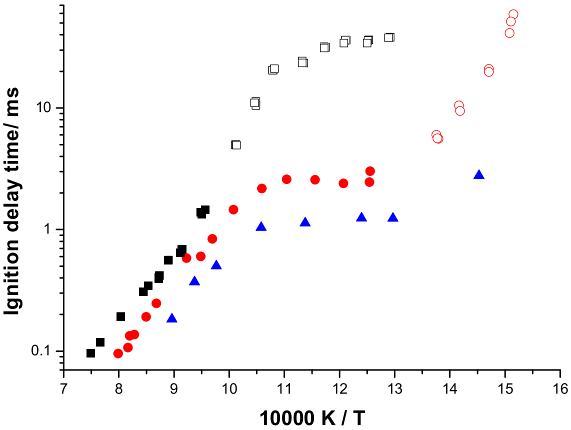

(a) $\phi = 0.3$

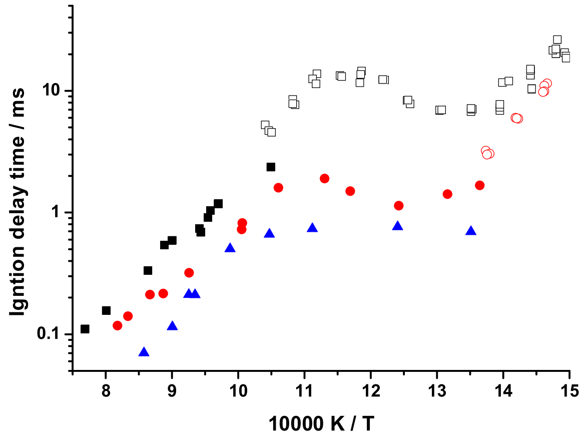

(b) $\phi = 0.5$

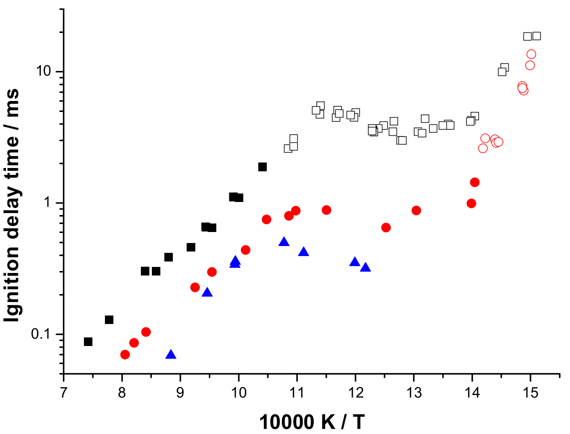

(c) $\phi = 1.0$

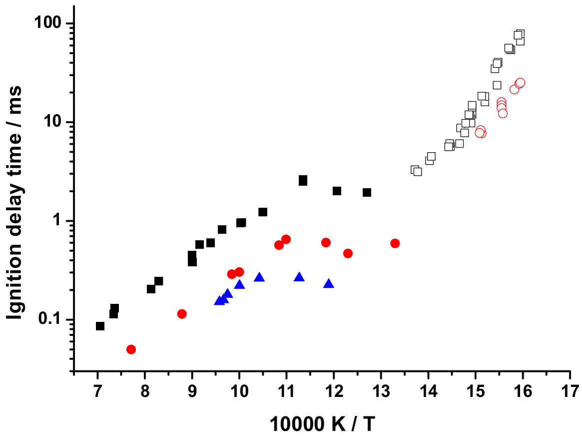

(d) $\phi = 2.0$

Figure 5.4: Effect of pressure on *n*-butylcyclohexane ignition delay times, (a) $\phi = 0.3$, (b) $\phi = 0.5$, (c) $\phi = 1.0$, (d) $\phi = 2.0$, ■ – 10 atm, ● – 30 atm, ▲ – 50 atm, filled symbols – shock tube data, open symbols – RCM data.

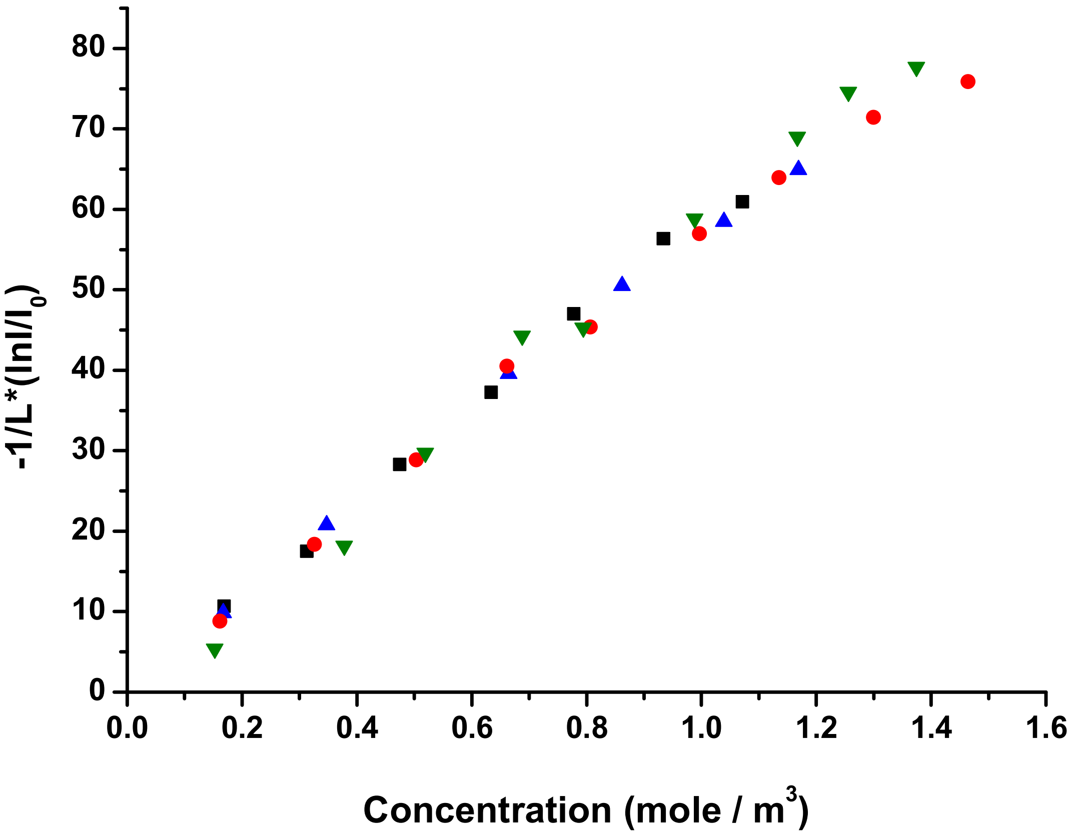

Figure 5.5: IR absorption of *n*-butylcyclohexane, test cell ■ – 80°C, ● – 100°C, ▲ – 120°C. In situ test ▼ – 110°C.

Chapter 6

n-Butylcyclohexane / n-Heptane Ignition Delay Time Study

Similar to pure n-butylcyclohexane, ignition delay times for a mixture of n-butylcyclohexane and n-heptane were also measured. These mixtures act as a surrogate for n-decylcyclohexane, mimicking the same hydrogen/carbon ratio, with that of the surrogate being 2.1 while that of n-decylcyclohexane is 2.0. At present it is extremely difficult to carry out experiments using n-decylcyclohexane in the gaseous phase as it has an extremely low vapour pressure. Camin *et al.* [21] have reported the vapour pressure of n-decylcyclohexane to be 52.08 Torr at 196.8°C. n-Butylcyclohexane (99%) and n-heptane (99%) were supplied by TCI. Oxygen (99%), nitrogen (99%) and helium (99%) gases were supplied by BOC. All reagents were used without further purification. Gas mixtures were prepared as per the procedure for direct fuel injection outlined previously for the high-pressure shock tube, Section 4.2, and the rapid compression machine, Section 4.4 Mixture compositions are provided in Table 6.1

ϕ	n-Heptane	n-Butylcyclohexane	Oxygen	Nitrogen
0.32	0.47	0.53	41.08	154.55
0.53	0.47	0.53	24.65	92.73
1.06	0.47	0.53	12.33	46.37
2.13	0.47	0.53	6.16	23.19

Table 6.1: Composition of n-butylcyclohexane / n-heptane / air gas mixtures.

6.1 Shock Tube Study

n-Butylcyclohexane / n-heptane mixtures were studied in the intermediate-pressure (1, 10 and 30 atm) and high-pressure (low temperature 30 atm and 50 atm) shock tubes over a range of equivalence ratios and pressures. Experiments were carried out at equivalence ratios of 0.3, 0.5, 1.0 and 2.0 in air. Experiments were carried out as per the procedure outline previously. Liquid fuel mixtures of n-butylcyclohexane and n-heptane were prepared by weighing the individual fuel components, a full procedure has been discussed in Section 4.2. All gas mixtures were prepared via direct injection of the fuel into the mixing tank.

6.2 Rapid Compression Machine Study

To extend the temperature range of the data obtained in the shock tube experiments were also carried out in the RCM at compressed pressures of 10 and 30 atm. Reactive and non-reactive gas mixtures were prepared via direct injection of the fuel into the mixing tank as per the procedure outlined previously.

6.3 Results and Discussion

6.3.1 Effect of Equivalence Ratio

1 atm

Ignition delay times were measure at a reflected shock pressure of 1 atm at equivalence ratios of 0.5, 1.0 and 2.0 in air in the temperature range 950 – 1820 K. Experiments were not carried out at an equivalence ratio of 0.3. Due to the low reflected shock pressure the pressure rise due to ignition was weak and hence it was difficult to measure the ignition delay times. Results obtained from these experiments followed no trend.

As part of the project outline 1 atm shock tube ignition delay times for mixtures of *n*-butylcyclohexane / *n*-heptane were also to be studied. Experiments were carried using the intermediate-pressure shock tube. It was found that experimental results that were obtained followed no well defined trend. It was found that there was a large signal to noise ratio, as a result of this the timer counters did not capture the passing shock wave. Times that have to be obtained using the trace recorded on the oscilloscope. In addition, the pressure rise due to ignition was often very weak and not well defined, this resulted in an inaccurate determination of the ignition delay time. Unfiltered light emission was also used as a diagnostic. This was also unsuccessful as there was not sufficient light emitted to accurately measure ignition delay times. Data which was obtained was sporadic with no clearly defined trend, Fig 6.1.

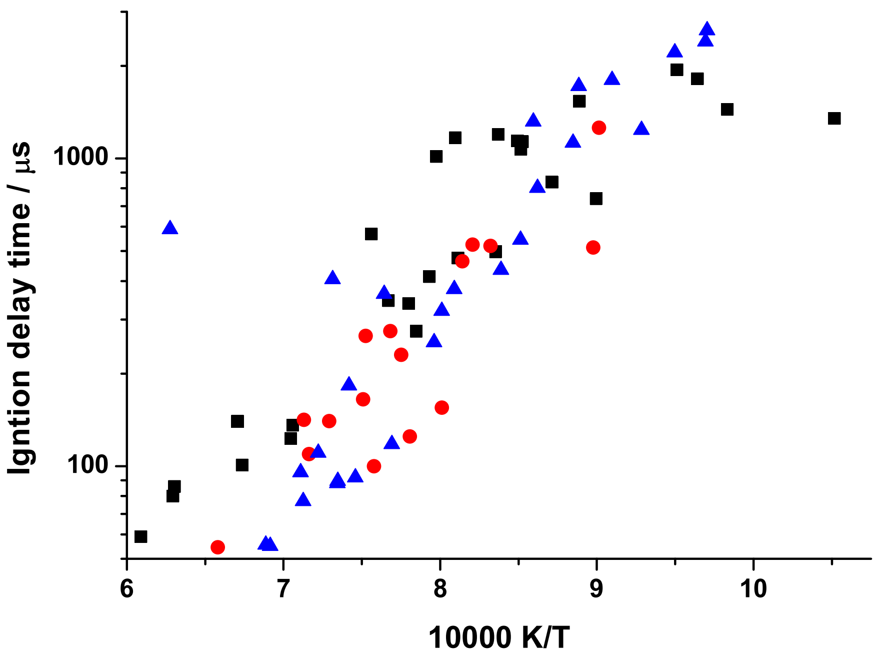

Figure 6.1: Effect of equivalence ratio on ignition delay time of mixtures of *n*-butylcyclohexane / *n*-heptane in air at 1 atm, ▲ – $\phi = 0.5$, ● – $\phi = 1.0$, ■ – $\phi = 2.0$.

10 atm

Ignition delay times were measured at a reflected shock and compressed gas pressure of 10 atm at equivalence ratios of 0.3, 0.5, 1.0 and 2.0 in the temperature range 600 – 1540 K, Fig. 6.2(a). Good agreement was observed between igniting delay times measured in the shock tube and those measured in the RCM.

At the highest temperatures of this study, 1030 – 1540 K, there was little effect of equivalence ratio on the ignition delay times. At 1220 K the ignition times for the various equivalence ratios are: $\phi = 0.3 - 240$ μs, $\phi = 0.5 - 219$ μs, $\phi = 1.0 - 200$ μs, $\phi = 2.0 - 179$ μs, and so the ignition time decreases by 8.8% from $\phi = 0.3$ to 0.5, by 8.6% from $\phi = 0.5$ to 1.0 and 10.5% from $\phi =$ 1.0 to 2.0, with a decrease in ignition delay time of 25.4% from $\phi = 0.3$ to 2.0.

The largest effect of equivalence ratio was observed in the NTC region, which was centred at approximately 850 K. At this temperature the ignition times of the various equivalence ratios are: $\phi = 0.3 - 31.6$ ms, $\phi = 0.5 - 13.9$ ms, $\phi = 1.0 - 8.05$ ms, $\phi = 2.0 - 1.92$ ms, and so the ignition time decreases by 56% from $\phi = 0.3$ to 0.5, by 42.1% from $\phi = 0.5$ to 1.0 and 76.2% from $\phi = 1.0$ to 2.0, with a decrease in ignition delay time of 93.9% from $\phi = 0.3$ to 2.0.

At lower temperatures, 600 – 715 K, the effect of equivalence ratio on the ignition delay decreased. At 670 K the ignition times of the various equivalence ratios are: $\phi = 0.5 - 15.6$ ms, $\phi = 1.0 - 8.74$ ms, $\phi = 2.0 - 5.13$ ms, and so the ignition time decreases by 43.9% from $\phi = 0.5$ to 1.0 and 41.3% from $\phi = 1.0$ to 2.0, with a decrease in ignition delay time of 67.1% from $\phi =$ 0.5 to 2.0.

At the highest temperatures studied (1100 – 1540 K) it can be seen that the fuel-lean mixtures were most reactive while the fuel-rich mixtures were slowest to ignite. However at lower temperatures (580 – 1100 K)fuel-rich mixtures were fastest and fuel-lean mixtures are slowest to ignite. At approximately 1250 K the reactivies of the various equivalence ratios cross over. In the temperature range studied in the RCM, 590 – 1000 K, strong NTC behaviour was observed.

30 atm

Ignition delay times were also measured at a reflected shock and compressed pressure of 30 atm at equivalence ratios of 0.3, 0.5, 1.0 and 2.0 in the temperature range 600 – 1430 K, Fig. 6.2(b). Good agreement was observed between the ignition delay times measured in the shock tube and those measured at lower temperatures in the RCM.

At the highest temperatures of this study, 1000 – 1430 K, it was observed that there was a little effect of equivalence ratio on the ignition delay times. At 1075 K the ignition times of the various equivalence ratios are: $\phi = 0.3 - 550$ μs, $\phi = 0.5 - 330$ μs, $\phi = 1.0 - 260$ μs, $\phi = 2.0 -$ 190 μs, and so the ignition time decreases by 40% from $\phi = 0.3$ to 0.5, by 21.2% from $\phi = 0.5$ to 1.0 and 26.9% from $\phi = 1.0$ to 2.0, with a decrease in ignition delay time of 65.5% from $\phi =$ 0.3 to 2.0.

The greatest effect of equivalence ratio was observed in the NTC region, centred at approximately 850 K. At this temperature the ignition times of the various equivalence ratios are: $\phi =$ 0.3 – 2.43 ms, $\phi = 0.5 - 1.2$ ms, $\phi = 1.0 - 0.62$ ms, $\phi = 2.0 - 0.46$ ms, and so the ignition time decreases by 50.6% from $\phi = 0.3$ to 0.5, by 48.3% from $\phi = 0.5$ to 1.0 and 25.8% from $\phi = 1.0$ to 2.0, with a decrease in ignition delay time of 81.1% from $\phi = 0.3$ to 2.0.

At the lowest temperatures of this study, 600 – 750 K, the effect of equivalence ratio on the ignition delay times was lessened and the data converges slightly. At 660 K the ignition times of the various equivalence ratios are: $\phi = 0.3 - 45$ ms, $\phi = 0.5 - 26.8$ ms, $\phi = 1.0 - 15.2$ ms, $\phi =$ 2.0 – 6.46 ms, and so the ignition time decreases by 40.4% from $\phi = 0.3$ to 0.5, by 43.3% from $\phi = 0.5$ to 1.0 and 57.5% from $\phi = 1.0$ to 2.0, with a decrease in ignition delay time of 85.6% from $\phi = 0.3$ to 2.0.

Throughout the temperature range (560 – 1430 K) fuel-rich mixture are fastest and fuel-lean mixtures are slowest to ignite. At the highest temperatures of the study, approximately 1250 K, the equivalence ratios converge, with a possible crossover of reactivities outside the range available experimentally. Again strong NTC behaviour was observed.

50 atm

Ignition delay times were measured at a reflected shock pressure of 50 atm at equivalence ratios of 0.3, 0.5, 1.0 and 2.0 in the temperature range 760 – 1250 K, Fig. 6.2(c).

At the highest temperatures of this study, 1000 – 1250 K, there was a clear separation of the equivalence ratios studied. At 1040 K the ignition times of the various equivalence ratios are: ϕ = 0.3 – 520 μs, ϕ = 0.5 – 350 μs, ϕ = 1.0 – 195 μs, ϕ = 2.0 – 157 μs, and so the ignition time decreases by 32.7% from ϕ = 0.3 to 0.5, by 44.3% from ϕ = 0.5 to 1.0 and 19.5% from ϕ = 1.0 to 2.0, with a decrease in ignition delay time of 69.8% from ϕ = 0.3 to 2.0.

At lower temperatures, 760 – 1000 K, there was an enhanced effect of equivalence ratio. At 880 K the ignition times of the various equivalence ratios are: ϕ = 0.3 – 1185 μs, ϕ = 0.5 – 823 μs, ϕ = 1.0 – 339 μs, and so the ignition time decreases by 30.5% from ϕ = 0.3 to 0.5 and 58.8% from ϕ = 0.5 to 1.0, with a decrease in ignition delay time of 71.4% from ϕ = 0.3 to 1.0.

Through out the temperature range studied, 760 – 1250 K, fuel-rich mixtures were the most reactive while fuel-lean mixtures were slowest to ignite. There was a clear separation of the reactivies of the equivalence ratios with strong NTC behaviour also observed. Again strong NTC behaviour was observed.

In order to carry out experiments at a reflected shock pressure of 50 atm a large initial pressure of test gas was required. Due to the low vapour pressure of the *n*-butylcyclohexane component of this fuel condensation occurred during the preparation of large test gas mixture which were prepared directly in the shock tube. To overcome this problem the initial temperature of the shock tube was increased. This was sufficient to overcome the issue of condensation in fuel-lean cases. It was found that for fuel-rich conditions it was impossible to overcome the issue of condensation and hence it was not possible to obtain ignition delay times at low-temperatures. Experiments which were carried out under fuel-rich conditions had longer than expected ignition delay times.

It proved impossible to obtain experimental results for temperatures higher than approximately 1050 K for ϕ = 2.0 mixture. It was found when experiments were carried out under these conditions the ignition delay times obtained were too fast to measure accurately, i.e. less that 50 μs. A number of such experiments were carried out but none proved to be successful.

Due to the highly reactive nature of this fuel it was not possible to obtain ignition delay time data for this fuel in the rapid compression machine at a compressed pressure of 50 atm. The ignition delay times of such experiments was less than 5 ms, which is outside the range available experimentally in the RCM.

6.3.2 Effect of Pressure

Figure 6.3 shows the effect of reflected shock and compressed pressure on the ignition delay times of *n*-butylcyclohexane / *n*-heptane mixtures at various equivalence ratios studied. Shock tube ignition delay times are plotted with closed symbols, RCM ignition delay times are plotted with open symbols. Across all equivalence ratios and pressures studied a re-occurring trend is observed for all *n*-butylcyclohexane / *n*-heptane ignition delay times. In all cases the higher the pressure the more reactive the fuel. For all equivalence ratios the 10 atm ignition delay times are longer than those measured at 30 atm, which are in turn longer than those measured at 50 atm.

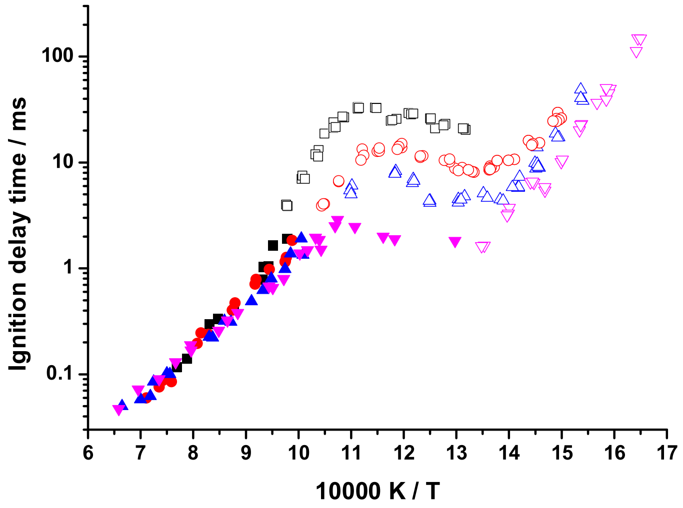

(a) 10 atm

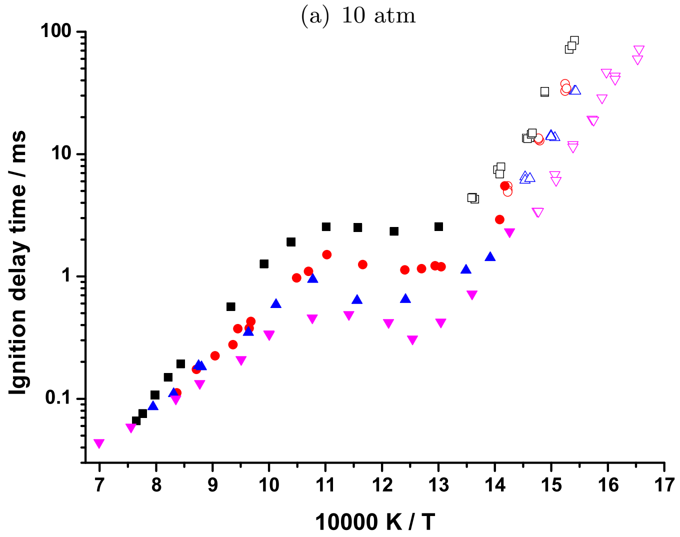

(b) 30 atm

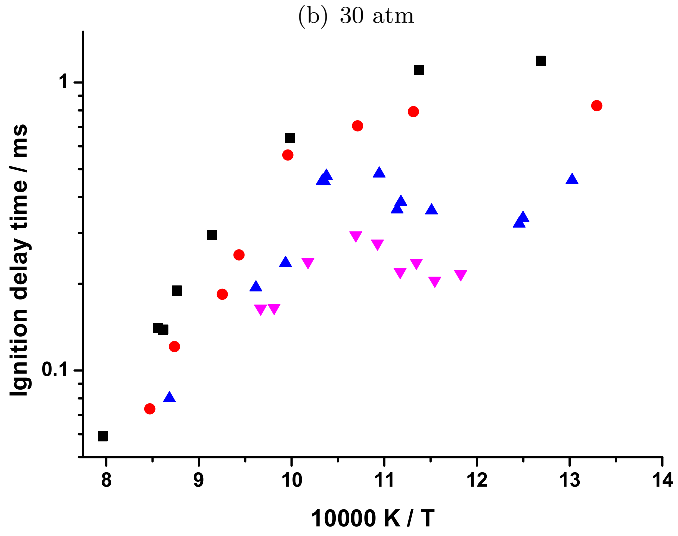

(c) 50 atm

Figure 6.2: Effect of equivalence ratio on ignition delay time of *n*-butylcyclohexane / *n*-heptane mixtures in air at 10, 30 and 50, ■ – ϕ = 0.3, ● – ϕ = 0.5, ▲ – ϕ = 1.0, ▼ – ϕ = 2.0, filled symbols – shock tube data, open symbols – RCM data.

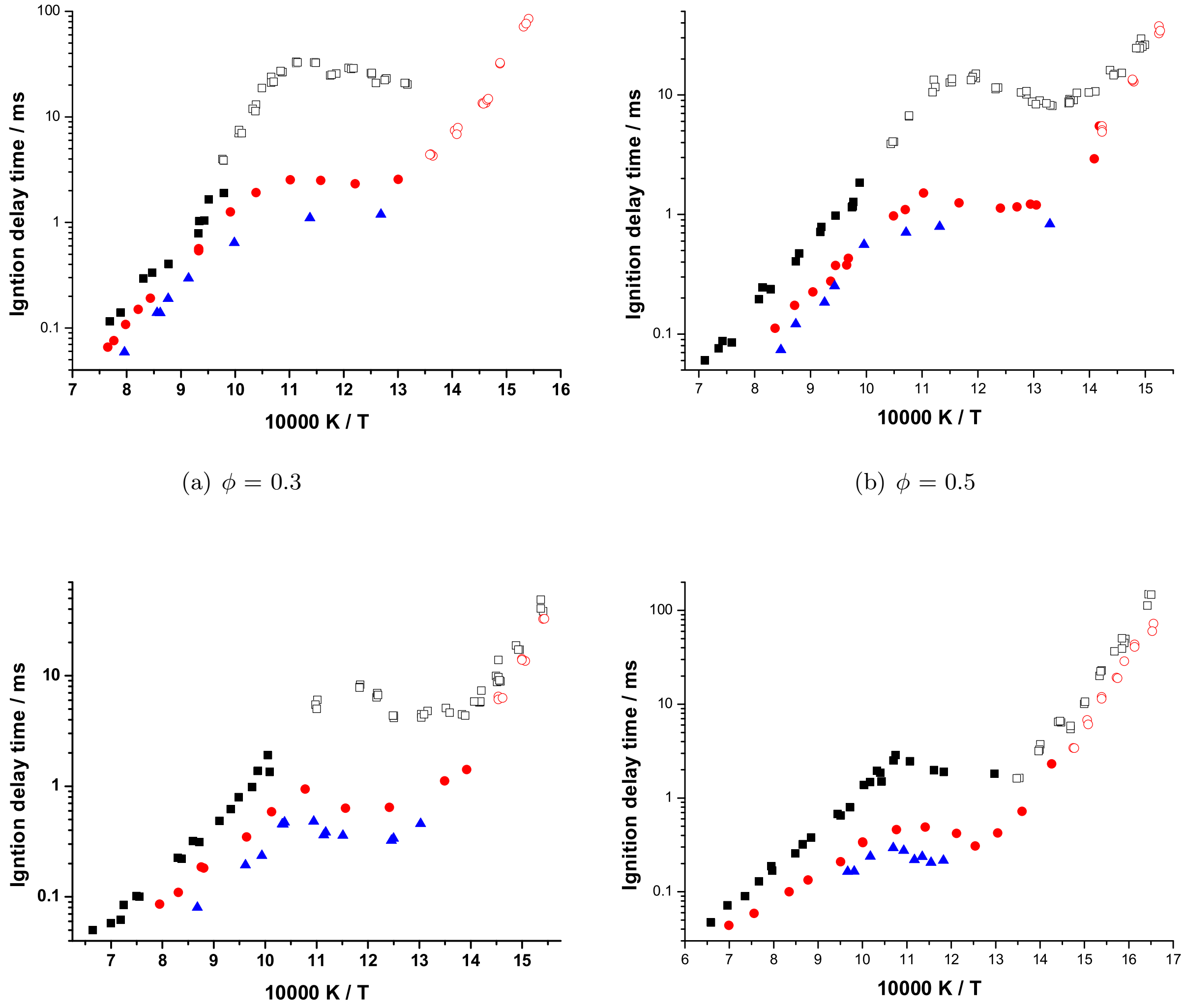

(a) $\phi = 0.3$

(b) $\phi = 0.5$

(c) $\phi = 1.0$

(d) $\phi = 2.0$

Figure 6.3: Effect of pressure on n-butylcyclohexane / n-heptane ignition delay times, (a) $\phi = 0.3$, (b) $\phi = 0.5$, (c) $\phi = 1.0$, (d) $\phi = 2.0$. ■ – 10 atm, ● – 30 atm, ▲ – 50 atm. Filled symbols – shock tube data, open symbols – RCM data.

Chapter 7

Comparison of *n*-Butylcyclohexane and a *n*-Decylcyclohexane Surrogate

It is interesting to compare *n*-butylcyclohexane ignition delay times obtained in the shock tube and rapid compression machine with those for mixtures of *n*-butylcyclohexane / *n*-heptane obtained under similar conditions in order to investigate the effect of the addition of *n*-heptane. Comparisons were carried out for all pressures and at all equivalence ratios studied, Fig. 7.1 – 7.3.

7.1 10 atm

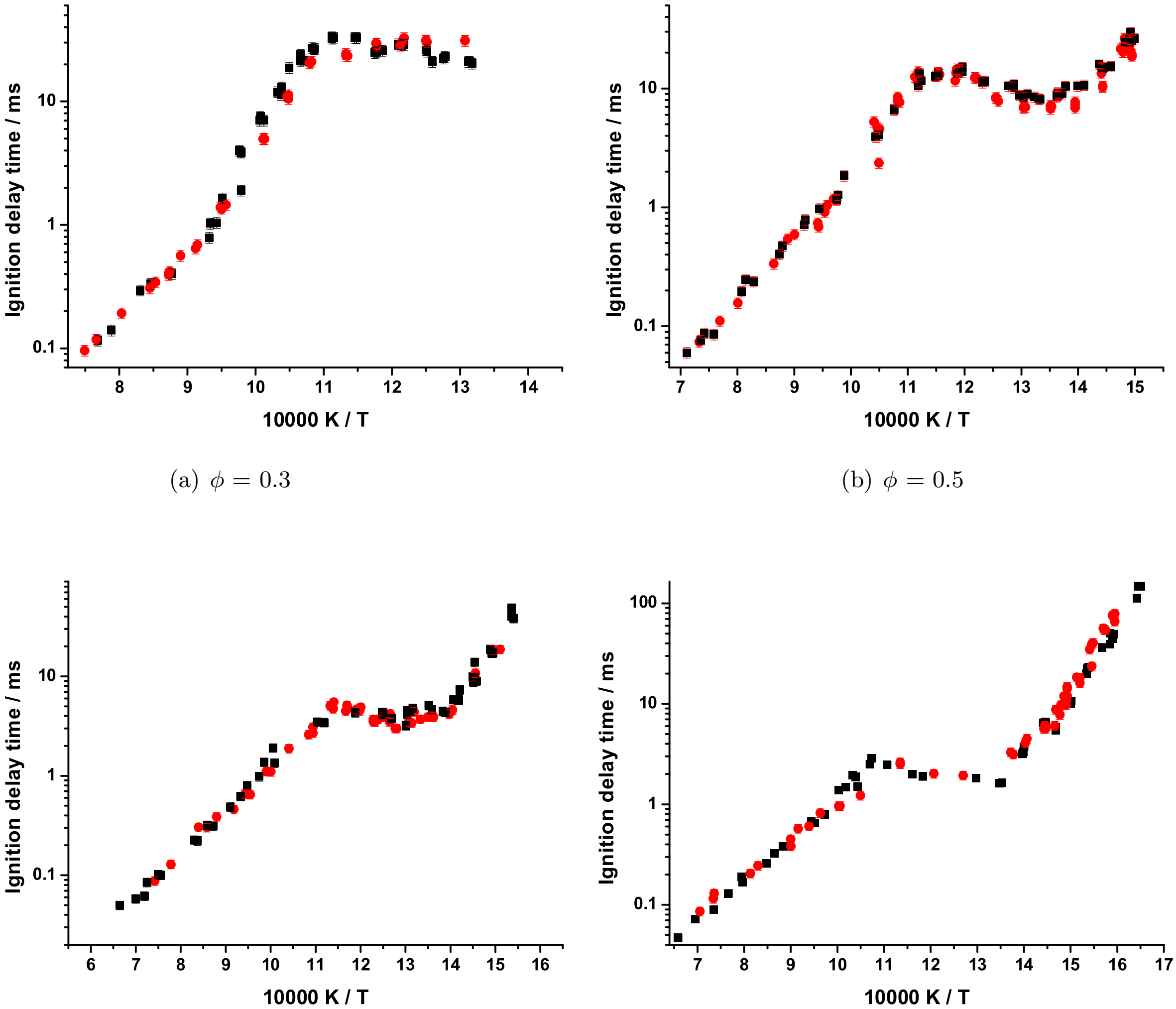

(a) $\phi = 0.3$

(b) $\phi = 0.5$

(c) $\phi = 1.0$

(d) $\phi = 2.0$

Figure 7.1: Comparison of *n*-butylcyclohexane and *n*-butylcyclohexane / *n*-heptane ignition delay times at 10 atm, $\phi = 0.3 - 2.0$, ● – *n*-butylcyclohexane ■ – *n*-butylcyclohexane / *n*-heptane, 10% error bars are included on data.

7.2 30 atm

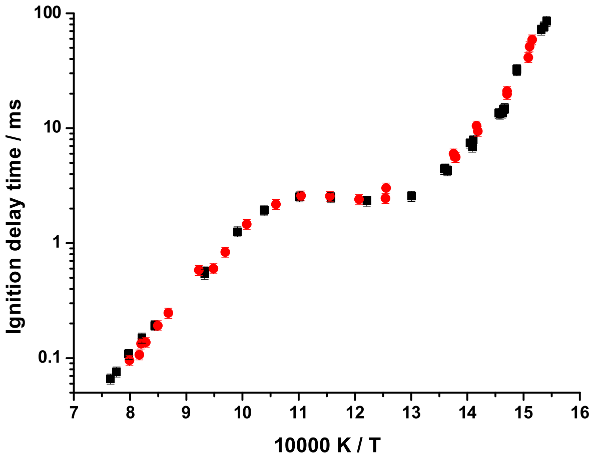

(a) $\phi = 0.3$

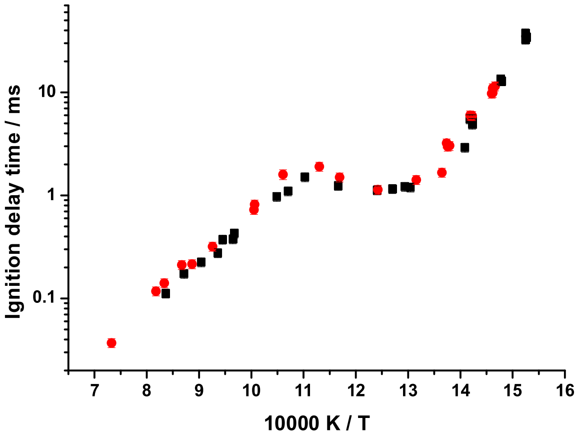

(b) $\phi = 0.5$

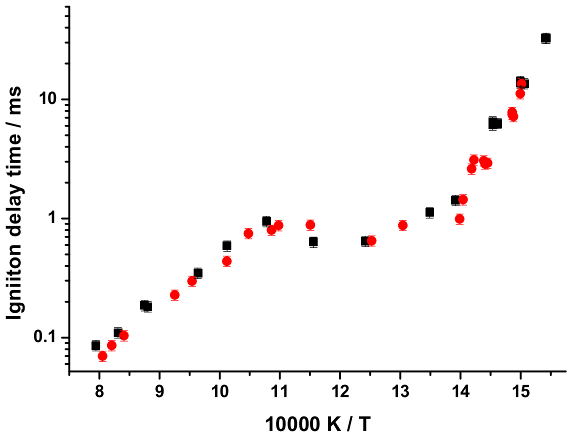

(c) $\phi = 1.0$

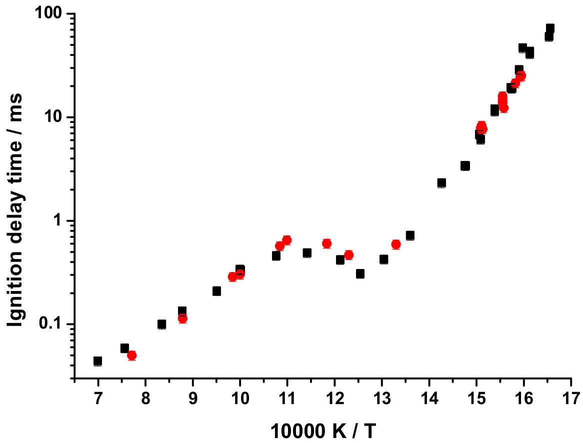

(d) $\phi = 2.0$

Figure 7.2: Comparison of n-butylcyclohexane and n-butylcyclohexane / n-heptane ignition delay times at 30 atm, $\phi = 0.3 - 2.0$, ● – n-butylcyclohexane ■ – n-butylcyclohexane / n-heptane, 10% error bars are included on data.

7.3 50 atm

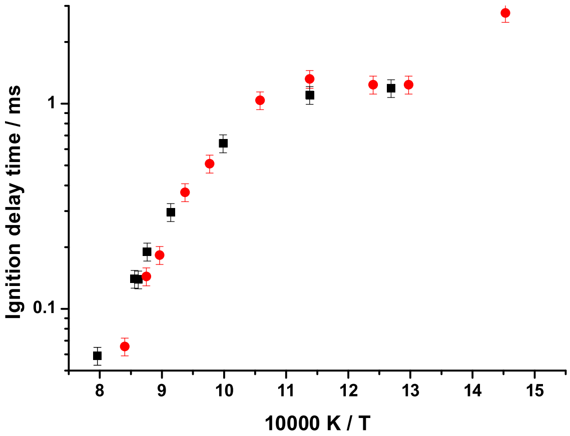

(a) $\phi = 0.3$

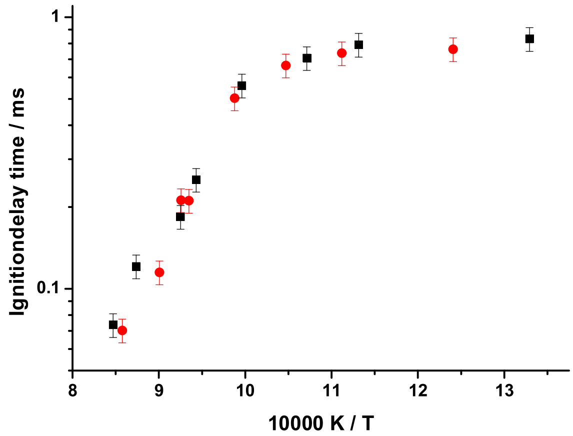

(b) $\phi = 0.5$

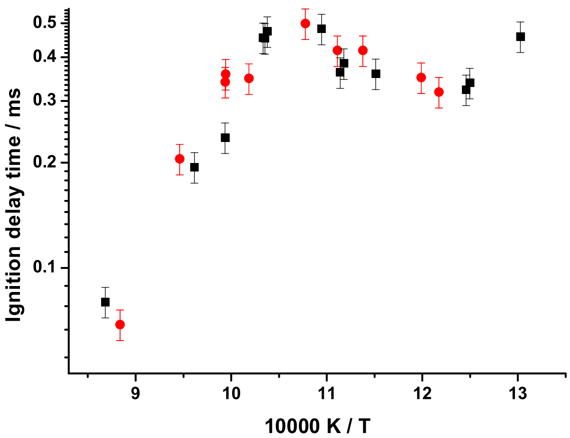

(c) $\phi = 1.0$

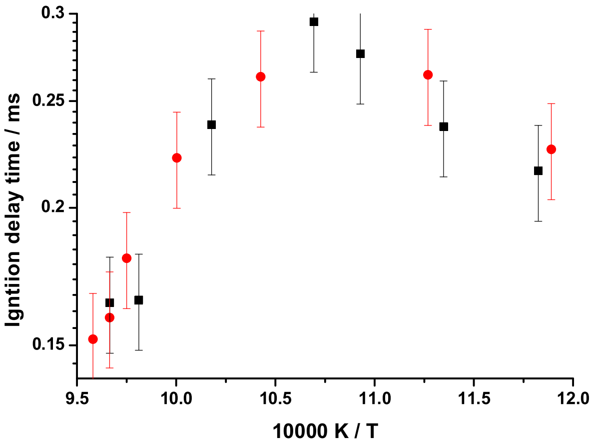

(d) $\phi = 2.0$

Figure 7.3: Comparison of *n*-butylcyclohexane and *n*-butylcyclohexane / *n*-heptane ignition delay times at 10 atm, $\phi = 0.3 - 2.0$, ● – *n*-butylcyclohexane ■ – *n*-butylcyclohexane / *n*-heptane, 10% error bars are included on data.

7.4 Comparison with *n*-Heptane

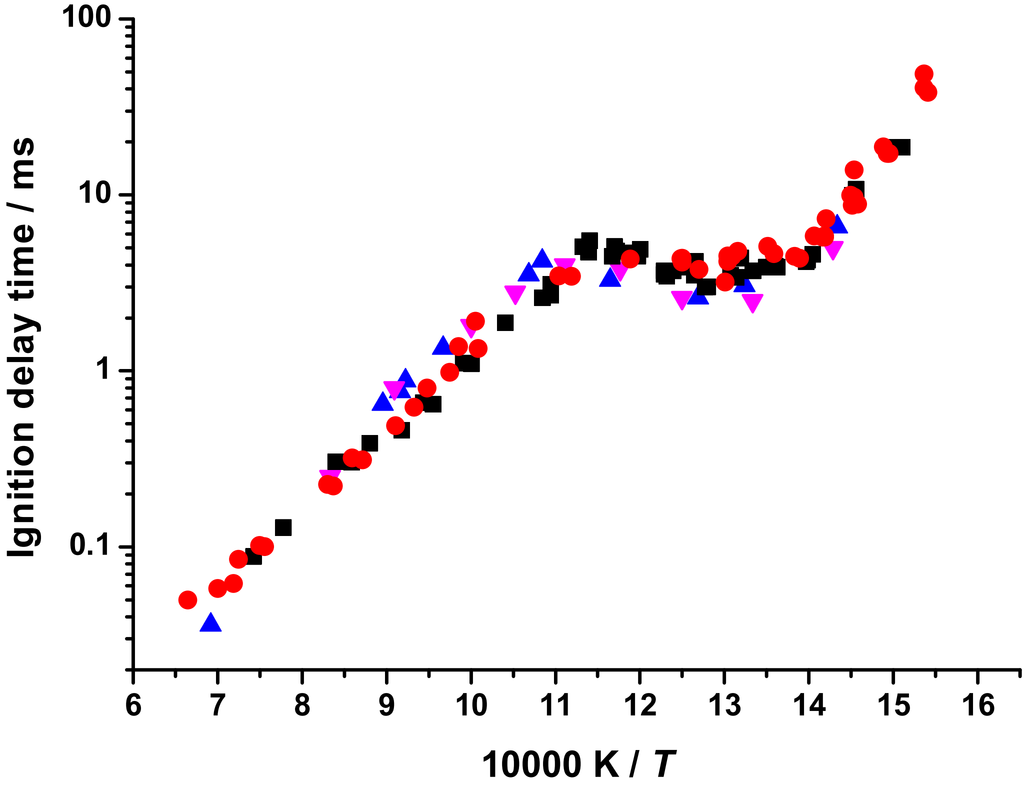

Figure 7.4: Ignition delay times of *n*-butylcyclohexane, mixtures of *n*-butylcyclohexane /*n*-heptane and *n*-heptane, ϕ = 1.0, 10 atm. ● – *n*-butylcyclohexane (1.38% fuel), ■ – *n*-butylcyclohexane /*n*-heptane (1.67% fuel), ▲ – *n*-heptane, Heufer *et al.* [84] (1.8% fuel), ▼ – *n*-heptane, NUI Galway high pressure shock tube validation (1.8% fuel).

Figure 7.4 illustrates the similar ignition delay times of *n*-butylcyclohexane, *n*-heptane and mixtures of *n*-butylcyclohexane /*n*-heptane carried out at similar initial fuel concentrations, ϕ = 1.0, 10 atm.

7.5 Discussion

It can be seen that for all pressures and equivalence ratios studied the ignition delay times for the two fuels are almost identical, Fig. 7.1 – 7.3.

At a reflected shock and compressed pressure of 10 atm the reactivites of the two fuels are very similar, Fig. 7.1. At ϕ = 0.3 it can be seen that the reactivities of the two fuels are very similar with some small discrepancies coming out of the NTC regime and at the lowest temperatures of the study. At ϕ = 0.5, 1.0 and 2.0 the reactivities of the two fuels are identical.

At a reflected shock pressure of 30 and 50 atm the two fuels are almost identical, Fig. 7.3.

7.6 Conclusions

It can be seen that under similar conditions *n*-butylcyclohexane and *n*-butylcyclohexane / *n*-heptane mixtures exhibits almost identical ignition delay times. When compared to *n*-heptane ignition delay times at similar conditions it was found that all three fuels exhibit similar reactivity. These results suggests that at the conditions of *this study* the reactivity large alkyl-cyclohexanes is similar to that of larger *n*-alkanes.

Chapter 8

Chemical Kinetic Modeling of *n*-Butylcyclohexane and a *n*-Decylcyclohexane Surrogate

8.1 Mechanisms

JetSurF 1.1 [47] and 2.0 [30] and the mechanism of Natelson *et al.* [17] can be used to simulate the combustion of *n*-butylcyclohexane.

JetSurF 2.0 [30] is the latest version of mechanisms produced by Prof. Hai Wang at USC. It consists of 348 species and 2163 reactions. The authors state that this mechanism is an "un-tuned work-in-progress" and it is only suitable for high-temperature simulations as it does not incorporate low-temperature chemistry.

Natelson *et al.* [17] have built on JetSurF 1.1 [47] and included a reaction scheme with 42 species and 80 reactions for the description of low temperature *n*-butylcyclohexane chemistry. Reaction rate constants were included based on analogy with similar systems and values were adapted. This study involved the simulation of low temperature, 600 – 800 K, fuel lean, 8 atm, *n*-butylcyclohexane pressurised flow reactor experiments. As this mechanism was optimised using pressurised flow reactor data only, the authors state that to use this model to simulate other experimental conditions extensive modification would be required.

JetSurF 2.0 is built upon the base mechanism of USC-Mech II, which describes the oxidation of $C_0 - C_4$ hydrocarbons. In an effort to see if the predicted ignition delay times predicted by JetSurF 2.0 could be improved Aramco Mech 1.0 [85], a $C_0 - C_4$ detailed sub-mechanism developed at NUI Galway, was substituted into JetSurF 2.0. Aramco Mech 1.0 is a detailed chemical kinetic mechanism which has been developed to describe the oxidation of small hydrocarbon and oxygenated hydrocarbon species. The mechanism has been validated over a wide range of initial conditions and experimental devices including flow reactor, shock tube, jet-stirred reactor and flame studies. The mechanism contains accurate kinetic descriptions for saturated and unsaturated hydrocarbons, namely; methane, ethane, ethylene, and acetylene, and oxygenated species; formaldehyde, methanol, acetaldehyde and ethanol.

10, 30 and 50 atm *n*-butylcyclohexane and mixtures of *n*-butylcyclohexane / *n*-heptane, shock tube ignition delay times were simulated using JetSurF 2.0, the combined Aramco Mech 1.0 and the C_5+ portion of JetSurF 2.0 and the mechanism of Natelson *et al.*

Model results for shock tube ignition delay times only are presented. Simulations carried out for rapid compression machine were unsuccessful. Low temperature rapid compression machine simulations carried out using JetSurF 2.0 did not yield results due to no low temperature chemistry being incorporated into this mechanism. The mechanism of Natelson *et al.* incorporates low temperature chemistry but this mechanism failed to reach a solution for rapid compression machine simulations.

8.2 Results and Discussion

n-Butylcyclohexane, 10 atm

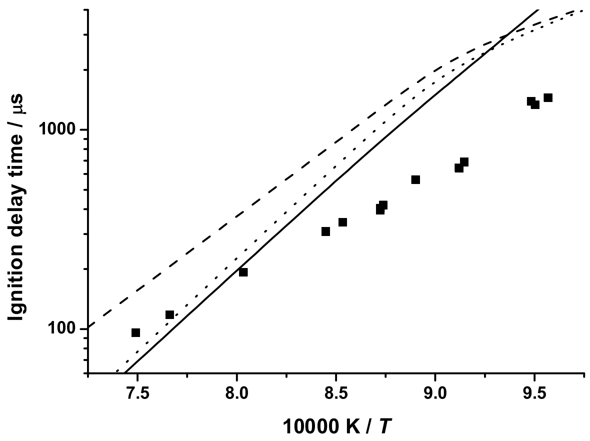

(a) $\phi = 0.3$

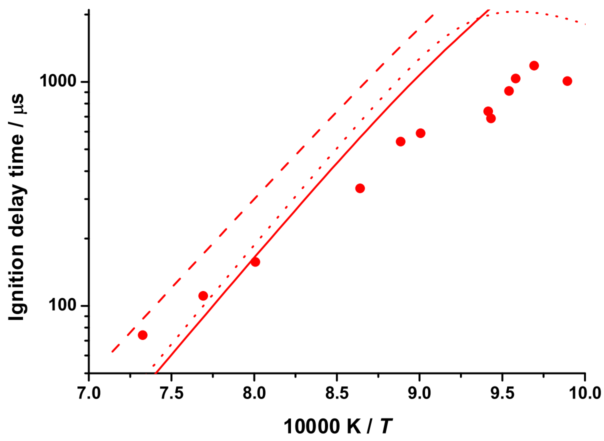

(b) $\phi = 0.5$

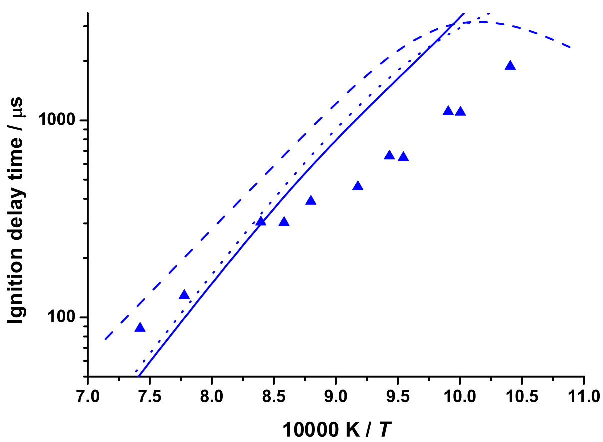

(c) $\phi = 1.0$

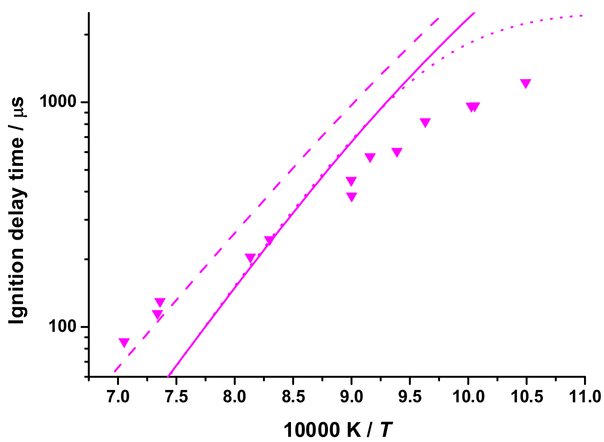

(d) $\phi = 2.0$

Figure 8.1: *n*-Butylcyclohexane shock tube ignition delay times (points) at $p = 10$ atm compared to model predictions. —— JetSurF 2.0, - - - JetSurF 2.0 + Aramco Mech 1.0, ··· Natelson *et al.*

Fig. 8.1 shows that at 10 atm JetSurF 2.0 over-predicts reactivity at high temperature but under-predicts reactivity at lower temperature in comparison with experimental data. The addition of Aramco Mech 1.0 increases the ignition delay times predicted. At $\phi = 0.3$ and 1.0 at temperatures lower than 1050 K the combined JetSurF 2.0 / Aramco Mech 1.0 model suggest NTC behaviour. The ignition delay times predicted by the mechanism of Natelson *et al.* are longer than those measured experimentally, Fig. 8.1, it predicts an NTC behaviour at $\phi = 0.5$, 1.0 and 2.0, which is not seen experimentally.

A rate of production analysis was carried out at 10 atm, $\phi = 1.0$, 1140 K to highlight the reactions that consume the fuel as shown in Fig. 8.2. Dominant channels include hydrogen abstraction from the fuel which results in the formation of eight $C_{10}H_{19}$ radical isomers. These radicals are consumed via hydrogen shift isomerisations, β scisson of the butyl side chain and ring opening reactions. Approximately 30% of the fuel undergoes ring opening and unimolecular decomposition reactions.

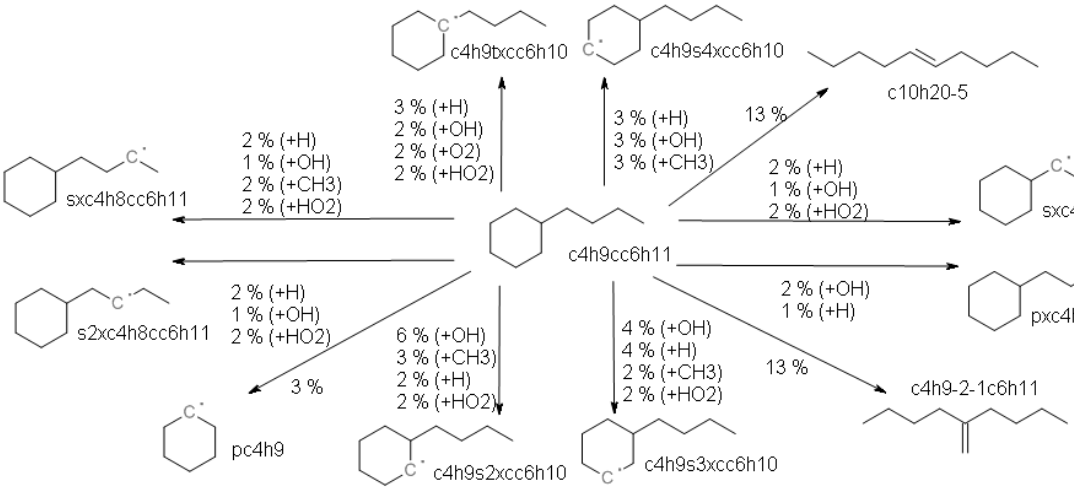

Figure 8.2: Rate of production showing the major pathways for n-butylcyclohexane decomposition carried out using JetSurF 2.0, 10% fuel consumption at 10 atm, $\phi = 1.0$, 1140 K.

n-Butylcyclohexane, 30 atm

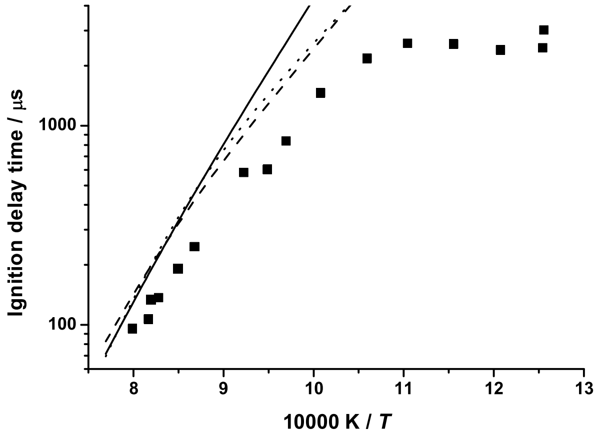

(a) $\phi = 0.3$

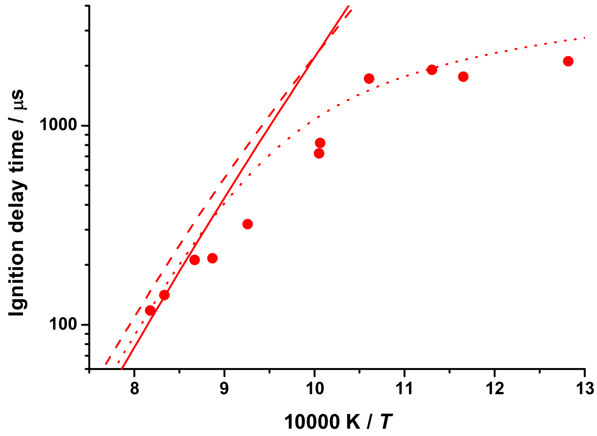

(b) $\phi = 0.5$

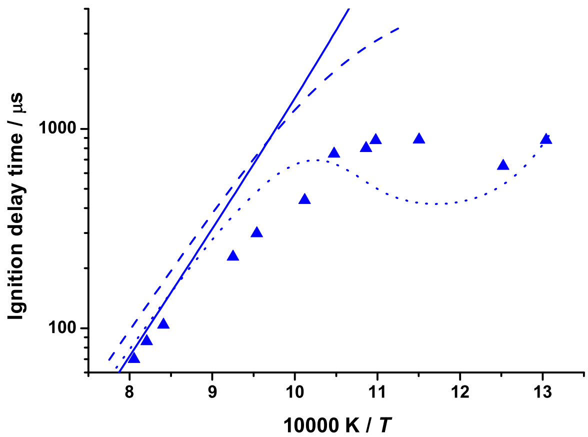

(c) $\phi = 1.0$

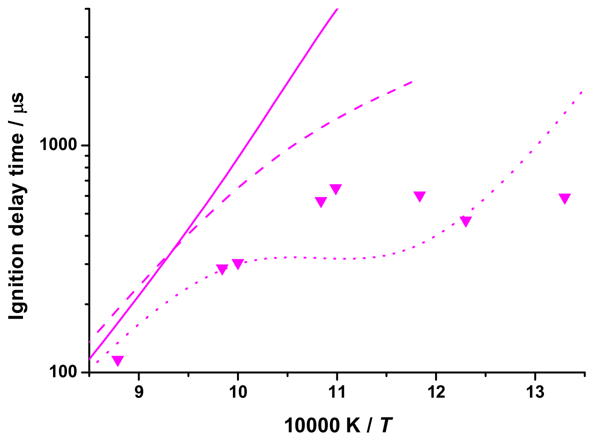

(d) $\phi = 2.0$

Figure 8.3: *n*-Butylcyclohexane shock tube ignition delay times (points) at $p = 30$ atm compared to model predictions. —— JetSurF 2.0, - - - JetSurF 2.0 + Aramco Mech 1.0, ··· Natelson *et al.*

At 30 atm the *n*-butylcyclohexane ignition times predicted by JetSurF 2.0 are longer than those measured experimentally throughout the temperature range as demonstrated in Fig. 8.3.

The addition of Aramco Mech 1.0 to JetSurF 2.0 has little effect at temperatures above 1000 K, below this temperature the addition of Aramco Mech 1.0 results in an increase in reactivity, Fig. 8.3. The largest effect of this is seen for rich mixtures, Fig. 8.3(d).

The mechanism of Natelson *et al.* performs well in the lower temperature regime unsurprisingly as it has been optimised to lower temperature data.

n-Butylcyclohexane, 50 atm

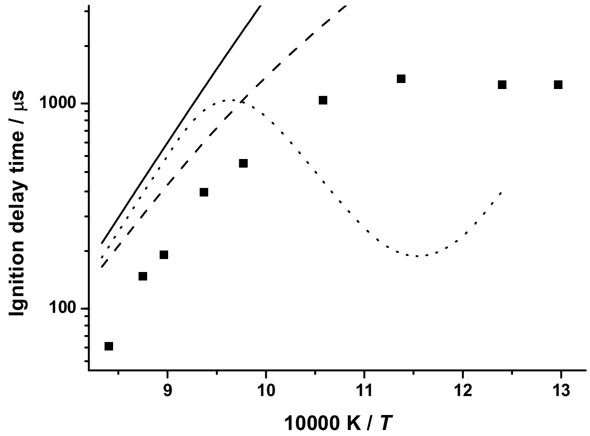

(a) $\phi = 0.3$

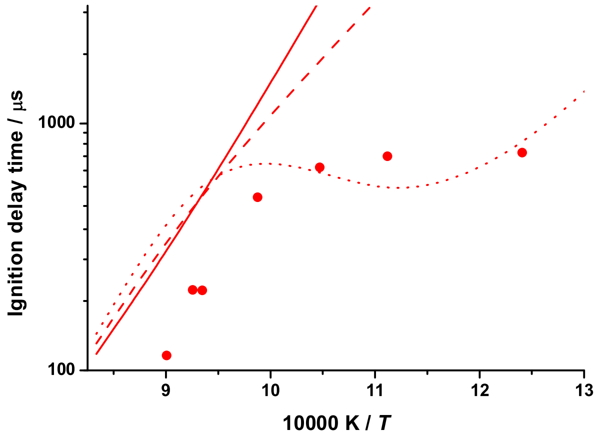

(b) $\phi = 0.5$

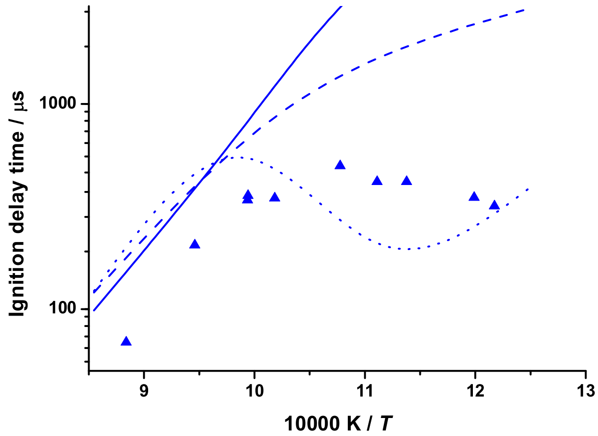

(c) $\phi = 1.0$

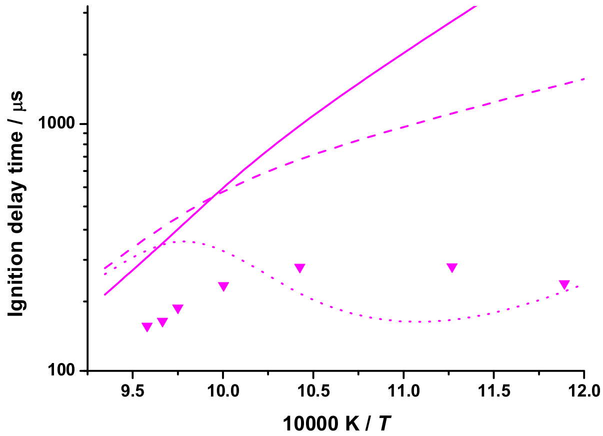

(d) $\phi = 2.0$

Figure 8.4: n-Butylcyclohexane shock tube ignition delay times (points) at $p = 50$ atm compared to model predictions.. —— JetSurF 2.0, - - - JetSurF 2.0 + Aramco Mech 1.0, $\cdots$ Natelson *et al.*

At 50 atm the n-butylcyclohexane JetSurF 2.0 under-predicts reactivity at all equivalence ratios by greater than a factor of two across the temperature range, as does the combined mechanism of Aramco Mech 1.0 and JetSurF 2.0, Fig. 8.4. While the mechanism of Natelson *et al.* also under-predicts reactivity at higher temperature it shows better agreement with the experimental data at low temperatures. At $\phi = 0.5$, 1.0 and 2.0 it is able to predict the NTC behaviour seen in the experimental data. However, it greatly over-predicts reactivity at $\phi = 0.3$.

n-Butylcyclohexane and *n*-Heptane Mixtures, 10 atm

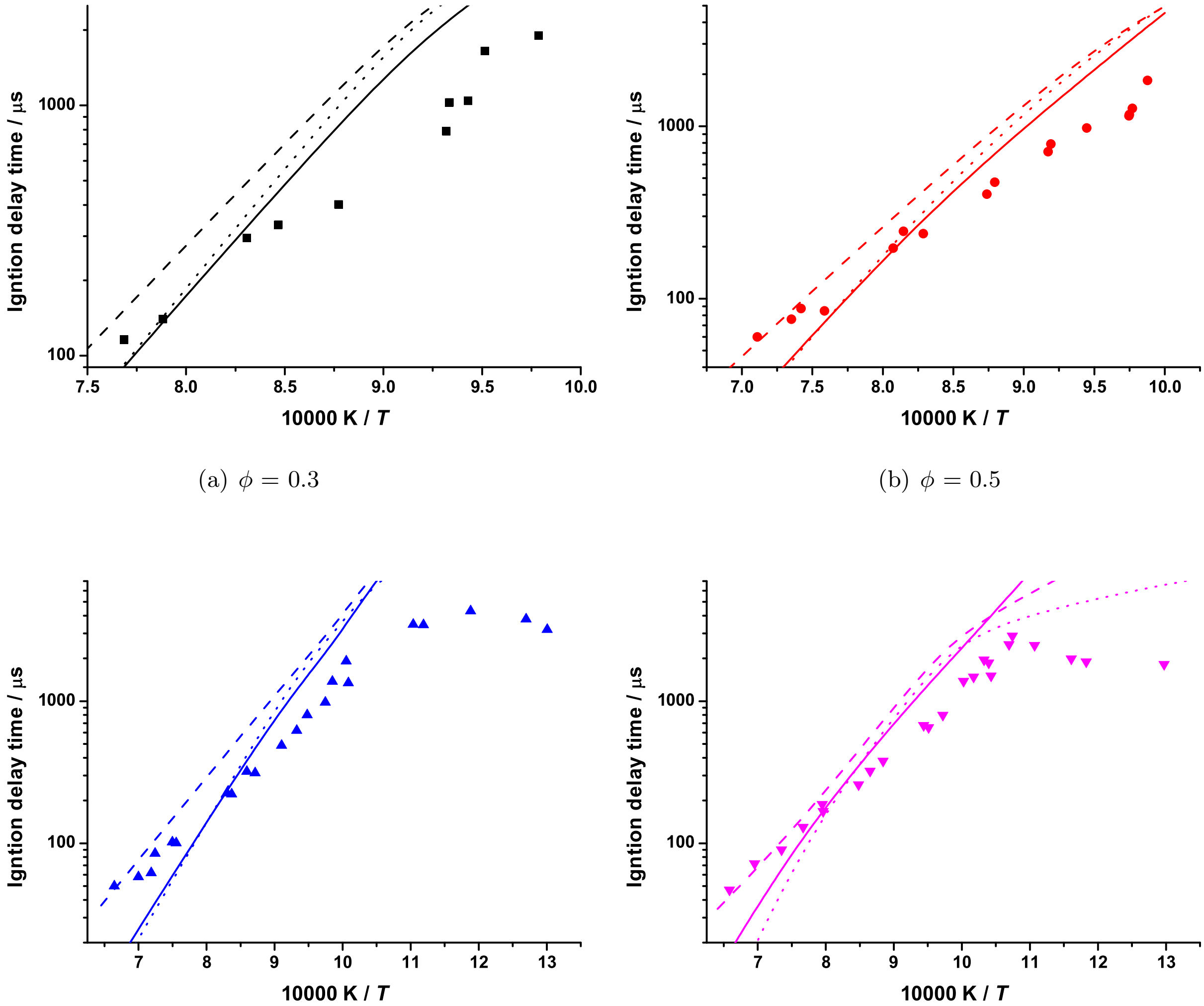

(a) $\phi = 0.3$

(b) $\phi = 0.5$

(c) $\phi = 1.0$

(d) $\phi = 2.0$

Figure 8.5: *n*-Butylcyclohexane / *n*-heptane shock tube ignition delay times (points) at $p = 10$ atm compared to model predictions. —— JetSurF 2.0, - - - JetSurF 2.0 + Aramco Mech 1.0, $\cdots$ Natelson *et al.*

All three mechanisms perform better of the *n*-butylcyclohexane / *n*-heptane mixtures than for *n*-butylcyclohexane only. They are all largely based on the same *n*-heptane sub-mechanism. The addition of Aramco Mech 1.0 to JetSurF 2.0 resulting the prediction of longer ignition delay time. None of the mechanisms predict the NTC behaviour seen in the experimental data at ϕ = 1.0.

n-Butylcyclohexane and n-Heptane Mixtures, 30 atm

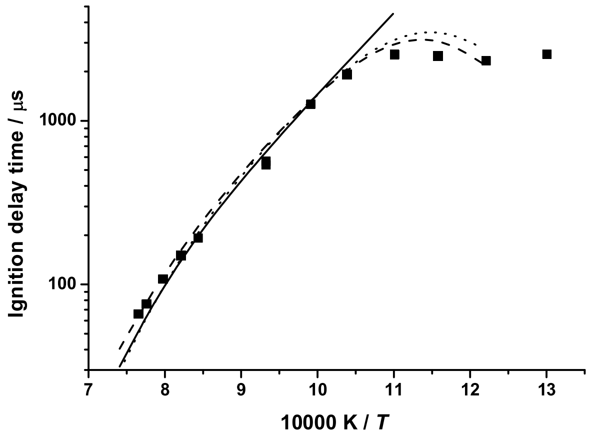

(a) $\phi = 0.3$

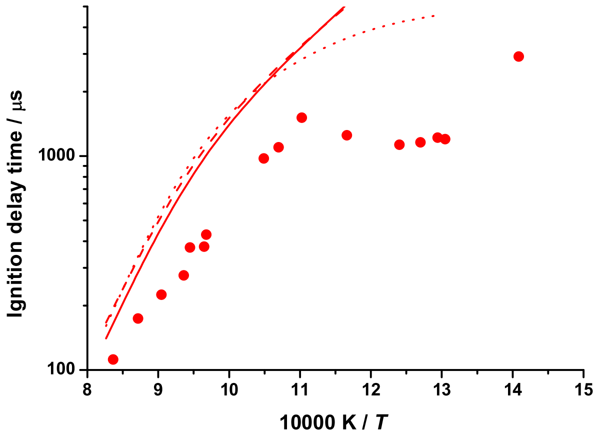

(b) $\phi = 0.5$

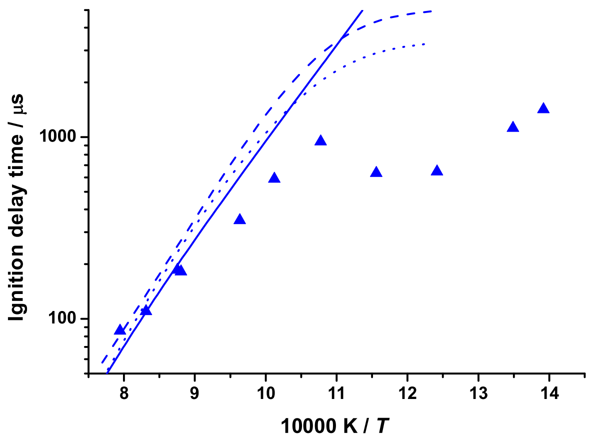

(c) $\phi = 1.0$

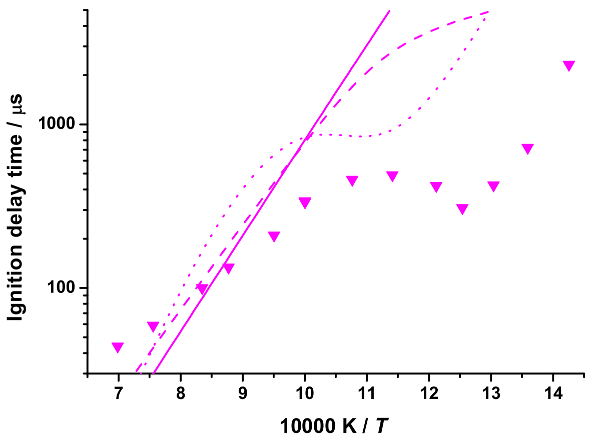

(d) $\phi = 2.0$

Figure 8.6: n-Butylcyclohexane / n-heptane shock tube ignition delay times (points) at p = 30 atm compared to model predictions. —— JetSurF 2.0, - - - JetSurF 2.0 + Aramco Mech 1.0, $\cdots$ Natelson *et al.*

Figure 8.6 shows that all three mechanisms predict similar ignition delay times for temperatures above 1000 K, however, the Natelson mechanism and the combined Aramco Mech 1.0 / JetSurF 2.0 mechanism predict NTC behaviour below this temperature while JetSurF 2.0 does not. The best agreement between model predictions and experimental results is seen at $\phi = 0.3$, Fig. 8.6(a).

A 'brute force' sensitivity analysis was performed to highlight the most important reactions controlling shock tube ignition delay times. This analysis involves increasing and decreasing each reaction rate expression by a factor of two and calculating the effect on the predicted ignition delay time. The sensitivity coefficient (σ) is defined as;

$$\sigma = \log\left(\frac{\tau'}{\tau''}\right) / \log\left(\frac{2.0}{0.5}\right) \tag{8.1}$$

where τ' is the ignition delay time calculated with the increased rate coefficient and τ'' is the ignition delay time calculated using the decreased rate expression. This definition results in negative sensitivity coefficients for reactions promoting reactivity and positive coefficients for those inhibiting reactivity.

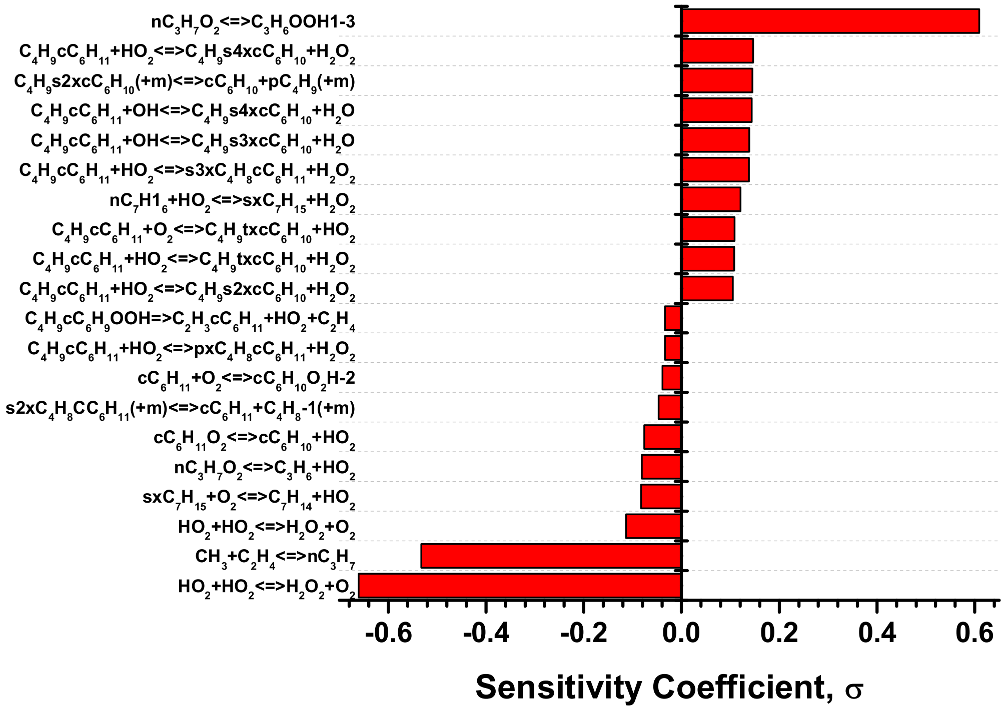

Figure 8.7: Sensitivity analysis carried out using JetSurF 2.0 with NUIG C_0 - C_4 sub-mechanism for n-butylcyclohexane / n-heptane mixtures at 30 atm, $\phi = 0.3$ atm, 865 K.

Figure 8.7 shows the sensitive reactions for n-butylcyclohexane / n-heptane mixtures at 30 atm $\phi = 0.3$, 865 K. It is important to note that many of the sensitive reactions are from the sub-mechanism with C_3 chemistry being highlighted as very important. At this condition on temperature and pressure the most sensitive reaction is the reaction of hydrogen peroxide and molecular oxygen resulting in two hydroxyl radicals, which in turn react with the fuel. Reactions of the fuel that are sensitive include hydrogen abstraction by hydroperoxyl and hydroxyl radicals.

JetSurF 2.0 does not include low temperature chemistry hence this sensitivity analysis has a number of missing pathways. At this temperature reactions of the fuel and molecular oxygen are important. Such reactions are not present in this mechanism.

n-Butylcyclohexane and n-Heptane Mixtures, 50 atm

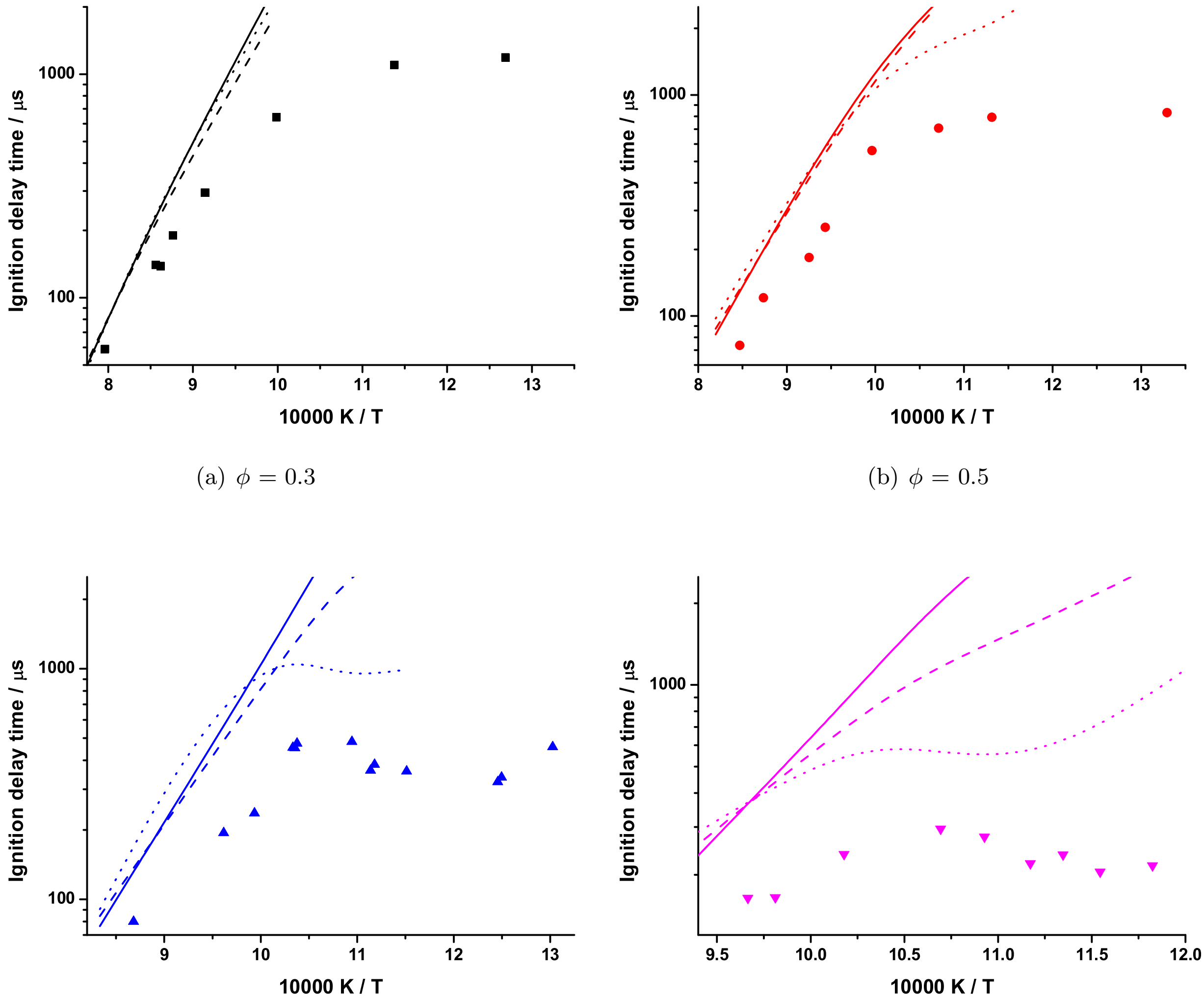

(a) $\phi = 0.3$

(b) $\phi = 0.5$

(c) $\phi = 1.0$

(d) $\phi = 2.0$

Figure 8.8: n-Butylcyclohexane / n-heptane shock tube ignition delay times (points) at $p = 50$ atm compared to model predictions. —— JetSurF 2.0, - - - JetSurF 2.0 + Aramco Mech 1.0, ··· Natelson *et al.*

For 50 atm data at high temperatures and all equivalence ratios there is little difference in the predictions of the three mechanisms, all under-predicts reactivity, Fig 8.8. However at ϕ = 2.0, at temperatures below 1000 K, Natelson *et al.* predicts ignition delay times which are four times faster than the predictions of JetSurF 2.0. At this condition NTC behaviour is also predicted by Natelson *et al.* and to a lesser extent the combined JetSurF 2.0 and Aramco Mech 1.0 mechanism.

In order to elucidate the reactions that cause the large difference in reactivity between the mechanisms a sensitivity analysis was carried out at $\phi = 2.0$, 940 K for JetSurF 2.0 and combined JetSurF 2.0 and Aramco Mech 1.0 as seen in Fig 8.9. It can be seen that for both mechanisms reactions of n-heptane and n-butylcyclohexane are among the most sensitive. At this condition of temperature and pressure the most sensitive reaction for both mechanisms is the decomposition reaction of hydrogen peroxide resulting in two hydroxyl radicals, which in turn react with the fuel. Reactions of the fuel components which are sensitive include unimolecular decomposition of the fuel radicals and hydrogen abstraction by hydroperoxyl radicals.

A sensitivity analysis was also carried out using the mechanism of Natelson *et al.* at $\phi = 2.0$, 940 K. At this condition of temperature and pressure the most sensitive reaction is the decomposition of hydrogen peroxide giving two hydroxyl radicals, which in turn react with the fuel. This mechanism contains low temperature pathways for n-butylcyclohexane. Sensitive low temperature reactions include reaction of the fuel radicals with molecular oxygen and isomerisation reactions.

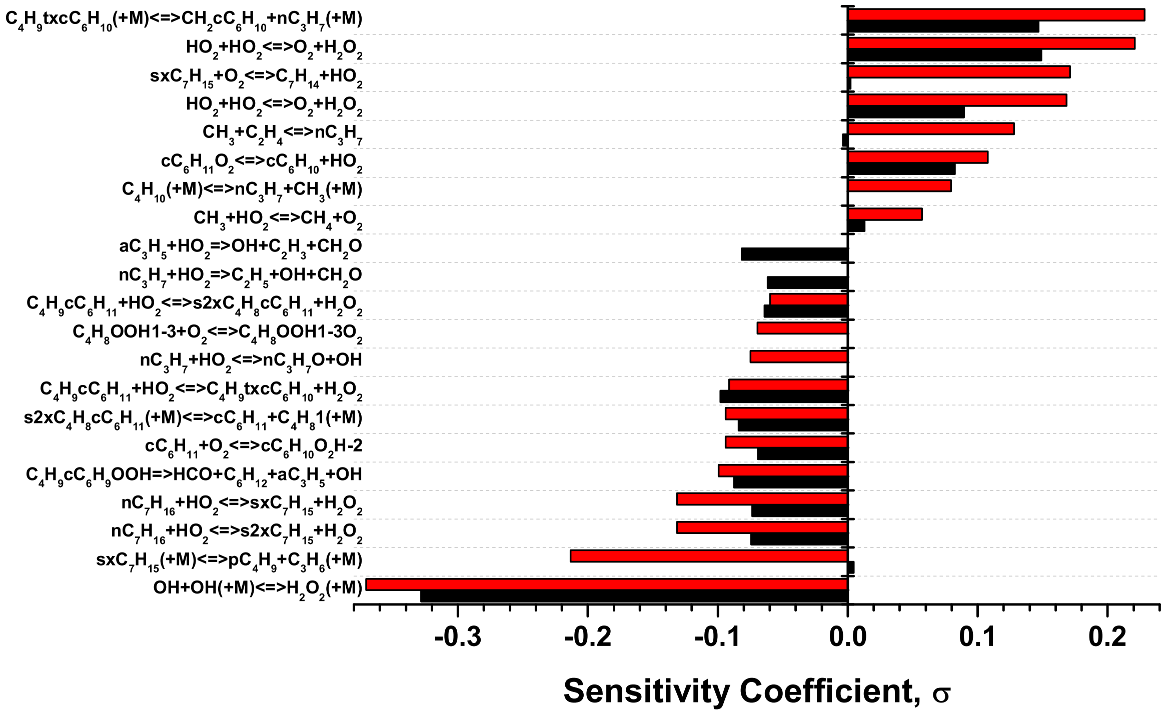

Figure 8.9: Sensitivity analysis carried out using JetSurF 2.0 and combined JetSurF 2.0 and Aramco Mech 1.0 mechanisms for n-butylcyclohexane / n - heptane mixtures at 50 atm, ϕ = 2.0 atm, 940 K. ■ – JetSurF 2.0, ■ – JetSuef 2.0 / Aramco 1.0

8.3 Conclusions

10, 30 and 50 atm n-butylcyclohexane and mixtures of n-butylcyclohexane / n-heptane, shock tube ignition delay times were simulated using JetSurF 2.0, the combined Aramco Mech 1.0 and C_5+ portion of JetSurF 2.0 and the mechanism of Natelson *et al.*, Fig. 8.1 – 8.8. The addition of Aramco Mech 1.0 to JetSurF 2.0 did not improve agreement with the experimental data. The mechanism of Natelson *et al.* performed the best as it incorporated low temperature chemistry.

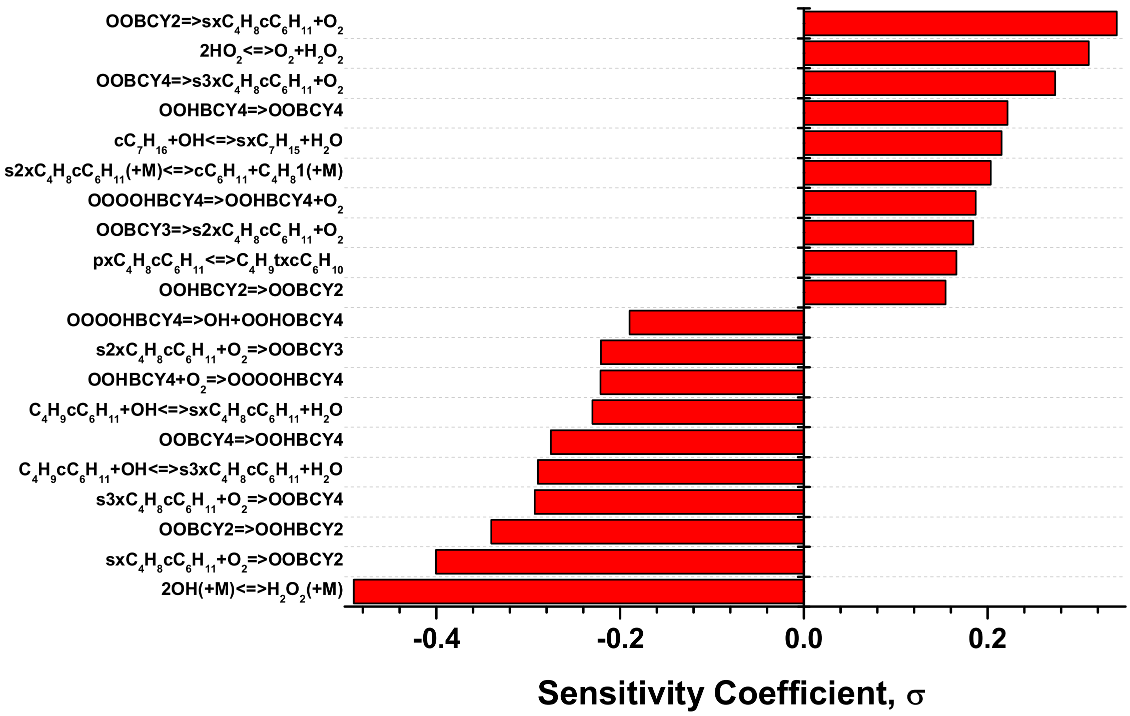

Figure 8.10: Sensitivity analysis carried out using the mechanism of Natelson *et al.* for n-butylcyclohexane / n - heptane mixtures at 50 atm, ϕ = 2.0 atm, 940 K.

Chapter 9

Low Pressure Shock Tube Study of the Isomers of Pentene

Alkenes that are found in transportation fuels are formed during the refining of crude oil by fluid catalytic cracking of heavier fractions in the presence of a zeolite catalyst. In this process hydrocarbons with higher boiling points, which are of little use for transportation fuels, are broken into smaller, more useful hydrocarbons. This process results in the formation of alkene products. Another process, alkylation, uses an acid catalyst to convert smaller alkenes to larger, branched alkanes which have a higher octane number and are hence a more valuable component of automotive fuels [86]. Despite this process a considerable amount of alkenes (approximately 5% [3]) are present in transportation fuels. Hence it is important that the combustion of such fuel components is understood.

The presence of such unsaturated components has both advantages and disadvantages. Short-chained alkenes have higher resistance to knock than alkanes of a similar length. Engine knock occurs as resut of detonation of the fuel outside the flame front, this is undisirable as this can leas to damage of engine parts. High concentrations of such components on the other hand, can affect the stability of the fuel and can result in the formation of gums in the engine. Another reason for interest in such unsaturated fuels is the presence of double bonds in biofuels such as fatty acid esters and their influence on a fuel's combustion characteristics.

The ignition delay times for both 1- and trans-2-pentene are presented here and the effect of the location of the double bond on the reactivity of the fuel is discussed.

9.1 Previous Work

A small number of studies have been carried out on the oxidation of the isomers of pentene. These include RCM studies [87, 88] and a flow reactor study [89].

Ribaucour *et al.* [87] carried out a study on the oxidation of 1-pentene in an RCM in the temperature range 600 – 900 K, at compressed pressures in the range 6 – 9 bar using stoichiometric fuel/air mixtures. Also as part of this work n-pentane was studied under similar conditions. For both of the fuels two-stage ignition and an NTC region was observed. A model for the combustion of n-pentane and 1-pentene was also presented as part of this work.

The oxidation of n-pentane and 1-pentene were studied in a rapid compression machine by Minetti *et al.* [88] at low-temperatures, 600 – 900 K, at pressures in the range of 6.8 – 9.2 bar and at $\phi = 1.0$ diluted in air. In this study, two series of experiments were conducted for each fuel. In the first series the pressure traces and light emissions were recorded during and after the ignition event. In the second, the chemical composition of the reacting mixtures were analysed using gas chromatography and mass spectrometry at various times during the pre-ignition period for selected initial conditions. Major products include water, ethene, propene, methanol, 1,3-butadiene, methanal, ethanal, 1-butene, propenal, propanal, propanone and 1,4-pentadiene. Reaction schemes were also proposed.

Prabhu *et al.* [89] have studied the oxidation of 1-pentene and the effect of the addition of nitric oxide. This work was carried out in a pressurised flow reactor at 6 atm, in the temperature range 600 – 800 K, and at an equivalence ratio of 0.4. Nitric oxide was added in small quantities, 0 – 500 ppm mole fraction. It was found that 1-pentene exhibited low-temperature reactivity and strong NTC behaviour. With the addition of NO it was found that the reactivity began at higher temperatures compared to experiments where only 1-pentene was used. In addition, the distribution of reaction products was altered by NO addition as well as the NTC behaviour of the fuel. The reactivity in the NTC region was enhanced by the concentrations of NO used in the study.

Earlier work carried out in the 1970's and 1980's was mainly concerned with the use of the pentene isomers as additives. Pentene was added to mixtures of *n*-heptane [90] and mixtures of hydrogen and oxygen [91] and the effect of this addition on the combustion was noted.

The effect of various additives on the cool flame combustion of *n*-heptane was studied by Tipper and Titchard [90]. In this work the pressure and temperature rise associated with the onset of a cool flame in 1:1 *n*-heptane:oxygen mixtures in the temperature range 240 – 270°C were recorded. The effect of the addition of 29 organic inorganic and organometallic species on the combustion of *n*-heptane was also recorded. Both 1- and 2-pentene were used in this study. It was found that both 1- and 2-pentene had an inhibiting effect with reduced reactivity observed for both additives. 2-Pentene was found to have a greater inhibiting effect than 1-pentene.

Baldwin *et al.* [91] have studied the effect of adding pentene to mixtures of hydrogen and oxygen. In this work an analysis of the products formed by the reaction of 1% 1-pentene and cis-2-pentene with slowly reaction mixtures of hydrogen and oxygen was carried out. These reactions were performed at 480°C in boric acid coated vessels. Reaction products were analysed at 5% pentene consumption. The analysis was preformed using gas chromatography. The major products for 1-pentene included propene, ethene, methane, butadiene, butene, pentadiene, 2-pentene, 2-ethyloxetane, propionaldehyde, methylethylketone, 2,4-dimethyloxetane, tetrahydropyran, 2-propyloxirane, butyraldehyde, 2-methyltetrahydrofuran and acetaldehyde. Similar products were observed for 2-pentene. Reaction pathways were proposed to account for the products observed.

The combustion of pentenes in the cool flame region was studied by Hughes and Prodhan [92], where the temperature and pressure changes associated with the passage of cool flames though mixtures were measured for each of the three isomers of pentene; 1-pentene and cis- and trans-2-pentene. These experiments were carried out at a 1:1 fuel:oxygen ratio in the temperature range 280 – 330°C. It was found that the induction periods for 1-pentene were much shorter than those for 2-pentene.

9.2 This Work

9.2.1 Experimental

Experiments were performed in the low-pressure shock tube. 1-Pentene (99.5%) and trans-2-pentene (99%) were supplied by TCI. Oxygen (99.99%), argon (99.99%) helium (99.99%) and nitrogen (99.95%) gases were supplied by BOC. All reagents were used without further purification. Gas mixtures were prepared as per the procedure outlined previously for the low-pressure shock tube, Section 4.1. Experiments were carried out for mixtures of 1% fuel at equivalence ratios of 0.5, 1.0 and 2.0 and at a reflected shock pressure of 1 atm. Mixtures compositions are provided in Table 9.1.

ϕ	Fuel	Oxygen	Argon
0.5	1.0	15.0	84.0
1.0	1.0	7.5	91.5
2.0	1.0	3.75	95.25

Table 9.1: Percentage composition of 1-pentene and 2-pentene gas mixtures.

9.2.2 Computational

A computational study was carried out in collaboration with the group at Lawrence Livermore National Laboratory [93]. The mechanism was validated using the experimental data presented here and also using 10 atm shock tube ignition delay times and 1-, 2- and 3-hexene 10 atm shock tube and RCM data.

This mechanism was based on a $C_1 - C_4$ detailed core mechanism developed at NUI Galway. In addition to this model reactions were added to take into account linear, branched and aromatic hydrocarbons. The alkene chemistry was based on a previous mechanism by Mehl et al. [94]. Rates of reactions for abstraction, radical decomposition, internal isomerisations and initiation reactions have been reviewed and replaced based on previous works published in the literature [95–98].

9.2.3 Results

Experimental Work

The experiments were carried out in the low-pressure shock tube using 1% fuel at equivalence ratios of 0.5, 1.0 and 2.0, at a reflected shock pressure of 1 atm and reflected shock temperatures in the range 1250 – 1900 K. Both 1- and trans-2-pentene were studied under these conditions, Fig. 9.1. It can be seen that there is a clear effect of equivalence ratio for both fuels. Throughout the temperature range studied the fuel lean data is the most reactive while the fuel lean data is the least reactive. This is true for both fuels.

Computational Work

Ignition delay times were calculated using the Mehl *et al* [93] mechanism. The computational results can be seen in Fig. 9.1 where the simulation results are plotted as lines. It can be seen that at lean and stoichiometric conditions the model captures the experimental data well. At fuel rich conditions the model deviates slightly from then experimental data at the highest temperatures studied.

Comparison of 1- and 2-Pentene

When comparing the reactivity of 1- and 2-pentene, Fig. 9.2, it can be seen that 2-pentene has a slightly higher reactivity than 1-pentene with ignition delay times for 2-pentene being slightly shorter than those observed for 1-pentene. This is due to the underlying chemistry, to investigate this a rate of production analysis was carried out for 1- and 2-pentene at $\phi = 1.0$, 1470 K, Fig. 9.3.

The dominant pathway for 1-pentene consumption is unimolecular decomposition resulting in the formation of a resonantly stable allyl radical and ethyl radical. Other pathways see the abstraction of hydrogen from the fuel resulting in fuel radicals which decompose to give alkyl and alkenyl radicals and dienes.

The dominant pathway for 2-pentene consumption is unimolecular decomposition of the fuel forming a methyl radical and alkneyl radical, this decomposed further to form a diene and

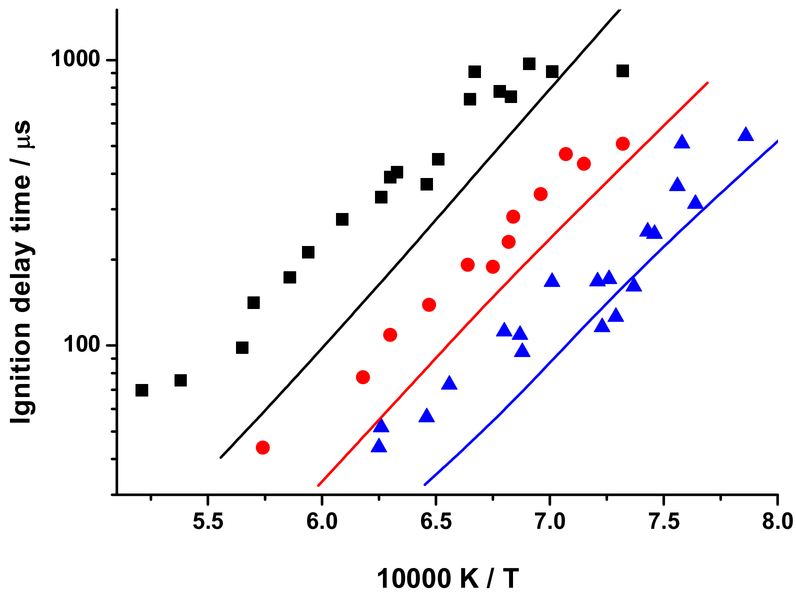

(a) 1-pentene

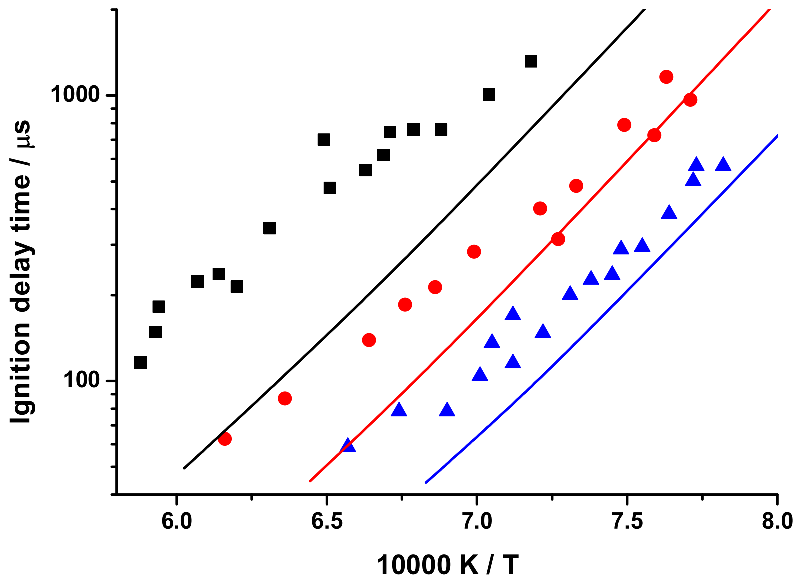

(b) trans-2-pentene

Figure 9.1: 1% 1-pentene and 2-pentene, 1 atm , experimental data and model predictions, ■ – $\phi = 2.0$, ● – $\phi = 1.0$, ▲ – $\phi = 0.5$. Lines represent model predictions.

hydrogen atom. Other pathways see the abstraction of hydrogen from the fuel resulting in small alkyl and alkenyl radicals and dienes.

Over the temperature range of this study the dominant pathway for the consumption of the 1-pentene fuel is to form an allyl and ethyl radical. Allyl radicals have resonance stability and are hence less reactive. The dominant pathway for the consumption for the 2-pentene fuel at these temperatures is to form a diene and a hydrogen atom which promotes reactivity resulting in 2-pentene having shorter ignition delay times than that of 1-pentene.

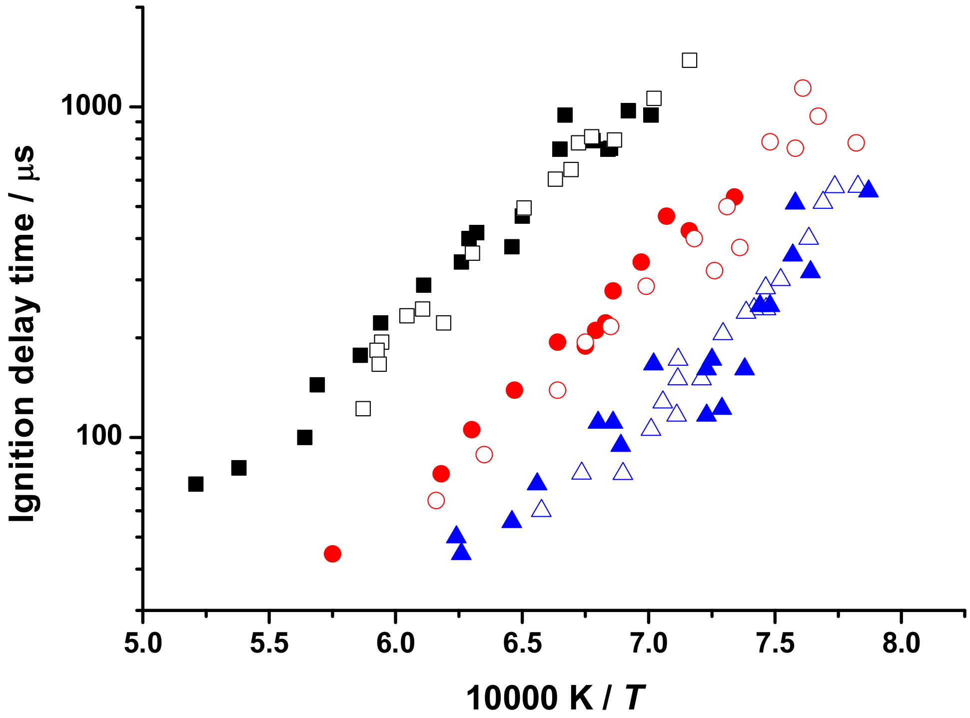

Figure 9.2: Comparison of 1- and 2-pentene 1 atm ignition delay times. 1-pentene, ■ − $\phi = 2.0$, ● − $\phi = 1.0$, ▲ − $\phi = 0.5$. 2-pentene, open symbols.

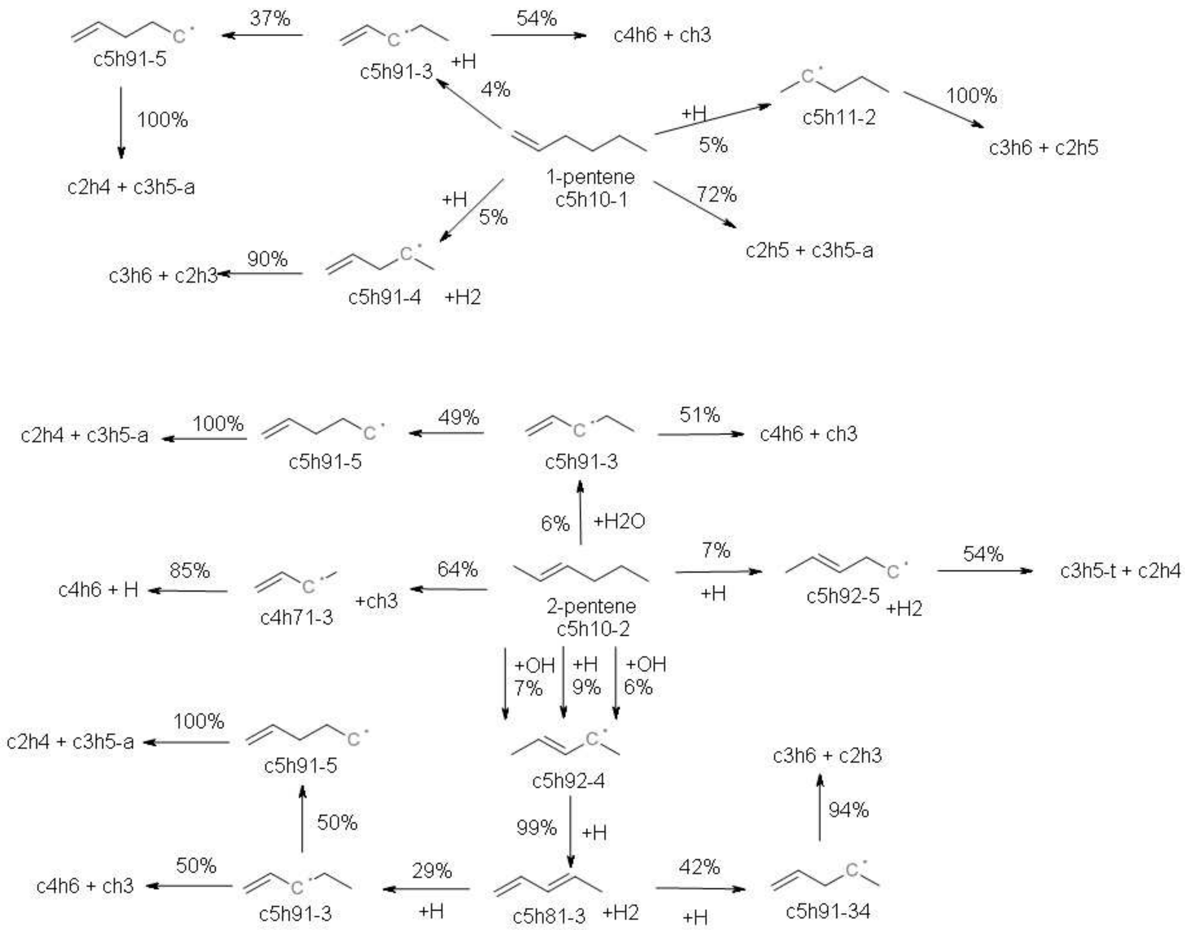

Figure 9.3: Rate of production showing the major pathways for 1- and 2-pentene decomposition carried out using the mechanism of Mehl *et al.* [93] at 1 atm, $\phi = 1.0$ atm, 1470 K.

Chapter 10

Low Pressure Shock Tube Study of 2,5-Dimethylfuran

Biofuels, that is fuels derived from biomass, have in recent years generated a great deal of interest. This is mainly due to increasing fuel prices, the need for greater energy security and increasing restrictions concerning emissions.

2,5-Dimethylfuran holds great potential as a biofuel which is currently underutilised. Ethanol is currently a widely used biofuel but is not without its disadvantages. Ethanol has a low energy density, is highly volatile and can be contaminated by the adsorption of water from the atmosphere. By comparison, 2,5-dimethylfuran has more desirable properties. It is less volatile, has a higher energy density and is not soluble in water. In the literature routes have been described to produce 2,5-dimethylfuran including a catalytic route using fructose, obtained directly from biomass or from the isomerisation of glucose, as a starting material, Fig. 10.1 [99]. Another proposed pathway to the production of 2,5-dimethylfuran is to firstly produce 5-hydroxymethylfurfural from corn stover, the inedible waste from the harvesting of crops such as the stalks and husks [100]. The 5-hydroxymethylfurfural produced, when purified, can be converted to 2,5-dimethylfuran via hydrogenolysis using a copper catalyst.

2,5-Dimethylfuran also may help overcome the "food v's fuel" debate that arises in the production of biofuels. Bio-ethanol, for example, is typically produced via the fermentation of sugars and starches which occur in plants. The debate arises whether food which was once intended for human consumption should be used for this purpose or should land that was once used for agricultural purposes now be devoted to the production of such crops. Another real fear is the potential loss of natural habitats to land for this purpose. It has been suggested that the large increase in the production of biofuels is to blame for the rise in global food prices.

Second generation biofuels such as 2,5-dimethylfuran may hold an answer to these problems because it can be produced from cellulose which is unsuitable for human consumption.

10.1 Previous Work

One of the first 2,5-dimethylfuran studies reported in the literature is a pyrolysis study carried out by Lifshitz *et al.* [101]. In this work the thermal decomposition of 2,5-dimethylfuran was studied in a single pulse shock tube in the temperature range 1070 – 1370 K for mixtures of 0.5% 2,5-dimethylfuran. Analysis of the post shock gas was carried out using gas chromatography. A reaction scheme of 50 species and 180 reactions was proposed based on the product distributions observed over the temperature range of the study.

Wu *et al.* [103] have measured the laminar burning velocity and Markstein length of premixed mixtures of 2,5-dimethylfuran in air diluted with nitrogen and carbon dioxide. Measurements were taken at atmospheric pressure, at an initial temperature of 393 K and at equivalence ratios

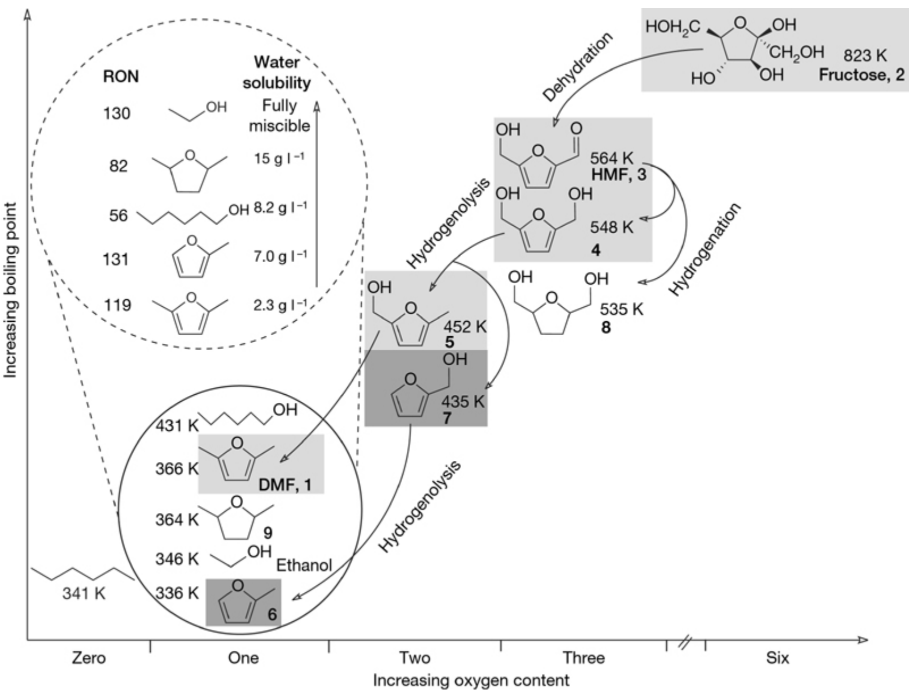

Figure 10.1: Production of 2,5-dimethylfuran form fructose [99].

in the range $\phi = 0.9 - 1.5$. Three different dilution ratios of N_2/CO_2 were used over a number of equivalence ratios. It was found that the addition of the N_2/CO_2 diluents decreases the unstretched flame propagation rate and the laminar burning velocity. The addition of CO_2 has a much larger influence than N_2. It was also found that the stability of the flame increased with increasing dilution ratios. This is more evident in fuel-lean mixtures than in fuel-rich ones.

Wu *et al.* [102] have studied 2,5-dimethylfuran laminar flames at low pressure. Mixtures of 2,5-dimethylfuran/O_2/Ar were studied with tunable vacuum ultraviolet synchrotron radiation photoionisation and molecular beam mass spectrometry. Photoionsiation mass spectra of the flames were recorded and photoionisation efficiency curves of combustion intermediates measured. Species were identified by comparing measured ionisation energies with those which have been reported in the literature or to values which had been calculated. In all, more than 70 species were detected using this technique, including furan and its derivatives, aromatics and free radicals. Also reported was possible reaction pathways for 2,5-dimethylfuran, 2-methylfuran and furan based on the intermediates identified.

Tian *et al.* [104] carried out a comparative study of 2,5-dimethylfuran, ethanol and conventional gasoline using laminar flame velocities. Experiments were performed at initial temperatures in the range 50 – 100°C and at a number of equivalence ratios in the range $\phi = 0.6 - 2.0$. The fuel-air mixtures were examined in a constant volume vessel and recorded using high speed schlieren visualisation, hence measurements of flame growth following ignition and the laminar flame velocity were calculated. It was found that for all fuels flame propagation was fastest at slightly richer conditions, between equivalence ratios of 1.0 and 1.2. At all initial temperatures it was found that ethanol has the fastest burning velocity while those of gasoline and 2,5-dimethylfuran were quite similar.

Zhong *et al.* [105] have studied 2,5-dimethylfuran in a direct ignition spark ignition engine. Tests were carried out at an inlet temperature of 25°C, at a constant engine speed of 1500 RPM and at an equivalence ratio of 1.0. 2,5-Dimethylfuran, ethanol and gasoline were all tested under these conditions. Fuel consumption, thermal efficiency, engine knock, legislated gaseous emissions and particulate matter emissions were studied. It was concluded that the use of pure 2,5-dimethylfuran in a research engine did not show any adverse effects on the engine and the combustion duration of 2,5-dimethylfuran was shorter than that of ethanol. For both 2,5-dimethylfuran and gasoline the concentration of CO, hydrocarbons and $NO_{\times}$ emissions were similar. This was also true for particulate matter, although the mean diameter size of the particulate matter was smaller for 2,5-dimethylfuran.

Wu *et al.* [106] have studied the laminar burning velocities and Markstein lengths of 2,5-dimethylfuran as part of a blend with iso-octane. This study was carried out using the outwardly propagating spherical flame method and high speed schlieren photography. The experiments were performed at initial pressures of 1.0, 2.5 and 5.0 bar, at initial temperatures of 393, 433 and 473 K and at equivalence ratios in the range 0.9 – 1.5 at 0.1 intervals. It was found that the flame speeds for 2,5-dimethylfuran/iso-octane mixtures were higher than those for iso-octane/air.

Friese *et al.* [107] performed an experimental and theoretical study of the reaction of 2,5-dimethylfuran with hydrogen atom. The experimental part of this study was carried out in a shock tube at reflected shock pressures near 1.6 and 4.8 bar with reflected shock temperatures in the range 970 – 1240 K and initial mole fractions of 2,5-dimethylfuran in the range of 12 – 40 ppm. Ethyliodine was used as the source of hydrogen atoms as it decomposes to give ethene, hydrogen and iodine. For this investigation, initial mole fractions used were in the range of 2 – 4 ppm. Quantum chemical and statistical rate theory calculations were also carried out. Energies of reactants, transition states and products were calculated.

Sirjean and Fournet [108] carried out a theoretical study of the reaction of 2,5-dimethylfuran with hydrogen atom and the products formed. The reaction of 2,5-dimethylfuran with H-atom was studied using a calculated potential energy surface. Hydrogen abstraction by H-atom and hydrogen addition to 2,5-dimethylfuran were considered.

Sirjean *et al.* [109] carried out a shock tube and chemical kinetic modelling study of the oxidation of 2,5-dimethylfuran. Experiments were carried out at reflected shock pressure of 1 and 4 bar, equivalence ratios of 0.5, 1.0 and 1.5 and with reflected shock temperatures in the range 1300 – 1831 K. A kinetic model is also presented as part of this work. This model was validated using shock tube ignition delay times and pyrolysis speciation data of Lifshitz *et al.* [101]. The model was in good agreement with the experimental data.

10.2 This Work

10.2.1 Experimental

This study was undertaken to compliment work which had been previously been carried out by Black at NUI Galway [110]. Experiments were performed using the low-pressure shock tube at equivalence ratios of 1.0 and 2.5 and at a reflected shock wave pressure of 1 atm. To expand on these data sets ignition delay times were recorded for equivalence ratios of 0.5 and 2.0 at 1 atm and at equivalence ratios of 0.5, 1.0, 2.0 and 2.5 at 2 atm using 0.75% fuel.

2,5-Dimethylfuran (99%) was supplied by Sigma Aldrich. Oxygen (99.99%), argon (99.99%), helium (99.99%) and nitrogen (99.95%) gases were supplied by BOC. All reagents were used without further purification. Gas mixtures were prepared as per the procedure outlined previously for the low-pressure shock tube, Section 4.1. The composition of the mixtures used are provided in Table 10.1.

ϕ	Fuel	Oxygen	Argon
0.5	0.75	11.25	88
1.0	0.75	5.625	93.625
2.0	0.75	2.8125	96.4375

Table 10.1: Percentage composition of 2,5-dimethylfuran gas mixtures.

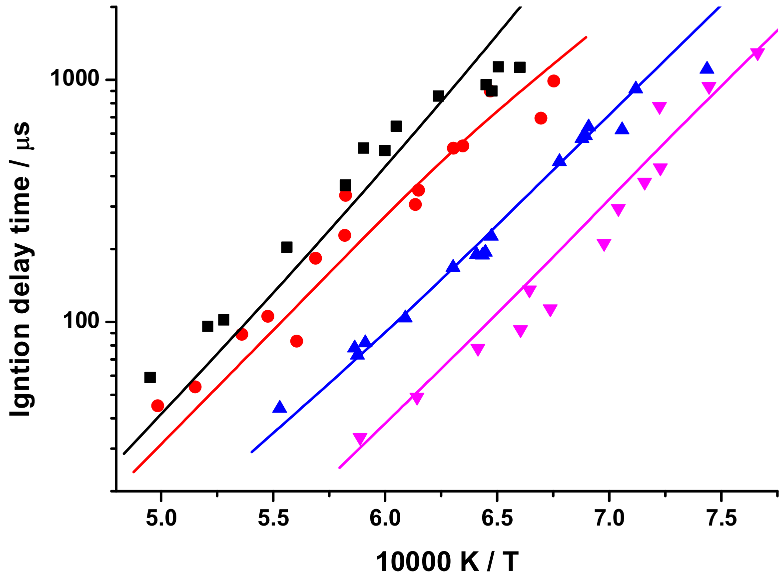

(a) 1 atm

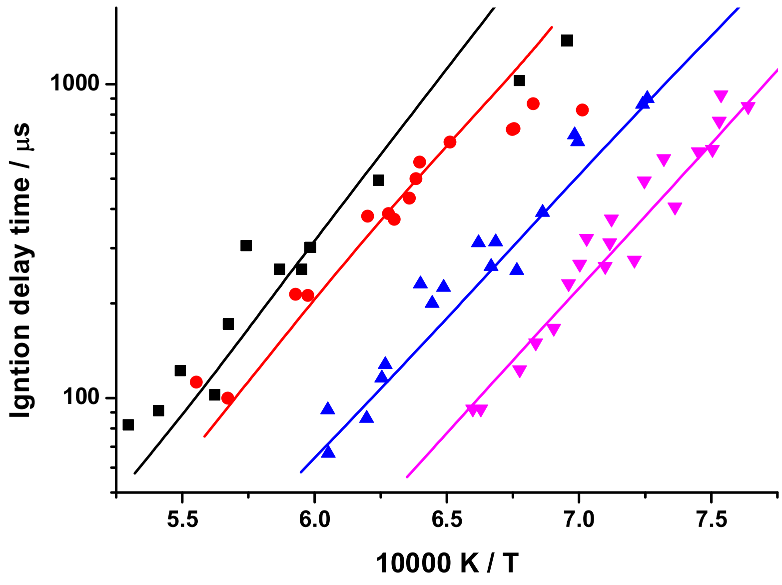

(b) 2 atm

Figure 10.2: 2,5-dimethylfuran experimental results, 1 atm, ■ – ϕ = 2.5 (Black), ● – ϕ = 2.0 (Conroy), ▲ – ϕ = 1.0 (Black), ▼ – ϕ = 0.5 (Yasunaga). 2 atm, ■ – ϕ = 2.5 (Yasunaga), ● – ϕ = 2.0 (Conroy), ▲ – ϕ = 1.0 (Conroy), ▼ – ϕ = 0.5 (Conroy). Lines represent model predictions of Somers *et al.* [111]

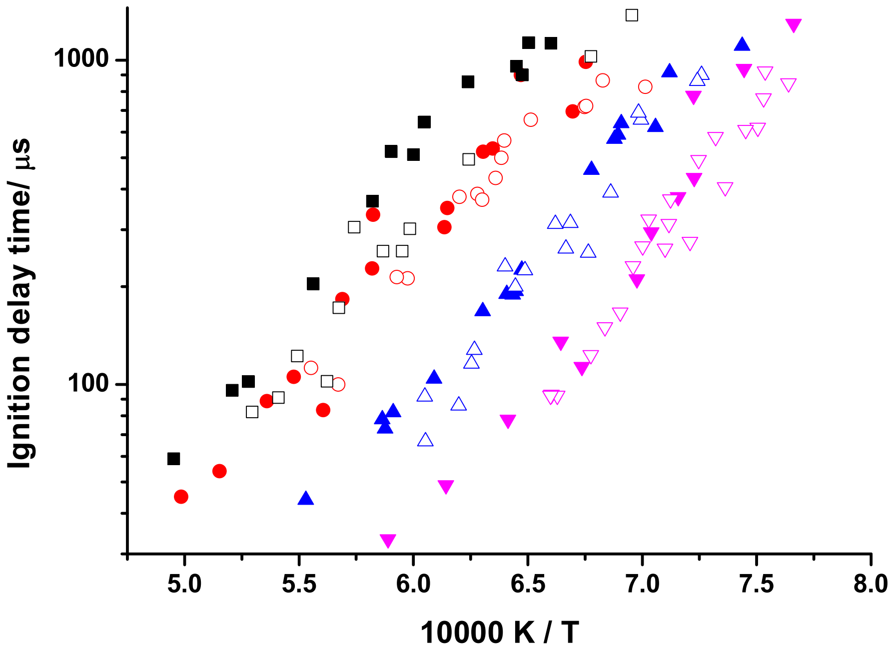

Figure 10.3: Effect of pressure on 2,5-dimethylfuran ignition delay times, ■ – ϕ = 2.5, ● – ϕ = 2.0, ▲ – ϕ = 1.0, ▼ – ϕ = 0.5. 1 atm - closed symbols, 2 atm - open symbols.

10.3 Results

10.3.1 Experimental

From Fig. 10.2 it can be seen that there is a clear effect of equivalence ratio and that there are differences in the separation of the reactivities of the equivalence ratios. The reactivities of the ϕ = 0.5, 1.0 and 2.0 are equally spaced while the reactivity of the ϕ = 2.5 is somewhat less reactive than the trend. This is true for both pressures. In the temperature range studied, 1300 – 2000 K, it is clear that fuel lean mixtures are the most reactive over the temperature range studied while the fuel rich are the least reactive. This is also true for both data taken at both 1 and 2 atm.

The effect of pressure can be seen in Fig. 10.3. It can be seen that there is little effect of pressure with the 2 atm data being only slightly faster than the 1 atm data.

10.3.2 Model Simulations

A computational study was carried out at NUI Galway by Somers *et al.* [111]. A detailed chemical kinetic mechanism containing 2768 reactions and 545 species was developed. This mechanism was validated using shock tube pyrolysis data and ignition delay times, flame speeds and jet stirred reactor speciation data.

Ignition delay times were calculated using the mechanism of Somers *et al.* [111]. Computational results can be seem in Fig. 10.2 where the simulated results are plotted as lines. It can be seen that the model predicts the experimental data well for all conditions of this study.

To investigate the chemistry taking place a rate of production analysis was carried out at ϕ = 1.0 and 1650 K at 1 atm, Fig 10.4. It can be seen that under these conditions the majority of the fuel, dmf25, undergoes H abstraction from one of the methyl groups attached to the furan ring resulting in a fuel radical. This radical undergoes a ring opening reaction to give a ketone which decomposes further. Other less dominant pathways include unimolecular decomposition of the fuel to give a diene and aldehyde. Also the fuel may decompose to give 2-methylfuran and a methyl radical.

A sensitivity analysis was also carried out at 1 atm, ϕ = 1.0, 1550 K, Fig. 10.5 to investigate the reactions which the ignition delay time was sensitive to. It was found that the most sensitive reaction was $\dot{H} + O_2 \longrightarrow \dot{O}H + \ddot{O}$. This reaction was hugely promoting to the system. Reactions of the fuel and fuel radicals are also important.

10.4 Conclusions

The low-pressure shock tube data for 2,5-dimethylfuran taken by Black was greatly expanded upon by this study. Previously experiments had only been carried out over a small number of equivalence ratios, at one pressure. In completing this experimental investigation ignition delay time data is now available at reflected shock wave pressures of 1 and 2 atm and over a range of equivalence ratios, ϕ = 0.5 – 2.5.

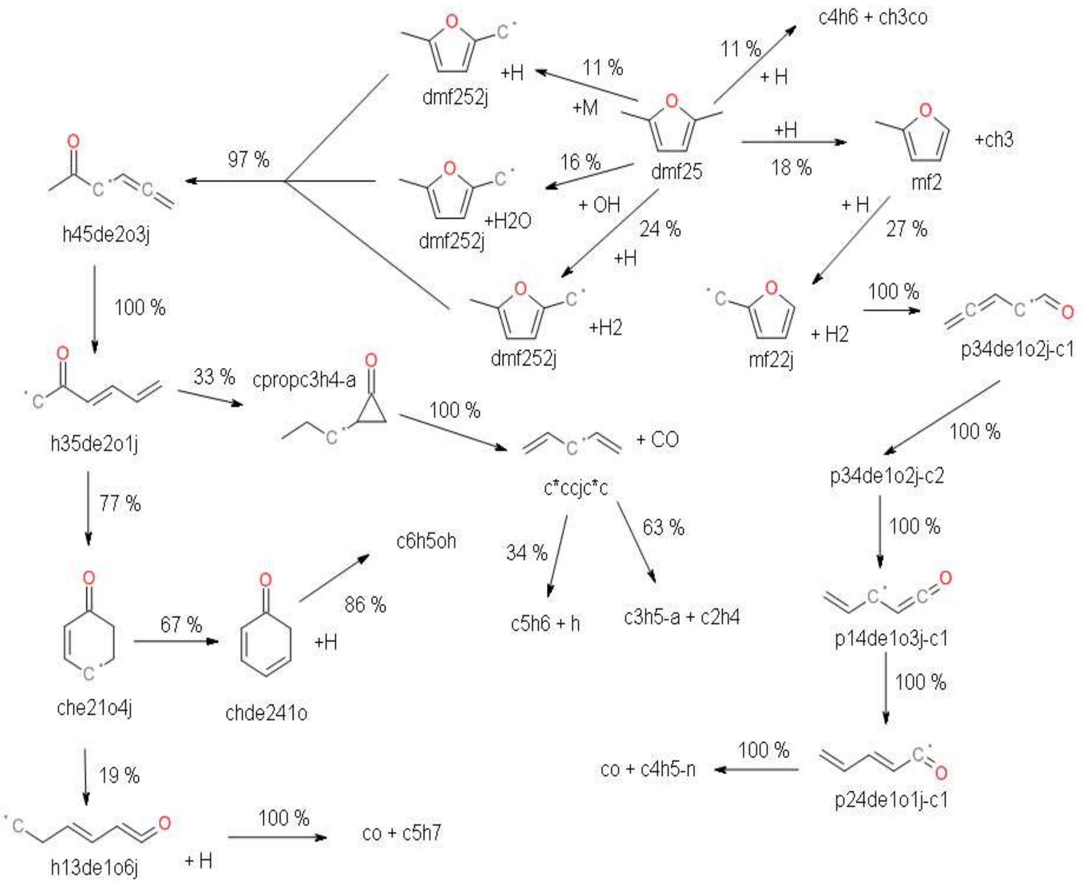

Figure 10.4: Rate of production carried out using the mechanism of Somers *et al.* [111], 10% fuel consumption at 1 atm, $\phi = 1.0$ atm, 1650 K.

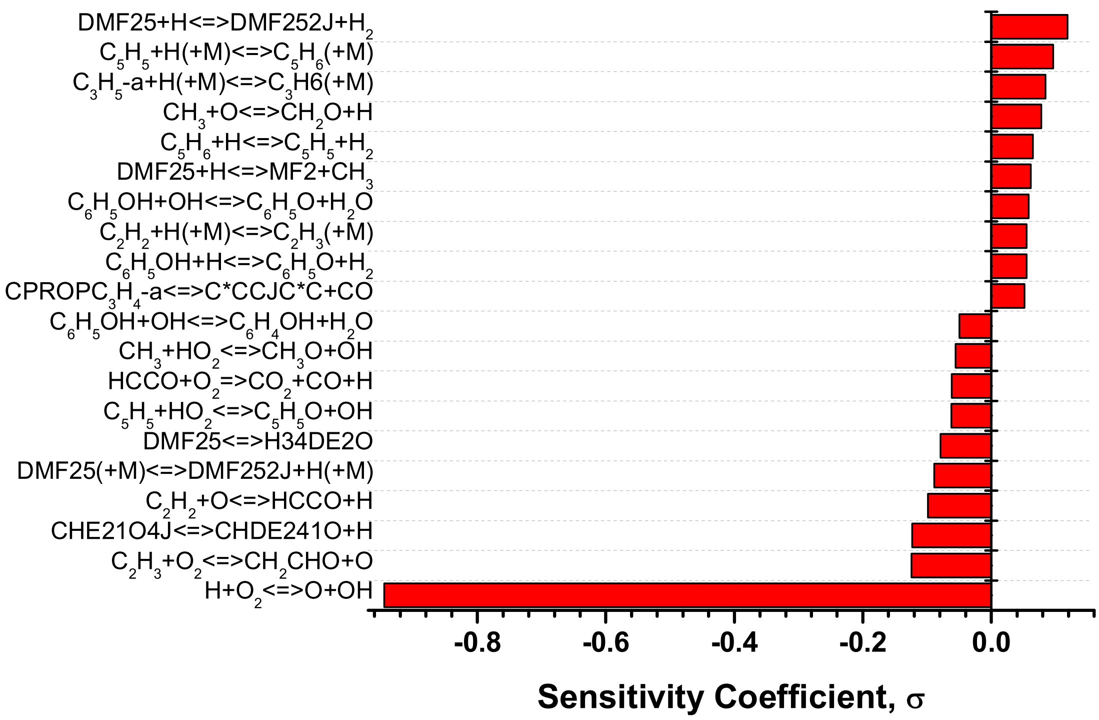

Figure 10.5: Sensitivity analysis carried out using the mechanism of Somers *et al.* [111] at 1 atm, $\phi = 1.0$, 1550 K.

Chapter 11

Conclusion

This study represents the first high pressure ignition delay time study of n-butylcyclohexane. This fuel was studied extensively in both the shock tube and the rapid compression machine over a wide range of temperatures, pressures and equivalence ratios. Ignition delay times were measured in the temperature range 580 – 1550 K, at reflected shock wave and compressed gas pressures of 1, 10, 30 and 50 atm and at equivalence ratios of 0.3, 0.5, 1.0 and 2.0 in air. High temperature experiments were carried out in the high pressure shock tube while experiments at lower temperatures were carried out using the rapid compression machine.

In addition ignition delay times were also measured for mixtures of n-butylcyclohexane and n-heptane. Experiments were carried out at similar conditions to those outlined for n-butylcyclohexane. This mixture was chosen to represent a surrogate for n-decylcyclohexane as it has a similar hydrogen/carbon ratio. n-Decylcyclohexane is a large alkyl-cyclohexane fuel component which has an extremely low vapour pressure and is impossible to study in the gaseous phase hence this surrogate was used to emulate this fuel.

Experiments carried out at 1 atm were unsuccessful, however experiments carried out at 10, 30 and 50 atm for both fuels were successful and a large amount of data was collected over a range of equivalence ratios and wide temperature range. As a result a large range of engine relevant experimental conditions were covered producing data with is suitable for model validation.

Due to the low vapour pressure of n-butylcyclohexane heating of the experimental facilities used was necessary. Heating systems were installed onto the shock tube, rapid compression machine, manifolds and mixing tanks to ensure that all fuel remained in the gaseous phase for the duration of the experiment. Infra-red absorption test were carried in a heated test cell and in situ in the rapid compression machine. Results of these tests confirmed fuel concentration and hence no condensation of the fuel was occurring during experiments.

Ignition delay times of n-butylcyclohexane were compared to those of the n-decylcyclohexane surrogate. It was found that over the range of conditions of this study the ignition delay times of the two fuels exhibit similar reactivity. When these ignition delay times were compared to 10 atm, $\phi = 1.0$, n-heptane ignition delay times measured under similar conditions, all three fuels exhibited similar reactivity suggesting that at this condition large alkyl-cyclohexanes have similar reactivity as larger n-alkanes.

Experimental results for both n-butylcyclohexane and n-butylcyclohexane / n-heptane mixtures were compared to simulations using two mechanisms from literature, JetSurF 2.0 and Natelson *et al.* In an effort to improve the simulation results Aramco Mech 1.0, a highly validated C_0 - C_4 sub-mechanism, was substituted into JetSurF 2.0. This did not improve the simulation results. The mechanism of Natelson *et al.* performed the best, however extensive modification of the mechanism is required to capture the experimental data.

The isomers of pentene were studied in the low pressure shock tube. Ignition delay times were measured for 1- and trans-2-pentene in the temperature range 1250 – 1900 K, at a reflected shock wave pressure of 1 atm and at equivalence ratios of 0.5, 1.0 and 2.0 at 1% fuel concentration. For both isomers, throughout the temperature range of the study fuel rich mixtures are slowest to ignite while fuel lean mixtures are fastest to ignite. This data was used in conjunction with high pressure shock tube and rapid compression machine data to validate the chemical kinetic mechanism of Mehl *et al.* The model captures the trend of the experimental data, however the simulated ignition delay times are faster than those seen experimentally. At $\phi = 2.0$ at the highest temperature of the study the model deviates from the experimental data. This is seen for both isomers.

In addition 2,5-dimethyfuran was also studied in the low pressure shock tube. Ignition delay times were measured in the temperature range 1300 – 2000 K, at a reflected shock wave pressures of 1 and 2 atm and at equivalence ratios of 0.5, 1.0, 2.0 and 2.5 at 0.75% fuel concentration. For both pressures studied, throughout the temperature range fuel rich mixtures are slowest to ignite while fuel lean mixtures are fastest to ignite. This shock tube data was used in conjunction with high pressure shock tube, pyrolysis, flame speed and jet stirred reactor data to validate the chemical kinetic mechanism of Somers *et al.* The model captures the experimental data for all pressures and equivalence ratios studied.

Bibliography

[1] http://www.seai.ie/Publications/Statistics_Publications/Energy_in_Ireland/Key_statistics_booklet_1990_to_2010.pdf

[2] J. G. Speight, Environmental Analysis and Technology for the Refining Industry (2005)

[3] F. Battin-Leclerc, 'Detailed Chemical Kinetic Models for the Low-Temperature Combustion of Hydrocarbons with Applications to Gasoline and Diesel Fuel Surrogates' *Progress in Energy and Combustion Science* vol. 34 (2008) p. 440 – 498.

[4] H.K. Ciezki, G. Adomeit, 'Shock-tube Investigation of Self-ignition of n-Heptane-Air Mixtures Under Engine Relevant Conditions' *Combustion and Flame* vol. 93 (1993) p. 421 – 433.

[5] R. Minetti, M. Carlier, M. Ribaucour, E. Therssen, L.R. Sochet, 'A Rapid Compression Machine Investigation of Oxidation and Auto-Ignition of n-Heptane; Measurements and Modelling' *Combustion and Flame* vol. 102 (1995) p. 298 – 309.

[6] H.J. Curran, P. Gaffuri, W.J. Pitz, C.K. Westbrook, 'A Comprehensive Modelling Study of n-Heptane Oxidation' *Combustion and Flame* vol. 114 (1998) p. 149 – 177.

[7] H. Curran, W.J. Pitz, C.K. Westbrook, C.V. Callahan, F.L. Dryer, 'Oxidation of Automotive Primary Reference Fuels at Elevated Pressures' *Twenty-Seventh Symposium (International) on Combustion* (1998) p. 379 – 387.

[8] J. Herzler, L. Jerig, P. Roth, 'Shock Tube Study of the Ignition of Lean n-Heptane/Air Mixtures at Intermediate Temperatures and High Pressures' *Proceedings of the Combustion Institute* vol. 30 (2005) p. 1147 – 1153.

[9] E. J. Silke, H. J. Curran, J. M. Simmie, 'The influence of fuel structure on combustion as demonstrated by the isomers of heptane: a rapid compression machine study' *Proceedings of the Combustion Institute* vol. 30 (2005) p. 2639 – 2647.

[10] D.F. Davidson, Z. Hong, G.L. Pilla, A. Farooq, R.D. Cook, R.K. Hanson, 'Multi-species Time-history Measurements During n-Heptane Oxidation Behind Reflected Shock Waves' *Combustion and Flame* vol. 157 (2010) p. 1899 – 1905.

[11] S. Humer, U. Niemann, R. Seiser. K. Seshadri, E. Pucher, 'Combustion of Jet Fuels and its Surrogate in Laminar Nonuniform Flows' *Proceedings of the European Combustion Meeting* (2009).

[12] J. Yu, S. Eser, 'Supercritical Decomposition of Jet Fuel Components; Model Compound Studies' *American Chemical Society* vol.43 (1998) p. 74 – 79.

[13] R.H. Natelson, M.S. Kurman, N.P. Cernansky, D.L. Miller, 'Experimental Investigation of Surrogates for Jet and Diesel Fuels' *Fuel* vol. 87 (2008) p. 2339 – 2342.

[14] C.Ji, E. Damesa, B. Sirjeana, H. Wanga, F. N. Egolfopoulos, 'An Experimental and Modelling Study of the Propagation of Cyclohexane and Mono-Alkylated Cyclohexane Flames' *Proceedings of the Combustion Institute* vol. 33, (2011) p. 971 – 978.

[15] Z. Hong, K.-Y. Lam, D. F. Davidson, R. K. Hanson, 'A Comparative Study of the Oxidation Characteristics of Cyclohexane, Methylcyclohexane, and *n*-Butylcyclohexane at High Temperatures' *Combustion and Flame* vol. 156 (2011) p. 1456 – 1468.

[16] R.H. Natelson, R.O. Johnson, M.S. Kurman, N.P. Cernansky, D.L. Miller, 'Comparison of Reactivity in a Flow Reactor and a Single Cylinder Engine' *Experimental Thermal and Fuel Science* vol. 34 (2010) p. 928 – 932.

[17] R.H. Natelson, M.S. Kurman, N.P. Cernansky, D.L. Miller, 'Low Temperature Oxidation of *n*-Butylcyclohexane' *Combustion and Flame* vol. 158 (2011) p. 2325 – 2337.

[18] N. Liu, C. Ji, F. N. Egolfopoulos, 'Ignition of Non-Premixed Cyclohexane and Mono-Alkylated Cyclohexane Flames' *Proceedings from the Combustion Institute* vol.34 (2012) p. 873 – 880.

[19] S. Honnet, K. Seshadri, H. Niemann, N. Peter, 'A Surrogate Fuel for Kerosene' *Proceedings from the Combustion Institute* vol. 32 (2009) p. 458 – 492.

[20] R. Natelson Ph.D. 2010 Drexel University

[21] D. L. Camin, A. F. Forziati, F. D. Rossini, 'Physical Properties of *n*-Hexadecane, *n*-Decylcyclopentane, *n*-Decylcyclohexane, 1-Hexadecene and *n*-Decylbenzene' *The Journal of Physical Chemistry* vol. 58 (1954) p. 440 – 442.

[22] D. R. Lide, Handbook of Chemistry and Physics, 87th Edition, CRC Press

[23] S. Zeppieri, K. Brezinsky, I. Glassman, 'Pyrolysis Studies of Methylcyclohexane and Oxidation Studies of Methylcyclohexane and Methylcyclohexane/Toluene Blends' *Combustion and Flame* vol. 108 (1997) p. 266 – 286.

[24] J. P. Orme, H. J. Curran, J. M. Simmie, 'An Experimental and Modelling Study of Methylcyclohexane Pyrolysis and Oxidation' *Journal of Physical Chemistry* vol. 110 (2006) p. 114 – 131.

[25] W. J. Pitz, C. V. Naik, T. Ni Mhaolduin, H. J. Curran, J. P. Orme, J. M. Simmie, C. K. Westbrook, 'Modelling and Experimental Investigation of Methylcyclohexane Oxidation in a Rapid Compression Machine' *Proceedings for the Combustion Institute* vol. 31 (2007) p. 267 – 273.

[26] J. Vanderover, M. A. Oehlschlaeger, 'Ignition Time Measurements for Methylcylcohexane- and Ethylcyclohexane-Air Mixtures at Elevated Pressures' *International Journal of Chemical Kinetics* vol. 41 (2009) p. 82 – 91.

[27] A. Roubaud, R. Minetti, L. R. Sochet, 'Oxidation and combustion of Low Alkylbenzenes at High Pressure: Comparative Reactivity and Auto-Ignition' *Combustion and Flame* vol. 121 (2000) p. 535 – 541.

[28] Y. Yang, A. L. Beohman, 'Experimental Study of Cyclohexane and Methylcyclohexane Oxidation at Low to Intermediate Temperature in a Motored Engine' *Proceedings of the Combustion Institute* vol. 32 (2009) p. 419 – 426.

[29] F. Wu, A. P. Kelley, C. K. Law, 'Laminar Flame Speeds of Cyclohexane and Mono-alkylated Cyclohexanes at Elevated Pressures' *Combustion and Flame* vol. 159 (2012) p. 1417 – 1425.

[30] H. Wang, E. Dames, B. Sirjean, D. A. Sheen, R. Tangko, A. Violi, J. Y. W. Lai, F. N. Egolfopoulos, D. F. Davidson, R. K. Hanson, C. T. Bowman, C. K. Law, W. Tsang, N. P. Cernansky, D. L. Miller, R. P. Lindstedt, 'A High-Temperature Chemical Kinetic Model of *n*-Alkane (up to *n*-Dodecane), Cyclohexane, and Methyl-, Ethyl-, *n*-Propyl and *n*-Butyl-Cyclohexane Oxidation at High Temperatures, JetSurF version 2.0, September 19, 2010 (http://melchior.usc.edu/JetSurF/JetSurF2.0).

[31] B. Husson, O. Herbinet, P. A. Glaude, S. S. Ahmed, F. Battin-Leclerc, 'Detailed Product Analysis during Low- and Intermediate-Temperature Oxidation of Ethylcyclohexane' *Journal of Physical Chemistry A* vol. 116 (2012) p. 5100 – 5111.

[32] A. Ristori, P. Dagaut, A. El Bakali, M. Cathonnet, 'The Oxidation of *n*-Propylcyclohexane: Experimental Results and Kinetic Modelling'*Combustion Science and Technology* vol. 165 (2001) p. 197 – 228.

[33] M. Crochet, G. Vanhove, M. Ribaucour, R. Minetti, '*n*-Propylcyclohexane Lean Oxidation and Autoignition at Low Temperatures and Elevated Pressures' *Proceedings of the European Combustion Meeting* (2009).

[34] T. Dubois, N. Chaumeix, C. E. Paillard, F. Douce, G. Pengloan, P. Manuelli, 'Experimental Study of the Oxidation of Surrogates for Diesel Fuels at HCCI Conditions' *European Combustion Meeting* (2007).

[35] T. Dubois, N. Chaumeix, C. E. Paillard, 'Experimental and Modelling Study of *n*-Propylcyclohexane Oxidation under Engine- relevant Conditions' *Energy and Fuel* vol. 23 (2009) p. 2453 – 2466.

[36] E. Pousse, R. Porter, V. Warth, P.A. Glaude, R. Fournet, F. Battin-Leclerc, 'Lean Methane premixed Laminar Flame Doped by Components of Diesel Fuel II: *n*-Propylcyclohexane' *Combustion and Flame* vol. 157 (2010) p. 75 – 90.

[37] P. Dagaut, S. Gail, 'Chemical Kinetic Study of the Effect of a Biofuel Additive on Jet-A1 Combustion' *Journal of Physical Chemistry* vol. 111 (2007) p. 3992 – 4000.

[38] K. Mati, A. Ristori, S. Gail, G. Pengloan, P. Dagaut, 'The Oxidation of a Diesel Fuel at 1-10 atm: Experimental Study in a JSR and Detailed Chemical Kinetic Modelling *Proceedings of the Combustion Institute* vol. 31 (2007) p. 2939 – 2946.

[39] M.Yahyaoui, N. Djebaili-Chaumeix, P. Dagaut. C. E. Paillard, S. Gail, 'Kinetics of 1-Hexene Oxidation in a JSR and a Shock Tube: Experimental and Modeling Study' *Combustion and Flame* vol. 147 (2009) p. 67 – 78.

[40] E. Pousse, P.A. Glaude, R. Fournet, F. Battin-Leclerc, 'Lean Methane premixed Laminar Flame Doped by Components of Diesel Fuel I: *n*-Butylbenzene' *Combustion and Flame* vol. 156 (2009) p. 957 – 974.

[41] E. Pousse, Z.Y. Tian, P.A. Glaude, R. Fournet, F. Battin-Leclerc, 'Lean Methane premixed Laminar Flame Doped by Components of Diesel Fuel III: Indane and a Comparison Between *n*-Butylbenzene, *n*-Propylcyclohexane and Indane' *Combustion and Flame* vol. 157 (2010) p. 1236 – 1260.

[42] W.C. Lai, C. Song, 'Pyrolysis of Alkycyclohexanes in or Near the Supercritical Phase, Product Distribution and Reaction Pathways' *Fuel Process Technology* vol. 48 (1996) p. 1 – 27.

[43] J. Yu, S. Eser, 'Thermal Decomposition of Jet Fuel Model Compounds Under Near Critical and Supercritical conditions 1.*n*-Butylcyclohexane and *n*-Butylcyclohexane' *American Chemical Society* vol. 37 (1998) p. 4591 – 4600

[44] M. Colket, T. Edwards, S. Williams, N .P. Cernansky, D. L. Miller, F. Egolfopoulos, P. Linstedt, K. Seshadri, F.L. Dryer, C. K. Law, D. Friend, D. Lenhert, H. Pitsch, A. Sarofim, M. Smooke, W. Tsang, 'Development of an Experimental Database and Kinetic Models for Surrogate Jet Fuels' *45th AIAA Aerospace Sciences Meeting and Exhibit* (2007) p. 1 – 21.

[45] R. Nateleson, R. Johnson, M. Kurman, N. Cernansky, D. Miller, 'Low Temperature Oxidation of Selected Jet Fuel and Diesel Fuel Components at Elevated Pressures' *5^{th} US Combustion Meeting* (2007).

[46] P.A. Glaude, D. Fournet, R. Bounaceur, M. Moliere, 'Gas Turbines and Biodiesel; A Clarification of the Relative $NO_{\times}$ Indices of FAME, Gasoil and Natural Gas' *ASME Turbo Expo* (2009) p. 1 – 7.

[47] B. Sirjean, E. Dames, D. A. Sheen, F. N. Egolfopoulos, H. Wang, D. F. Davidson, R. K. Hanson, H. Pitsch, C. T. Bowman, C. K. Law, W. Tsang, N. P. Cernansky, D. L. Miller, A. Violi, R. P. Lindstedt, 'A High-Temperature Chemical Kinetic Model of *n*-Alkane, Cyclohexane, and Methyl-, Ethyl-, *n*-Propyl and *n*-Butyl-Cyclohexane Oxidation at High Temperatures, JetSurF version 1.1, September 15, 2009 (http://melchior.usc.edu/JetSurF/JetSurF1.1).

[48] R. Di Sante 'Measurements of the Auto-Ignition of *n*-Heptane/Toluene Mixtures Using a Rapid Compression Machine' *Combustion and Flame* vol. 159 (2012) p. 55 – 63.

[49] J. Zhang, S. Niu, Y. Zhang, C. Tang, X. Jiang, E. Hu, Z. Huang, 'Experimental and Modelling Study of the Auto-Ignition of *n*-Heptane/*n*-Butanol Mixtures' *Combustion and Flame* vol. 160 (2013) p. 31 – 39.

[50] A. G. Gaydon, I. R. Hurle, The Shock Tube in High-Temperature Chemical Physics (1963).

[51] H. B. Dixon, 'On the Movements of the Flame in the Explosion of Gases' *Proceedings of the Royal Society of London. Series A, Containing Papers of a Mathematical and Physical Character* vol. 200 (1903) p. 315 – 352.

[52] W. Payman, D. W. Woodhead, 'Explosion Waves and Shock Waves. Part I. The Wave-Speed Camera and Its Application to the Photography of Bullets in Flight' *Proceedings of the Royal Society of London. Series A, Containing Papers of a Mathematical and Physical Character* vol. 132 (1931) p. 200 – 213.

[53] W. Payman, D. W. Woodhead, H. Titman, 'Explosion Waves and Shock Waves. Part II. The Shock Wave and Explosion Products Sent out by Blasting Detonators' *Proceedings of the Royal Society of London. Series A, Mathematical and Physical Sciences* Vol. 148 (1935) p. 604 – 622.

[54] W. Payman, H. Titman, 'Explosion Waves and Shock Waves. III. The Initiation of Detonation in Mixtures of Ethylene and Oxygen and of Carbon Monoxide and Oxygen' *Proceedings of the Royal Society of London. Series A, Containing Papers of a Mathematical and Physical Character* vol. 152 (1935) p. 418 – 445.

[55] W. Payman, W. C. F. Shepherd, 'Explosion Waves and Shock Waves. IV. Quasi-Detonation in Mixtures of Methane and Air' *Proceedings of the Royal Society of London. Series A, Mathematical and Physical Sciences* Vol. 158 (1937) p. 348 – 367.

[56] W. Payman, W. C. F. Shepherd, 'Explosion Waves and Shock Waves. VI. The Disturbance Produced by Bursting Diaphragms with Compressed Air' *Proceedings of the Royal Society of London. Series A, Mathematical and Physical Sciences* Vol. 186 (1946) p. 293 – 321.

[57] W. B. Cybulski, W. Payman, D. W. Woodhead, 'Explosion Waves and Shock Waves. VII. The Velocity of Detonation in Cast T.N.T.' *Proceedings of the Royal Society of London. Series A, Mathematical and Physical Sciences* vol. 197, (1949) p. 51 – 72.

[58] W. Bleakney, D. K. Weimer, C. H. Fletcher, 'The Shock Tube: A Facility for Investigations in Fluid Dynamics' *Review of Scientific Instruments* vol. 20 (1949) p. 807 – 815.

[59] A. Hertzberg, A. Kantrowitz, 'Studies with an Aerodynamically Instrumented Shock Tube' *Journal of Applied Physics* vol. 21 (1950) p. 874 – 878.

[60] J. Huang, P.G. Hill, W.K. Bushe, S.R. Munshi, 'Shock-tube Study of Methane Ignition Under Engine-Relevant Conditions: Experiments and Modelling' *Combustion and Flame* vol, 136 (2004) p. 25 – 42.

[61] A. R. Amadio, M. W. Crofton, E. L. Petersen 'Test-Time Extension Behind Reflected Shock Waves Using CO_2-He and C_3H_8-He Driver Mixtures' *Shock Waves* vol. 16 (2006) p. 157 – 165.

[62] L. R. Cancino, M. Fikri, A. A. M. Oliveira, C. Schulz, 'Measurement and Chemical Kinetics Modelling of Shock-Induced Ignition of Ethanol-Air Mixtures' *Energy and Fuel* vol. 24 (2010) p. 2830 – 2840.

[63] K.G. Falk 'The Ignition Temperatures of Hydrogen-Oxygen Mixtures' *Journal of the American Chemical Society* vol. 28 (1906) p. 1517 – 1534.

[64] H.B. Dixon, L. Bradshaw, C. Campbell, 'The Firing of Gases by Adiabatic Compression. Part I. Photographic Analysis of the Flame' *Journal of the Chemical Society, Transactions* vol. 105 (1914) p. 2027 – 2035.

[65] H.B. Dixon, J.M. Crofts, 'The Firing of Gases by Adiabatic Compression. Part II. The Ignition-points of Mixtures Containing Electrolytic Gas' *Journal of the Chemical Society, Transactions* vol. 105 (1914) p. 2036 – 2053.

[66] H. Cassel, 'Über Entflammung und Verbrennung von Sauerstoff-Wasserstoff-Gemischen' *Annalen der Physik* vol. 356 (1917) p. 685 – 704.

[67] H.T. Tizard, 'The Cause of Detonation in Internal Combustion Engines' *North East Coast Institution of Engineers and Shipbuilders* (1920 – 1921).

[68] H.T. Tizard, D.R. Pye, 'Experiments on the Ignition of Gases by Sudden Compression' *Philosophical Magazine* vol. 44 (1922) p. 79 – 121.

[69] H.T. Tizard, D.R. Pye, 'Ignition of Gases by Sudden Compression' *Philosophical Magazine* vol. 1 (1926) p. 1094 – 1105.

[70] M. Aubert, 'Étude Physico-Chemique de Quatre Combustible Liquides Extraits d'un Goudron Primaire, Obtenueà Partit des Déchets d'Extraction des Mines Domaniales Francaises de la Sarre' Chaleur et Industrie' VOL. 6 (1929) p. 373 – 379.

[71] R.W. Fenning, F.T. Cotton 'Experiments on the Ignition of Gases by Sudden Compression' *Reports and memoranda, Great Britain Aeronautical Research Committee* (1930).

[72] W. S. Affleck, A. Thomas, 'An Opposed Piston Rapid Compression Machine for Preflame Reaction Studies' *Proceedings of the Institution of Mechanical Engineers* vol. 183 (1968-69) p. 365 – 382.

[73] M. Carlier, C. Corre, R. Minetti, J-F. Pauwels, M. Ribaucour, L-R. Sochet, 'Autoignition of Butane: A Burner and a Rapid Compression Machine Study' *Twenty-Third Symposium (International) on Combustion* vol. 23, (1991) p. 1753 – 1758.

[74] J.F. Griffiths, Q. Jiao, M. Schreiber, J. Meyer, K.F. Knoche, 'Development of Thermokinetic Models for Autoignition in a CFD Code: Experimental Validation and Application of the Results to Rapid Compression Studies' *Twenty-Fourth Symposium on Combustion* vol. 24, (1992) p. 1809 – 1815.

[75] P. Park Ph.D. 1990 Massachusetts Institute of Technology http://hdl.handle.net/1721.1/14068

[76] M.T. Donovan, X. He, B.T. Zigler, T.R. Palmer, M.S. Wooldridge, A. Atreya 'Demonstration of a Free-Piston Rapid Compression Facility for the Study of High Temperature Combustion Phenomena' *Combustion and Flame* vol. 137 (2004) p. 351 – 365.

[77] J. Würmel Ph.D. 2004 National University of Ireland, Galway.

[78] L. Brett, J. Mc Namara, P. Musch, J.M. Simmie, 'Simulation of Methane Autoignition in a Rapid Compression Machine with Creviced Pistons' *Combustion and Flame* vol. 124 (2001) p. 326 – 329.

[79] J. Smith Ph.D. 2004 National University of Ireland, Galway.

[80] C. Morley, http://www.c.morley.ukgateway.net/gseqrite.html

[81] R. Mével, P.A. Boettcher, J.E. Shepherd 'Absorption Cross Section at 3.39 μm of Alkanes, Aromatics and Substituted Hydrocarbons' *Chemical Physics Letters* vol. 531 (2012) p. 22 – 27.

[82] H-P. S. Shen, J. Vanderover, M. A. Oehlschlager, 'A Shock Tube Study of the Auto-Ignition of Toluene/Air Mixtures at High Pressures', *Proceedings from the Combustion Institute* vol. 32 (2009) p. 165 – 172.

[83] D. F. Davidson, R. K. Hanson, Fundamental Kinetics Database Utilizing Shock Tube Measurements Volume 1: Ignition Delay Time Measurements, Mechanical Engineering Department, Stanford University, Stanford (2005).

[84] K. A. Heufer, H. Olivier 'Determination of Ignition Delay Times of Different Hydrocarbons in a New High Pressure Shock Tube' *Shock Waves* vol. 20 (2010) p. 307 – 316.

[85] C. J. Aul, W, K. Metcalfe, S. M. Burke, H. J. Curran, E. L. Petersen 'Ignition and Kinetic Modelling of Methane and Ethane Fuel Blends with Oxygen: A Design of Experiments Approach' *Combustion and Flame* vol. 160 (2013) p. 1153 – 1167

[86] T. G. Kaufamann, A. Kaldor, G. F. Stuntz, M. C. Kerby, L. L. Ansell, 'Catalysis Science and Technology for Cleaner Transportation Fuel' *Catalysis Today* vol. 62 (2000) p. 77 – 90.

[87] M. Ribaucour, R. Minetti, L. R. Sochet, 'Autoignition of *n*-Pentane and 1-Pentene: Experimental Data and Kinetic Modelling', *Twenty Seventh (International) Symposium on Combustion* (1998) p. 345 – 351.

[88] R .Minetti, A. Roubaud, E. Therssen, M. Ribaucour, L. R. Sochet, 'The Chemistry of Pre-ignition of *n*-Pentane and 1-Pentene', *Combustion and Flame* vol. 118 (1999) p. 213 – 220.

[89] S. K. Prabhu, R. K. Bhat, D. L. Miller, N. P. Cernansky, '1-Pentene Oxidation and its Interaction with Nitric Oxide in the Low and Negative Temperature Coefficient Regions', *Combustion and Flame* vol. 104 (1996) p. 377 – 390.

[90] C. F. H. Tipper, A. Titchard, 'The Effect of Additives on the Cool Flame Combustion of *n*-Heptane' *Combustion and Flame* vol. 16 (1971) p. 223 – 232.

[91] R. R. Baldwin, J. P. Bennett, R. W. Walker, 'Addition of Pentenes to Slowly Reacting Mixtures of Hydrogen and Oxygen at 480°C' *Journal of the Chemical Society, Faraday Transactions 1: Physical Chemistry in Condensed Phases* vol. 76 (1980) p. 2396 – 2412.

[92] R. Hughes, A. S. Prodhan, 'The Combustion of the *n*-Pentenes in the Cool Flame Region' *Combustion and Flame* vol. 21 (1973) p. 297 – 301.

[93] M. Mehl, W. J. Pitz, C. K. Westbrook, K. Yasunaga, C. Conroy, H. J. Curran, 'Autoignition Behaviour Of Unsaturated Hydrocarbons in the Low and High Temperature Regions' *Proceedings from the Combustion Institute* vol. 33 (2011) p. 201 – 208.

[94] M. Mehl, G. Vanhove, W. J. Pitz, E. Ranzi, 'Oxidation and Combustion of the *n*-Hexene Isomers: A Wide Range Kinetic Modelling Study' *Combustion and Flame* vol. 155 (2008) p. 759 – 772.

[95] M. V. Johnson, S. S. Goldsborough, Z. Serinyel, P. O'Toole, E. Larkin, G. O'Malley, H. J. Curran, 'A Shock Tube Study of *n*- and *iso*-Propanol Ignition' *Energy and Fuel* vol. 23 (2009) p. 5886 – 5898.

[96] J. Moc, G. Black, J. M. Simmie, H. J. Curran, 'The Unimolecular Decomposition and H Abstraction Reactions by HO and HO_2 from *n*-Butanol' *AIP Conference Proceedings* vol. 1148 (2008) p. 161 – 164.

[97] H. J. Curran, P. Gaffuri, W. J. Pitz, C. K. Westbrook, 'A Comprehensive Modelling Study of iso-Octane Oxidation' *Combustion and Flame* vol. 129 (2002) p 253 – 280.

[98] M. Mehl, H. J. Curran, W. J. Pitz, C. K. Westbrook, 'Chemical Kinetic Modelling of Component Mixtures Relevant to Gasoline' *European Combustion Meeting* (2009).

[99] Y. Roman-Leshkov, C. J. Barrett, Z. Y. Liu, J. A. Dumesic, 'Production of Dimethylfuran for Liquid Fuels from Biomass Derived Carbohydrates' *Nature* vol. 447 (2007) p. 982 – 986.

[100] J. B. Binder and R. T. Raines, 'Simple Chemical Transformation of Lignocellulosic Biomass into Furans for Fuels and Chemicals' *Journal of the American Chemical Society* vol. 131 (2009) p. 1979 – 1985.

[101] A, Lifshitz, C, Tamburu, R. Shashua, 'Thermal Decomposition of 2,5-Dimethylfuran. Experimental Results and Computer Modelling' *Journal of Physical Chemistry* vol. 102 (1998) p. 10655 – 10670.

[102] X. Wu, Z. Huang, T. Yuan, K. Zhang, L. Wei, 'Identification of Combustion Intermediates in a Low-Pressure Premixed Laminar 2,5-Dimethylfuran/Oxygen/Argon Flame with Tunable Synchrotron Photoionization' *Combustion and Flame* vol. 156 (2009) p. 1365 – 1376.

[103] X. Wu, Z. Huang, C. Jin, X. Wang, B. Zheng, Yi. Zhang, L. Wei, 'Measurements of Laminar Burning Velocities and Markstein Lengths of 2,5-Dimethylfuran-Air-Diluent Premixed Flames' *Energy and Fuel* vol. 23 (2009) p. 4355 – 4362.

[104] G. Tian, R. Daniel, H. Li, H. Xu, S. Shuai, P. Richards, 'Laminar Burning Velocities of 2,5-Dimethylfuran Compared with Ethanol and Gasoline' *Energy & Fuel* vol. 24 (2010) p. 3898 – 3905.

[105] S. Zhong, R. Daniel, H. Xu, J. Zhang, D. Turner, M. L. Wyszynski, P. Richards, 'Combustion and Emissions of 2,5-Dimethylfuran in a Direct-Injection Spark-Ignition Engine' *Energy and Fuel* vol. 24 (2010) p. 2891 – 2899.

[106] X. Wu, Q. Li, J. Fu, C. Tang, Z. Huang, R. Daniel, G. Tian, H. Xu, 'Laminar Burning Characteristics of 2,5-Dimethylfuran and iso-Octane Blend at Elevated Temperatures and Pressures' *Fuel* vol. 95 (2012) p. 234 – 240.

[107] P. Friese, J. M. Simmie, M. Olzmann, 'The Reaction of 2,5-Dimethylfuran with Hydrogen Atoms - An Experimental and Theoretical Study' *Proceedings of the Combustion Institute* vol. 34 (2013) p. 233 – 239.

[108] B. Sirjean, R. Fournet, 'Theoretical Study of the Reaction of 2,5-Dimethylfuran + H $\rightarrow$ Products' *Proceedings of the Combustion Institute* vol. 34 (2013) p. 241 – 249.

[109] B. Sirjean, R. Fournet, P.-A. Glaude, F. Battin-Leclerc, W. Wang, M. A. Oehlschlaeger, 'Shock Tube and Chemical Kinetic Modeling Study of the Oxidation of 2,5-Dimethylfuran' *Journal of Physical Chemistry A* vol. 117 (2013) p. 1371 – 1392.

[110] G. Black, Ph. D. 2009, National University of Ireland, Galway.

[111] K. P. Somers, J. M. Simmie, F. Gillespie, C. Conroy, G. Black, W. K. Metcalfe, F. Battin-Leclercb, P. Dirrenberger, O. Herbinet, P.-A. Glaude, P. Dagaut, C. Togbé, K. Yasunaga, R. X. Fernandes, C. Lee, R. Tripathi, H. J. Curran, 'A Comprehensive Experimental and Detailed Chemical Kinetic Modelling Study of 2,5-Dimethylfuran Pyrolysis and Oxidation' *Combustion and Flame* In press (2013)

Appendix A

n-Butylcyclohexane Data

A.1 Shock Tube

p_1/Torr	ν/ms^{-1}	p_5/atm	T_5/K	$\tau/\mu s$
175.2	1041.9	8.9	1335.0	96.0
204.4	1024.6	9.8	1305.1	118.0
225.8	990.1	9.7	1244.7	193.0
255.0	959.5	10.5	1183.7	308.0
309.2	946.8	11.3	1171.9	344.0
325.4	930.7	11.2	1146.4	395.0
253.4	938.6	9.7	1146.3	405.0
301.6	937.5	11.5	1144.4	420.0
306.6	919.4	10.5	1123.6	563.0
358.0	901.1	11.2	1096.7	645.0
355.4	899.5	11.1	1093.4	690.0
355.6	884.1	11.4	1054.5	1386.4
327.4	883.6	10.6	1052.4	1338.4
256.6	877.8	8.2	1045.2	1452.0

Table A.1: 0.42% n-butylcyclohexane, 20.91% oxygen, 78.67% nitrogen $\phi = 0.3$, $p_5 = 10$ atm.

p_1/Torr	ν/ms^{-1}	p_5/atm	T_5/K	$\tau/\mu s$
157.2	1070.7	9.0	1365.1	74.0
175.6	1033.6	9.1	1300.2	111.0
206.6	1003.9	9.6	1248.9	157.0
255.4	950.1	10.1	1157.4	335.0
275.8	930.4	10.2	1125.5	542.0
300.0	920.4	10.6	1110.4	591.0
300.6	891.6	9.8	1062.2	740.0
325.8	889.7	10.5	1060.2	687.0
360.4	880.8	11.1	1048.1	912.0
358.4	878.8	11.0	1043.8	1037.0
350.6	870.5	10.4	1031.7	1182.0
451.2	826.6	12.1	953.3	2364.0

Table A.2: 0.69% n-butylcyclohexane, 20.85% oxygen, 78.45% nitrogen $\phi = 0.5$, $p_5 = 10$ atm.

p_1/Torr	ν/ms^{-1}	p_5/atm	T_5/K	$\tau/\mu s$
153.2	1086.2	9.8	1347.4	88.0
150.6	1052.7	9.0	1285.5	129.0
208.2	991.0	10.0	1190.9	304.0
207.2	980.0	10.1	1165.2	303.0
253.2	955.8	10.9	1136.5	388.0
255.6	927.3	10.2	1089.5	460.0
303.2	907.7	11.2	1060.2	659.0
305.8	898.4	10.9	1047.7	648.0
356.6	871.8	11.4	1009.4	1108.0
355.8	866.2	11.3	999.5	1100.0
404.6	839.6	11.6	960.9	1880.0

Table A.3: 1.38% *n*-butylcyclohexane, 20.71% oxygen, 77.91% nitrogen $\phi = 1.0$, p_5 =10 atm.

p_1/Torr	ν/ms^{-1}	p_5/atm	T_5/K	$\tau/\mu s$
101.4	1180.6	9.8	1417.6	86.0
113.6	1144.2	9.9	1362.8	115.0
106.0	1141.2	9.1	1358.8	130.0
137.6	1058.7	9.5	1229.4	205.0
152.0	1041.7	9.9	1205.0	245.0
202.4	975.1	10.6	1111.4	450.0
203.6	974.7	10.7	1110.8	383.0
208.8	963.4	10.8	1091.8	573.0
256.8	943.9	12.4	1065.1	605.0
253.8	922.9	11.3	1038.1	820.0
257.4	904.7	11.0	997.3	961.2
308.3	890.6	12.2	994.6	956.0
276.6	871.4	11.2	953.1	1225.2
367.2	815.4	11.0	881.4	2513.2
324.0	813.1	10.2	881.2	2625.2
457.4	770.3	11.5	828.8	2018.8
509.6	737.1	11.5	787.5	1938.8

Table A.4: 2.72% *n*-butylcyclohexane, 20.43% oxygen, 76.48% nitrogen ϕ =2.0, p_5 = 10 atm.

p_1/Torr	ν/ms^{-1}	p_5/atm	T_5/K	$\tau/\mu s$
625.8	995.9	27.6	1251.8	95.5
651.4	983.9	28.6	1224.9	107.0
606.2	977.9	25.3	1220.2	133.6
675.4	969.9	27.2	1207.8	137.0
705.6	951.3	26.6	1177.3	192.0
801.6	936.2	28.7	1152.1	247.0
859.5	898.7	28.4	1084.1	582.0
1003.6	876.5	29.1	1054.4	602.0
1051.8	861.6	28.6	1031.6	837.0
1105.0	841.3	29.5	992.4	1462.0
1253.0	809.9	30.2	944.0	2182.0
1442.8	784.5	30.6	905.7	2590.0
1635.0	757.3	30.7	865.4	2567.0
1977.4	731.7	33.1	828.3	2402.0
3518.4	707.9	33.0	797.3	2461.0
2369.7	709.3	35.6	796.5	3025.0

Table A.5: 0.42% n-butylcyclohexane, 20.91% oxygen, 79.67% nitrogen $\phi = 0.3$, $p_5 = 30$ atm.

p_1/Torr	ν/ms^{-1}	p_5/atm	T_5/K	$\tau/\mu s$
452.2	1074.3	27.1	1365.0	37.0
558.2	993.0	26.3	1222.9	118.0
650.6	973.5	27.2	1199.9	141.0
622.4	951.7	25.7	1153.5	212.0
850.6	930.3	31.0	1127.7	216.0
750.2	890.2	26.3	1080.2	320.0
1050.8	846.0	28.2	994.9	726.0
905.6	851.6	26.0	993.8	820.0
1187.8	814.9	29.5	942.9	1600.0
1526.7	754.9	28.1	855.5	1650.0
2048.5	719.5	33.3	805.0	1140.0
2215.0	682.6	29.5	760.0	1420.0
2540.6	665.9	30.5	732.8	1370.0

Table A.6: 0.695% n-butylcyclohexane, 20.854% oxygen, 78.451% nitrogen $\phi = 0.5$, $p_5 = 30$ atm.

p_1/Torr	ν/ms^{-1}	p_5/atm	T_5/K	$\tau/\mu s$
525.4	1022.9	28.0	1241.7	70.0
552.6	1012.4	29.6	1218.5	86.0
650.0	1000.5	33.4	1189.1	104.0
751.4	926.1	30.9	1080.9	228.0
860.4	895.8	29.5	1048.2	298.5
952.6	854.0	27.8	988.3	438.5
1150.6	833.1	31.7	954.6	750.0
1009.9	864.8	30.1	920.7	800.0
1350.4	807.2	34.9	910.9	875.0
1395.0	776.3	31.6	869.2	883.0
1692.0	723.4	30.5	798.5	651.0
2018.6	698.9	31.5	766.7	877.0
2009.8	685.3	30.2	715.0	992.0
2522.2	657.1	33.4	712.0	1440.0

Table A.7: 1.381% n-butylcyclohexane, 20.71% oxygen, 77.909% nitrogen $\phi = 1.0$, $p_5 = 30$ atm.

p_1/Torr	ν/ms^{-1}	p_5/atm	T_5/K	$\tau/\mu s$
350.6	1106.5	28.6	1296.7	56.0
550.4	1000.0	32.4	1138.0	114.0
707.6	907.4	29.9	1015.9	288.0
835.2	894.7	33.5	1000.0	304.0
990.6	837.7	32.5	922.7	570.0
910.6	831.4	30.0	910.0	650.0
1146.4	779.1	29.1	845.0	604.0
1340.2	753.6	30.2	813.0	468.0
1689.0	702.5	30.0	752.0	591.0

Table A.8: 2.742% n-butylcyclohexane, 20.428% oxygen, 76.848% nitrogen $\phi = 2.0$, $p_5 = 30$ atm.

p_1/Torr	ν/ms^{-1}	p_5/atm	T_5/K	$\tau/\mu s$
1198.2	962.6	48.0	1190.3	65.5
1265.4	934.7	46.1	1143.2	144.0
1321.2	918.1	47.2	1115.7	183.0
1635.0	888.3	50.8	1067.1	370.0
1799.2	861.2	52.1	1023.7	510.0
2102.2	810.5	50.8	945.1	1039.0
2412.4	776.3	49.0	879.0	1320.0
3298.0	716.1	51.2	806.4	1240.0
4093.4	691.0	55.5	771.0	1238.0
4822.5	630.3	48.7	688.2	2774.0

Table A.9: 0.42% n-butylcyclohexane, 20.91% oxygen, 79.67% nitrogen $\phi = 0.3$, $p_5 = 50$ atm.

p_1/Torr	ν/ms^{-1}	p_5/atm	T_5/K	$\tau/\mu s$
1219.4	957.7	47.1	1166.0	70.3
1288.4	938.3	49.1	1110.4	115.0
1348.2	904.6	45.9	1080.4	212.0
1543.8	890.0	53.9	1069.8	211.0
1739.4	854.1	49.2	1012.5	503.0
1994.6	817.6	49.6	955.0	664.0
2268.4	780.3	49.7	899.4	737.0
3125.6	716.1	49.5	806.0	762.0
4821.5	671.8	50.0	740.0	695.0

Table A.10: 0.695% *n*-butylcyclohexane, 20.854% oxygen, 78.451% nitrogen $\phi = 0.5$, $p_5 = 50$ atm.

p_1/Torr	ν/ms^{-1}	p_5/atm	T_5/K	$\tau/\mu s$
1166.6	956.9	50.1	1131.5	69.0
1252.1	907.9	47.2	1057.0	205.0
1342.0	873.7	45.7	1006.3	340.0
1329.2	873.4	45.1	1005.9	358.0
1517.8	856.8	47.2	981.9	348.0
1621.0	818.9	43.8	928.0	499.0
1736.2	799.3	44.8	900.0	418.0
2009.4	783.4	48.1	878.9	418.0
2182.4	755.1	48.9	834.1	350.0
2273.8	821.5	44.2	821.5	318.0

Table A.11: 1.381% *n*-butylcyclohexane, 20.71% oxygen, 77.909% nitrogen $\phi = 1.0$, $p_5 = 50$ atm.

p_1/Torr	ν/ms^{-1}	p_5/atm	T_5/K	$\tau/\mu s$
963.4	931.9	46.8	1043.8	152.0
968.8	925.3	45.0	1034.7	159.0
962.8	918.6	44.8	1025.6	180.0
1063.8	899.4	45.5	999.7	222.0
1179.6	868.7	45.8	959.2	263.0
1390.2	813.0	45.3	887.4	264.0
1836.1	776.4	45.6	841.0	226.0

Table A.12: 2.742% *n*-butylcyclohexane, 20.428% oxygen, 76.848% nitrogen $\phi = 2.0$, $p_5 = 50$ atm.

A.2 Rapid Compression Machine

p_i/bar	T_i/K	p_c/bar	T_c/K	τ/ms	diluent
0.334	413.3	10.1	989.0	5.0	N_2 : 100%
0.334	414.5	10.0	988.0	5.0	N_2 : 100%
0.331	414.6	9.9	987.0	5.0	N_2 : 100%
0.329	397.3	9.9	956.0	11.0	N_2 : 100%
0.327	397.1	9.9	954.0	11.3	N_2 : 100%
0.333	396.8	10.1	954.0	10.5	N_2 : 100%
0.328	384.7	9.9	927.0	20.5	N_2 : 100%
0.328	383.6	9.9	926.0	20.4	N_2 : 100%
0.328	383.2	9.9	924.0	21.1	N_2 : 100%
0.528	413.5	9.9	883.0	24.4	N_2 : 100%
0.535	414.0	10.1	883.0	23.5	N_2 : 100%
0.538	412.9	10.1	881.0	23.4	N_2 : 100%
0.539	397.3	10.0	850.0	29.6	N_2 : 100%
0.534	397.5	9.9	849.0	29.4	N_2 : 100%
0.537	397.2	10.0	849.0	28.4	N_2 : 100%
0.530	382.6	10.1	825.0	28.4	N_2 : 100%
0.532	382.4	10.0	822.0	31.8	N_2 : 100%
0.530	382.5	9.9	821.0	32.7	N_2 : 100%
0.523	368.2	10.1	800.0	31.1	N_2 : 100%
0.522	368.5	10.0	800.0	31.3	N_2 : 100%
0.526	368.3	10.1	799.0	30.3	N_2 : 100%
0.517	352.1	9.8	765.0	31.1	N_2 : 100%
0.525	352.1	9.4	765.0	31.3	N_2 : 100%
0.526	352.6	9.9	765.0	31.2	N_2 : 100%

Table A.13: 0.42% *n*-butylcyclohexane, 20.91% oxygen, 78.67% nitrogen $\phi = 0.3$, $p_5 = 10$ atm.

p_i/bar	T_i/K	p_c/bar	T_c/K	τ/ms	diluent
0.346	413.5	10.3	961.0	5.3	N_2 : 100%
0.336	413.2	9.8	956.0	4.7	N_2 : 100%
0.333	412.6	9.6	952.0	4.6	N_2 : 100%
0.340	397.8	9.9	924.0	8.5	N_2 : 100%
0.336	397.6	9.8	924.0	7.8	N_2 : 100%
0.336	397.1	9.7	921.0	7.7	N_2 : 100%
0.337	383.1	10.0	899.0	12.5	N_2 : 100%
0.337	383.7	9.7	895.0	11.4	N_2 : 100%
0.337	383.5	9.7	894.0	13.8	N_2 : 100%
0.544	418.1	10.0	867.0	13.4	N_2 : 100%
0.544	418.2	9.9	865.0	13.1	N_2 : 100%
0.538	403.9	10.1	845.0	11.6	N_2 : 100%
0.534	403.4	10.0	844.0	13.6	N_2 : 100%
0.526	403.5	9.8	843.0	14.6	N_2 : 100%
0.520	388.3	9.9	821.0	12.3	N_2 : 100%
0.533	388.3	10.2	821.0	12.4	N_2 : 100%
0.531	388.1	10.1	819.0	12.3	N_2 : 100%
0.523	372.9	10.3	797.0	8.3	N_2 : 100%
0.517	372.9	10.1	796.0	8.4	N_2 : 100%
0.537	372.8	10.4	794.0	7.8	N_2 : 100%
0.610	414.5	10.1	767.0	6.9	60% N_2 : 40% CO_2
0.614	414.5	10.1	767.0	7.0	60% N_2 : 40% CO_2
0.619	414.3	10.1	765.0	7.0	60% N_2 : 40% CO_2
0.612	398.1	10.0	740.0	6.7	60% N_2 : 40% CO_2
0.611	398.2	10.0	740.0	7.2	60% N_2 : 40% CO_2
0.611	397.8	10.0	739.0	7.1	60% N_2 : 40% CO_2
0.613	382.9	10.1	717.0	6.9	60% N_2 : 40% CO_2
0.608	383.2	10.1	717.0	7.3	60% N_2 : 40% CO_2
0.607	383.2	10.0	717.0	7.7	60% N_2 : 40% CO_2
0.534	363.9	10.2	694.0	13.4	50% N_2 : 50% CO_2
0.534	364.1	10.2	694.0	14.7	50% N_2 : 50% CO_2
0.538	363.7	10.3	694.0	15.1	50% N_2 : 50% CO_2
0.607	367.9	10.1	693.0	10.5	60% N_2 : 40% CO_2
0.607	367.9	10.1	693.0	10.3	60% N_2 : 40% CO_2
0.611	367.9	10.1	693.0	10.4	60% N_2 : 40% CO_2
0.535	352.0	10.5	678.0	21.6	50% N_2 : 50% CO_2
0.545	351.4	10.6	676.0	20.2	50% N_2 : 50% CO_2
0.533	351.9	10.3	676.0	22.1	50% N_2 : 50% CO_2
0.531	351.7	10.3	675.0	26.4	50% N_2 : 50% CO_2
0.618	353.3	10.3	670.0	20.6	60% N_2 : 40% CO_2
0.609	352.9	10.2	669.0	19.3	60% N_2 : 40% CO_2
0.604	353.1	10.1	669.0	18.6	60% N_2 : 40% CO_2

Table A.14: 0.69% *n*-butylcyclohexane, 20.85% oxygen, 78.45% nitrogen $\phi = 0.5$, $p_5 = 10$ atm.

p_i/bar	T_i/K	p_c/bar	T_c/K	τ/ms	diluent
0.375	398.0	10.2	922.0	2.6	60% N_2 : 40% Ar
0.374	397.5	9.8	914.0	3.1	60% N_2 : 40% Ar
0.376	397.0	10.2	914.0	2.7	60% N_2 : 40% Ar
0.392	412.0	10.2	883.0	5.1	100% : N_2
0.392	411.0	10.1	878.0	4.7	100% : N_2
0.391	412.0	9.9	877.0	5.5	100% : N_2
0.386	398.0	10.0	857.0	4.5	100% : N_2
0.381	398.0	9.8	855.0	5.1	100% : N_2
0.388	398.0	9.9	853.0	4.8	100% : N_2
0.354	354.0	9.8	839.0	4.7	60% N_2 : 40% Ar
0.374	382.0	10.2	835.0	4.4	100% : N_2
0.376	382.0	10.1	833.0	4.9	100% : N_2
0.455	351.7	9.2	813.0	3.6	50 % N_2 : 50% Ar
0.401	393.0	10.7	812.0	3.5	80% N_2 : 20% CO_2
0.516	387.6	9.6	807.0	3.7	N_2 : 100%
0.514	386.9	9.3	801.0	3.9	N_2 : 100%
0.525	377.8	9.9	791.0	3.5	N_2 : 100%
0.500	371.4	10.1	790.0	4.2	N_2 : 100%
0.396	373.0	11.0	783.0	3.0	80% N_2 : 20% CO_2
0.393	372.5	10.8	781.0	3.0	80% N_2 : 20% CO_2
0.506	369.5	9.8	778.0	4.5	N_2 : 100%
0.522	378.9	8.4	765.0	3.5	N_2 : 100%
0.515	378.5	8.1	761.0	3.4	N_2 : 100%
0.393	363.5	9.8	750.0	3.7	80% N_2 : 20% CO_2
0.396	361.0	9.6	741.0	3.9	80% N_2 : 20% CO_2
0.382	352.8	9.9	736.0	4.0	80% N_2 : 20% CO_2
0.383	354.5	9.6	735.0	3.9	80% N_2 : 20% CO_2
0.391	352.9	9.9	734.0	3.9	80% N_2 : 20% CO_2
0.563	394.3	9.6	716.0	4.2	50% N_2 : 50% CO_2
0.563	394.3	9.5	715.0	4.3	50% N_2 : 50% CO_2
0.562	394.4	9.3	712.0	4.6	50% N_2 : 50% CO_2
0.563	376.3	9.7	689.0	10.0	50% N_2 : 50% CO_2
0.564	376.4	9.7	689.0	10.0	50% N_2 : 50% CO_2
0.566	376.6	9.6	687.0	10.8	50% N_2 : 50% CO_2
0.562	362.1	9.8	669.0	18.6	50% N_2 : 50% CO_2
0.559	361.2	9.4	662.0	18.7	50% N_2 : 50% CO_2

Table A.15: 1.38% *n*-butylcyclohexane, 20.71% oxygen, 77.91% nitrogen ϕ = 1.0, p_5 =10 atm.

p_i/bar	T_i/K	p_c/bar	T_c/K	τ/ms	diluent
0.554	393.3	10.0	729.0	3.3	100% N_2
0.558	392.6	10.0	726.0	3.1	100% N_2
0.545	382.2	10.0	713.0	4.1	100% N_2
0.547	381.7	9.9	711.0	4.5	100% N_2
0.556	384.0	10.1	693.0	5.6	20% N_2 : 80% CO_2
0.556	384.3	10.1	692.0	6.1	20% N_2 : 80% CO_2
0.555	384.1	10.0	691.0	5.7	20% N_2 : 80% CO_2
0.559	375.0	10.5	682.0	6.1	20% N_2 : 80% CO_2
0.547	375.4	10.1	681.0	8.8	20% N_2 : 80% CO_2
0.55	374.9	9.9	677.0	7.8	20% N_2 : 80% CO_2
0.548	353.3	10.7	676.0	9.8	100% N_2
0.535	352.6	10.3	673.0	11.9	100% N_2
0.547	366.7	10.4	672.0	11.7	20% N_2 : 80% CO_2
0.548	366.6	10.4	671.0	10.7	20% N_2 : 80% CO_2
0.547	366.5	10.4	671.0	9.8	20% N_2 : 80% CO_2
0.591	393.0	10.2	670.0	12.1	50% N_2 : 50% CO_2
0.597	392.9	10.3	670.0	14.2	50% N_2 : 50% CO_2
0.591	392.9	10.2	670.0	14.8	50% N_2 : 50% CO_2
0.516	384.4	10.3	661.0	18.4	50% N_2 : 50% CO_2
0.586	384.2	10.2	658.0	16.1	50% N_2 : 50% CO_2
0.588	384.3	10.2	658.0	18.2	50% N_2 : 50% CO_2
0.58	375.8	10.3	649.0	34.8	50% N_2 : 50% CO_2
0.58	375.6	10.2	647.0	23.7	50% N_2 : 50% CO_2
0.582	375.8	10.2	647.0	39.3	50% N_2 : 50% CO_2
0.586	375.7	10.1	646.0	40.6	50% N_2 : 50% CO_2
0.571	367.6	10.1	637.0	56.4	50% N_2 : 50% CO_2
0.579	367.7	10.2	636.0	54.8	50% N_2 : 50% CO_2
0.568	367.6	9.9	635.0	54.2	50% N_2 : 50% CO_2
0.557	359.1	10.3	629.0	76.1	50% N_2 : 50% CO_2
0.558	359.0	10.2	627.0	79.0	50% N_2 : 50% CO_2
0.556	359.1	10.1	627.0	66.1	50% N_2 : 50% CO_2

Table A.16: 2.72% *n*-butylcyclohexane, 20.43% oxygen, 76.48% nitrogen ϕ =2.0, p_5 = 10 atm.

p_i/bar	T_i/K	p_c/bar	T_c/K	τ/ms	diluent
1.604	378.4	30.6	727.0	6.0	50% N_2 : 50% CO_2
1.605	378.7	30.3	726.0	5.6	50% N_2 : 50% CO_2
1.601	378.5	30.2	725.0	5.6	50% N_2 : 50% CO_2
1.596	364.5	30.9	706.0	10.5	50% N_2 : 50% CO_2
1.603	364.6	30.8	705.0	9.4	50% N_2 : 50% CO_2
1.596	350.6	30.2	680.0	21.0	50% N_2 : 50% CO_2
1.604	350.7	30.5	680.0	19.8	50% N_2 : 50% CO_2
1.602	337.3	31.4	663.0	41.3	50% N_2 : 50% CO_2
1.606	337.2	31.4	662.0	51.4	50% N_2 : 50% CO_2
1.605	337.1	30.5	660.0	59.0	50% N_2 : 50% CO_2

Table A.17: 0.42% *n*-butylcyclohexane, 20.91% oxygen, 79.67% nitrogen ϕ = 0.3, p_5 = 30 atm.

p_i/bar	T_i/K	p_c/bar	T_c/K	τ/ms	diluent
1.477	384.0	30.4	728.0	3.2	50% N_2 : 50% CO_2
1.475	384.1	30.7	727.0	3.0	50% N_2 : 50% CO_2
1.470	383.9	30.3	725.0	3.0	50% N_2 : 50% CO_2
1.441	369.5	30.3	705.0	6.0	50% N_2 : 50% CO_2
1.445	369.7	30.2	704.0	6.0	50% N_2 : 50% CO_2
1.440	369.9	29.7	703.0	5.9	50% N_2 : 50% CO_2
1.405	356.9	29.7	685.0	9.8	50% N_2 : 50% CO_2
1.571	356.9	33.0	684.0	11.0	50% N_2 : 50% CO_2
1.398	356.8	29.5	684.0	9.9	50% N_2 : 50% CO_2
1.602	356.7	33.2	682.0	11.5	50% N_2 : 50% CO_2

Table A.18: 0.695% *n*-butylcyclohexane, 20.854% oxygen, 78.451% nitrogen ϕ = 0.5, p_5 = 30 atm.

p_i/bar	T_i/K	p_c/bar	T_c/K	τ/ms	diluent
1.177	353.0	33.0	705.0	2.6	50% CO_2 : 50% N_2
1.352	354.0	37.1	703.0	3.1	50% CO_2 : 50% N_2
1.616	381.9	29.6	695.0	3.1	50% CO_2 : 50% N_2
1.616	381.9	29.4	694.0	2.9	50% CO_2 : 50% N_2
1.596	381.6	28.7	692.0	2.9	50% CO_2 : 50% N_2
1.615	368.2	29.3	673.0	7.8	50% CO_2 : 50% N_2
1.617	368.3	29.3	673.0	7.5	50% CO_2 : 50% N_2
1.608	368.1	29.2	672.0	7.2	50% CO_2 : 50% N_2
1.608	361.9	29.5	667.0	11.2	50% CO_2 : 50% N_2
1.566	361.5	29.3	666.0	13.6	50% CO_2 : 50% N_2

Table A.19: 1.38% *n*-butylcyclohexane, 20.71% oxygen, 77.91% nitrogen ϕ = 1.0, p_5 = 30 atm.

p_i/bar	T_i/K	p_c/bar	T_c/K	τ/ms	diluent
1.665	385.3	28.7	663.0	7.8	50% N_2 : 50% CO_2
1.663	385.3	29.4	662.0	8.3	50% N_2 : 50% CO_2
1.662	385.0	29.3	661.0	7.7	50% N_2 : 50% CO_2
1.650	373.4	28.8	643.0	16.0	50% N_2 : 50% CO_2
1.626	373.3	28.4	643.0	14.8	50% N_2 : 50% CO_2
1.658	373.2	29.1	643.0	13.9	50% N_2 : 50% CO_2
1.650	373.3	28.6	642.0	12.3	50% N_2 : 50% CO_2
1.747	358.5	33.5	632.0	21.4	50% N_2 : 50% CO_2
1.605	360.3	29.0	628.0	24.6	50% N_2 : 50% CO_2
1.601	360.3	28.6	627.0	25.2	50% N_2 : 50% CO_2

Table A.20: 2.72% *n*-butylcyclohexane, 20.43% oxygen, 76.48% nitrogen ϕ =2.0, p_5 = 30 atm.

Appendix B

n-Butylcyclohexane and n-Heptane Data

B.1 Shock Tube

p_1/Torr	ν/ms^{-1}	p_5/atm	T_5/K	$\tau/\mu s$
202.2	1023.9	9.6	1301.0	116.0
209.6	1008.5	10.3	1268.6	140.0
258.4	969.4	10.5	1203.7	295.5
252.6	956.2	9.8	1181.0	334.0
301.6	930.1	10.6	1140.0	402.0
325.6	890.2	10.0	1073.1	787.5
352.4	890.0	11.0	1071.2	1027.0
355.2	882.4	10.7	1060.6	1042.5
368.4	884.1	10.9	1051.1	1648.0
382.6	865.8	10.1	1021.9	1824.0

Table B.1: 0.239%n-heptane, 0.296% n-butylcyclohexane, 20.893% oxygen, 78.598% nitrogen ϕ = 0.3, p_5 = 10 atm.

p_1/Torr	ν/ms^{-1}	p_5/atm	T_5/K	$\tau/\mu s$
151.6	1094.0	9.1	1406.6	60.0
156.8	1069.8	8.9	1360.3	76.0
175.6	1060.9	9.6	1347.9	87.5
204.6	1043.8	10.6	1318.4	85.0
205.8	999.7	9.5	1238.7	196.0
206.8	994.7	9.5	1227.7	246.0
206.8	981.5	9.0	1206.8	238.0
225.4	947.0	9.1	1144.4	404.0
250.6	939.8	9.6	1137.2	473.0
325.8	909.5	11.2	1090.2	712.0
308.2	909.2	10.7	1087.9	788.0
352.8	889.2	11.2	1058.6	977.0
402.8	867.5	11.7	1026.1	1150.0
375.4	866.4	10.8	1025.8	1170.0
353.2	865.0	10.1	1023.6	1270.0
406.2	867.4	12.0	1012.4	1844.0

Table B.2: 0.422% n-heptane, 0.448% n-butylcyclohexane, 20.823% oxygen, 78.333% nitrogen ϕ = 0.5, p_5 = 10 atm.

p_1/Torr	ν/ms^{-1}	p_5/atm	T_5/K	$\tau/\mu s$
106.2	1181.9	8.9	1504.8	50.0
119.2	1137.8	8.8	1428.8	58.0
125.8	1116.6	8.8	1391.4	62.0
125.8	1109.9	8.7	1380.2	85.0
150.4	1081.9	9.6	1333.7	102.0
153.2	1076.5	9.6	1323.7	100.5
205.6	1004.1	10.5	1204.6	226.0
202.2	997.6	10.1	1194.7	222.0
201.6	978.3	9.5	1163.8	320.0
250.4	967.1	11.3	1147.4	313.0
251.6	934.6	10.2	1098.3	488.0
300.4	917.4	11.4	1072.3	622.0
301.6	906.1	11.1	1054.8	800.0
353.2	886.0	12.0	1026.1	983.0
350.2	887.8	12.0	1015.1	1376.0
375.2	874.2	12.0	994.8	1912.0
361.8	863.3	11.4	991.5	1343.0
369.6	810.3	10.3	906.0	3475.0
437.4	801.4	11.5	893.8	3443.0
439.6	762.88	10.4	841.6	4317.0
511.2	721.93	10.0	787.6	3784.0
617.4	707.29	10.7	768.7	3198.0

Table B.3: 0.787% n-heptane, 0.88% n-butylcyclohexane, 20.648% oxygen, 77.327% nitrogen ϕ = 1.0, p_5 = 10 atm.

p_1/Torr	ν/ms^{-1}	p_5/atm	T_5/K	$\tau/\mu s$
80.8	1246.4	9.2	1518.5	47.0
76.4	1199.7	7.8	1437.4	72.0
100.4	1150.6	9.0	1360.7	90.0
109.2	1114.4	8.9	1304.3	130.0
125.9	1082.6	9.3	1257.7	188.0
109.2	1082.0	8.1	1255.9	168.0
153.0	1030.1	9.8	1178.7	258.0
156.6	1013.0	9.4	1155.8	323.0
175.8	995.9	10.1	1130.7	380.0
200.2	945.5	9.8	1059.4	677.0
200.8	939.0	9.6	1051.3	653.0
250.8	921.3	11.2	1028.5	798.0
275.4	910.4	12.0	997.3	1384.0
275.8	895.6	11.0	982.9	1484.0
300.6	882.4	12.2	968.5	1952.0
274.8	879.6	11.2	962.0	1860.0
303.4	868.7	11.2	958.7	1507.0
289.6	853.0	11.6	935.1	2510.0
325.2	853.6	11.6	930.9	2880.0
345.2	835.1	12.0	903.3	2473.0
448.4	795.9	12.7	861.4	1990.0
413.4	783.3	11.1	845.4	1894.0
618.2	122.7	12.0	770.8	1820.0

Table B.4: 1.548% n-heptane, 1.746% n-butylcyclohexane, 20.307% oxygen, 76.397% nitrogen ϕ = 2.0, p_5 = 10 atm.

p_1/Torr	ν/ms^{-1}	p_5/atm	T_5/K	$\tau/\mu s$
558.2	1028.0	27.1	1306.9	66.0
576.6	1018.1	27.3	1288.5	76.0
609.6	998.2	27.2	1253.2	108.0
709.6	976.8	29.3	1217.9	150.0
754.2	958.1	29.4	1185.4	192.0
1004.8	890.1	31.1	1072.4	565.0
1007.2	890.3	31.2	1072.3	539.0
1098.0	852.9	30.3	1009.0	1260.0
1248.6	823.5	31.0	963.0	1920.0
1434.6	787.0	32.2	908.0	2540.0
1674.6	757.0	32.6	864.0	2500.0
1980.4	725.9	32.0	819.0	3300.0
2359.8	690.5	31.9	769.0	2560.0

Table B.5: 0.239% n-heptane, 0.296% n-butylcyclohexane, 20.893% oxygen, 78.598% nitrogen ϕ = 0.3, p_5 = 30 atm.

p_1/Torr	ν/ms^{-1}	p_5/atm	T_5/K	$\tau/\mu s$
609.2	971.6	27.1	1195.5	112.0
751.4	941.1	27.7	1147.4	174.0
907.2	915.6	30.2	1105.8	225.0
952.2	891.4	29.4	1068.3	277.0
1106.4	884.1	33.0	1058.4	374.2
975.8	870.8	27.9	1036.6	377.0
1009.2	867.8	28.2	1033.3	429.5
1206.5	814.9	27.4	953.5	974.2
1254.8	808.3	29.4	934.7	1100.0
1355.2	792.3	31.0	907.0	1510.0
1581.2	757.5	31.9	857.6	1250.0
1860.9	720.9	30.5	806.3	1130.0
2867.2	707.3	32.5	787.5	1160.0
2245.6	696.5	32.0	772.8	1220.0
2244.2	691.8	32.0	766.5	1200.0
2794.6	649.4	32.0	709.9	2920.0
2761.2	646.0	31.9	705.4	5500.0

Table B.6: 0.422% *n*-heptane, 0.448% *n*-butylcyclohexane, 20.823% oxygen, 78.333% nitrogen $\phi = 0.5$, $p_5 = 30$ atm.

p_1/Torr	ν/ms^{-1}	p_5/atm	T_5/K	$\tau/\mu s$
477.2	1037.9	27.0	1258.7	86.0
555.0	1001.7	27.7	1203.3	110.0
608.2	965.0	27.5	1142.4	186.0
660.8	960.6	29.4	1135.7	182.0
906.8	893.0	31.3	1037.8	348.5
1106.4	858.5	33.5	987.9	588.5
1003.6	818.4	26.5	928.0	945.0
1303.9	780.3	31.4	865.0	634.0
1500.0	735.5	29.6	805.3	645.0
1988.9	680.8	29.0	741.3	1120.0
2461.4	662.5	32.0	718.4	1420.0

Table B.7: 0.787% *n*-heptane, 0.88% *n*-butylcyclohexane, 20.648% oxygen, 77.327% nitrogen $\phi = 1.0$, $p_5 = 30$ atm.

p_1/Torr	ν/ms^{-1}	p_5/atm	T_5/K	$\tau/\mu s$
258.0	1196.5	26.4	1431.0	44.0
308.4	1125.7	25.8	1323.1	59.0
501.6	1042.6	33.1	1197.8	100.0
607.2	1000.2	34.0	1139.7	133.5
603.8	937.9	28.3	1051.9	210.0
797.2	899.4	32.7	999.9	340.0
1054.8	876.3	31.3	999.5	335.0
900.6	846.1	30.6	928.9	460.0
1123.8	802.3	31.5	876.1	490.0
1176.2	762.0	27.9	825.2	421.0
1414.6	739.3	30.4	797.4	309.0
1508.8	711.1	27.9	766.6	425.0
1994.1	690.9	31.4	735.6	721.0
2244.6	660.7	32.0	701.3	2320.0

Table B.8: 1.548% n-heptane, 1.746% n-butylcyclohexane, 20.307% oxygen, 76.397% nitrogen $\phi = 2.0$, $p_5 = 30$ atm.

p_1/Torr	ν/ms^{-1}	p_5/atm	T_5/K	$\tau/\mu s$
998.4	1001.5	45.9	1256.0	59.0
1147.0	954.5	48.2	1168.3	140.0
1194.4	945.9	45.5	1160.2	139.0
1265.8	938.4	50.4	1141.1	190.0
1394.6	909.8	50.4	1093.8	296.0
1610.4	852.3	48.7	1001.7	641.0
2251.6	771.3	48.8	878.8	1103.0
3090.6	708.4	48.6	788.2	1191.0

Table B.9: 0.239% n-heptane, 0.296% n-butylcyclohexane, 20.893% oxygen, 78.598% nitrogen $\phi = 0.3$, $p_5 = 50$ atm.

p_1/Torr	ν/ms^{-1}	p_5/atm	T_5/K	$\tau/\mu s$
1115.4	967.9	47.8	1180.7	73.6
1260.6	946.1	47.3	1144.7	121.0
1450.2	910.6	50.4	1080.9	184.0
1397.0	893.3	46.6	1060.1	252.0
1522.0	857.1	45.9	1004.0	560.0
1654.2	835.9	47.4	965.5	654.0
1737.4	817.4	45.2	933.4	707.0
3205.7	776.0	48.7	883.9	792.0
2304.6	754.6	49.7	846.9	553.0
2466.8	736.6	50.7	821.7	557.0
2903.7	707.2	46.3	781.0	609.0
3731.5	681.3	47.6	752.3	831.0

Table B.10: 0.422% n-heptane, 0.448% n-butylcyclohexane, 20.823% oxygen, 78.333% nitrogen $\phi = 0.5$, $p_5 = 50$ atm.

p_1/Torr	ν/ms^{-1}	p_5/atm	T_5/K	$\tau/\mu s$
1150.0	976.7	46.5	1151.7	80.0
1308.4	901.0	44.5	1040.0	194.0
1316.6	876.7	44.4	1006.5	236.0
1486.6	849.7	45.1	967.8	455.0
1371.6	852.9	44.9	965.8	453.0
1483.0	846.8	45.6	963.7	474.0
1696.2	811.0	45.7	913.6	482.0
1638.6	804.2	45.8	897.7	362.0
1725.0	801.9	47.8	894.5	384.0
1853.4	783.0	48.1	868.7	359.0
2440.6	728.5	44.8	802.7	323.0
2251.4	731.6	44.8	800.2	338.0
2817.4	701.4	45.1	767.7	458.0

Table B.11: 0.787% *n*-heptane, 0.88% *n*-butylcyclohexane, 20.648% oxygen, 77.327% nitrogen ϕ = 1.0, p_5 = 50 atm.

p_1/Torr	ν/ms^{-1}	p_5/atm	T_5/K	$\tau/\mu s$
937.7	930.5	46.3	1034.6	164.0
996.8	949.1	46.8	1019.2	165.0
1134.7	891.5	44.2	982.5	238.0
1072.9	860.0	45.0	935.1	295.0
1261.8	844.5	46.6	915.1	276.0
1412.7	823.5	46.8	895.1	220.0
1543.6	812.5	46.4	881.3	237.0
1606.1	800.3	45.5	866.2	205.0
1524.8	789.1	45.0	845.7	216.0

Table B.12: 1.548% *n*-heptane, 1.746% *n*-butylcyclohexane, 20.307% oxygen, 76.397% nitrogen ϕ = 2.0, p_5 = 50 atm.

B.2 Rapid Compression Machine

p_i/bar	T_i/K	p_c/bar	T_c/K	τ /ms	diluent
0.384	379.9	10.3	1024.0	4.0	70% Ar : 30% N_2
0.381	379.1	10.2	1022.0	3.9	70% Ar : 30% N_2
0.386	379.7	10.2	1021.0	3.9	70% Ar : 30% N_2
0.385	367.5	10.3	994.0	7.0	70% Ar : 30% N_2
0.381	367.1	10.2	993.0	7.5	70% Ar : 30% N_2
0.387	366.8	10.2	988.0	7.0	70% Ar : 30% N_2
0.382	354.8	10.4	969.0	12.0	70% Ar : 30% N_2
0.385	354.6	10.3	964.0	11.4	70% Ar : 30% N_2
0.385	354.9	10.3	963.0	13.1	70% Ar : 30% N_2
0.405	342.2	11.7	953.0	18.8	70% Ar : 30% N_2
0.386	342.0	10.6	938.0	23.9	70% Ar : 30% N_2
0.382	341.9	10.5	938.0	21.2	70% Ar : 30% N_2
0.381	341.6	10.3	934.0	21.6	70% Ar : 30% N_2
0.423	376.7	10.3	923.0	27.2	60% N_2 : 40% Ar
0.420	377.1	10.1	921.0	26.5	60% N_2 : 40% Ar
0.423	376.5	10.2	920.0	26.7	60% N_2 : 40% Ar
0.419	364.7	10.3	899.0	32.3	60% N_2 : 40% Ar
0.410	364.3	10.1	899.0	33.3	60% N_2 : 40% Ar
0.415	364.1	10.2	897.0	32.9	60% N_2 : 40% Ar
0.416	352.7	10.3	873.0	32.9	60% N_2 : 40% Ar
0.412	352.4	10.1	871.0	32.9	60% N_2 : 40% Ar
0.414	351.9	10.2	871.0	32.6	60% N_2 : 40% Ar
0.415	339.3	10.6	851.0	24.8	60% N_2 : 40% Ar
0.413	339.2	10.5	849.0	25.1	60% N_2 : 40% Ar
0.415	339.4	10.2	843.0	25.8	60% N_2 : 40% Ar
0.482	380.4	9.9	827.0	29.2	N_2 : 100%
0.486	380.1	9.8	824.0	28.5	N_2 : 100%
0.483	379.9	9.6	821.0	28.9	N_2 : 100%
0.474	367.4	9.6	800.0	26.1	N_2 : 100%
0.474	367.0	9.7	799.0	25.4	N_2 : 100%
0.473	367.0	9.6	799.0	26.1	N_2 : 100%
0.471	354.5	10.6	794.0	21.0	N_2 : 100%
0.463	354.4	9.9	784.0	22.4	N_2 : 100%
0.460	354.5	9.8	783.0	23.0	N_2 : 100%
0.460	354.6	9.7	782.0	23.2	N_2 : 100%
0.460	342.2	9.9	762.0	21.0	N_2 : 100%
0.461	342.1	9.9	761.0	21.0	N_2 : 100%
0.466	342.2	9.9	759.0	20.3	N_2 : 100%

Table B.13: 0.239% n-heptane, 0.296% n-butylcyclohexane, 20.893% oxygen, 78.598% nitrogen $\phi = 0.3$, $p_5 = 10$ atm.

p_i/bar	T_i/K	p_c/bar	T_c/K	τ /ms	diluent
0.346	413.7	10.3	958.0	3.9	N_2 : 100%
0.349	413.0	10.1	955.0	4.1	N_2 : 100%
0.346	413.9	10.0	953.0	4.1	N_2 : 100%
0.343	399.3	10.2	929.0	6.6	N_2 : 100%
0.345	399.3	10.3	929.0	6.7	N_2 : 100%
0.34	384.5	9.8	894.0	10.6	N_2 : 100%
0.33	384.1	9.8	892.0	13.4	N_2 : 100%
0.341	384.3	9.7	890.0	11.7	N_2 : 100%
0.329	368.3	10.8	870.0	12.7	N_2 : 100%
0.329	367.6	10.7	867.0	12.8	N_2 : 100%
0.328	367.6	10.7	867.0	13.7	N_2 : 100%
0.328	353.7	10.9	842.0	13.3	N_2 : 100%
0.381	412.3	11.1	840.0	14.0	60% N_2 :40% CO_2
0.324	353.2	10.7	840.0	14.1	N_2: 100%
0.375	412.5	10.8	839.0	14.4	60% N_2 :40% CO_2
0.381	414.0	10.9	836.0	13.8	60% N_2 :40% CO_2
0.328	353.1	10.7	836.0	15.0	N_2: 100%
0.378	399.9	10.5	812.0	11.2	60% N_2 :40% CO_2
0.377	397.4	10.7	812.0	11.5	60% N_2 :40% CO_2
0.377	397.9	10.6	809.0	11.5	60% N_2 :40% CO_2
0.374	383.3	10.4	783.0	10.5	60% N_2 :40% CO_2
0.379	383.7	10.1	777.0	10.1	60% N_2 :40% CO_2
0.377	382.6	10.2	777.0	10.8	60% N_2 :40% CO_2
0.375	368.9	11.4	771.0	8.8	60% N_2 :40% CO_2
0.55	393.5	11.6	769.0	8.5	60% N_2 :40% CO_2
0.376	369.1	11.2	767.0	8.4	60% N_2 :40% CO_2
0.552	392.6	11.4	765.0	8.2	60% N_2 :40% CO_2
0.566	392.6	11.6	763.0	8.1	60% N_2 :40% CO_2
0.37	369.1	10.6	763.0	9.0	60% N_2 :40% CO_2
0.545	380.4	11.4	746.0	8.5	60% N_2 :40% CO_2
0.544	380.4	11.4	746.0	8.8	60% N_2 :40% CO_2
0.541	380.2	11.3	746.0	8.6	60% N_2 :40% CO_2
0.364	353.1	10.3	733.0	9.2	60% N_2 :40% CO_2
0.367	353.5	10.3	732.0	9.0	60% N_2 :40% CO_2
0.368	353.6	10.1	729.0	9.1	60% N_2 :40% CO_2
0.541	368.4	11.4	727.0	10.5	60% N_2 :40% CO_2
0.546	367.4	11.5	726.0	10.4	60% N_2 :40% CO_2
0.541	365.9	11.3	721.0	10.7	60% N_2 :40% CO_2
0.533	354.7	11.5	708.0	16.1	60% N_2 :40% CO_2
0.536	354.9	11.3	705.0	14.6	60% N_2 :40% CO_2
0.536	354.2	11.3	704.0	15.0	60% N_2 :40% CO_2
0.538	351.3	11.3	698.0	15.3	60% N_2 :40% CO_2
0.535	342.7	11.5	686.0	24.6	60% N_2 :40% CO_2
0.537	341.1	11.4	683.0	26.0	60% N_2 :40% CO_2
0.536	341.9	11.3	683.0	24.5	60% N_2 :40% CO_2
0.532	341.8	11.1	681.0	29.6	60% N_2 :40% CO_2
0.53	341.4	11.1	681.0	25.3	60% N_2 :40% CO_2
0.536	341.2	11.1	679.0	26.3	60% N_2 :40% CO_2

Table B.15: 0.422% *n*-heptane, 0.448% *n*-butylcyclohexane, 20.823% oxygen, 78.333% nitrogen $\phi = 0.5$, $p_5 = 10$ atm.

p_i/bar	T_i/K	p_c/bar	T_c/K	τ /ms	diluent
0.348	383.0	9.9	911.0	5.5	50% N_2 : 50% Ar
0.345	383.0	9.7	909.0	5.0	50% N_2 : 50% Ar
0.349	383.0	9.7	908.0	6.0	50% N_2 : 50% Ar
0.402	413.0	9.7	845.0	7.9	90% N_2 : 10% CO_2
0.407	413.0	9.8	845.0	7.8	90% N_2 : 10% CO_2
0.402	413.0	9.7	844.0	8.3	90% N_2 : 10% CO_2
0.406	398.0	10.0	822.0	6.4	90% N_2 : 10% CO_2
0.405	398.0	9.9	821.0	7.0	90% N_2 : 10% CO_2
0.402	398.0	9.9	820.0	6.7	90% N_2 : 10% CO_2
0.401	383.0	10.2	801.0	4.4	90% N_2 : 10% CO_2
0.416	383.0	10.5	800.0	4.2	90% N_2 : 10% CO_2
0.400	383.0	10.1	800.0	4.4	90% N_2 : 10% CO_2
0.395	368.0	9.6	767.0	4.5	90% N_2 : 10% CO_2
0.396	368.0	9.7	767.0	4.2	90% N_2 : 10% CO_2
0.398	368.0	9.5	764.0	4.5	90% N_2 : 10% CO_2
0.386	368.0	9.1	760.0	4.8	90% N_2 : 10% CO_2
0.375	353.0	9.5	740.0	5.1	90% N_2 : 10% CO_2
0.388	352.0	9.7	736.0	4.6	90% N_2 : 10% CO_2
0.541	381.1	10.0	723.0	4.5	75% N_2 : 25% CO_2
0.547	381.1	9.9	720.0	4.4	75% N_2 : 25% CO_2
0.532	368.1	10.4	711.0	5.9	75% N_2 : 25% CO_2
0.554	391.2	10.1	706.0	5.8	50% N_2 : 50% CO_2
0.556	390.6	10.1	705.0	5.8	50% N_2 : 50% CO_2
0.551	390.0	10.1	705.0	5.8	50% N_2 : 50% CO_2
0.537	368.3	10.0	704.0	7.3	75% N_2 : 25% CO_2
0.551	378.0	10.4	690.0	9.9	50% N_2 : 50% CO_2
0.554	377.8	10.4	689.0	8.8	50% N_2 : 50% CO_2
0.522	355.6	10.0	688.0	13.9	75% N_2 : 25% CO_2
0.519	355.2	10.1	688.0	9.7	75% N_2 : 25% CO_2
0.521	356.1	9.9	687.0	9.1	75% N_2 : 25% CO_2
0.557	377.2	10.2	686.0	8.9	50% N_2 : 50% CO_2
0.555	365.5	10.5	672.0	18.8	50% N_2 : 50% CO_2
0.559	364.9	10.5	670.0	17.2	50% N_2 : 50% CO_2
0.555	365.0	10.3	669.0	17.2	50% N_2 : 50% CO_2
0.564	352.2	10.6	651.0	48.8	50% N_2 : 50% CO_2
0.550	351.4	10.5	651.0	40.6	50% N_2 : 50% CO_2
0.550	351.6	10.3	649.0	38.3	50% N_2 : 50% CO_2

Table B.16: 0.787% *n*-heptane, 0.88% *n*-butylcyclohexane, 20.648% oxygen, 77.327% nitrogen $\phi = 1.0$, $p_5 = 10$ atm.

p_i/bar	T_i/K	p_c/bar	T_c/K	τ /ms	diluent
0.435	398.0	10.2	742.0	1.6	80% N_2 : 20% CO_2
0.437	398.0	10.0	739.0	1.6	80% N_2 : 20% CO_2
0.436	383.0	10.0	716.0	3.2	80% N_2 : 20% CO_2
0.437	383.0	9.9	715.0	3.3	80% N_2 : 20% CO_2
0.434	383.0	9.8	714.0	3.7	80% N_2 : 20% CO_2
0.436	368.0	10.6	694.0	6.5	80% N_2 : 20% CO_2
0.431	368.0	10.3	692.0	6.6	80% N_2 : 20% CO_2
0.410	368.0	9.7	691.0	6.4	80% N_2 : 20% CO_2
0.601	392.4	9.4	681.0	5.4	80% N_2 : 20% CO_2
0.605	392.1	9.5	681.0	5.9	80% N_2 : 20% CO_2
0.590	380.3	9.5	667.0	10.1	80% N_2 : 20% CO_2
0.593	380.0	9.5	666.0	10.7	80% N_2 : 20% CO_2
0.623	389.6	9.8	652.0	20.1	50% N_2 : 50% CO_2
0.622	389.6	10.0	651.0	22.5	50% N_2 : 50% CO_2
0.620	389.4	9.6	650.0	23.0	50% N_2 : 50% CO_2
0.579	354.0	9.6	638.0	36.6	80% N_2 : 20% CO_2
0.614	375.0	9.7	631.0	50.4	50% N_2 : 50% CO_2
0.679	353.8	9.7	631.0	39.2	80% N_2 : 20% CO_2
0.614	374.4	9.6	629.0	45.0	50% N_2 : 50% CO_2
0.615	372.0	9.8	628.0	49.6	50% N_2 : 50% CO_2
0.601	359.3	9.5	609.0	112.9	50% N_2 : 50% CO_2
0.610	358.4	9.6	608.0	148.9	50% N_2 : 50% CO_2
0.617	357.3	9.7	606.0	147.6	50% N_2 : 50% CO_2

Table B.17: 1.548% *n*-heptane, 1.746% *n*-butylcyclohexane, 20.307% oxygen, 76.397% nitrogen $\phi = 2.0$, $p_5 = 10$ atm.

p_i/bar	T_i/K	p_c/bar	T_c/K	τ /ms	diluent
1.112	383.1	28.6	733	4.3	20% N_2 :80% CO_2
1.183	384.4	30.3	736	4.4	20% N_2 :80% CO_2
1.211	384.3	30.8	735	4.4	20% N_2 :80% CO_2
1.182	368.2	30.1	710	6.9	20% N_2 :80% CO_2
1.191	368.5	31.0	712	7.5	20% N_2 :80% CO_2
1.155	368.4	29.4	709	7.9	20% N_2 :80% CO_2
1.205	352.1	31.3	686	13.3	20% N_2 :80% CO_2
1.235	325.3	32.2	687	13.5	20% N_2 :80% CO_2
1.161	352.2	29.7	684	13.6	20% N_2 :80% CO_2
1.553	354.5	29.0	683	14.5	50% N_2 :50% CO_2
1.574	354.6	29.2	682	14.9	50% N_2 :50% CO_2
1.714	367.4	30.5	672	31.9	30% N_2 :70% CO_2
1.704	367.1	30.2	672	32.6	30% N_2 :70% CO_2
1.731	353.2	31.4	653	71.7	30% N_2 :70% CO_2
1.703	353.3	30.5	651	76.7	30% N_2 :70% CO_2
1.683	353.1	29.7	649	85.3	30% N_2 :70% CO_2

Table B.18: 0.239% *n*-heptane, 0.296% *n*-butylcyclohexane, 20.893% oxygen, 78.598% nitrogen $\phi = 0.3$, $p_5 = 30$ atm.

p_i/bar	T_i/K	p_c/bar	T_c/K	τ /ms	diluent
1.607	369.4	31.1	703.0	5.5	50% N_2 : 50% CO_2
1.601	369.5	31.0	703.0	5.1	50% N_2 : 50% CO_2
1.601	369.3	31.0	703.0	4.9	50% N_2 : 50% CO_2
1.605	356.1	30.1	677.0	13.2	50% N_2 : 50% CO_2
1.602	356.2	29.9	677.0	13.3	50% N_2 : 50% CO_2
1.6	356.2	29.8	676.0	12.9	50% N_2 : 50% CO_2
1.6	343.5	29.8	656.0	32.7	50% N_2 : 50% CO_2
1.604	343.5	29.9	656.0	37.6	50% N_2 : 50% CO_2
1.611	343.4	29.9	655.0	34.5	50% N_2 : 50% CO_2

Table B.19: 0.422% n-heptane, 0.448% n-butylcyclohexane, 20.823% oxygen, 78.333% nitrogen ϕ = 0.5, p_5 = 30 atm.

p_i/bar	T_i/K	p_c/bar	T_c/K	τ /ms	diluent
1.621	378.4	29.8	688.0	6.5	50% N_2 : 50% CO_2
1.627	378.5	29.7	688.0	6.1	50% N_2 : 50% CO_2
1.624	378.2	28.9	684.0	6.3	50% N_2 : 50% CO_2
1.609	365.3	29.4	667.0	14.2	50% N_2 : 50% CO_2
1.610	365.4	29.5	667.0	13.9	50% N_2 : 50% CO_2
1.615	365.1	28.9	664.0	13.6	50% N_2 : 50% CO_2
1.604	351.9	29.9	649.0	32.6	50% N_2 : 50% CO_2
1.608	352.0	29.8	648.0	32.7	50% N_2 : 50% CO_2

Table B.20: 0.787% n-heptane, 0.88% n-butylcyclohexane, 20.648% oxygen, 77.327% nitrogen ϕ = 1.0, p_5 = 30 atm.

p_i/bar	T_i/K	p_c/bar	T_c/K	τ /ms	diluent
1.742	392.6	25.7	678.0	3.4	75% N_2 : 25% CO_2
1.741	392.2	25.7	677.0	3.4	75% N_2 : 25% CO_2
1.735	380.3	26.6	664.0	6.8	75% N_2 : 25% CO_2
1.733	379.9	26.4	663.0	6.1	75% N_2 : 25% CO_2
1.829	390.3	28.1	650.0	12.0	50% N_2 : 50% CO_2
1.822	390.2	27.9	650.0	11.5	50% N_2 : 50% CO_2
1.807	378.5	28.5	636.0	19.3	50% N_2 : 50% CO_2
1.819	378.3	28.4	635.0	19.0	50% N_2 : 50% CO_2
1.733	353.6	29.4	629.0	28.8	75% N_2 : 25% CO_2
1.742	353.8	28.8	626.0	46.7	75% N_2 : 25% CO_2
1.817	366.0	29.1	620.0	43.4	50% N_2 : 50% CO_2
1.816	366.2	28.8	620.0	40.9	50% N_2 : 50% CO_2
1.808	353.5	29.5	605.0	60.1	50% N_2 : 50% CO_2
1.815	353.7	29.5	604.0	72.4	50% N_2 : 50% CO_2

Table B.21: 1.548% n-heptane, 1.746% n-butylcyclohexane, 20.307% oxygen, 76.397% nitrogen ϕ = 2.0, p_5 = 30 atm.

Appendix C

Non-Reactive Rapid Compression Machine Pressure Profiles

Non-reactive pressures profiles and volume histories for *n*-butylcyclohexane and mixtures of *n*-butylcyclohexane / *n*-heptane rapid compression machine experiments are available on an accompanying CD.

Appendix D

Pentene Isomer Data

D.1 1-Pentene

p_1/Torr	ν/ms^{-1}	p_5/atm	T_5/K	$\tau/\mu s$
17.5	916.8	1.1	1651.4	50.0
18.0	900.5	1.0	1601.5	50.0
17.8	898.7	1.0	1596.2	44.0
19.0	882.4	1.0	1547.3	56.0
20.1	874.5	1.1	1524.1	72.0
21.5	855.9	1.1	1469.8	111.0
22.2	851.5	1.1	1457.1	111.0
21.0	849.6	1.0	1451.5	94.0
22.3	840.0	1.1	1424.0	167.0
23.0	825.8	1.0	1384.0	161.0
22.6	825.3	1.0	1382.6	117.0
25.0	824.1	1.1	1379.3	172.0
22.3	821.4	1.0	1371.6	122.0
20.0	815.4	0.9	1355.0	161.0
24.5	811.7	1.1	1344.8	250.0
22.0	808.7	0.9	1336.5	250.0
24.1	803.1	1.0	1321.2	356.0
26.0	802.3	1.1	1318.9	511.0
25.8	798.3	1.1	1308.1	317.0
25.5	784.6	1.0	1271.0	556.0

Table D.1: 1% 1-pentene, 15% oxygen, 84% argon, $\phi = 0.5$, $p_5 = 1$ atm.

p_1/Torr	ν/ms^{-1}	p_5/atm	T_5/K	$\tau/\mu s$
17.0	920.2	1.0	1738.2	44.0
19.0	882.9	1.0	1618.4	78.0
18.1	873.0	1.0	1586.8	106.0
20.2	859.4	1.0	1544.5	139.0
21.0	846.8	1.0	1505.9	194.0
22.1	838.8	1.0	1481.5	189.0
22.0	835.7	1.0	1472.0	211.0
23.5	832.7	1.1	1463.2	222.0
22.5	830.8	1.0	1457.5	278.0
22.3	844.6	1.1	1449.1	150.0
22.8	823.4	1.0	1435.4	339.0
23.0	816.1	1.0	1413.6	467.0
25.0	810.5	1.1	1397.3	422.0
24.3	798.7	1.0	1362.8	533.0

Table D.2: 1% 1-pentene, 7.5% oxygen, 91.5% argon, $\phi = 1.0$, $p_5 = 1$ atm.

p_1/Torr	ν/ms^{-1}	p_5/atm	T_5/K	$\tau/\mu s$
15.0	961.1	1.0	1920.5	72.0
16.1	943.6	1.0	1859.3	81.0
16.3	918.0	1.0	1771.6	100.0
16.5	913.7	1.0	1757.3	144.0
17.0	898.6	1.0	1706.9	177.0
19.0	891.4	1.1	1682.9	222.0
18.0	877.5	1.0	1637.4	289.0
20.2	865.3	1.0	1597.8	339.0
21.1	862.5	1.1	1588.9	400.0
21.3	860.2	1.1	1581.6	417.0
22.0	850.0	1.1	1549.1	378.0
21.5	847.0	1.0	1539.3	467.0
22.3	835.5	1.0	1503.5	744.0
22.3	834.0	1.0	1499.0	944.0
22.5	826.1	1.0	1474.7	789.0
23.0	822.3	1.0	1463.0	744.0
21.8	821.1	1.0	1459.3	750.0
22.8	816.8	1.0	1446.0	972.0
22.1	810.2	0.9	1426.1	944.0
21.2	786.4	0.8	1363.9	911.0

Table D.3: 1% 1-pentene, 3.75% oxygen, 95.25% argon, ϕ= 2.0, $p_5 = 1$ atm.

D.2 Trans-2-Pentene Data

p_1/Torr	ν/ms^{-1}	p_5/atm	T_5/K	$\tau/\mu s$
19.1	874.0	1.0	1520.7	60.0
19.5	860.7	1.0	1484.6	78.0
20.0	860.3	1.0	1481.4	139.0
21.0	849.5	1.1	1449.4	78.0
20.4	841.3	1.0	1426.6	106.0
22.5	837.4	1.1	1417.2	128.0
21.1	834.3	1.0	1406.2	117.0
22.0	834.1	1.1	1405.5	150.0
23.6	833.8	1.1	1405.1	172.0
24.5	827.4	1.1	1387.0	150.0
25.8	821.0	1.2	1371.0	206.0
20.0	856.3	0.9	1362.1	100.0
23.8	814.1	1.1	1353.9	239.0
23.5	813.5	1.0	1348.4	244.0
25.0	810.4	1.1	1339.9	283.0
24.0	810.3	1.0	1339.6	244.0
25.5	806.0	1.1	1329.3	300.0
26.0	799.0	1.1	1310.0	400.0
24.0	795.4	1.0	1300.4	513.0
23.2	793.2	1.0	1292.5	572.0
26.4	787.5	1.1	1277.6	574.0

Table D.4: 1% trans-2-pentene, 15% oxygen, 84% argon, $\phi = 0.5$, p_5= 1 atm.

p_1/Torr	ν/ms^{-1}	p_5/atm	T_5/K	$\tau/\mu s$
20.0	884.8	1.1	1623.0	64.0
19.3	869.6	1.0	1574.7	89.0
19.0	847.3	0.9	1506.0	139.0
20.5	838.9	1.0	1480.6	194.0
21.5	831.7	1.0	1458.9	217.0
21.0	822.5	1.0	1431.3	287.0
24.5	809.6	1.1	1393.3	400.0
22.0	804.0	1.0	1377.1	320.0
25.3	800.9	1.1	1367.9	500.0
23.2	797.5	1.0	1358.3	376.0
24.3	790.3	1.0	1337.5	783.0
24.8	783.9	1.0	1319.1	750.0
24.0	782.4	0.9	1314.8	1139.0
26.2	779.6	1.0	1304.6	938.0
25.0	769.9	0.9	1279.5	778.0

Table D.5: 1% trans-2-pentene, 7.5% oxygen, 91.5% argon, $\phi = 1.0$, $p_5 = 1$ atm.

p_1/Torr	ν/ms^{-1}	p_5/atm	T_5/K	$\tau/\mu s$
17.5	897.9	1.0	1703.2	122.0
19.3	894.5	1.1	1687.6	183.0
18.0	892.5	1.0	1685.2	167.0
19.0	892.9	1.1	1682.3	194.0
18.5	883.1	1.0	1654.4	233.0
19.6	878.0	1.1	1637.5	244.0
18.5	872.0	1.0	1615.8	222.0
19.8	863.5	1.0	1586.5	361.0
21.0	849.7	1.0	1547.0	724.0
20.1	846.5	1.0	1536.8	494.0
23.0	837.3	1.1	1508.0	605.0
23.5	834.0	1.1	1494.1	647.0
22.0	830.7	1.0	1487.4	778.0
24.0	827.0	1.1	1476.0	811.0
25.0	820.7	1.1	1456.7	794.0
22.5	811.1	1.0	1424.2	1061.0
23.5	801.8	1.0	1396.2	1383.0
26.0	777.9	1.0	1325.8	1356.0
25.5	775.4	1.0	1318.7	1444.0

Table D.6: 1% trans-2-pentene, 3.75% oxygen, 95.25% argon, $\phi = 2.0$, $p_5 = 1$ atm.

Appendix E

Dimethylfuran Data

p_1/Torr	ν/ms^{-1}	p_5/atm	T_5/K	$\tau/\mu s$
15.5	952.9	1.0	1940.7	54.0
17.6	932.3	1.1	1865.8	89.0
16.5	927.9	1.0	1850.1	72.0
17.8	921.0	1.1	1825.9	106.0
18.1	901.4	1.0	1757.9	183.0
19.1	889.9	1.1	1718.2	228.0
22.0	862.9	1.1	1626.5	350.0
20.0	856.6	1.0	1606.1	428.0
22.4	850.7	1.1	1586.1	522.0
21.1	847.5	1.0	1575.6	533.0
23.4	822.1	1.0	1493.6	994.0

Table E.1: 0.75% dimethylfuran, 2.8125% oxygen, 96.4375% argon, $\phi = 2.0$, $p_5 = 1$ atm.

p_1/Torr	ν/ms^{-1}	p_5/atm	T_5/K	$\tau/\mu s$
37.3	853.1	1.9	1515.4	92.0
37.1	850.9	1.9	1508.7	92.0
37.6	840.1	1.8	1475.9	103.0
38.1	825.7	1.8	1462.7	150.0
39.1	830.9	1.8	1448.3	167.0
40.1	827.0	1.9	1436.7	232.0
41.1	824.1	1.9	1428.1	267.0
43.0	822.3	2.0	1422.7	322.0
43.0	817.5	1.9	1408.6	263.0
42.2	816.4	1.9	1405.3	313.0
44.2	815.9	1.9	1403.9	372.0
41.1	810.2	1.8	1387.1	275.0
45.1	807.7	1.9	1379.9	492.0
48.1	802.9	2.0	1365.9	579.0
46.1	800.2	1.9	1358.1	406.0
46.6	794.6	1.9	1342.0	610.0
47.1	791.3	1.9	1332.5	619.0
47.5	789.7	1.9	1327.9	762.0
50.1	789.3	2.0	1326.8	924.0
49.6	783.0	2.0	1308.9	848.0
48.6	773.1	1.8	1281.0	1129.0

Table E.2: 0.75% dimethylfuran, 11.25% oxygen, 88% argon, $\phi = 0.5$, $p_5 = 2$ atm.

p_1/Torr	ν/ms^{-1}	p_5/atm	T_5/K	$\tau/\mu s$
34.0	879.5	1.8	1652.9	92.0
35.1	879.3	1.9	1652.2	67.0
36.1	867.5	1.9	1613.5	86.0
37.1	863.0	1.9	1598.9	116.0
38.1	862.0	2.0	1595.6	128.0
41.1	851.7	2.0	1562.4	231.0
39.0	848.3	1.2	1551.5	200.0
40.1	845.1	1.9	1541.3	225.0
42.3	835.4	2.0	1510.6	313.0
41.5	832.3	1.9	1499.9	263.0
43.0	830.7	2.0	1495.8	314.0
41.5	825.1	1.9	1478.3	255.0
42.0	818.3	1.9	1457.2	390.0
42.1	815.1	1.8	1447.3	276.0
43.6	810.1	1.9	1432.3	689.0
46.1	809.3	2.0	1429.5	656.0
43.3	802.8	1.8	1409.7	530.0
44.1	801.5	1.8	1405.7	650.0
47.2	783.3	1.9	1381.0	863.0
50.1	792.2	2.0	1377.7	900.0
45.0	791.8	1.8	1376.4	800.0
49.0	777.6	1.9	1334.2	1229.0
48.0	776.3	1.8	1330.3	933.0

Table E.3: 0.75% dimethylfuran, 5.625% oxygen, 93.625% argon, $\phi = 1.0$, $p_5 = 2$ atm.

p_1/Torr	ν/ms^{-1}	p_5/atm	T_5/K	$\tau/\mu s$
33.1	913.9	2.0	1800.9	113.0
32.5	903.1	1.9	1763.2	100.0
33.3	880.9	1.8	1687.0	214.0
33.8	877.0	1.8	1673.8	213.0
36.1	858.8	1.8	1612.8	379.0
33.5	858.4	1.7	1611.5	313.0
34.0	858.1	1.7	1610.5	578.0
38.0	852.6	1.9	1592.4	387.0
37.2	851.0	1.8	1587.1	372.0
42.0	846.6	2.0	1572.7	433.0
39.0	844.7	1.9	1566.5	500.0
40.0	843.7	1.9	1563.2	565.0
35.1	863.9	1.7	1541.1	300.0
43.1	835.2	2.0	1535.6	654.0
45.1	818.4	2.0	1481.9	717.0
44.0	818.0	1.9	1480.6	722.0
47.0	817.8	2.1	1480.0	828.0
45.5	813.8	2.0	1467.3	1222.0
43.5	813.0	1.9	1464.8	867.0
49.5	806.0	2.1	1442.8	1756.0
46.1	799.5	1.9	1442.6	961.0
48.0	801.2	2.0	1427.9	1217.0
41.0	800.6	1.7	1426.0	828.0
49.8	793.9	2.0	1405.3	1800.0
49.0	790.0	2.0	1393.3	1189.0
50.0	778.8	1.9	1359.1	1561.0

Table E.4: 0.75% dimethylfuran, 2.8125% oxygen, 96.4374% argon $\phi = 2.0$, $p_5 = 2$ atm.